

An Integrated Method for Optimizing Bridge Maintenance Plans

Eslam Mohammed Abdelkader

A Thesis

In the Department of

Building, Civil and Environmental Engineering

Presented in the Partial fulfillment of the Requirements

For the Degree of

Doctor of Philosophy (Building Engineering) at

Concordia University

Montreal, Quebec, Canada

September 2020

©Eslam Mohammed Abdelkader

CONCORDIA UNIVERSITY
SCHOOL OF GRADUATE STUDIES

This is to certify that the thesis prepared

By: **Eslam Mohammed Abdelkader**

Entitled: **An Integrated Method for Optimizing Bridge Maintenance Plans**

and submitted in partial fulfillment of the requirements for the degree of

DOCTOR OF PHILOSOPHY (Building Engineering)

complies with the regulations of the University and meets the accepted standards with respect to originality and quality.

Signed by the final examining committee:

_____	Chair
Dr. Chun Wang	
_____	External Examiner
Dr. Yasser Mohamed	
_____	External to Program
Dr. Amr Youssef	
_____	Examiner
Dr. Ashutosh Bagchi	
_____	Examiner
Dr. Mazdak Nik-Bakht	
_____	Thesis Co-Supervisor
Dr. Osama Moselhi	
_____	Thesis Co-Supervisor
Dr. Mohamed Marzouk	
_____	Thesis Co-Supervisor
Dr. Tarek Zayed	

Approved by: _____
Dr. M. Nokken, Graduate Program Director

November 3, 2020 _____
Dr. A. Asif Dean of Gina Cody School of Engineering and Computer
Science

ABSTRACT

An Integrated Method for Optimizing Bridge Maintenance Plans

Eslam Mohammed Abdelkader, Ph.D.

Concordia University, 2020

Bridges are one of the vital civil infrastructure assets, essential for economic developments and public welfare. Their large numbers, deteriorating condition, public demands for safe and efficient transportation networks and limited maintenance and intervention budgets pose a challenge, particularly when coupled with the need to respect environmental constraints. This state of affairs creates a wide gap between critical needs for intervention actions, and tight maintenance and rehabilitation funds. In an effort to meet this challenge, a newly developed integrated method for optimized maintenance and intervention plans for reinforced concrete bridge decks is introduced. The method encompasses development of five models: surface defects evaluation, corrosion severities evaluation, deterioration modeling, integrated condition assessment, and optimized maintenance plans. These models were automated in a set of standalone computer applications, coded using C#.net in Matlab environment. These computer applications were subsequently combined to form an integrated method for optimized maintenance and intervention plans. Four bridges and a dataset of bridge images were used in testing and validating the developed optimization method and its five models.

The developed models have unique features and demonstrated noticeable performance and accuracy over methods used in practice and those reported in the literature. For example, the accuracy of the surface defects detection and evaluation model outperforms those of widely-recognized machine learning and deep learning models; reducing detection, recognition and evaluation of surface defects error by 56.08%, 20.2% and 64.23%, respectively. The corrosion

evaluation model comprises design of a standardized amplitude rating system that circumvents limitations of numerical amplitude-based corrosion maps. In the integrated condition, it was inferred that the developed model accomplished consistent improvement over the visual inspection procedures in-use by the Ministry of Transportation in Quebec. Similarly, the deterioration model displayed average enhancement in the prediction accuracies by 60% when compared against the most commonly-utilized weibull distribution. The performance of the developed multi-objective optimization model yielded 49% and 25% improvement over that of genetic algorithm in a five-year study period and a twenty five-year study period, respectively. At the level of thirty five-year study period, unlike the developed model, classical meta-heuristics failed to find feasible solutions within the assigned constraints. The developed integrated platform is expected to provide an efficient tool that enables decision makers to formulate sustainable maintenance plans that optimize budget allocations and ensure efficient utilization of resources.

ACKNOWLEDGEMENT

I would like to express my deepest gratitude to my supervisors: prof. Osama Moselhi, prof. Mohamed Marzouk and prof. Tarek Zayed for their patience, constructive guidance, motivation and enthusiasm throughout my PhD studies. Their immense knowledge and instructions assisted me a lot in all the time of research and writing of my thesis. I also would like to express my sincere appreciation to my examining committee members: Dr. Yasser Mohamed, Dr. Ashutosh Bagchi, Dr. Mazdak Nik-Bakht and Dr. Amr Youssef for their constructive comments and encouragement.

I would like to thank and acknowledge my colleagues at the construction automation lab: Mohamed Elmasry, Ahmed Abdelmawgood, Abobakr AlSakkaf, Ahmed Assad and Tarek Salama for their advice, motivation and welcoming atmosphere.

Last but not least, I would like to specially thank and express my extreme gratefulness towards my father Tarek, my mother Nahla and my sisters Nehal and Hadeel for their continuous encouragement, care and support. I owe a lot to my family and it is my greatest pleasure to dedicate my thesis to them.

TABLE OF CONTENTS

LIST OF FIGURES	VIII
LIST OF TABLES	XI
List of ABBREVIATIONS	XIII
CHAPTER I: INTRODUCTION	1
1.1 Problem Statement	1
1.2 Research Objectives	1
1.3 Thesis Organization	2
CHAPTER II: LITERATURE REVIEW	4
2.1 Overview	4
2.2 Condition Assessment Models	4
2.2.1 Previous research studies	4
2.2.2 Research Gaps	8
2.3 Surface Defects Detection and Evaluation	12
2.3.1 Related work	12
2.3.2 Bibliometric analysis and research gaps	22
2.4 Deterioration Modeling	30
2.4.1 Previous research works	30
2.4.2 Research gaps	34
2.5 Maintenance Optimization and Planning	35
2.5.1 Previous research efforts	36
2.5.2 Bibliometric mapping and research shortcomings	42
2.6 Summarized Research Gaps	47
CHAPTER III: INTEGRATED METHOD FOR OPTIMIZED MAINTENANCE PLANS	49
3.1 Overview	49
3.2 Developed Integrated Method	49
3.3 Surface Defects Evaluation	55
3.3.1 Restoration of degraded images	55

3.3.2	Automated recognition of defects	62
3.3.3	Evaluation of defects severities	67
3.4	Corrosion Evaluation	85
3.5	Integrated Condition Assessment	91
3.6	Deterioration Modeling.....	98
3.6.1	Hybrid Bayesian-based method	98
3.6.2	Semi Markov-based method	105
3.7	Maintenance Optimization.....	108
3.7.1	Resource planning method.....	109
3.7.2	Maintenance planning method.....	119
CHAPTER IV:	COMPUTER AIDED APPLICATIONS.....	139
4.1	Overview.....	139
4.2	Autonomous Surface Defects Evaluation	139
4.3	Autonomous Deterioration Modeling.....	144
4.4	Autonomous Maintenance Planning.....	150
CHAPTER V:	TESTING AND VALIDATION	153
5.1	Overview.....	153
5.2	Validation of Developed Computer Aided Applications.....	155
CHAPTER VI:	CONCLUSION AND FUTURE RESEARCH.....	252
6.1	Summary and Conclusions	252
6.2	Research Limitations	255
6.3	Recommendations for Future Research	255
REFERENCES.....		256
APPENDIX I:	SAMPLE OF C#.NET CODE	289

LIST OF FIGURES

Figure 2.1: Bibliometric co-occurrence map of the surface defects assessment models.....	23
Figure 2.2: Bibliometric co-occurrence map of the surface defects detection models.....	25
Figure 2.3: Bibliometric co-occurrence map of the machine learning algorithms adopted for surface defects evaluation.....	27
Figure 2.4: Bibliometric co-occurrence map of the maintenance planning models bridges	43
Figure 3.1: Schematic diagram of the developed research methodology	54
Figure 3.2: Framework of the developed method for the evaluation of surface defects severities	55
Figure 3.3: Flowchart of the developed noise detection and restoration method	61
Figure 3.4: Flowchart of the developed defects’ detection and recognition method.....	66
Figure 3.5: Flowchart of the developed spalling detection and assessment method	79
Figure 3.6: Extracted spatial domain features using singular value decomposition.....	81
Figure 3.7: Flowchart of the developed corrosion evaluation method	90
Figure 3.8: Flowchart of the developed bridge intervention prioritization method.....	95
Figure 3.9: Flowchart of the developed hybrid Bayesian-based method for deterioration modeling	104
Figure 3.10: Flowchart of the developed semi Markov-based method for deterioration modeling	107
Figure 3.11: Framework of the two-tier method for bridge maintenance planning.....	108
Figure 3.12: Flowchart of the developed integrative evolutionary-based method	114
Figure 3.13: Schematic representation of a solution structure for resource	116
Figure 3.14: Flowchart of the developed maintenance planning method.....	125
Figure 3.15: Schematic representation of a solution structure for a typical bridge network	131
Figure 4.1: Interface of the developed preprocessing module of surface defects.....	141
Figure 4.2: Interface of the developed feature extraction model for bridge defects recognition	142
Figure 4.3: Interface of the developed SVD – ENN – IWO model for bridge defects recognition	142
Figure 4.4: Interface of the developed spalling detection model.....	143
Figure 4.5: Interface of the developed feature extraction model for bridge defects evaluation	144
Figure 4.6: A sample of the C#.net code written for the deterioration model platform	145
Figure 4.7: Interface and output of the conditional probabilities module.....	146
Figure 4.8: Interface of the unknown conditional probabilities module.....	146
Figure 4.9: Interface of the Metropolis-Hastings algorithm model	147
Figure 4.10: Interface of the stochastic optimization model.....	148
Figure 4.11: Interface of the performance metrics computation module.....	149
Figure 4.12: Sample of STROBOSCOPE source code for optimizing resource allocation plans	150
Figure 4.13: User interface of the multi-objective differential evolution model for resource allocation.....	151

Figure 4.14: Interface of the developed ECDE-based models for maintenance planning of bridge network	152
Figure 5.1: Breakdown of transition and censored events	155
Figure 5.2: Sample of bridge defects images	157
Figure 5.3: Another sample of bridge defects images	158
Figure 5.4: Corrupted images by (a) Gaussian noise, (b) salt and pepper noise, (c) speckle noise and (d) combination of Gaussian and speckle noises	159
Figure 5.5: Corrupted images by (a) combination of Gaussian and salt and pepper noises, and (b) combination of speckle and salt and pepper noises	160
Figure 5.6: Convergence of the ENN – IWO separate noise recognition model.....	162
Figure 5.7: Distribution of the singular values for image image Spalling-Image “G”	168
Figure 5.8: Convergence of the SVD – ENN – IWO model for defects detection based on dataset I	170
Figure 5.9: Convergence of the SVD – ENN – IWO model for defects recognition.....	171
Figure 5.10: ROC curves of the prediction models for defects detection based on entire dataset I	173
Figure 5.11: Sample of the spalling images.....	178
Figure 5.12: Segmentation outcome of different detection models for spalling-Image “A”	182
Figure 5.13: Segmentation outcome of different detection models for spalling-Image “F”	183
Figure 5.14: Segmentation outcome of different detection models for spalling-Image “T”	184
Figure 5.15: Convergence Curve of the developed ENN – IWO model for predicting spalling area based on original dataset	185
Figure 5.16: Picking the amplitude values of the top reinforcing rebars.....	191
Figure 5.17: Interface of the RapidMiner platform	192
Figure 5.18: Clusters obtained from expectation maximization clustering algorithm.....	192
Figure 5.19: Pareto frontier points of the three adopted evolutionary algorithms- A.....	195
Figure 5.20: Pareto frontier points of the three evolutionary algorithms- B	196
Figure 5.21: Corrosion map of the first bridge deck.....	199
Figure 5.22: Corrosion map of the second bridge deck	200
Figure 5.23: Convergence of the NSGA – II for optimum fuzzy scale computation	202
Figure 5.24: Convergence of invasive weed optimization algorithm for the automated calibration of fuzzy membership functions	205
Figure 5.25: Convergence of genetic optimization algorithm for the automated calibration of fuzzy membership functions	207
Figure 5.26: Calibrated fuzzy membership functions of corrosion	209
Figure 5.27: Histogram and cumulative distribution of the IBDCI using Latin hypercube sampling.....	211
Figure 5.28: Output of the corrosion model for the first bridge deck.....	217
Figure 5.29: Posterior distribution of the in-state probability P33	220
Figure 5.30: Trace plot of the in-state probability P33	221

Figure 5.31: Trace plot of the mean convergence of the in-state probability P33	222
Figure 5.32: Trace plot of the autocorrelation function for the in-state probability P33	223
Figure 5.33: Convergence curve of the negative log likelihood of the unknown transition probabilities.....	224
Figure 5.34: Condition states' distribution and deterioration curve of the hybrid Bayesian model	226
Figure 5.35: 3D optimal surface obtained from the multi-objective particle swarm optimization model.....	232
Figure 5.36: 3D optimal surface obtained from the multi-objective differential evolution model	233
Figure 5.37: Pareto optimal solutions computed from the multi-objective particle swarm optimization model and multi-objective differential evolution model	234
Figure 5.38: Behavior of different chaotic maps	238
Figure 5.39: Behavior of different chaotic maps (Continued).....	239
Figure 5.40: Optimum maintenance plans of the twenty five-year study period.....	241
Figure 5.41: Optimum maintenance plans of the twenty five year-study period (Continued) ...	242
Figure 5.42: Optimum maintenance plans of the thirty five-year study period.....	243
Figure 5.43: Plot of the average and standard deviation of rankings of the meta-heuristic-based optimization models.....	248
Figure 5.44: Box plots of the hypervolume of the meta-heuristic-based maintenance optimization models.....	249

LIST OF TABLES

Table 3.1: Intervention actions and their corresponding unit costs for bridge deck.....	133
Table 5.1: Comparison of the performance metrics of the six classification models for separate noise recognition based on split validation.....	162
Table 5.2: Comparison of the performance metrics of the six classification models for separate noise recognition based on 10-fold cross validation.....	163
Table 5.3: Statistical comparison of the developed noise classification model against other models based on non-parametric tests	163
Table 5.4: Overall performance evaluation of the different types of restoration models	166
Table 5.5: Filtering protocol for different types of noises	167
Table 5.6: Performance evaluation of the prediction models for defects detection based on entire dataset I using 10-fold cross validation	172
Table 5.7: Performance evaluation of the prediction models for defects recognition based on entire dataset using 10-fold cross validation.....	175
Table 5.8: Performance evaluation of the prediction models for defects detection based on entire dataset II using 10-fold cross validation	176
Table 5.9: Mean and standard deviation of rankings obtained by the prediction models	177
Table 5.10: Performance comparison between the different spalling detection models	179
Table 5.11: Statistical comparison between the different spalling detection models using balanced accuracy	181
Table 5.12: Performance comparison between the prediction models based on the original dataset	187
Table 5.13: Performance comparison between the prediction models based on the augmented dataset	188
Table 5.14: Anderson Darling tests for probability distributions of spalling area.....	189
Table 5.15: Sample of the cluster memberships of spalling area obtained from fuzzy C-means clustering algorithm	189
Table 5.16: Severity rating system of spalling based on its area and depth	190
Table 5.17: Sample of the optimal solutions of the shuffled frog leaping algorithm	194
Table 5.18: Comparison between shuffled frog-leaping, particle swarm algorithm and genetic algorithm for the twenty runs.....	197
Table 5.19: Entropy values, variation coefficients, and the weights of the attributes	198
Table 5.20: Sample of the solutions' ranking obtained from TOPSIS	199
Table 5.21: Sample of the pair-wise comparisons with respect to the condition of the bridge deck	203
Table 5.22: Sample of the pair-wise comparisons with respect to the corrosion	203
Table 5.23: Un-weighted supermatrix, weighted supermatrix, and limit supermatrix of the different affecting bridge defects	204
Table 5.24: A comparative analysis between the performances of IWO, GA and NLP	206

Table 5.25: Optimized parameters of the fuzzy membership functions using the invasive weed optimization algorithm.....	208
Table 5.26: A sample of chi-squared test for some bridge condition categories.....	210
Table 5.27: A sample of the cluster memberships obtained from the FCM algorithm.....	213
Table 5.28: Rating systems of the bridge defects based on their severity indices.....	216
Table 5.29: Bridge intervention recommendations based on the IBDCI.....	217
Table 5.30: A comparison between corrosion evaluation using ground penetrating radar and half-cell potential.....	218
Table 5.31: Bridge maintenance prioritization for a sub network of bridges.....	218
Table 5.32: Calculated transition probabilities for each zone.....	225
Table 5.33: Comparison between the different deterioration models.....	228
Table 5.34: Boundary condition of the output variables from discrete event simulation model.....	229
Table 5.35: Performance comparison between the different machine learning models for the prediction of greenhouse gases based on 10-fold cross validation.....	231
Table 5.36: Entropy values, variation coefficients, and the weights of the attributes.....	235
Table 5.37: Sample of the solutions' rankings obtained from PROMETHEE II.....	236
Table 5.38: Performance comparison between the different multi-objective meta-heuristics for maintenance planning of the thirty five-year study period.....	245
Table 5.39: Performance comparison between the different multi-objective meta-heuristics for maintenance planning of the thirty five-year study period (Continued).....	246
Table 5.40: Sample of the solutions' rankings obtained from COPRAS, GRA and AR for the maintenance planning of five-year study period.....	250
Table 5.41: Sample of the solutions' rankings obtained from COPRAS, GRA and AR for the maintenance planning of twenty five-year study period.....	251
Table 5.42: Sample of the solutions' rankings obtained from COPRAS, GRA and AR for the maintenance planning of thirty five-year study period.....	251

List of ABBREVIATIONS

AHP	Analytical hierarchy process
ANP	Analytical network process
TOPSIS	Technique of order preference by similarity to ideal solution
GPR	Ground penetrating radar
DA	Discriminant analysis
KNN	K-nearest neighbors
RF	Random forest
SVM	Support vector machines
ANN	Back-propagation artificial neural network
PSNR	Peak signal to noise ratio
MSE	Mean-squared error
NAE	Normalized absolute error
IEF	Image enhancements factor
SVD	Singular value decomposition
ENN	Elman neural network
IWO	Invasive weed optimization
DT	Decision tree
CONVNET	Deep convolutional neural network trained from scratch
BACC	Balanced accuracy
MCC	Matthews's correlation coefficient
AUC	Area under curve

AR	Average ranking
MAE	Mean absolute error
RBNN	Radial basis neural network
GRNN	Generalized regression neural network
LSVM	Linear kernel support vector machines
RSVM	Radial kernel support vector machines
GBDT	Gradient boosted decision trees
GP	Gaussian process
MAPE	Mean absolute percentage error
MOGA	Multi-objective genetic algorithm
MOPSO	Multi-objective particle swarm optimization algorithm
MODA	Multi-objective dragonfly algorithm
MOGWO	Multi-objective grey wolf optimization algorithm
MOJAYA	Multi-objective Jaya algorithm
MOSFL	Multi-objective shuffled frog-leaping algorithm
DE	Differential evolution algorithm
MDE	Modified differential evolution algorithm
GOA	Grasshopper optimization algorithm
TLO	Teaching-learning optimization algorithm
BBO	Biogeography-based optimization algorithm

CHAPTER I: INTRODUCTION

1.1 Problem Statement

Bridges are one of the core civil infrastructure systems that are vital for economic developments and public welfare. Their large numbers, expeditious deteriorating condition, increase in public demands for safe, functional and serviceable transportation networks in the light of squeezed maintenance and intervention budgets constitute an escalating challenge, especially when coupled with the need to address social and environmental constraints. The research question here is how one can contribute to the development of innovative, accurate and reliable tools and integrated methods to support optimization of maintenance and intervention plans for bridges, particularly reinforced concrete bridge decks that account for their safe use, serviceability conditions and sustainability in light of budget and environmental constraints. Such optimization requires accurate and reliable condition assessment methods, deterioration models as well as integrated optimization algorithms that address the limitation of current related methods, improve and extend them as well as augmenting current practice in this field (Felio, 2016; National Research Council Canada, 2013; Kim et al., 2018; Shreyas and Dai, 2020; Demertzis and Iliadis, 2020; Choi and Song, 2019).

1.2 Research Objectives

The main objective is to study the essential requirement for optimized maintenance plans of reinforced concrete bridge decks with due consideration to social and environmental impacts of these plans. To achieve this objective, the following sub-objectives are considered.

- 1- Review state of the art in relation to methods required to plan, develop and execute optimized maintenance plans.

- 2- Evaluate and consider possible use of different methods for capturing inspection data such as computer vision-based methods and those based on penetrating radar for efficient detection, diagnosis and evaluation of the severity of defects in reinforced concrete bridge decks.
- 3- Model deterioration of several bridge components under multiple intervention actions.
- 4- Design and develop an integrated condition-driven method for bridge deck maintenance prioritization and utilize it for optimizing those maintenance plans.
- 5- Automate the method in 4 above in a standalone computer aided platform, and test and validate it using cases of bridges constructed in Canada and the United States of America.

1.3 Thesis Organization

The thesis is organized in in six chapters:

Chapter 2: It describes a review of literature related to the stated objectives, focusing on condition assessment of reinforced concrete bridges, surface defects evaluation, deterioration modeling and optimization of maintenance plans. Also, it highlights research shortcomings of the previously-developed models.

Chapter 3: It describes the developed integrated condition assessment method, its components and its use in development of optimized maintenance plans. These components include models developed for detection of surface defects, corrosion severity, deterioration modeling as well as the developed optimization model.

Chapter 4: It focuses on automating the developments made in Chapter 3 in a set of partially integrated standalone set of computer applications, along with their respective user interactive screens and samples of their developed programming codes.

Chapter 5: It is dedicated to testing and validation of the developed method for optimized maintenance plans and its individual models using cases of bridges constructed in Canada and the United States of America. This chapter includes also discussion of the results obtained and highlights the limitations of the developments made in this thesis.

Chapter 6: It describes summary and conclusions of the research performed, and lists recommendations for future work.

CHAPTER II: LITERATURE REVIEW

2.1 Overview

In this chapter, previously-conducted research is analyzed in relation to the fields of evaluating the condition of bridge decks, assessing of surface defects, predicting the condition of bridge components and optimizing bridge maintenance plans. Additionally, it documents the critical research gaps of the previous studies based on a group of bibliometric analyses.

2.2 Condition Assessment Models

This section reports previous research studies in relevance to condition assessment modeling and the identified research gaps.

2.2.1 Previous research studies

Condition assessment is vital for delegated transportation agencies because it enables them to establish an accurate description of extent of severities of bridge deterioration. Several efforts were conducted for the purpose of establishing condition assessment models of reinforced concrete bridges. Alsharqawi et al. (2020) developed a numerical amplitude-based ground penetrating radar scale to evaluate the corrosiveness in reinforced concrete bridges. K-means clustering method was applied to compute the thresholds of the amplitude values. Some statistical analysis tests were adopted to define the best-fit distribution of the thresholds, namely Kolmogorov-Smirnov test, Anderson Darling, and chi-squared test. They highlighted that the thresholds that separate the “Very Poor” category from “Poor” category, “Poor” category from “Medium” category, and “Medium” category from “Good” category follow logistic distribution, logistic distribution and triangular distribution, respectively. Then, weibull distribution was adopted to simulate the deterioration of the bridge decks using the output of the ground penetrating radar. Prasetyo et al. (2019) presented an approach for the purpose of prioritization of

bridge maintenance. Analytical hierarchy process was utilized to compute the weighting vector of a set of attributes, namely average daily traffic, bridge length, bridge width, population, etc. Preference Ranking Organization Method for Enrichment Evaluation was applied to obtain a unified ranking index based on the evaluation of the bridge inventory across the different attributes. It was revealed that the condition rating attribute constituted the highest priority among the different criteria.

Amiri et al. (2019) adopted a group of multi-criteria decision-making techniques for sorting maintenance actions taking into consideration the risks that may threaten the bridges during the operational stage. The multi-criteria decision-making models involved AHP, ANP and TOPSIS. Furthermore, the risks on bridges were analyzed using failure mode and effects analysis (FMEA) method. Fitriani et al. (2019) presented a maintenance prioritization model of truss bridges using analytical hierarchy process. The prioritization model was designed with respect to a set of attributes, namely level of damage, technical aspects, financial aspects, vehicle load and resources. Level of damage represented the highest weight (27.6%) while resources constituted the lowest weight (12.1%) as per the feedback of 12 respondents. They highlighted that the developed model could provide transportation agencies with efficient bridge maintenance program.

Gao and Li (2018) proposed a simplified corrosion index to evaluate the actual corrosion of reinforced concrete superstructure. Fuzzy analytical hierarchy process was applied to compute the weighting factors, namely corrosion damage, environment change factor and material vulnerability factor. They pointed out the developed model signified promise results when dealing with the assessment of the extent of severities of corrosion. Omar et al. (2018a) created a condition map for concrete bridge decks using infrared thermography. In it, K-means clustering

algorithm was applied to compute the threshold values of temperature. The condition map was developed based on three categories of “sound”, “monitoring” and “warning”, whereas it was found that sound condition ranged from 1 °C to 2.5°C. The developed condition maps were compared against corrosion map created using visual analysis of ground penetrating radar profiles. It was concluded that the differences between the percentages of defected regions created using these two non-destructive evaluation techniques were approximately 5%.

Alsharqawi et al. (2018) developed a model for the evaluation of concrete bridges using an integration of ground penetrating radar and visual inspection. Quality Function Deployment (QFD) was introduced to establish a comprehensive bridge deck condition index based on the severities of set of defects such as corrosion, delamination, spalling, scaling, etc. The developed QFD was divided into five main components, which are: house of quality (HOQ), customer demands (Whats), quality characteristics (Hows), relationship matrix, correlation matrix, and absolute weights of Whats. Wasserman’s normalization technique was adopted in order to map the interdependencies between the bridge defects. Weibull distribution function was then utilized to forecast the deterioration of the bridged deck. It was highlighted that the developed model could provide bridge managers with robust MR&R recommendations. Omar et al. (2018b) developed a model for the generation of an overall bridge deck condition map based on the integration of ground penetrating radar and infrared thermography. Passive infrared thermography testing and ground penetrating radar scanning were conducted to create a delamination map and corrosion map, respectively. In the developed model, K-means clustering was applied to compute the thresholds of the corrosion and delamination maps. A combined condition map was then developed based on average normalized method. It was stated that the

integration of the ground penetrating radar and infrared thermography could enhance bridge deck inspection programs and maintenance budget allocation models.

Abu Dabous et al. (2017) developed an integrated model that adopted ground penetrating radar and infrared thermography for evaluating the condition rating of bridge decks. In the developed model, the threshold values of the ground penetrating radar and infrared thermography maps were identified subjectively on a case by case basis. These maps were then superimposed to simulate possible delamination locations through eliminating non-coinciding areas. The condition rating of bridge deck was then identified based on the percentage of defected regions. It was found that the ground penetrating radar and infrared thermography coincides with delaminated areas identified by hammer sounding by 85% and 75%, respectively. Additionally, it was found that the integrated method and hammer sounding accomplished the same overall condition rating. Suthanaya and Artamana (2017) proposed a multi-criteria decision making model for the prioritization of bridge maintenance in developing countries. The ranking system was capitalized on four criteria which were: road network system, institutional system, land use system and movement system. They concluded that the most influential attributes were bridge condition, road narrowing, transportation strategic area, traffic volume and bridge function. They deduced that the developed model was efficient in building a bridge maintenance ranking system in Bali province.

Dinh and Zayed (2016) introduced an automated software that calculates the bridge deck corrosiveness index (BDCI) based on the weighted fuzzy union (WFU) operation in order to take into consideration the fuzziness associated with the expert opinions. The corrosion index was calculated based on GPR to evaluate the corrosion of the rebar in the concrete bridge decks.

Martino et al. (2016) introduced a method to compute threshold value for the ground penetrating

radar based on the receiver operating characteristic curves (ROC) using half-cell potential as a ground truth. They concluded that -1.6 DB is the universal threshold that separates the healthy areas from the corroded areas in concrete bridge decks. However, the developed method can be only used for the binary classification since it is based on the ROC curves, i.e., for the separation of the corroded areas from the non-corroded areas.

Moufti et al. (2014) applied fuzzy hierarchical evidential reasoning (HER) to provide a detailed condition assessment under uncertainty. The proposed methodology modeled the three levels of the concrete bridge, which were: bridge components, elements, and measured defects. Dempster-Shafer (D – S) theory was implemented to aggregate the multiple sources of information. The weights of the bridge elements and the structural defects were calculated based on Analytical Hierarchy process. Deng et al. (2014) presented a methodology for the bridge condition assessment using D numbers, which is an extension of the Dempster-Shafer theory. The proposed methodology was divided into four main stages, which were: establishing a hierarchical model for the bridge condition assessment model, calculating the weight and assessment rating for each factor, aggregating the assessment results of the bottom factors, and aggregating of all the assessment results by stepwise weighting to calculate the overall condition index. Bolar et al. (2013) applied HER for the condition assessment of the bridges. The HER framework classified the bridge data to primary, secondary, tertiary or life safety-critical elements. The information and bodies of evidence were aggregated using Dempster–Shafer and Yager rule of combination in order to deal with aleatory and epistemic uncertainties.

2.2.2 Research Gaps

In view of the previous studies, it can be observed that ground penetrating radar-based models lack the presence of a generic standardized amplitude rating scale, whereas there is no clear

value for the thresholds that define the different categories of corrosion. The presence of standardized thresholds for the ground penetrating radar is very essential in order to provide an equal basis for comparison between the different concrete bridge decks. Their absence can lead in return to inaccurate maintenance prioritization and budget allocation models.

In this regard, most of the previously developed models relied on K-means clustering algorithm to compute the amplitude threshold values. However, K-means clustering is an un-supervised learning algorithm which means that they are highly dependent on the input dataset since there is no prior information about the model. Thus, if another bridge deck is investigated, the amplitude threshold values will be different consequently and subsequently; no fair comparison can be conducted between two bridge decks. Some models capitalized on statistical goodness of fit tests to compute the standardized thresholds based on 34 bridge decks. However, these tests require huge dataset to build a reliable amplitude rating scale. In this context, Fornell (1983) illustrated that the minimum sample size required to perform goodness of fit tests is 200. In addition to that, Grant et al. (2017) stated that the Kolmogorov-Smirnov test is performed when the sample size is more than 50 observations. Some models also utilized ROC curves to compute the threshold values. Nevertheless, the developed model is limited for two point category scale (corroded and non-corroded areas) and cannot be generalized to provide the amplitude thresholds in the case of the existence of more than two condition categories.

Some models focused on one or two types of defects to design the bridge maintenance prioritization models. This induces incomprehensive and inefficient condition assessment models because the prioritization index doesn't reflect the actual condition of the bridge. Also, it is worth mentioning that most of the prioritization models capitalized on visual inspection and conventional methods to evaluate the physical condition of the bridge elements. However, these

methods are subjective and deal with only the defects visible on the surface. In this regard, the condition assessment models established based on the visual inspection are error-prone and often lead to imprecise judgements because of the inherent subjectivity arising from being extensively dependent on the skills and experience of inspectors, which creates wide variations among the evaluations of the inspectors. Furthermore, visual inspection is criticized for being labour-intensive, time-consuming and hazardous in some cases (Kim et al., 2018; Lei et al., 2018). Although the integration of non-destructive evaluation techniques have been previously investigated in evaluating the condition of bridge decks. However, these models overlooked the evaluation of surface defects despite their considerable importance, whereas it was reported that surface defects play an important role in visual inspection manuals because they are able to establish an accurate reflection of condition ratings of structural members (Koch et al., 2015). Some models also relied on crisp or deterministic paradigms to derive the condition assessment model. Thus, they fail to capture the considerable inherent uncertainties elicited during the inspection process or inability to precisely evaluate subsurface deterioration, which may lead to imprecise and misleading decision-making platforms. Another issue could be observed is that some models did not consider the uncertainty of the importance weightings or correlation matrices of the different attributes that influence the decision-making process. These uncertainties arise from the vagueness and subjectivity provided by experts' judgements such that the lack of their modeling may result in inefficient intervention actions. Some models were mainly driven by the AHP to compute the weights of the attributes of the maintenance prioritization models. AHP assumes independencies between the attributes of the model. As such, it does not model the dependencies and interaction between the different attributes, which may heavily influence the decision-making process taken by delegating authorities.

It is also noted that there is a lack of systematic bridge maintenance decision-making strategies and comprehensive severity rating systems in the element-level, whereas most of the conducted studies with regard to that level were basically condition assessment models. Furthermore, these models don't provide the decision-makers with the flexibility to delineate a synthesis evaluation of the extent of severities of the bridge defects separately. It can be also noticed that there is lack of maintenance prioritization models that support both element and network levels decision making. These decision support systems are highly needed since separate network-level decision making platform may not yield the optimum decisions for transportation agencies resulting from their failure to capture the actual deterioration of individual bridge elements.

With respect to the fuzzy-based decision-making models, it is observed that most of them were structured on subjective methods to formulate the fuzzy expert systems. This includes the shape and spans of membership functions in addition to the fuzzy rules of the inference models. They were defined subjectively based on the engineer's expertise or intuition, which are inconsistent, time-consuming and hardly generalized to fit the case in hand. Furthermore, they are highly dependent on the size and demography of the respondents. For instance, the feedback obtained from 50 experts can be different from the feedback obtained from 100 experts. Moreover, the feedback obtained from engineers of twenty years' experience can be different from the feedback obtained from engineers of thirty years' experience. Another issue of concern is that with possible increase in the number of fuzzy rules in the fuzzy inference system, there is higher potential of experiencing underlying disparities among the rules that are difficult to be observed (Sharma and Goyal, 2019). Therefore, the absence of empirical objective interpretation methods for tuning the fuzzy inference systems may not provide optimal and efficient fuzzy-based decision-making models. In order to circumvent the limitations of subjective methods of fine-

tuning the fuzzy inference systems, an optimization-based method needs to be proposed for the purpose of automated calibration of fuzzy membership functions.

2.3 Surface Defects Detection and Evaluation

This section highlights key research shortcomings by analyzing existing literature using a set of bibliometric maps.

2.3.1 Related work

Proper surface defects detection and quantification plays an important role in designing efficient image-based bridge condition rating systems. Several previous computer vision-based models were developed for the automated detection and evaluation of surface defects in reinforced concrete bridges. Yang et al. (2020) proposed a transfer learning-based model for crack detection in infrastructures. Visual Geometry Group of 16 layers (VGG16) was utilized for the sake of improving detection performance and reducing the training time. The training and validation of the model was carried out using a set of well-known crack datasets, namely SDNET dataset, CCIC dataset and BCD dataset. It was found that the developed model could achieve an improvement in the crack detection accuracies by 2.33% and 5.06% for the SDNET and BCD dataset, respectively when compared against other deep convolutional neural networks.

Xu et al. (2019) introduced a method to automatically detect cracks in images using convolutional neural network. Atrous Spatial Pyramid Pooling was applied to detect the input feature map with multiple sampling rates. Atrous convolutions of size 3×3 and with rates of 2, 4 and 8 were applied in parallel whereas the extracted feature maps are further processed by the depthwise separable convolution in a separate branch. Atrous convolution was utilized to obtain larger receptive field and more context information without reducing the resolution and increasing number of parameters. The multi-scale feature maps of Atrous convolutions were

integrated with the globally pooled input feature map to generate the final feature map. The depthwise separable convolution in the Atrous spatial pyramid pooling module was used to minimize the computational complexity and enhance the computational efficiency. They deduced that the developed model outperformed a set of pre-trained networks by achieving accuracy, precision, sensitivity, specificity and F-measure of 96.37%, 78.11%, 100%, 95.83% and 0.8771, respectively.

Kruachottikul et al. (2019) utilized a pre-trained deep convolutional neural network called “Halcon” for the detection of defects in bridge sub structure surface. They established a binary classification model that enabled to determine whether the images encompassed defects or not. They highlighted that the developed transfer learning-based model achieved a total accuracy of 89.3% which could improve the inspection process conducted by the departments of highways. Dung and Anh (2019) presented a crack detection method capitalizing on deep fully convolutional neural network. The main pillar of the fully convolutional neural network was VGG16 that was pre-trained using the ImageNet dataset. In this regard, the proposed encoder incorporated all the convolutional and pooling layers of the VGG16 except the fully connected and softmax layers. VGG16 was selected over other pre-trained networks including ResNet and InceptionV3 since it provided better performance in crack image classification. The encoder-decoder fully convolutional neural network was then trained end to end based on crack-labeled images dataset. It was highlighted that the developed segmentation method achieved average precision and maximum F1-score of 89.3% for the testing dataset.

Wang et al. (2019) utilized an integration of AlexNet and VGG11 pre-trained deep convolutional neural networks for bridge crack identification. The feature maps created by the two networks are concentrated in series to be sent to a softmax classifier for categorization of cracks. It was

found that the developed model yielded improvements in the prediction accuracies by 0.32% and 0.41% with respect to AlexNet and VGG11 networks, respectively. Słonski (2019) compared the performances of four different architectures of deep convolutional neural networks in the automated detection of concrete surface cracks. This comprised small convolutional network with and without data augmentation, pre-trained VGG16 with data augmentation alongside VGG16 with a combination of data augmentation and fine-tuning. It was reported that the VGG16 coupled data augmentation and fine-tuning provided the highest classification performance achieving training and validation accuracies of 95% and 93%, respectively.

Wang et al. (2019) proposed a method for crack detection in concrete bridges based on a set of image processing techniques. Adaptive filtering was integrated with contrast enhancement to eliminate the background noise and facilitate the accurate extraction of crack features. Then, a hybridization of Otsu and modified Sobel operator was applied for the detection of cracks. The proposed method achieved an absolute error of 0.02 mm in the detection of cracks width. Chen et al. (2019) proposed a method for the detection of concrete cracks using Otsu algorithm. In the developed model, Gaussian filter was applied to remove noise from background. Morphological operations were applied to remove noise from the segmented image while maintaining the shape features of the cracking. It was highlighted that the developed model could efficiently generate a binary image of cracks.

Dorafshan et al. (2018a) studied the implementation of two modes of deep convolutional neural network in concrete crack detection. In the first mode, the AlexNet architecture was fully-trained from scratch capitalizing on the dataset captured using small unmanned aerial systems. In the second mode, a transfer learning-based network of same topology was pre-trained using ImageNet dataset. The performances of the deep neural networks were assessed using three

datasets. It was reported that the transfer learning-based network had higher training accuracy than the fully trained network. Furthermore, it accomplished higher validation accuracies for the three datasets by values ranged from 5.3% to 10%. Kim et al. (2018) introduced a region-based convolutional neural network model coupled with transfer learning for identification of cracks in an aging concrete bridge. A 3D point-cloud based background model was generated for the visualization of cracks on the inspection map. In this model, the deep neural network model was pre-trained using the Cifar-10 dataset. Furthermore, a dataset of 384 images was utilized for training and testing purposes. It was concluded that this model achieved a relative error of 1-2% in the quantification of cracks.

Pavithra et al. (2018) proposed a computer vision-based method for the detection of cracks in reinforced concrete bridges. Then, median filter was applied to remove the salt and pepper noise present in images. Morphological segmentation was utilized to detect cracks in images using some operations such as dilation and erosion. The grey level co-occurrence matrix and statistical features were used to feed the detection model. Finally, the cascaded random forest classifier was applied to decide whether the images contain cracks or not. Li et al. (2018) introduced a two-stage crack detection method based on convolutional neural network. A median filter was applied to de-noise the input images for further processing stages. The first stage involved feeding a small patch centering each pixel into the predictor to compute the probability that a pixel belongs to a cracked area. In the second stage, a bigger patch elicited from the first confidence map is fed into the second predictor to obtain a second confidence map. Finally, the two confidence maps are combined to generate a final confidence map, which is used to map whether or not a certain pixel belong to cracked regions. The introduced method outperformed

the canny edge detector method and spatially tuned robust multi-feature method (STRUM) as per accuracy, precision and sensitivity.

Lei et al. (2018) developed a method for the crack detection based on the crack central point (CCPM) algorithm. Gaussian filter was applied to remove noise from images and restore them. They highlighted that the crack can be distinguished capitalizing on the existing minimum gray value in the row crack area, which usually takes the form of parabolic distribution. They also urged that the developed method can accurately compute a separating threshold that can efficiently extract the crack from the images collected using the unmanned aerial vehicle. Zhang et al. (2018) presented a model to classify the bridge cracks using convolutional neural network. Wavelet de-noising was used to remove noise that corrupted images. Otsu algorithm was utilized as the segmentation method to differentiate the bridge cracks from the background. The proposed model achieved accuracies of 92%, 95% and 90% for small cracks, larger cracks and serious cracks, respectively.

Zhang et al. (2018) proposed an improved watershed algorithm to enhance the detection process of bridge cracks. They utilized a combination of H-minima method, morphological forced minimum operation and watershed algorithm to enhance the segmentation capacity and avoid the over segmentation. H-minima was used to capture the local minima values of the target region which are highly correlated with bridge cracks from low frequency components in the image. They demonstrated that the developed method introduced higher accuracy and robustness when compared to the conventional watershed segmentation method. Cha et al. (2017) employed convolutional neural network for the detection of concrete cracks. The architecture of the deep convolutional neural network (DCNN) was composed of four convolutional layers, two pooling layers, one rectified linear unit layer and one softmax layer. The developed model was validated

through comparisons against Canny and Sobel edge detection methods. It outperformed them providing training accuracy and testing accuracy of 98.22% and 97.42%, respectively.

Zhang et al. (2017) proposed a modified beamlet tree-based method for the detection of cracks in concrete bridges. The images were collected using unmanned aerial vehicle from the underside of bridges. The proposed method relied on beamlet data structure and a corresponding binary tree to segment the cracks. Then, a set of morphological operations including: top-hat, dilation, erosion and thinning were applied to remove the irregular illuminations and fill small holes. The developed method provided superior detection results when compared against the original beamlet tree, Canny and structured edges models. Lee et al. (2017) developed a bridge inspection system using an unmanned aerial vehicle (UAV). Median filter was used to remove the noises and blurring present in images. Otsu method was applied to segment the images to objects of interest and background. Then, the crack properties in the HSV space were used to distinguish between cracks and other surface irregularities. HSV is a color space that is identified using hue, saturation and value of the color. Hue stands for pure color resemblance. Saturation stands for how white a color is and the value of the color indicates its lightness. They highlighted that their model was capable of detecting cracks measured in micrometers.

Cen et al. (2017) utilized convolution neural network to detect the presence of cracks in reinforced concrete bridges. The images were captured using unmanned aerial vehicle such that images of size 48×48 pixels were used as an input to train the model. They investigated different sizes of filter window, whereas they concluded that the filter window size 48×2 achieving the highest accuracy. The proposed detection method was capable of achieving 93.12% prediction accuracy using 2304 crack images and 5368 non-crack images. Xuejun and Yan (2017) developed a bridge crack detection system using video frame processing. The classification of

bridge cracks was performed via deep belief network (DBN). The proposed model was capable to achieve a classification accuracy of 94%, 93% and 90% for the transverse cracks, longitudinal cracks, and network cracks. The developed DBN model outperformed some conventional utilized classification methods such as support vector machines and back propagation neural network.

Yao et al. (2016) presented a bridge crack detection and classification model based on a climbing root using a set of image processing techniques. Wiener filtering method was applied to remove the motion blur of the acquired images. Then, the wavelet transform was employed to minimize the texture effects of the crack area and finally, support vector machine (SVM) was implemented to classify the cracks and evaluate their severity levels. Dinh et al. (2016) established a computer vision-based method for concrete crack detection. Average filter was applied to smooth the input images and remove the blob-like noise. A non-parametric peak detection algorithm was developed for binarization purpose, so that it was able to differentiate defected and non-defected regions. They highlighted that the automated peak detection algorithm provided satisfactory results in the case of high noisy background images and low contrast images.

Ellenberg et al. (2016) developed a bridge damage quantification model using digital images collected from unmanned aerial vehicles. Median filter was applied to remove the noise and enhance the contrast in images. The proposed method combined high-resolution cameras with camera calibration and homography for tracing of cracks. They highlighted that the proposed method was capable of detecting cracks in images, which could eventually provide efficient bridge inspection models. Bu et al. (2015) introduced a model that integrates both wavelet features and support vector machines to detect bridge cracks automatically in images. They compared between three feature extraction methods which are: Daubechies Wavelet features, Gabor filter and Zernike moments. They concluded that Daubechies Wavelet features provides

the best performance followed by Gabor filter and finally Zernike moments. They also highlighted that support vector machine achieved an accuracy of 93% in normal images, 90% in complex images, and 92% in overall images.

Yeboah et al. (2015) developed an approach for the automatic detection and classification of bridge cracks using a robotic system. They utilized radon transform and directional projection variance for feature extraction. Finally, adaBoosted Relevance Vector Machines (RVM) was utilized to classify the cracks into no-cracks, simplex cracks and complex cracks. The proposed method outperformed a set of classifiers such as adaboost, RVM, back propagation artificial neural network and prior mathematical modelling. Shuang-rui et al. (2015) developed an android-based method to automatically measure the crack width in bridges. The developed method encompassed gray scale conversion, binarization, dednoising, edge recognition, and crack evaluation. The threshold value in the image segmentation stage was computed based on Otsu algorithm. They highlighted that the proposed model attained an accuracy of 95.26% for a dataset of ten cracks.

Adhikari et al. (2014) developed an artificial neural network-based model to predict the depth of the crack given a certain crack width based on an input dataset of 101 images. They developed a method the cracking depth computation, which helps in providing a more accurate condition rating of concrete elements. They presented an approach based on spectral analysis to detect the change in crack patterns over time by converting digital images to the frequency domain using Fast Fourier Transform (FFT). Tao et al. (2014) presented a method to detect bridge cracks in underwater conditions. Spatial median filtering was applied to enhance the smoothing of the images. The image was divided into several blocks such a threshold segmentation value which was computed as per the gray-level intensities present in each block. After the detection of the

cracks, the proposed model was capable to retrieve some parameters from the images such as area, length, width and perimeter.

Prasanna et al. (2014) presented an automated crack detection algorithm based on the STRUM classifier. The utilized an algorithm that employs robust curve fitting methods to localize potential crack regions spatially in the existence of noise. The STRUM classifier was able to achieve accuracy of 95%, which is compared to 69% accuracy in the case of typical image-based approaches. Ho et al. (2013) introduced a method for the damage detection of cable surface in cable-stayed bridges. Median filter was applied for noise reduction and histogram equalization. Then, the input images are mapped to principal component analysis space, where the Mahalanobis square distance was utilized to determine the distances between the input images and sample patterns, and eventually building the pattern recognition model.

Xue-jun and Xiao-ning (2013) designed a computer program using C++ programming language to detect and quantify cracks in reinforced concrete bridges. They compared the median filter, mean filter and combination of both filters by adding noise to the original image and they concluded that the median filter provided better noise removal efficiency as per the mean-squared error. Sobel algorithm was adopted to automatically identify the edges of the crack. Sobel operator algorithm is implemented by computing the gradient of image intensity at each pixel within the image. It determines the direction of largest increase from light to dark and the rate of increase in this direction. The developed method was capable of achieving a relative percentage error of 6% for cracks of width less than 0.3 mm, and error more than 30% for cracks of width less than 0.1 mm. Su (2013) proposed a computer vision method based on Charge Coupled Devices (CCD) cameras to automatically detect cracks during the bridge inspection. Weighted mean filter was utilized to remove environmental noises from images. They

highlighted that 5×5 weighted median filter provides better accuracy when compared to 3×3 weighted median filter. Otsu thresholding was adopted for the binary transformation of the image. They stated that their model was capable to achieve accuracies of 90% and 84% for the training dataset and testing dataset, respectively.

Tong et al. (2011) presented a new method for image-based crack detection to facilitate the automatic bridge inspection process. Gaussian filter was used to remove the noise and enhance the image quality. Morphological operations are used to ensure the connection between the crack segments. The objective of the model was to decide whether the binary images represent a crack or not based on some criteria such as circularity of the region, aspect ratio, perimeter and area. The proposed model achieved an accuracy of 93% and it outperformed some other methods such as Fujita method, canny edge detection method and Sobel edge detection method. Moon and Kim (2011) proposed an automatic system for crack detection using some image processing techniques to enable the inspectors to perform the crack monitoring task effectively. The irregular illumination present in the images was removed using improved subtraction method by applying a median filter and then gray image is subtracted from the enhanced image. Then a Gaussian low-pass filter was utilized to connect small gaps and to adjust the distortion in the crack shape. The tuning parameters such as threshold value, median filter size, Gaussian filter size, standard deviation of the Gaussian filter, were determined via a set of organized experiments using signal to noise ratio metric. Finally, a back-propagation artificial neural network is designed to binary classify whether the concrete images contain cracks or not. The model was capable to detect crack images by 90% and non-crack images by 92%, whereas the number of hidden layers was defined based on experience.

Lee et al. (2008) designed a machine vision robotic system to automate the inspection process of bridges. The developed system enables the user to evaluate the cracks in real time, whereas it was evaluated using 100 noisy images. Median smoothing filter was applied to remove noises and to ensure uniform brightness through the image. Then, dilation and thinning morphological operations were utilized to maintain the connections between the crack segments. They demonstrated that the developed method yielded higher detection accuracies when compared against Sobel, Canny and Fujita methods.

2.3.2 Bibliometric analysis and research gaps

Three bibliometric co-occurrence maps are structured for the purpose of establishing a comprehensive overview of the developed bridge defects' assessment models in bridges, buildings and pavement. This is accomplished using VOSviewer which enables to extract and analyse the co-occurrences of keywords related to a given topic. VOS in the term "VOSviewer]" stands for the visualization of similarities, and it is a freely-available platform that aids in creating and visualizing bibliometric networks. Van Eck and Waltman (2014) defined the number of co-occurrences of two keywords as the number of publications in which the keywords were mentioned together either in the title, abstract or the keywords list. This scientometric analysis aids in delineating the shortcomings of the previous literature which paves the way for building more efficient bridge defects' assessment models. In the bibliometric co-occurrence maps, the font and circle sizes imply co-occurrences of the keywords in the dataset while the connections between the keywords signify their Interrelatedness. The developed bibliometric maps are used to highlight the frequencies of the developed crack detection-based models, classical segmentation-based models alongside developed machine learning and transfer learning-based models. They are not used for deriving other research gaps. Figure 2.1 provides a

Figure 2.2 depicts a bibliometric co-occurrence map of the bridge defects detection models based on 224 publications from 1998 to 2019, and 194 keywords. These figures indicate that most of the previous publications relied on Otsu algorithm followed by K-means clustering and then fuzzy C-means clustering and watershed algorithm for the segmentation of the defects from the background. However, these classical segmentation methods are inefficient in the case of complex, non-uniformly illuminated and low contrast images, whereas they diverge and provide poor segmentation results. In this regard, complex images are usually associated with multimodal gray level histograms rather than unimodal ones. Solving multimodal search spaces are very complicated and exhaustive task to be achieved. The multimodality of the histograms makes it exhaustive for the classical segmentation methods to find the optimum solution much more than the unimodal histograms. It can be also inferred that there is lack of investigation of the optimization-based methods which are less invariant to the noise that may corrupt the images and yield more accurate results when compared against the classical segmentation methods mostly in the complex images.

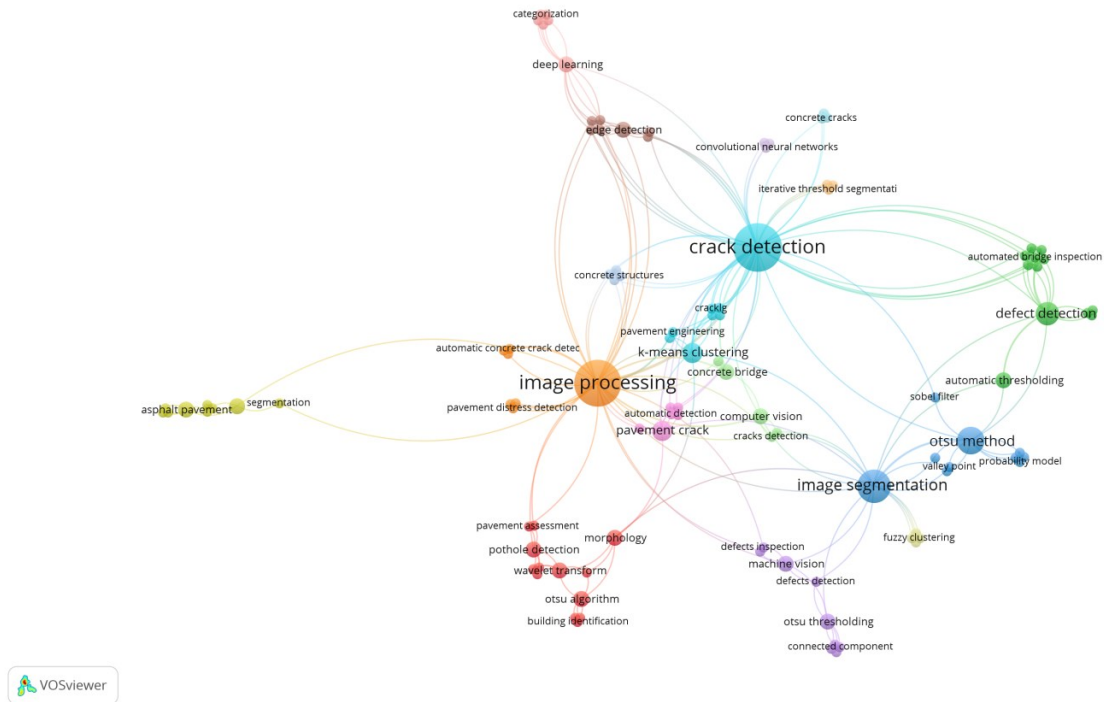


Figure 2.2: Bibliometric co-occurrence map of the surface defects detection models

It can be also noticed that most of the restoration methods of bridge defects images are lacking a comprehensive investigation of the type of noise that the images are corrupted with. Moreover, the restoration of bridge defects images is a problem-dependent in real-time environment, i.e., applying a filtering method without specifying the type of noise leads to poor de-noising results under these conditions. Thus, it is decisive to find a method which aims to intelligently evaluate if an image is corrupted with noise, and what type of separate or mixed noise is corrupting the image before applying the de-noising method. The images which are corrupted with a mixture of noises create an amplified challenge to remove the mixed noise without compromising the edge sharpness and important features. As such, building a generic model which is irrespective of a specific type of noise can provide more robustness to the proposed method. Absence of noise detection models can lead to image blurring due to the application of incorrect or underperforming image restoration models. This will remarkably affect the following bridge

defects evaluation procedures including: bridge defects severities extraction and detection, and eventually the accuracy of diagnosis of bridge defects severities.

In addition to that, most of the previous studies utilized a single filter such as median, mean or Gaussian filters to deal with different types of noises. Nevertheless, a single filter fails to deal with all types of noises, whereas some filters behave efficiently with some types of noises and fail to deal with others. Another issue in the reported de-noising methods is the parameter of the filters, whereas most of the filtering methods proposed in the literature are attribute or threshold governed such as mask size of 4×4 . The window size selection in the neighborhood filters is a key issue in de-noising, whereas smaller window sizes sometimes don't completely remove the noise while larger window sizes sometimes lead to edge blurring. The absence of noise detection models and inefficient restoration methods lead to the establishment of inaccurate condition assessment models and unreliable deterioration models, which eventually leads to inefficient bridge management systems.

Figure 2.3 depicts a bibliometric co-occurrence network of the machine learning algorithms adopted for the recognition and evaluation of surface defects. This is fulfilled using a database of 107 articles from 1993 to 2020, which produced 224 keywords. In the light of previous studies, it can be noticed that some models rely on feeding the whole input image directly to the machine learning model for the detection and recognition of surface defects. Nevertheless, this necessitates high computational cost and resources are consumed per epoch during the training process endeavoring to explore the multi-dimensional space. A feature extraction algorithm is necessitated in the case of presence of complex and noisy texture of images of bridge deck, which are mainly characterized by weak signals of defects patterns, in homogeneity of defects and the diversity of defects. The absence of efficient feature extraction algorithm may undermine

the discrimination and learning capacity of the machine learning elicited from its failure to delineate the important features in the input images. In this context, more attention should be dedicated to the implementation of feature extraction algorithm in an attempt to improve the learning capacity of the machine learning model.

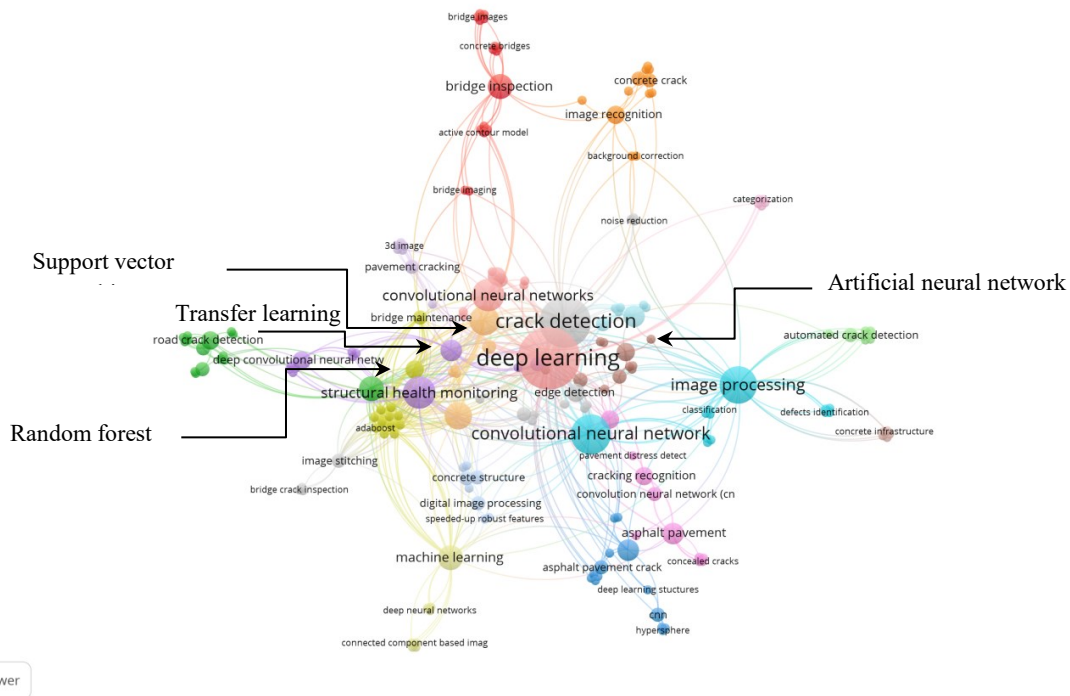


Figure 2.3: Bibliometric co-occurrence map of the machine learning algorithms adopted for surface defects evaluation

Another shortcoming can be observed is that some of the reported models required conducting segmentation as a pre-processing to build the automated detection model of surface defects. In this context, the segmented image is mainly utilized as an input to the machine learning model. This increases the net computational time and complexity as a result of the increase in number of pre-processing stages. Furthermore, these models are highly variant and sensitive to noise, non-uniformly illumination and low contrast between the defect and background. This may induce many error points and significant degradation in defects' extraction because the prediction

accuracy of the machine learning model is becoming highly dependent on the defects' segmentation algorithm. In this context, it is more practical and efficient to rely on the gray-level images to design the classification model of surface defects.

As shown in Figure 2.3, convolutional neural network is the most adopted machine learning model followed by support vector machines then random forest and eventually artificial neural network models. Deep learning has been adopted in the recent years to analyze and evaluate the surface defects in the different assets. However, deep learning suffers from the following shortcomings. Deep learning requires huge training dataset to capture the features and build the relationships between the set of independent variables and the dependent variables, which sometimes can be difficult and tedious to create. Another disadvantage of deep learning is that it is a high resource demanding paradigm that necessitates the presence of highly computational infrastructure demonstrated in the form of high graphics processing units in addition to the presence of efficient data storage. The high computational cost is elicited from the need of large amount of data, memory and extensive training cycles to learn the deep learning model. It is worth mentioning that the deep learning sometime induces detection latency as a result of the high processing demands. Deep learning models sometimes induce over-fitting triggered by the presence of small dataset, which may drastically influence of the recognition capacity of the machine learning models (Demertzis and Iliadis, 2020; Al Najada et al., 2018; Dundar et al., 2015).

Another shortcoming of the deep learning models is the presences of wide range of hyper parameters that substantially influence the performance of the deep learning models. This includes the number of filters, stride size, padding size and kernel sizes to create the feature map, number of convolutional layers, type of transfer function, type of pooling operation, number of

fully connected layers, number of neurons, and weights of the connections between neurons. There are infinite numbers of possible solutions that needs exhaustive search to be carried out, which causes the manual tuning of the hyper parameters to be a very challenging task. In this context, the absence of automated systematic method to define the optimum parameters of the convolutional neural network can lead to its entrapment in local minima which yields inferior solutions triggered by the long computational time and slow convergence (Alhamdoosh and Wang, 2014; AL-Allaf, 2011). Hence, this necessitates the development of a self-adaptive method that can autonomously tune its parameters based on the available dataset with minimum human intervention. Transfer learning has recently attracted significant research attention to be utilized in the detection of surface defects. However, transfer learning-based deep neural network models are vulnerable to negative transfer, which allude to the situations where the transfer of information from the source domain has a detrimental implication on the prediction of the target domain. The absence of sufficient degree of similarity between the features of the source domain and target domain undermines the learning performance of the target errand (Dhillon and Verma, 2019; Stamate et al., 2015).

Some previous models counted on artificial neural network models to model the surface defects. In this regard, gradient descent algorithm is considered as one of the most commonly utilized for their training. It is based on finding the partial derivative of the error function to update the weights of the connections. The training process based on the gradient descent often gets trapped in a local minima or premature convergence and sometimes causes over-fitting problems especially in the case of presence of multilayer neural network. The multi-layer neural network is normally linked with large search space, multi-local minima points, non-differential function and complex multi-dimensional curve. Furthermore, in some cases, the global minimum is hidden

between the local minima. Thus, the gradient descent algorithm can end up oscillating between the local minima (Shreyas and Dai, 2020; Jabin, 2014).

2.4 Deterioration Modeling

This section reviews the previous research works on modeling the deterioration of bridges. It also demonstrates their main shortcomings.

2.4.1 Previous research works

Deterioration models are essential for department of transportation because it enables them to emulate the future condition state or performance of bridges. Recently, several studies have been conducted to model the deterioration of the concrete bridges. Martinez et al. (2020) compared a set of machine learning models in the prediction of future bridge condition indices including: K-nearest neighbors, decision tree, linear regression, artificial neural network and deep learning neural network. The comparative analysis demonstrated that decision tree outperformed other prediction models accomplishing root mean-squared error, mean absolute error, mean relative error and correlation coefficient of 1.607, 0.179, 0.23% and 0.977, respectively. Furthermore, it was highlighted that linear regression generated different prediction from other machine learning models capitalizing on paired t-test. Nguyen and Dinh (2019) developed an artificial neural network model for predicting the future condition ratings of highway bridges. The input parameters encompassed age, average daily traffic, number of main spans, percentage of daily traffic, etc. It was found that the developed model achieved a testing accuracy of 73.5%. Additionally, it was reported that the current bridge age is the most influential factor that affects the bridge deck deterioration based on the coefficient of determination analysis.

Ali et al. (2019) introduced artificial neural network model for simulating the future performances of deck, substructure and superstructure. The input variables comprised age,

average daily traffic, deck width, percentage of trucks in average daily traffic, etc. The developed model was validated through comparison against the linear regression. They investigated several configurations of artificial neural network and it was reported that artificial neural network of three hidden layers with three hidden neurons in the first and second layers, and one neuron in the last layer attained the lowest average testing error. Hussein and Abu Tair (2019) applied feed forward neural network to predict the deterioration age of reinforced concrete bridges based on actual historical records. They investigated the significance of design parameters of feed forward artificial neural network. They highlighted that artificial neural network provided better performance than regression models. Moreover, they illustrated that Levenberg Marquardt algorithm provided a faster learning rate than Gradient descent algorithm. It was also found that number of hidden neurons has a more significant influence than number of hidden layers on the performance of neural network.

Zambon et al. (2017) compared between homogenous and non-homogenous Markov chain with waiting times of weibull and exponential distributions in addition to the gamma process. The developed models were based on 1100 concrete bridge decks from the Portuguese inventory. They concluded that the prediction capability of the gamma process outperformed the Markov chain model. Shim and Lee (2017) developed a Markovian deterioration model to predict the future condition rating based on the national bridge inventory (NBI) condition rating. The transition probabilities were calculated based on the median duration years.

Muñoz et al. (2016) presented a methodology to predict the deterioration of the bridges using both Markov chain and regression analysis in the case of small sample size. They illustrated that the proposed methodology provided conservative estimates for the future condition ratings as well as similar estimates to the traditional methods in calibrating the Markovian models and

regression analysis. Lu et al. (2016) developed a group of regression models for the deterioration prediction of highway bridges. They stated that the multiple linear regression with data filtering provided the best prediction accuracy based on some performance metrics. Bu et al. (2015) incorporated both state-based model and time-based model to predict the future bridge condition ratings. The state-based model was based on both Elman neural network and backward prediction model. For the time-based model, the transition probabilities were calculated based on the Kaplan and Meier (K – M) method. They compared the proposed model against the traditional regression-based optimization method to calibrate the Markov model. The proposed model provided better performance than the traditional method, whereas 464 inspection records were used as an input for the model.

Hasan (2015) utilized a combination of both artificial neural network and Markov chain to model the deterioration of different bridge components in Victoria, Australia. The most significant factors that affect the deterioration were determined using weight analysis connection method which is a function of the weights between the input neurons and hidden neurons as well as the weights between the hidden neurons and output neurons. Annual average daily traffic was found to be the most significant factor with an overall significance of 1.21. The transition probabilities were calculated using three different techniques which are: percentage prediction method, non-linear optimization, and Bayesian approach. Le and Andrews (2015) modeled the deterioration of the bridge elements based on the two-parameter weibull distribution. Anderson Darling test is used to compare a group of probability distributions. The parameters of the weibull distribution were defined based on the rank regression.

Mašović and Hajdin (2014) utilized expectation maximization (EM) to estimate the transition probabilities of the Markov chain model. The developed model was applied to data from the

Serbian Bridge Information Database to improve the deterioration of the bridge elements. They highlighted that the introduced developed model can be used when limited inspection records are available. Ranjith et al. (2013) developed a Markov chain model to predict the deterioration of the timber bridge elements. They calculated transition probabilities using three methods which are: percentage prediction method, regression-based optimization method, and non-linear optimization method. The comparison was based on chi-squared goodness of fit test and reliability test and they concluded that the deterioration model that utilized non-linear optimization method achieved the best accuracy.

Hong et al. (2013) developed deterioration curves for a group of bridge elements using historical data for bridges in South Korea. The deterioration model is constructed based on Markov chain and the transition probability matrix is established using non-linear optimization. They utilized zoning concept where a certain transition probability matrix is assumed for each age group. Callow et al. (2013) applied time-delay neural network (TDNN) to model the deterioration of bridge elements. Genetic algorithm optimization was employed to optimize the backward prediction model (BPM) output while case-based reasoning (CBR) was implemented to retrieve similar cases from the database.

Lee et al. (2011) utilized statistical regression to model the time-dependent performance of bridge decks, prestressed girders, and piers in Korea. An equation was introduced for each bridge component, whereas the condition grade is a function of the elapsed time. Jiang (2010) compared between the Markov chain model and polynomial regression model to predict the deterioration of the bridge condition. The polynomial regression model was built using bridge age and bridge condition rating as an input of the model. Forty bridges from the Indiana bridge condition

database were used to construct the deterioration model. They concluded that the Markov chain model provided more accurate results when compared to the polynomial regression model.

Agrawal (2010) compared between Markov chain approach and weibull-based approach to predict the deterioration of group of bridge elements based on historical data from the New York State Department of Transportation (NYSDOT). The transition probabilities were calculated based on non-linear optimization by minimizing the sum of the absolute difference between the condition rating obtained from the regression model and the condition rating obtained from the Markov chain. They concluded that weibull-based approach performed better than the Markov chain-based approach. Huang (2010) developed an artificial neural network (ANN) model to predict the deterioration of bridge decks. The ANN model was based on back-propagation approach multilayer perceptron (BP – MLP) classifier. Eleven significant factors that affect the deterioration of the bridge decks were identified such as age, deck area, length of deck, number of spans, average annual daily traffic, design load, etc. These factors were used as an input for the ANN model and they are selected based on the P-value.

2.4.2 Research gaps

Previously-developed deterioration models have several limitations which are described as follows. Deterministic models such as artificial neural network and multiple regression, often fail to capture the uncertainty and randomness of the deterioration process, whereas there is no certainty associated with the condition state the bridge element will enter within the next period of time. Additionally, they require a large dataset in order to construct a relationship between the set the independent variables and the condition rating of the bridge element. State-based models do not consider the sojourn times (waiting times). However, it is more realistic to model the

deterioration in terms of a function of the time spent in a certain condition state (Ravirala and Grivas, 1995).

Probability-distribution-based models such as weibull and gamma process distribution simulated the deterioration based on the condition ratings rather than considering the transition time that a bridge element takes to deteriorate from a certain condition state (CS_i) to the next lower condition state (CS_{i+1}) separately. Some time-based models simulated the sojourn time based on weibull and exponential distributions which is not necessarily true without conducting goodness of fit tests to ensure that the sojourn times follow these distributions

Regression-based Markov-chain models are not suitable for long-term prediction, whereas the deterioration curve deviates when predicting the future condition of the bridge elements (Bu et al., 2015). Some-Markovian models utilized one transition probability to predict the future performance of the bridge element, which is not logically true, whereas the deterioration process does not follow the same pattern for the whole study period. Some previous models did not consider the uncertainty associated with the transition probability and focus only the uncertainty associated with the transition time. Some Markovian and deterministic models did not map the inherent sequence or the logic of the deterioration process, which is essential to build a reliable deterioration prediction model.

2.5 Maintenance Optimization and Planning

In this section, previous research efforts related to maintenance planning are revealed. It also delineates their critical shortcomings that need to be addressed.

2.5.1 Previous research efforts

A cost-effective maintenance schedule is necessary for delegated agencies in order to obtain the exact information about the need and timing of maintenance activities for a certain planning horizon. Additionally, it enables them to manage the imbalance between the extensive needs for maintenance, repair and rehabilitation actions, and the limited available funds. Several studies were carried out for bridge maintenance planning and prioritization through modeling several objective functions for the purpose of bridge maintenance management. Allah Buksh et al. (2020) proposed a framework for multi-year maintenance planning for a group of bridges. Markov decision process was applied to forecast the deterioration process of the bridge, such that percentage prediction method was used to calibrate the transition probability matrices. In the framework, multi-attribute utility theory (MAUT) was utilized to rank the bridges through a universal score that simulates the preferences of the decision makers. A five-year optimal maintenance plan was established capitalizing on the genetic algorithm given a certain condition threshold and budget constraint. They pointed out that the developed framework can aid asset managers in implementing various maintenance scenarios within different performance and financial requirements.

Dromey et al. (2020) developed a model to rank the rehabilitation priority of bridges based on a set of characteristic attributes. Linear regression analysis was used to predict the annual degradation in the condition ratings of the bridges. The prioritization index was established based on ten influencing factors including: overall structural condition, number of spans, bridge material, rehabilitation cost, etc. Afterwards, stepwise multiple regression analysis was conducted to generate the best combination of independent variables that constitute the

prioritization index. They highlighted that the developed model could serve as a robust process to optimize the annual investments designated for bridge network rehabilitation.

Mao et al. (2020) designed an optimal maintenance scheduling strategy that was formulated in the form of two levels. The upper level incorporated a multi-objective non-linear programming model, which aimed at minimizing the total traffic delays during the maintenance period and maximizing the total number of bridges to be repaired. The lower level comprised simulating users' route choice using a modified user equilibrium model, whereas simulated annealing algorithm was deployed to solve the optimization model. Contreras-Nieto et al. (2019) introduced a geographical information system (GIS)-based model for the prioritization of bridge maintenance. The ranking system was formed based on the average daily traffic alongside the weighted average rating that considered deck, substructure, superstructure and scour. They evaluated the bridges based on a set of four attributes, namely bridge resiliency, riding comfort, safety and serviceability, whereas their relative importance weighting was obtained via analytical hierarchy process. They pointed out their model could be used by highways agencies to schedule the maintenance of deficit bridges.

Allah Bukhsh et al. (2019) presented an approach for network level maintenance planning using multi-attribute utility theory. The proposed approach prioritized the bridges by accommodating different attributes which were: improving assets' reliability, minimizing agency cost, minimizing impact on users and maintaining the bridge network safety. They suggested that the proposed approach can improve the decision-making of maintenance planning through modeling performance, economic and social aspects. Mahdi et al. (2019) developed a decision support system for identifying optimum maintenance plan of bridges stepping on bridge overall priority index (BOPI). The evaluation of the bridge depends on three performance indicators, namely

structural performance, functional performance and external factors. The optimal maintenance budget allocation is generated through a dynamic programming-based model that aimed at minimizing the total repair cost, and subject to performance and financial constraints.

Gao et al. (2019) proposed a method to rank the concrete bridge repairs based on the VIKOR (VlseKriterijumska Optimizacija I Kaompromisno Resenje in Serbian). The final multi-criteria ranking index was obtained based on a set of attributes including: average daily traffic, average daily truck traffic, service years, service environment alongside the sufficiency rating attributes. The sufficiency ratings attributes encompassed the ratings of deck, substructure, superstructure, culvert, etc. The relative importance weighting of the criteria set was computed based on the criteria importance through inter-criteria correlation (CRITIC). They suggested that the developed ranking system could efficiently rank the bridge maintenance order. Yossyafra et al. (2019) presented a hybrid multi-criteria decision making model for maintenance prioritization of bridges in West Sumatra Province. They utilized fuzzy analytical hierarchy process to compute the weights of attributes, which were technical condition, age, average daily traffic, economic benefits, road function, budget fund, disaster impact and spatial conditions. Then, a multi-criteria ranking index was calculated using VIKOR method, which mapped the priority order of bridges to be repaired prior to others.

Markiz and Jrade (2018) introduced a stochastic fuzzy logic decision support system combined with bridge information management system (BrIMS) to predict the bridge deterioration and to sort the MR&R actions. The priority rankings of the bridge components were established using quality function deployment and Technique of Order Preference Similarity to the Ideal Solution. The deterioration process of the bridge elements was simulated using time-dependent gamma shock models, such that the gamma function parameters were estimated through regression

analysis. It was revealed that the developed deterioration model could efficiently mimic the future performance of the bridge elements with a percentage of error ranged from 10% to 15%. Ghodoosi et al. (2018) developed an optimization model that comprised genetic algorithm to select the cost-effective intervention actions. In the developed model, a biquadratic deterioration function was incorporated to model the reliability of the bridge superstructure across the planning horizon. The fitness function involved minimization of the equal uniform annual worth of MR&R expenditures for a composite reinforced concrete superstructure.

Wu et al. (2017) presented a life-cycle optimization model for highway bridge maintenance. using Semi-Markov decision process to simulate the deterioration of bridges of the 2012 national bridge inventory dataset for the state of Texas. Then, the optimum maintenance strategies can be identified relying on the deterioration pattern and the repair costs. They highlighted that the developed model could provide more effective decision-making plans in the light of limited repair funds for maintaining critical bridges. Shim et al. (2017) proposed a bi-objective optimization method for the budget allocation of MR&R decisions over six years of planning horizon. Stochastic Markov decision process was employed to predict the deterioration of the network of bridge decks based on the national bridge inventory. In the developed model, two interrelated objective functions were considered, which were minimizing the percentage area of structurally deficient deck, and minimizing the total annual MR&R expenditures. The proposed multi-objective optimization technique was based on modification of “Normal Boundary Intersection” method. It was found that the proposed model could better generate efficient Pareto optimal solutions when compared against normal boundary intersection, normal constraint, goal attainment and weighted sum techniques.

Yoon and Hastak (2017) developed a multi-tiered method for the prioritization of bridge deck rehabilitation relying on urgency scale and total prioritization scale. The urgency scale was based on computing the timeframe that the rehabilitation process of the bridge deck can be delayed until its structural condition goes beyond the acceptable limit. The total prioritization scale integrates the normalized magnitudes of the performance, economic and criticality scales. Nurdin et al. (2017) developed a multi-criteria decision making model to set a priority scale for bridge maintenance and rehabilitation. Three attributes were introduced to set the maintenance prioritization index, whereas the criteria for condition of damage represented the largest weight followed by the volume traffic and criteria policy. The weights of attributes were computed based on analytical hierarchy process by aggregating the feedback of 27 respondents using geometric mean. ArcGIS was utilized to visualize the output of the maintenance prioritization model. Bridge condition was found to be of the highest weight (49.1%) while traffic volume constituted the lowest weight (18.5%). Subsequently, the intervention action, either maintenance or rehabilitation, was assigned as per the prioritization index.

Shim and Lee (2017) constructed a multi-objective optimization model with linearly weighted sum method to define the optimum MR&R activities for a network of bridge decks. Two objective functions were used in the optimization model which were: minimizing the area percentages of structurally deficient decks and minimizing the annual MR&R budget. The beta distribution was used to model the uncertainties of the unit cost of the intervention actions rather than employing deterministic values. Badawy (2017) presented a single-objective genetic algorithm to obtain the optimum maintenance plan of the expansion joints. Markovian models were used to obtain the future performance of the expansion joints, whereas the transition probability matrix was calibrated based on minimizing the differences between the predicted

condition and the inspected condition. The optimum intervention actions were identified based on the maximization of the annual overall condition index of the expansion joints while satisfying a total budget constraint.

Nurani et al. (2017) investigated the implementation of AHP, fuzzy AHP and TOPSIS for the identification of bridge maintenance priorities. Triangular fuzzy numbers were utilized to model the linguistic human judgment based on a nine-point scale. The ranking platform was established based on the average daily traffic alongside the bridge damage condition, which was based on the aggregated weighted average of the condition of the different components. Results revealed that AHP and TOPSIS produced close priority rankings to each other. Rashidi et al. (2017) developed a decision support system to select the optimum remediation strategies for steel bridges. Simplified analytical hierarchy process (S – AHP) was used to compute the weighting vector of the six main attributes of the decision making model, namely service life, safety, cost, environmental impact, traffic disruption and aesthetic appeal. They considered four different alternatives of rehabilitation actions: splice plates, steel plate strengthening, fiberglass reinforced plastic strengthening and partial member replacement. They concluded that safety had the highest global importance among the different attributes. Additionally, it can provide decision makers with reliable recommendations for the prioritization and selection of remediation actions of deteriorated bridges. Amini et al. (2016) proposed a decision-making model to prioritize the urban roadway bridges for maintenance and rehabilitation actions. Four main factors were defined for the bridge maintenance prioritization model. These factors involved destruction and environmental, destruction losses, funds, logistic and information, and strategic and condition. The weights of the factors were computed based on the analytical hierarchy process.

2.5.2 Bibliometric mapping and research shortcomings

Bibliometric co-occurrence map is structured for the purpose of creating a comprehensive overview of the bridge maintenance planning and prioritization. Figure 2.4 depicts a bibliometric co-occurrence map for the bridge maintenance planning and prioritization using VOSviewer 1.6.14. The created bibliometric map is used to highlight the frequencies of the developed genetic algorithm-based models. This map is obtained capitalizing on a total of 101 articles published from 1997 to 2020 that induces a network of 222 keywords. In view of the previous studies, most of them supported strategic planning decisions. In this regard, there is lack of operational planning models and their integration with strategic planning. The absence of these models or the imbalance between them could lead to misleading and inefficient bridge maintenance planning models.

The operational planning models encompass investigating the optimization of the rehabilitation work at the element level, which is primarily concerned with resource allocation under multiple conflicting objective functions. Most of the previous research supported either element-level, project-level or network-level decisions separately. Despite their interrelatedness, the previous literature lacks the integration of the different levels of decision-making. This absence of integration between the different levels of decision-making process can yield inefficient maintenance budget allocation models (Thompson et al., 2003). It is worth mentioning that the integration of the different levels is a more complicated task because of the necessity to model the various deterioration patterns of the bridge components instead of dealing with one type of them, which were usually bridge decks.

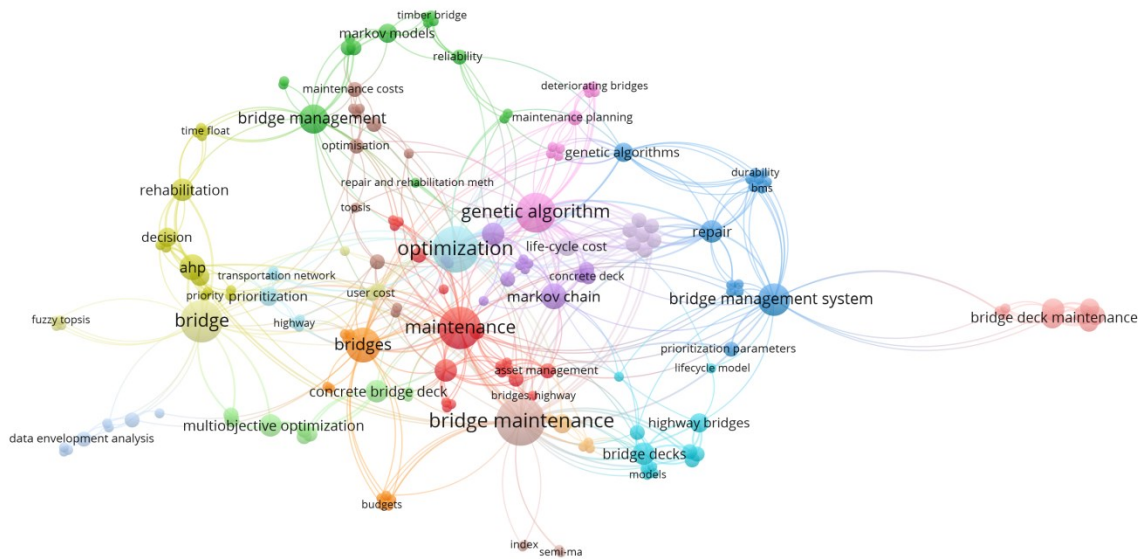


Figure 2.4: Bibliometric co-occurrence map of the maintenance planning models bridges

Some studies relied on single-objective optimization models for maintenance budget allocation. Single-objective optimization models focus on one fitness function at the expense of other functions. This induces a significant sacrifice in the performance of the optimization model and the quality of the generated optimal solutions. Most of the maintenance planning models dealt with short-term planning, whereas the previous models lack the exploration of long-term strategic planning. The allocation of MR&R decisions in short-term study periods is a simplified process and experience less interruptions when compared against the long-term maintenance planning. It is expected that the short-term maintenance models will diverge when applied to the more exhaustive nature of the combinatorial optimization model associated with long-term planning. This elicited from the amplified increase in the possible solutions of MR&R decisions. As such, the short-term periods are not sufficient to validate the performance capacity of the

maintenance optimization models. Additionally, previous researches efforts were concerned with relatively smaller number of bridge elements, which causes these models to be incomprehensive enough to model current transportation networks of large numbers of bridge elements. It can be also noticed that multi-criteria decision-making-based maintenance models are mainly concerned with prioritization of intervention actions at a certain instance of time based on the current condition ratings of bridge elements. In this regard, they fail to generate a MR&R schedule over a certain planning horizon while accommodating a set of conflicting objective functions.

Some models assumed that the deterioration behavior experienced by the bridge elements after the application of the intervention action will be in the same manner as before its application. In this context, the deterioration rates of the bridge elements are predicted to decelerate when intervention action is applied. Additionally, some models optimize the MR&R actions for the entire bridge rather than the different elements of the bridge. Dealing with the bridge as a single unit regardless the physical condition of the bridge elements may create misleading maintenance schedule. This stems from the fact that different bridge elements experience different deterioration rates over the course of the study period, which implies that they will reach their critical stages at different periods. Furthermore, the maintenance decision support systems that capitalized on a universal ranking index for prioritization purposes may be inefficient because of their incapability to monitor the degradation of the various bridge elements, whereas the overall bridge may be in a good condition while some building elements separately are experiencing high levels of deterioration. Some of the developed planning solutions presume deterministic unit costs and don't deal with them as stochastic random variables. Failure to address the encountered inherent uncertainties of the performance indices in the decision-making model alongside the randomness of construction process can yield inferior maintenance plans.

Also, it is worth mentioning that most of the prioritization and maintenance optimization models are deterministic and they don't capture the inherent uncertainties of the construction process, which usually don't lead to optimal solutions. Also, some of the maintenance prioritization models were mainly driven by preferences of domain experts and subjective rankings, which may not be necessarily applicable to be generalized to be applied elsewhere. Most of the previous studies relied on historical records to determine the cost of the maintenance actions, which are not necessarily accurate and may not fit the case in hand. The absence of precise and resource-driven cost estimation models can heavily influence the decision-making process at different levels of management. It is noted that bridge deck replacement has been rarely investigated within the state of the art despite its criticality from technical, economic and social aspects.

Most of the previous research adopted genetic algorithm for the optimization of maintenance scheduling and resource allocation of construction processes. However, genetic algorithm is often criticized by its low exploration and exploitation capacity, which leads to its premature convergence and stagnation in local minima than true optimal solutions; taking into consideration that the number of local minima increase exponentially with the increase in the size of the search space (Choi and Song, 2019). Moreover, it was found that previous studies mostly focused on agency costs in their maintenance evaluation models and overlooked the user-incurred costs. Nonetheless, user costs can substantially outweigh the direct agency costs in the bridges carrying high volumes of traffic. The accurate quantification and integration of user costs with agency cost can establish more comprehensive maintenance decision-making strategies.

Besides, many previous efforts viewed the maintenance management of bridges from the perspective of traditional pillars of structural condition and cost meanwhile ignoring other

important performance aspects. However, Van dam et al. (2012) suggested that infrastructure management should no longer be modeled from technical perspective solely. Furthermore, transportation networks are profoundly embedded in the community. Thus, management of existing bridges should satisfy the societal and environmental requirements in addition to the technical performance aspects, which aligns with the increase in the public attention towards environmentally conscious construction in the last decade. Additionally, the integration of environmental and societal principles of sustainability with the conventional pillars of asset management will provide decision-makers with a more comprehensive and efficient assessment of the implications of their maintenance decisions on the three main pillars of sustainable communities, i.e., economy, society and environment.

In the last two decades, several simulation-based optimization frameworks were designed for resource allocation of different construction processes. However, these models suffer from low computational capacity in the case of complex and hyper search space problems demonstrated in the form of exhaustive resource-based processes, which often causes appending inferior solutions. Another shortcoming of some of the simulation-based optimization models is the lack of practicality because of the absence of user friendly and computational efficient automated paradigm to facilitate its implementation by users.

Also, imposing constraints like the total budget and ignore the presence of annual budget constraints is considered as one of the limitations of the previous maintenance planning models. In this regard, the maintenance budget is usually assigned annually. Furthermore, the maintenance optimization model may satisfy the total budget constraint and violate the annual budget constraints. This causes that the importance of assigning this constraint is better demonstrated in the presence of large numbers of bridge elements. Some of the developed

maintenance optimization plans experience large number of intervention actions within small portion of the planning horizon because they overlooked the maximum number of visits when formulating the optimization model which induces significant traffic disruption to the users of the bridge. Furthermore, some of the developed annual MR&R cost profiles witness substantial fluctuations. Nonetheless, transportation agencies are interested in establishing timely maintenance plans with balanced expenditures over the planning period. In this context, a constraint needs to be assigned to stabilize the fluctuations of the annual MR&R cost profiles.

2.6 Summarized Research Gaps

The main shortcomings of the previous research work pertinent to surface defects evaluation, condition assessment, deterioration modeling and maintenance optimization are discussed in the following lines. Most of the previous studies focused on bridge crack detection. They overlooked some importance surface defects such as spalling and scaling. Furthermore, the developed models are not sufficient to evaluate the severity levels of the bridge defects. Classical segmentation models are highly variant to low contrast and non-uniformly illuminated images. Most of the developed machine learning models lacked advanced feature extraction algorithm in the case of presence of noisy texture images and weak signals of defects' patterns. Deep learning models are criticized by their need for huge dataset to capture the most important features in the images, their high computational cost and detection latency. Transfer learning-based deep neural networks are vulnerable to negative transfer. Manual tuning of hyper parameters of machine learning and deep learning models in addition to the use of gradient descent-based methods leads to local minima and inferior accuracy.

Ground penetrating radar-based models suffer from the absence of standardized amplitude rating system. Single defect-based and visual inspection-based maintenance prioritization models are

inefficient in evaluating the condition rating of bridge elements. It was also found that there is lack of systematic bridge maintenance decision-making strategies and severity rating systems in the element-level. Additionally, it can be interpreted that most of the previous studies overlooked inherent uncertainties encountered during the inspection process and associated with experts' judgements. Deterministic-based models for modelling deterioration fail to capture the randomness of deterioration process and require huge dataset for calibration. Developed stochastic-based models did not simulate the relationship between extent of severities of bridge defects and their influence on deterioration process. They also assumed unrealistic same deterioration pattern for the whole length of study period. State-based models are incapable of modeling the transition times between the different condition states.

Most of the developed maintenance optimization models suffered from the absence between different levels of decision-making process despite their interrelatedness. It was also observed that there is lack of operational planning models and their integration with strategic planning. Most of previous studies focused on a short-term maintenance planning and relied on single-objective optimization models. It is also observed that most of the developed cost estimation models overlooked user costs with highly fluctuated cost profiles. Developed maintenance optimization models focused on technical and economic aspects and they ignored social and ignored environmental aspects in bridge maintenance management. Genetic algorithm-based models suffer from local minima entrapment rather than true optimal solutions. Multi-criteria decision making models fail to monitor actual degradation in the condition ratings of bridge elements. Furthermore, they bridge maintenance prioritization at a certain instance of time rather than maintenance schedule over a certain planning horizon.

CHAPTER III: INTEGRATED METHOD FOR OPTIMIZED MAINTENANCE PLANS

3.1 Overview

This chapter enumerates the main stages of the developed integrated method for optimizing maintenance plans. Additionally, it provides an overview of some of the models encompassed in each of the developed methods. In this regard, it first explains a three-tier method designated for detection, recognition of surface defects and evaluation of their level of severities. It also describes a ground penetrating radar-based method devised for the evaluation of corrosion severities in reinforced concrete bridge decks based on a designed amplitude rating system. It also explains an integrated condition driven method for bridge intervention prioritization in element and network levels. In this chapter, two deterioration prediction methods are presented to simulate the future condition state of bridge components. The last section of the chapter demonstrates a two-tier resource driven method for the purpose of bridge maintenance planning.

3.2 Developed Integrated Method

This research introduces a five-stage research methodology for bridge maintenance evaluation, management and planning in a network level (see Figure 3.1). The first stage involves building a computer vision-based method designated for the detection, recognition of surface defects and evaluation of their severity levels. It contains three tiers; the first tier is a self-adaptive method designed for the autonomous recognition of noise, and restoration of degraded bridge defects images. This method is developed to be able to detect and recognize separate and combined noises that corrupt bridge defects images. The utmost objective of the developed method is to develop a filtering protocol, which incorporates the optimum filters to deal with each type of the different noises. The restored images are then fed into the second tier which ops for the automated identification of presence of surface defects and recognition of their type. In this

regard, the developed method considers three types of bridge surface defects namely, cracking, spalling and scaling. The labelled images are patched into a third tier which is envisioned on two phases for the detection and assessment of severity levels of surface defects. The first phase encompasses non-parametric segmentation approach that explored the effectiveness of merging information theory functions and meta-heuristics for the sake of detecting defects in images. In the second, a novel feature extraction model is proposed for efficient modeling of information in the image through the concentration of spatial and frequency domain features. The developed autonomous assessment method relies on coupling Elman recurrent neural network with invasive weed optimization algorithm in an attempt to better quantify the surface defects through improve exploration and exploitation capabilities of Elman neural network. This is accomplished through formulating a variable-length optimization model that involves both parametric and structural learning. In this context, a separate evaluation method is constructed for each of surface defects based on a set of descriptors. The output of this method also encompasses a severity rating system for each bridge defect.

In the second stage, a ground penetrating radar-based method is developed for the evaluation of corrosion severities in reinforced concrete bridge decks. This stage is established on the premise of integration of clustering algorithms, multi-objective optimization algorithms and multi-criteria decision making algorithms for the sake of structuring a standardized amplitude rating system. A set of soft and hard clustering algorithms are adopted to obtain initial amplitude thresholds to facilitate the guidance of the multi-objective optimization module towards the most feasible search regions. It encompasses a set of objective functions that enables both local and global search. The hybrid multi-criteria decision making module is devised to generate a compromise

and standardized amplitude rating system. The magnitudes of corrosion severities are then obtained capitalizing on the standardized amplitude rating system.

The third stage incorporates an integrated condition driven method for bridge intervention prioritization in element and network levels in addition to structuring a bridge maintenance decision-making strategy. It is conceptualized on three primary models, whereas the first model is developed for obtaining the weighting vector of bridge defects. The second is a fuzzy-based condition assessment model is envisioned on the integration of two modes of non-destructive evaluation techniques which are ground penetrant radar and computer vision technologies for the purpose of establishing a proper trade-off between the computational accuracy and efficiency. The severities of the bridge defects are demonstrated in the form of fuzzy membership functions to address the inherent uncertainties of inspection. The integrated condition assessment method tackles five types of bridge defects, namely corrosion, delamination, cracking, spalling, and scaling. The output of this model involves a severity index for each bridge defect separately alongside an integrated bridge deck condition index for maintenance prioritization purposes. The third model is designed for structuring a bridge maintenance decision-making strategy stepping on the integrated condition index.

In the integrated condition driven method, corrosion and surface defects are selected to be mapped by non-destructive techniques because of corrosion which is now recognized as the predominant and major cause of the degradation of the concrete structures causing premature structural failure (Baji et al., 2017; Martino et al., 2014). Additionally, it is reported that surface defects play a fundamental role in inspection reports and they can be utilized to generate accurate condition ratings of structural members (Koch et al., 2015). Additionally, it was found that corrosion and spalling constituted the highest relative weight of importance based on the

optimized fuzzy analytical network process model. Furthermore, it is more practical to select the non-destructive techniques that are capable to analyze and map the largest number of surface defects, which in return leads to a more computationally efficient and less computationally expensive decision-making platform. It should be mentioned that sensitivity analysis is carried out in order to validate the selection of defects to be mapped by non-destructive techniques.

The fourth stage includes two deterioration methods to forecast the future performance of bridge components under multiple intervention actions based on the output fed from the previous method. The first deterioration method is a defect-based for modeling the deterioration process. The in-state probabilities are demonstrated in the form of posterior distributions, whereas the transition from a condition state to the next lower state is a function of the severities of five types of bridge defects. In this regard, Bayesian belief networks are employed to construct the likelihood function of in-state probabilities by modeling the dependencies between the bridge defects. Additionally, Markov chain Monte Carlo Metropolis-Hastings algorithm is adopted to derive the posterior distributions of in-state probabilities. A stochastic genetic algorithm optimization model is designed to calibrate the non-homogenous transposition probability matrices. The second is a probabilistic time-based method that utilizes semi-Markov decision process for simulating the deterioration performance.

The fifth stage comprises formulating a resource driven method for the sake of bridge maintenance optimization at both project and network levels. It encompasses a two-tier method that combines operational and strategic planning in an attempt to develop more efficient and reliable decision support system. In the first tier, is an integrative evolutionary-based method is proposed for simulating and optimizing resource allocation plans of bridge deck replacement

projects. It comprises three models, the first model aims at mimicking the bridge deck replacement process through discrete event simulation. Whereas, the second encompasses structuring an efficient and straightforward surrogate machine learning model for mimicking the computationally expensive discrete event simulation model. The machine learning model is established for the purpose of forecasting time, cost, greenhouse gases and utilization rates of resource allocation plans capitalizing on the database generated from the previous model. The third constitutes formulation of a multi-objective differential evolution optimization model subject to the utilization rates of the involved resources and their dispersion. The output of the first tier alongside the performance aspects obtained from the previous methods, are fed into the second tier. The second tier is conceptualized on formulating a multi-objective exponential chaotic differential evolution method that supports both project and network- level decision-making for optimizing bridge maintenance plans. It is a stochastic method that simultaneously simulates multiple objective functions; maximizing the condition of bridge elements, minimizing the total agency and user costs, minimizing the duration of traffic disruption and minimizing the environmental impact of intervention actions.

Each of the developed methods delineated in the different stages is validated through several levels of performance evaluation and statistical comparisons. The performance evaluation comparisons include analyzing and evaluating both accuracies and robustness of the developed methods. The developed optimization methods are compared against a set of high-performing meta-heuristics and exact optimization algorithms while the prediction methods are validated through comparisons against a set of widely-recognized machine learning and deep learning model using original and augmented datasets alongside benchmark datasets.

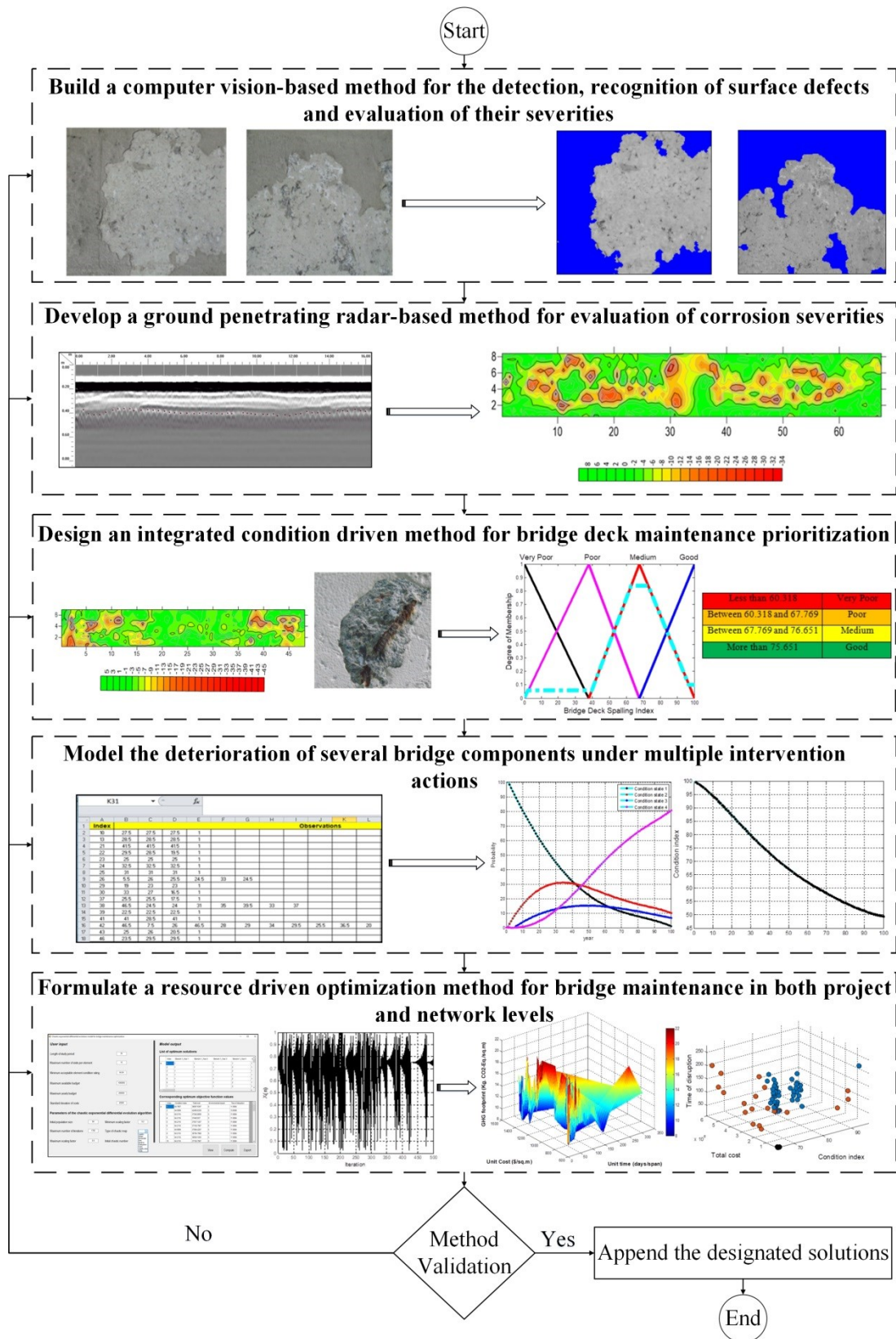


Figure 3.1: Schematic diagram of the developed research methodology

3.3 Surface Defects Evaluation

The developed framework for surface defects evaluation is composed of three main phases (see Figure 3.2). The first phase is self-adaptive two-tier method for detection of noises and restoration of bridge defects images. The restored image is passed to the second phase which is designated for the automated identification and recognition of bridge defects. The labeled image is fed into the third phase which is designed for the purpose of autonomous detection and assessment of each surface defects independently capitalizing on a set of descriptors.



Figure 3.2: Framework of the developed method for the evaluation of surface defects severities

3.3.1 Restoration of degraded images

The ultimate objective of the developed method is to design a filtering protocol for how to deal with different types of separate or mixed noises that corrupt bridge defects images. The developed method is a two-tier framework for the automatic recognition of noise and restoration of degraded bridge defects images (Mohammed Abdelkader et al., 2020a). The flowchart of the developed restoration method of bridge defects images is depicted in Figure 3.3. The first model is the automatic classification of noises, whereas three modules are developed for the detection and recognition of noise types based on the level of details the asset managers are concerned with. The first module is the noise detection, whereas a binary classification module is constructed to classify the images based on the existence of noise, i.e., to classify whether the

image is corrupted with noise or not. The second module is the separate noise recognition, whereas it is formulated as a four-point classification problem to provide a higher level of detail. The output of this module is to identify whether the image is corrupted with speckle noise, salt and pepper noise, or Gaussian noise or not corrupted with the noise. The third classification module is the combined noise recognition such that it provides the highest level of detail based on a formulation of a seven-point classification problem. This module is used to identify whether the image is corrupted with speckle noise, salt and pepper noise, Gaussian noise, combination of speckle and salt and pepper noises, combination of speckle and Gaussian noises, combination of salt and pepper and Gaussian noises, or not degraded with noise. Machine learning-based models proved their efficiency in noise detection of gray-scale and true color images in the recent few years resulting from their capabilities to accurately classify free-noise and corrupted images with noises (Basha and Venkateswarlu, 2020; Agarwal and Kumar, 2019; Ganesh and Kusagur, 2018; Kumar and Nagaraju, 2018). As such, a machine learning-based model is developed for the detection and recognition of noises corrupting bridge defects images.

For the first phase, the first step is to convert the RGB image into a gray-scale image, whereas the intensity values of the gray-scale image vary from 0 to 255. For the RGB image, R stands for red, G stands for green, and B stands for blue. The gray-scale images can minimize the computational effort without losing important features of the distress. The lowest possible intensity value of R, G and B is zero while the highest possible value is 255. The conversion to grayscale image is performed through weighted average of the R, G and B as follows (Yan et al., 2013).

$$G(i, j) = 0.299 \times R(i, j) + 0.587 \times G(i, j) + 0.114 \times B(i, j) \quad (3.1)$$

Where;

$G(i, j)$ stands for the grayscale image.

The original images are of size 3864×5152 pixels, the converted gray-scale images are then standardized to one size of 200×200 pixels as explained subsequently to ensure same size images in the training and testing processes of the neural network, and to speed up the computational process. Most of the previous studies suggested that images of size 200×200 pixels and 100×100 pixels are more suitable to capture the important features in the images in surface defects evaluation (Liu et al., 2020; Joni et al., 2020; Hoang, 2019). In this regard, a sensitivity analysis is conducted to find the most suitable size of image based on the prediction error. It was found that 200×200 pixels are more suitable in dealing with the developed models for noise detection and evaluation of surface defects' severities. It was also found that images of 100×100 pixels are more appropriate in the detection and recognition of surface defects. The next step is to convert the noise free image into a noisy image. To enable a larger and diverse dataset for training and testing, each of the individual images is corrupted artificially to generate a new one. Each one is corrupted with different combinations and intensities of separate and mixed noises using pre-defined Matlab function ("imnoise"). In this regard, different noise densities ranging from 10% to 30% were used in the present research to create a robust model against the variations in the noise densities. Then, a set of statistical features are extracted from the noisy images to be able to classify the noise present in the image. The statistical features include mean, mode, median, range, standard deviation, skewness, kurtosis, 75th percentile and 50th quartile.

Training Elman neural networks with meta-heuristic optimization algorithms is a powerful tool to improve the exploration and exploitation of Elman neural network. Exploration is the capability to investigate different regions in the problem space in order to locate a good optimum solution, which is hopefully to be the global optimum solution. Exploitation is the capability to

focus the search around a promising solution to find the optimum solution precisely. The training of Elman neural network is carried out through optimizing both the weights and architecture of Elman neural network. The optimization model encompasses formulating a single-objective function of minimization misclassification error of noise type. The optimized Elman neural network is saved and utilized to predict the input testing images.

The developed method is compared against five other machine learning models to demonstrate the capabilities of the developed noise detection and recognition method. The five models are DA, KNN, RF, SVM and ANN. The comparison is conducted based on six performance metrics, namely precision, F-measure, sensitivity, specificity, accuracy and Kappa coefficient. The performance of the different noise detection and recognition models were evaluated using split validation and 10-fold cross validation. Split validation is the most widely-used approach to evaluate classification and prediction models (Marcello et al., 2020; Bangaru et al., 2020; Chatterjee and Tsang, 2020). K-fold cross validation is applied to ensure the training and testing of the entire dataset, which rules out any possibility of over-fitting or over-learning in the pattern recognition phase. In the 10-fold cross validation, the dataset is divided into K equally sized segments or folds, then K iterations of training and testing are performed. A different fold is selected for testing within each iteration while the remaining K-1 folds are used for training (learning). The developed methods utilizes 10-folds cross validation in which the dataset was divided into 10 mutually exclusive subsamples (folds). Finally, non-parametric tests are performed between each pair of classifiers to evaluate the statistical significance level of the outcome of classifiers using the performances of the different folds. The non-parametric tests are Wilcoxon test, Mann-Whitney-U test, Kruskal–Wallis test, binomial sign test, Mood’s median

test, Friedman test and Friedman's aligned ranks test (Ning et al., 2019; Rodríguez-Fdez et al., 2015).

After mapping each image to a specific type of noise or noises, the second model is the restoration of bridge defects images. Image restoration aims at removing the maximum undesirable noise from the captured images and trying to bring the noisy image as much as possible to its un-degraded ideal state. Assume a degradation function H and a noise function $n(x, y)$ which are added to the original image $A(x, y)$ to produce the degraded image $G(x, y)$. The objective of the restoration function is to obtain the reconstructed image $\hat{A}(x, y)$ and at the same time to be as close as possible to the original image $A(x, y)$. The degraded image in the spatial domain can be expressed using Equation (3.2). As shown in Equation (3.2), based on the type of noise and degradation present in the image, an optimization problem is designed in order to define optimum configuration and parameters of the restoration method that can better filter out the noise present in the image and build the reconstructed image (Hoshyar et al., 2014).

$$G(x, y) = h(x, y) \times A(x, y) + n(x, y) \quad (3.2)$$

Where;

$h(x, y)$ represents the spatial representation for the degradation function. The symbol \times indicate the spatial convolution.

After loading the degraded image, a self-adaptive hybrid filtering model is developed based on designing a variable-length optimization problem that considers a combination of spatial domain and frequency domain filters to provide more in-depth evaluation and better-restored images. The utilized smoothing filters are median filter, mean filter, mode filter, Wiener filter, Gaussian filter, Lee filter and Frost filter of variable sizes. The developed model employs moth-flame

optimization algorithm to search for the optimum structure and parameters of the restoration method using a single objective function that maximizes the peak signal to noise ratio, i.e., minimize the difference between the original image and reconstructed image of bridge defects. The superior capacity of the moth-flame optimization in exploration and exploitation motivated its application in solving the restoration problem of bridge defects images.

In addition to investigating different combinations of filters, the developed method explores the effectiveness of the sequence of applying the filters, whereas the sequence of applying the smoothing filters can substantially affect the quality of the restored images. For instance, the quality of the restored image when applying the median filter followed by the Wiener filter is different from applying the Wiener filter followed by the median filter. Thus, the objective of the developed method is to define for each noise the following: optimum number of filters, optimum types of filters, optimum sequence of applying the filters, and optimum tuning parameters (governing attributes) of the applied filters.

The developed method is validated on two stages. In the first stage, the developed method is compared against the conventional filtering methods reported in the literature. For the second stage, the developed method is compared against a set of optimization algorithms which are: invasive weed optimization algorithm, differential evolution algorithm, modified differential evolution algorithm, grasshopper optimization algorithm, grey wolf optimization algorithm, particle swarm optimization algorithm, genetic algorithm and non-linear programming algorithm.

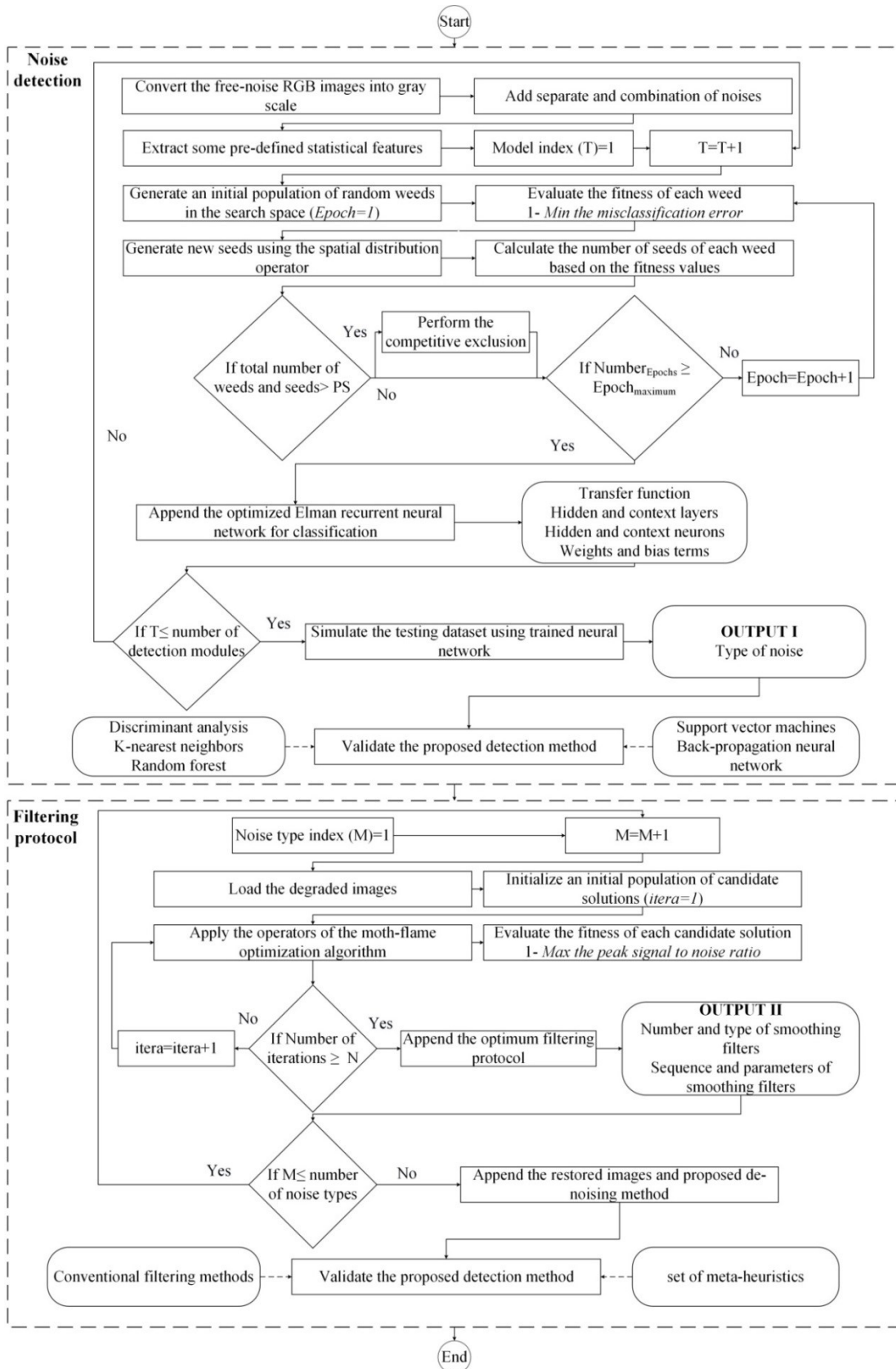


Figure 3.3: Flowchart of the developed noise detection and restoration method

The comparisons are conducted to investigate the capacity of the developed restoration method to search for the global optimum solutions in case of large search space and complex optimization problems against a set of well-known efficient meta-heuristics and exact optimization algorithm. The performances are assessed as per four performance metrics, namely PSNR, MSE, NAE and IEF. Eventually, the significance level of the optimal solutions of the different meta-heuristic optimization algorithms is evaluated using the same parametric and non-parametric tests of the noise detection and recognition model. Due to space limitations, brief information about the developed noise detection and restoration of bridge defects images are described briefly, more elaborate information can be adopted from Mohammed Abdelkader et al (2020a).

3.3.2 Automated recognition of defects

The ultimate thrust of this phase is to design a self-adaptive three-tier method that is envisioned on integration of singular value decomposition, Elman recurrent neural network and invasive weed optimization algorithm to automatically detect and classify the bridge defects in reinforced concrete bridges. The bridge defects detection is a binary classification model to detect whether or not the images contain defects. The bridge defects recognition model aims at identifying if the defected images contain cracking or spalling or scaling. In the present research, the images are manually labelled using visual inspection (Zhu and Song, 2020; Chaiyasarn et al., 2018). The flowchart of the developed defects' detection and recognition method is depicted in Figure 3.4. The developed method consists of three main modules which are: feature extraction, hybrid parameter-structural learning and performance evaluation, whereas the output of the first module is the feature vector set while the output of the second module is the classification scheme. Finally, the output of the third module is designated for evaluating the recognition capacity of the

developed method capitalizing on a set of performance prediction and statistical significance comparisons.

In the first module, close-range photographs are captured with proper focus on the object of interest or the defect. The natural targets are used for calibration of dimensions such as sharp corners of walls, beams and piers. In case of their inconvenience, colored cards and painted rods are used as artificial targets for calibration purposes (Jáuregui et al., 2006). The corrupted images are restored based on the noise type and designated filtering protocol structured in the previous section. Then, the images are standardized to size 100×100 pixels in order to facilitate the further processing stages. The developed method adopts un-supervised singular value decomposition (SVD) to capture the underlying essential features in the images by eliminating the insignificant features and reducing the computational complexity of the data, which leads to lesser computational time and more accurate analysis. SVD is utilized to compute the singular values of the images which are extracted in the form of feature vectors. This feature vector set is then used as an input to feed the Elman recurrent neural network.

There are different types of feature selection algorithms including principal component analysis, singular value decomposition, non-negative matrix factorization, latent semantic analysis and locality preserving projections. In this regard, singular value decomposition is preferred over other feature extraction algorithms because it proved its efficiency in dealing with wide range of engineering application including forecasting weekly solar radiation (Prasad et al., 2020), streamflow forecasting (Bhandari et al., 2019) and acoustic event classification (Mulimani and Koolagudi, 2019). Additionally, it is characterized by its low computational complexity (Yu et al., 2019; Guo et al., 2016). It is also worth mentioning that singular value decomposition

demonstrated superior dimensionality reduction accuracy against principal component analysis according to a set of performance evaluation tests (Tanwar et al., 2018; Chitsaz et al., 2016).

The second module is the hybrid parameter-structural learning, whereas the developed method utilizes invasive weed optimization to enhance the training process of the Elman neural network by resolving the exploration-exploitation trade-off dilemma. Invasive weed optimization algorithm is deployed for both parametric and structural learning, i.e., to automatically optimize the hyper parameters of Elman neural network including the weights alongside its best possible architecture. Invasive weed optimization is a meta-heuristic bio-inspired search algorithm that was proposed by Mehrabian and Lucas (2006). It emulates the natural and invasive behavior of weeds in colonizing and occupying territories in an attempt to find the most optimum place for growth and reproduction. The Elman neural network is trained by designing a variable-length single-objective optimization problem which encompasses a fitness function of minimization of misclassification error. The steps of the invasive weed optimization algorithm are repeated until satisfying the convergence criteria, i.e., reaching maximum number of iterations.

The optimum transfer functions, number of hidden and context layers, number of hidden and context neurons, and weights and bias terms establish the optimized Elman neural network, which is appended and utilized to simulate the instances of testing dataset. Invasive weed optimization algorithm is selected because it demonstrated its higher capacity in exploring complex and multi-local search spaces as well as solving diverse and sophisticated engineering problems such as optimal resource operation (Asgari et al., 2016), optimization of energy supply systems (Goharnejad et al., 2016) and prediction of compression index of limited-treated expansive clays (Nagaraju et al., 2020). In addition to this, invasive weed optimization algorithm outperformed a set of common well-known meta-heuristics including non-dominated sorting

genetic algorithm II, particle swarm optimization algorithm, artificial immune system and artificial bee colony (Mohammed Abdelkader et al., 2020c; Goli et al., 2019).

The third module is carried out for the purpose of validating the recognition accuracy of the developed method capitalizing on two folds of comparison namely, performance prediction and statistical significance tests. The comparative analysis is conducted against a set of conventional machine learning models and deep learning models reported for their higher accuracies. The well-performing machine learning models encompass discriminant analysis, K-nearest neighbors, random forest, support vector machines and DT, back propagation artificial neural network and Elman neural network. More details about the afore-mentioned classifiers can be found in Rathi and Palani (2012), Yang et al. (2018), Feng et al. (2016), Ahmad et al. (2017), and Kohestani and Hassanlourad (2016). The deep learning models involve a deep convolutional neural network trained from scratch alongside a group of different pre-trained deep neural network architectures, namely AlexNet, VGG16, VGG19 and CaffeNet. The prediction models are analyzed using both split validation and K-fold cross validation based on F-measure, Kappa coefficient, balanced accuracy, Matthews's correlation coefficient and area under curve. In the present research, 10-fold cross validation is adopted to guarantee the training and testing of the whole dataset, which truncates the risk of encountering over-learning or over-fitting by the prediction models.



Figure 3.4: Flowchart of the developed defects' detection and recognition method

The second fold of comparison comprises a set of statistical significance tests. In this context, Shapiro-Wilk is first utilized to test the normality of accuracies of the different folds at significance level of 0.05. Parametric or non-parametric testing is then carried out capitalizing on the normality assessment of observed data. A set of box plots are created for the purpose of graphical analysis the robustness of prediction models with respect to a certain performance indicator. They provide an efficient measure of statistical analysis of the accuracies generated from the prediction models. The recognition accuracies of the prediction models are analyzed using a constructed dataset which is denoted as Dataset I in addition to the bridge deck images existing in the public benchmark dataset SDNET2018 (Dorafshan et al., 2018b), which is denoted as Dataset II. This is carried out for the sake of conducting a further analysis of the robustness of the developed method in dealing with different sizes of datasets. Average ranking method is eventually utilized for the sake of establishing a unified assessment of the performances of prediction models across the different datasets. Further information about this method can be extracted from Mohammed Abdelkader et al. (2020b).

3.3.3 Evaluation of defects severities

The primary objective of this method is to develop a computerized platform for the automated detection and assessment of surfaced defects in reinforced concrete bridges. Each surface defect is assessed capitalizing on a set of descriptors (Mohammed Abdelkader et al., 2020d, Mohammed Abdelkader et al., 2020e, Mohammed Abdelkader et al., 2020f). The flowchart of spalling detection and evaluation of its severities is depicted in Figure 3.5. It is worth mentioning that the detection and evaluation of cracking and scaling follow the same computational procedures of spalling with some differences that are highlighted within the context of spalling evaluation method. This method encompasses an additional pre-processing stage of contrast

enhancement. In it, the images are re-scaled to a size of 200×200 because it is found to be able to better capture the descriptors of the defects. Bridges are complex structures due to the substantial amount of details and information present in images. Furthermore, they experience low contrast and inhomogeneous illumination conditions. Thus, min-max gray level discrimination approach is applied for contrast enhancement, and amplification of differences between gray level intensities of the spalling and non-spalling regions (background). This method increases the gray level intensities of the spalling pixels so that they become darker while it reduces the gray level intensities of the non-spalling pixels so they become lighter. The enhanced image capitalizing on the min-max gray level discrimination approach can be obtained as follows (Hoang, 2018).

$$I_a(x, y) = \begin{cases} \min(M, T) & \text{if } I_o(x, y) > I_o \min + \tau \times (S) \\ \max(N, F) & \text{if } I_o(x, y) \leq I_o \min + \tau \times (S) \end{cases} \quad (3.3)$$

Such that;

$$T = I_o(x, y) \times R_a, F = I_o(x, y) \times R_a^{-1}, S = I_o \max - I_o \min, M = I_o \max, \text{ and } N = I_o \min \quad (3.4)$$

Where;

$I_a(x, y)$ and $I_o(x, y)$ represent the adjusted image and original image, respectively. $I_o \max$ and $I_o \min$ represent the maximum and minimum gray level intensities in the original image. R_a and τ refer to the adjusted ratio and margin parameter, respectively. R_a and τ are assumed 1.1 and 0.5, respectively. It is worth mentioning that the grey level discrimination function is applied to each image separately.

The next stage is the image segmentation, which is defined as the process of partitioning the digital image into multiple segments based on some attributes such as colour, intensity and texture. The present research adopts bi-level thresholding (binarization) in order to generate a

single threshold T that classifies the image pixels into two segments, namely foreground (spalling) and background (surface). The bi-level thresholding function can be defined as follows.

$$G(x, y) = \begin{cases} 1, & \text{if } F(x, y) \geq T \\ 0, & \text{otherwise} \end{cases} \quad (3.5)$$

Where;

$G(x, y)$ represents the binary image. $F(x, y)$ represents the gray image. T denotes the threshold that separates the foreground from the background, whereas if the image pixels are above the threshold, they are appended to the foreground otherwise, they are appended to the background.

Image segmentation methods can be categorized into five main clusters, namely edge detection-based methods, clustering-based methods, region-based methods, histogram-based methods, and optimization-based methods. The detection of surface defects in reinforced concrete bridges is an exhaustive and challenging task for the following reasons:

- 1- Existence of low contrast between the defects and surrounding deck area, inhomogeneity of intensity and presence of shadows of similar intensity to the cracks. These conditions imply the existence of multimodal histograms. As such, the efficient exploration of multimodal search spaces is a hard and tedious task.
- 2- Higher potential of inaccurate segmentation, which results in imprecise extraction of the descriptors of surface defects. This eventually in inaccurate recognition and evaluation of spalling. It should be noted that small differences in the threshold values have also adverse effect on the decision-making process. Hence, the implications of failure to obtain the

optimum threshold further substantiate the use of the optimization-based methods for the spalling segmentation purpose.

3- Threshold values differ from one image to the other depending on its gray level intensities.

Thus, there is a need for an efficient and robust image segmentation model that can handle different conditions of images.

There are basically two approaches to handle the optimal thresholding problems which are: parametric and non-parametric approaches. For the parametric approaches, the gray-level of each class is assumed to follow a probability density function, normally a Gaussian probability density function is assumed. Then, the statistical parameters of each class are computed. The least-squared method can be used as one of the algorithms to estimate the parameters of the distribution that best-fits the gray-level histogram, leading to a non-linear optimization problem (Hammouche et al., 2008). However, the parametric approaches are computationally exhaustive and the performance is highly dependent on the initial conditions (Akay, 2013). The non-parametric approaches received considerable wide recognition by researchers in the recent years because they are computationally faster than parametric approaches. Furthermore, they demonstrated their superior segmentation capacities against other image segmentation methods. The non-parametric approaches tend to find the optimal thresholds that partition the gray-level regions based on some discriminating criteria such as Renyi entropy, cross entropy and the between-class variance (Otsu's function) (Zhang and Wu, 2011).

This research proposes the use of a non-parametric segmentation model for the detection of spalled concrete in images. This is accomplished through the accommodation of information theory-based formalism of images alongside invasive weed optimization algorithm (Mohammed Abdelkader et al., 2020c). The developed spalling detection model investigates more than one

objective function to enable the assessment of different types of images. Each one of them has its own assumption, and therefore it fits only a certain kind of images. The developed method investigates five objective functions which are: maximization of Kapur entropy, maximization of Tsallis entropy, maximization of Renyi entropy, minimization of cross entropy, and maximization of the between-class variance (Otsu function) for the inclusion of the best performing functions in the subsequent phase.

As shown in Figure 3.5, the developed image segmentation method is divided into two phases. In the first phase, five non-parametric models are investigated to solve the image segmentation problem by finding the optimum thresholds of the images. The optimum threshold is computed based on the five methods stated above. The developed method utilizes the invasive weed optimization algorithm to find the optimum threshold values based on each objective function separately. Then, the five image segmentation models are ranked based on three performance indicators namely, mean-squared error, peak signal to noise ratio and mean absolute error. These indicators are used to automatically analyze the performance of segmentation models. Subsequently, the best two performing image segmentation methods are selected to be used to design a bi-objective optimization problem. The best two performing objective functions are the ones which achieve the lowest mean-squared error, highest peak signal to noise ratio and lowest mean absolute error. In the second phase, the multi-objective optimization problem is also solved using the same optimization algorithm and the same initial setting of parameters in the first phase in order to provide an equal basis of comparison. The results obtained from the bi-objective optimization model are compared against the results of the single-objective optimization methods (best two segmentation models). If there is an improvement, the current design of the

bi-objective optimization model is appended and will be utilized for the subsequent steps. If not, the best segmentation obtained from the first phase, is utilized instead

Some imperfections may be present in the image after the segmentation process. These imperfections include some noise, holes, and non-uniform edges. These imperfections should be removed before the spalling quantification process using some morphological operations meanwhile preserving the shape of spalling. The noise and protrusions in images are reduced by removing the isolated unconnected pixels of area less than 50. Additionally, it utilizes operations like filling holes, closing operation with disk structuring element of size 6 and bridging unconnected pixels for the purpose of filling cavities within boundaries of objects and smoothing their borders. In this regard, the present research utilizes the standard 3×3 neighborhood in the bridging and filling holes operations. The bridging operator sets zero-value pixels (background pixels) to one (foreground pixel) if they have two non-zero neighbors that are not connected. The filling operation is used to fill isolated interior pixels in the spalling, which are the individual zero pixels that are surrounded by one-value pixels. It is worth mentioning that closing operation is dilation followed by erosion using a predefined structuring element. Suppose an image A of size $M \times N$ and structuring element SE . The closing operation can be described as follows (Pal and Chatterjee, 2017; Lv et al., 2014).

$$A \ominus SE = (A \oplus SE) \odot SE \quad (3.6)$$

Such that,

$$A \oplus SE = \max\{A(i, j) + SE(i, j)\} \quad (3.7)$$

$$A \odot SE = \min\{A(i, j) - SE(i, j)\} \quad (3.8)$$

Where;

The operators \ominus , \oplus and \odot refer to closing, dilation and erosion operations, respectively. The size and shape of structuring element are essential for performing the morphological operations. For example, the size of the structuring element has to be considerably smaller than the image to be processed and at the same time it has to be of a closer size to the object of interest in the image. The structuring element is expressed in the form of a binary image, which takes the value of zero and one. The structuring element can take the form of different shapes such as line, disk, square, diamond. In the present research, the size and type of structuring element alongside the minimum area of objects to be removed; are manually tuned for some images based on their implication on the quality of the segmented image. This setting of parameters is then appended to be applied to other images.

The validation process of the spalling detection model is three-folded for the sake of examining the robustness of the developed segmentation model, its non-dependency towards the kind of image and applicability to a wide range of images. The first fold is to substantiate the deployment of invasive weed optimization algorithm through comparison against high-performing state of art meta-heuristics. The second is to validate the formulation of the developed detection model. This is carried out through comparison against classical segmentation models including: Otsu, K-means clustering, region growing, fuzzy C-means clustering and expectation maximization. In this context, the performance comparisons are performed as per a set of image quality indicators and classification evaluation metrics. The image quality metrics encompass mean-squared error, peak signal to noise ratio and mean absolute error. The classification evaluation metrics include overall accuracy, F-measure, balanced accuracy and Matthews's correlation coefficient.

The third fold aims at evaluating the statistical significance of the output of the developed segmentation model against the afore-mentioned segmentation models using two-tailed paired student's t test. Student's paired t-test is a parametric statistical test utilized for the purpose of analyzing the statistical significance of the difference between two population means in a research study encompassing paired samples. In the present research, the student's t test is used to investigate whether or not the image quality indicators and classification evaluation metrics of two spalling detection models are different from each other based on a set of images. Student's t test is selected because it is a commonly utilized approach that proved its efficiency in analyzing statistical data and examining dissimilarities between different clusters in diverse applications including such as comparing core strength results (Reddy and Wanjari, 2018), verifying the effect of software on youth's learning process (Di Biasi et al., 2020) and analyzing international roughness index from multiple sources (Samsuri et al., 2019).

The second model aims at the automated assessment of spalling area. Feature extraction is a fundamental pre-processing stage in machine learning and pattern recognition problems because it enables to extract the features required as an input for the regression model. Feature extraction can be performed based on spatial domain analysis or frequency domain analysis. Spatial domain approach deals with physical parameters such that spatial domain features include texture, size, color, shape and edge intensity. Frequency domain approach relies on measuring parameters from an image, and the frequency domain features encompasses the coefficients of fast Fourier transform, discrete cosine transform (DCT) and discrete wavelet transform (DWT). It is worth mentioning that these transformation algorithms enable the transition from the spatial domain to frequency domain, and the inverse transformation enables returning back to the original spatial space. Frequency domain represents a space in which each image value at a certain position F

constitutes the amount that the intensity values in spatial domain image I vary over a specific distance with respect to position F . Thus, frequency domain demonstrates the rate at which image intensity values are changed in the spatial domain image I . High frequency components correspond to pixel values that transit rapidly across the image such as text and edges. Strong low frequency components correspond to large scale features in the images such as smooth regions, homogenous objects that dominate the image, and slow-varying character (Khan and Shah, 2014; Kaushik et al., 2012).

The present research proposes a novel feature extraction method that capitalizes on cascading the higher efficiency capabilities of singular value decomposition in capturing the intrinsic information and the robustness of discrete wavelet transform against proportion variance and rotation variance. In this context, singular value decomposition and discrete wavelet transform are adopted to model the spatial domain features and frequency domain features, respectively. This concatenation of features (SVD – DWT) is expected to establish a trade-off that minimizes the complexity of the training process and its computational time alongside enhancing the recognition capacity of the machine learning model. In this context, the speed up the computational process is accomplished by eliminating the insignificant features and reducing the computational complexity of the input dataset of gray-level images. Additionally, the improvement in the learning capacity of the prediction model is elicited from providing an accurate and comprehensive representation for the information in images.

The developed method adopts the energies of all discrete wavelet transform sub-bands are combined with non-negative singular values to create the feature vector set. Singular value decomposition is utilized to convert the input image of size 200×200 pixels into a spatial domain feature vector composed of singular values of size 1×200 . With respect to the frequency domain

features, DWT-based feature extraction exhibits three levels of decomposition, whereas N levels of decomposition result in $(3 \times N) + 1$ sub-bands. Thus, the frequency domain feature vector is composed of ten sub-bands. The increase in the levels of DWT increases the length of extracted features, which creates more computational burden. As such, the designated number of decompositions provides a trade-off between the computational complexity and computational accuracy. In this regard, the frequency domain feature vector is of size 1×10 encompassing the energies of ten sub-bands. As such, the spatial domain feature vector is cascaded with a frequency domain feature vector to establish a feature vector set of size 1×210 to serve as an input to build the automated spalling assessment model. The energy of each sub-band can be computed using the following equation (Shanavaz and Mythili, 2016).

$$E_k = \frac{1}{M \times N} \sum_{w=1}^M \sum_{h=1}^N |X_k(x, y)| \quad (3.9)$$

Where;

E_k represents the energy of k – th sub-band. $X_k(x, y)$ indicates the pixel value of k – th sub-band. M and N represent the width and height of sub-band, respectively.

After designing the feature vector set, it is used to feed the automated assessment model. In this regard, ENN – IWO model is established to autonomously evaluate the spalling area in reinforced concrete bridges. This model can be deployed by transportation agencies without domain knowledge in machine learning and meta-heuristics. The performance of the developed automated assessment model is compared against a set of widely-used machine learning models and high-performing deep learning models reported for their higher accuracies. The machine learning models comprises back-propagation artificial neural network, Elman neural network,

generalized regression neural network and radial basis neural network. The deep learning models encompass a deep convolutional neural network trained from scratch alongside a group of pre-trained deep neural network architectures, namely AlexNet, VGG16, VGG19 and CaffeNet. The performances of the prediction models are assessed based on mean absolute error percentage error, root mean-squared error (RMSE) and root mean squared percentage error (RMSPE). The comparative analysis is carried out using the original and augmented datasets for the purpose of testing the robustness of the developed method in dealing with different sizes of datasets. The original dataset is augmented for the sake of its enlargement by creating new training and testing instances (Dung et al., 2019). The data augmentation techniques can be applied alone or combined in computer vision. In the present research, different forms of data augmentation techniques are utilized including rotation, flipping and cropping. In this context, rotation and flipping are introduced to establish rotational invariant models, whereas the images are rotated by 90° , 180° and 270° .

The third model is designated for establishing a severity rating systems of spalling based on its area and depth. The spalling area is interpreted from the previous model while the spalling depth is adopted from the third-order polynomial regression function introduced by Dawood et al. (2017). The severity levels of spalling area are expressed in the form of percentage with respect to the whole zone area to reduce the effect of camera angle on crack detection. In this regard, spalling percentage is equal to number of pixels occupied by spalling divided by the total number of pixels. In order to establish efficient and robust rating system, sufficient amount of records should be present. As such, the spalling area and depth are assumed as random variables that follow certain probability distributions based on the available dataset. The best-fit distribution is

identified based on Anderson Darling statistic. Then, Latin hypercube sampling is employed to generate numerous scenarios to be used to structure the spalling severity rating system.

Fuzzy C-means clustering is eventually utilized to generate the thresholds of the severity levels of spalling area and depth. In this context, Fuzzy C-means clustering is selected over other clustering algorithms due to its capability in dealing with vagueness and uncertainties encountered during the bridge inspection process. Furthermore, it outperforms K-means hard clustering in terms of establishing more compact homogenous clusters as well as well-separated thresholds (Bhattacharjee et al., 2017; Hooda et al., 2014). It is worth mentioning that the severity of spalling in each image is evaluated based on its area and depth, and the worst case scenario is selected to establish a more conservative assessment of spalling severities. The previously-developed models are repeated for cracking and scaling. Scaling is evaluated based on its area and depth. Cracking is assessed according to its length and width. The crack length is obtained by the skeletonization of the binary image, whereas the length is assumed to be half of the perimeter of the crack skeleton. The area of the crack is obtained from the binary image, which is equal to the summation of the white pixels present in the image. Finally, the average width of the crack is computed by dividing the total area by the length of the crack segments.

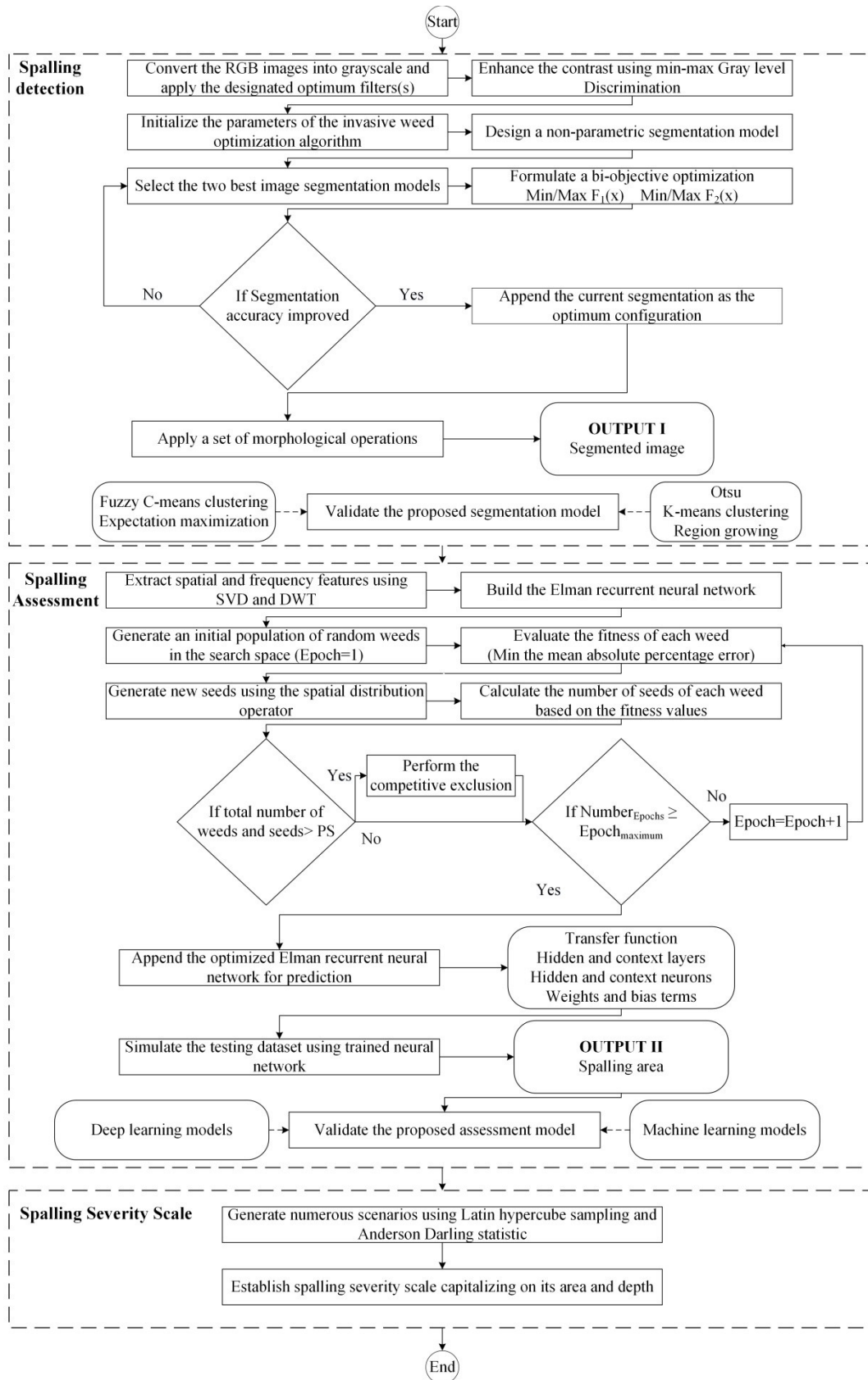


Figure 3.5: Flowchart of the developed spalling detection and assessment method

- **Singular value decomposition**

Singular value decomposition is a powerful tool that has many applications such as data compression and pattern recognition. SVD enables robust and reliable matrix factorization in order to extract the algebraic and geometric invariant features of an image. SVD factorizes a square or non-square matrix into two orthogonal matrices and a singular value matrix. The spatial domain features of an image of size 100×100 can be modelled using singular value decomposition by a feature vector set of size 1×100 (see Figure 3.6). This is expected to speed up the computational process by eliminating insignificant features meanwhile preserving as much as possible information in the image. The singular value decomposition of a rectangular real complex matrix A is expressed as follows (Chang et al., 2016; Jha and Chouhan, 2014).

$$A = U \Sigma V^T = \begin{bmatrix} u_{11} & \cdots & u_{1m} \\ u_{21} & \cdots & u_{2m} \\ \vdots & \ddots & \vdots \\ u_{m1} & \cdots & u_{mm} \end{bmatrix}_{m \times m} \times \begin{bmatrix} s_1 & 0 & \cdots & 0 \\ 0 & s_2 & \cdots & 0 \\ \vdots & \vdots & \ddots & \vdots \\ 0 & 0 & \cdots & s_m \end{bmatrix}_{m \times n} \times \begin{bmatrix} v_{11} & \cdots & v_{1n} \\ v_{21} & \cdots & v_{2n} \\ \vdots & \ddots & \vdots \\ v_{n1} & \cdots & v_{nn} \end{bmatrix}_{n \times n}^T \quad (3.10)$$

Such that;

$$U U^T = I \quad (3.11)$$

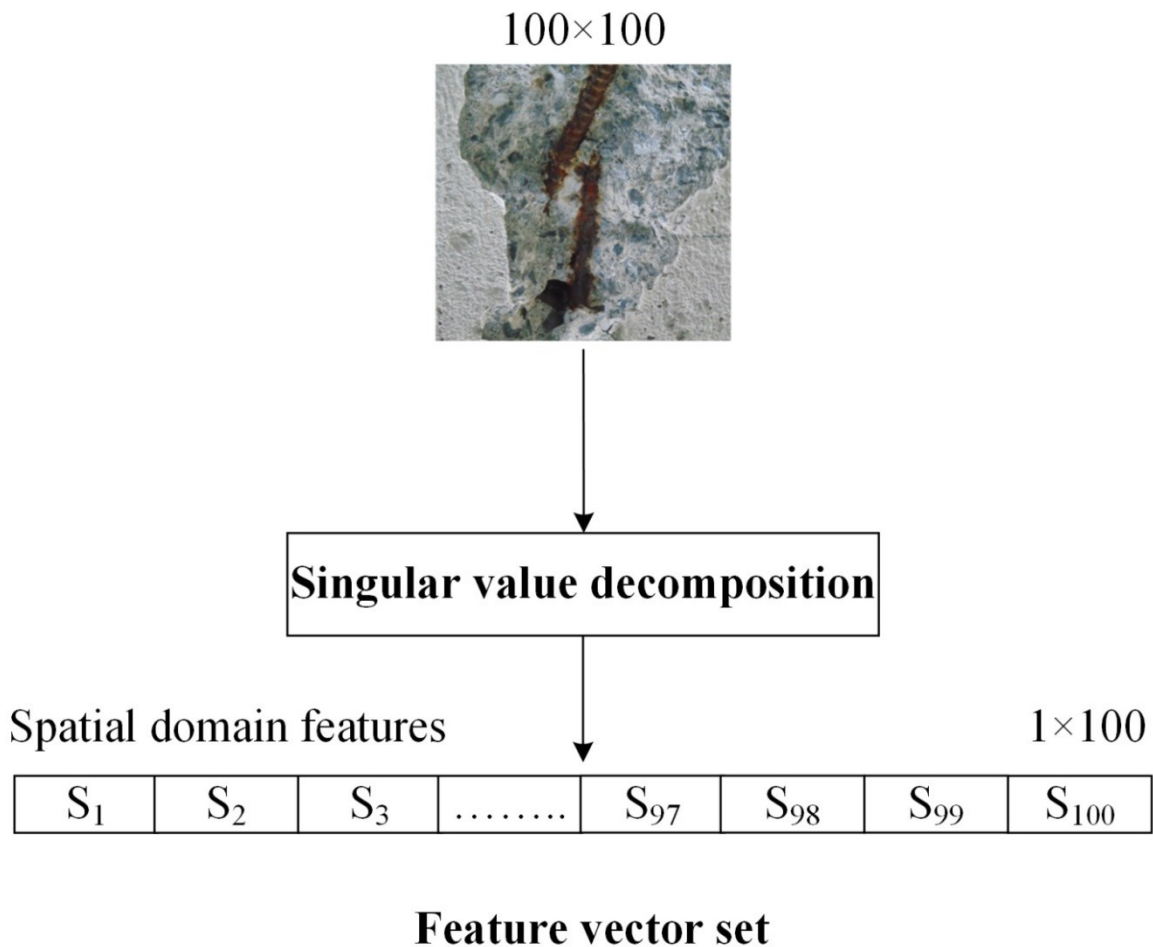
$$V V^T = I \quad (3.12)$$

$$s_1 \geq s_2 \geq s_3 \dots \dots \geq s_m \quad (3.13)$$

Where;

A is a $m \times n$ matrix. U is a $m \times m$ orthonormal matrix. V is a $n \times n$ orthonormal matrix. Σ is a diagonal matrix of size $m \times n$ which is composed of singular values of A such that it holds non-negative numbers. The diagonal entries of the Σ matrix represent the singular values and they

have higher values compared to the entries of U and V such that a matrix of size $m \times n$ can be reduced to a vector of size n . The singular values are ranked in a descending order, whereas the first entries of the singular value matrix contain the most substantial information while the last entries at the vector contain the least significant information. The singular values contain the energy information while the orthogonal matrices contain the intrinsic information. U^T and V^T are the transpose of matrices U and V , respectively. I is the identity matrix. The columns of U are called left singular vectors of A while the columns of V are called the right singular vectors of A .



S_i : Singular value of i -th dimension

Figure 3.6: Extracted spatial domain features using singular value decomposition

- **Autonomous training of Elman neural network**

As stated earlier, the ultimate objective of the present study is to develop an automated method for bridge defects detection and recognition. The bridge defects detection is formulated as a binary classification problem to classify images based on the existence of defects present in images. The output of this model is whether the images contain defects or not. The bridge defects recognition is articulated in the form of three-point classification problem. Its output is whether the image contains cracking, spalling or scaling. In the present study, the invasive weed optimization algorithm is utilized instead of the gradient descent algorithm to train the neural network for the following two reasons: inferior accuracy of the gradient descent and manual tuning of hyper parameters. The training process based on the gradient descent gets stagnated in local minima and premature convergence.

In addition to the above, there are wide ranges of hyper parameters of Elman neural network which significantly affect the prediction performance of Elman neural network. These parameters are highly sensitive to their initial values, whereas their initial setting is always variable from one case to the other. In this regard, there is no exact method reported in the literature to compute the number of context layers and context neurons. Most of these methods are case dependent and cannot be generalized to be applied in other case studies in addition to their time exhaustive nature. For instance, if the numbers of hidden layers and neurons are less than the optimal number this will result in a substantial decrease in the prediction accuracy. Furthermore, if the numbers layers and neurons are more than their optimum number this creates a lengthy training computational time. In this context, the blindness in determination of such hyper parameters and absence of systematic efficient method for their computation will have a considerable negative impact on the computational efficiency and accuracy of the prediction

model. Thus, a self-adaptive method is formulated for the sake of autonomous and dynamic tuning of the Elman neural network parameters and hyper parameters based on the present available dataset of images.

Invasive weed optimization algorithm is employed to train the Elman neural network by optimizing both the weights and structure of the ENN simultaneously in an attempt to amplify its learning capacity. The structural training includes both the topological structure and the transfer functions of the ENN model. This encompasses selection of most suitable transfer functions between the network layers, number of hidden layers and hidden neurons, number of context layers and context neurons. Eight types of transfer activation are analyzed namely, log-sigmoid transfer function, hyperbolic tangent sigmoid transfer function, Elliot symmetric sigmoid transfer function, positive linear transfer function, radial basis transfer function, triangular basis transfer function, linear transfer function and normalized radial basis transfer function. The parameter learning encompasses optimizing both the values of weights and bias terms.

Optimality theory is fundamentally focused on fixed-length assumption, such that most of the optimization models involve a fixed vector length of decision variables in order to simulate a particular set of possible solutions in the design space. Nonetheless, few cases reported in the literature comprised variable length optimization models. In them, the length of vector of solutions changes iteratively over the course of training epochs. It should be highlighted herein that the variable-length optimization problems are of more complex nature and they require more computational time and resources during the training process when compared against the fixed-length optimization problems. There is no clear definition for the gradient vector of the variable-length problem in the variable-length optimization problems. Hence, gradient-based methods are inefficient in dealing with the dynamic vector of solutions. One of the approaches to deal with

the variable-length optimization models is to presume a fixed length for the decision variables and to tune iteratively the decision variable that causes variability in length. Nevertheless, this approach often leads to suboptimal solutions. Additionally, it is time inefficient and impractical method especially in the presence of wide ranges of decision variables. This necessitates the formulation of a new approach which enables the estimation of the varying length of vector of possible solutions over the course of iterations (Ryerkerk et al., 2016).

In the present study, a self-adaptive optimization method is designed to handle the variability in the length of the optimization problem because the length of the optimization problem changes iteratively based on the number of hidden layers, number of context layers and number of hidden neurons. In order to be able to address the problem in hand, the variable length of the vector of solutions has to be known during the optimization process using a predefined function, i.e., the total number of connection weights has to be known during the training process. As such an estimator is designed to handle the dynamism of the configuration of the ENN by computing the total number of weighted connections using Equation (3.14). As shown in Equation (3.14), the optimization model gives the user the flexibility to design a multi-hidden layer neural network and a multi-context layer neural network based on the input dataset of images.

$$\text{Num} = ((I + 1) \times N) + ((N \times C \times P) + ((N + 1) \times N \times (P - 1)) + ((N + 1) \times O) \quad (3.14)$$

Where;

Num stands for the total number of weighted connections. The first term describes the number of weighted connections between the input and first hidden layer. The last term describes the number of weighted connections between the last hidden layer and output layer. The second term enables to compute the number of weighted connections between the hidden and context layers.

The third term enables to compute the number of weighted connections between the hidden layers. It should be noted that “+1” is added for the first and last terms to account for the weighted connections between the bias neurons and the output and hidden neurons. I represents the number of input neurons. N indicates the number of hidden neurons. C represents the number of neurons in the context layer. P represents number of hidden and context layers. O depicts the number of output neurons. In this regard, the number of context layers is assumed to be equal to the number of hidden layers for simplification purposes.

The structural and parameter training is conducted based on minimizing the single objective function of misclassification error of the total instances during each training epoch as follows.

$$MC_ERR = \min \frac{FAL_CLASS}{TOT_ISNT} \quad (3.15)$$

Where;

MC_ERR denotes the misclassification error. FAL_CLASS indicates number of falsely classified instances. TOT_ISNT represents total number of instances in the training dataset. It should be highlighted that misclassification error is preferred over other performance indicators since it is a well-known good performing performance indicator, unitless, and un-biased performance metric. Furthermore, it is usually more practical and efficient to deal with error cost functions in machine learning.

3.4 Corrosion Evaluation

The main thrust of the developed method is to structure standardized amplitude rating system that are then used to extract the percentages of corrosion severities for the sake of creating more reliable maintenance prioritization models. The flowchart of the developed method for corrosion

evaluation is shown in Figure 3.7. It is a hybrid method that integrates evolutionary algorithms, un-supervised clustering algorithms, and multi-criteria decision-making techniques. The multi-objective optimization module utilizes three evolutionary algorithms namely, genetic algorithm, particle swarm optimization algorithm, and shuffled frog-leaping algorithm. These three algorithms are selected due to their capability of solving the discrete and continuous optimization problems efficiently. The first step is to survey the bridge decks using the ground penetrating radar. Ground penetrating radar is one of the non-destructive techniques that are used for field investigation in structural engineering. Ground Penetrating radar can determine the subsurface structure easily and accurately. Moreover, it has the capability of locating metallic and non-metallic objects. GPR transmits pulsed electromagnetic waves from the transmitting antenna which is located on the ground surface and signals are then received by the receiving antenna.

The developed method utilizes GPR in order to evaluate the corrosion of the reinforcement rebars in the concrete bridge decks. GPR system is composed of data collection system and antennas. There are two types of antennas which are: mono-static antenna, and bi-static antenna. Mono-static antennas are composed of one antenna that performs both transmitting and receiving. Bi-static antennas include separate antennas for transmitting pulses and receiving those that are reflected. There are three basic components of GPR system which are: display unit, control unit, an antenna, and cart. The display unit is used to display the recorded data such as laptop. Control unit manages the operation of transmitting and receiving electromagnetic pulses. The antenna is used to perform the task of transmitting electromagnetic waves and receive the reflected pulse.

Then, the scanned profiles are imported into the GSSI RADAN7 software in order to extract the needed information. GSSI RADAN7 software is used to extract the amplitude values of the top reinforcing rebars. The numerical-amplitude method is used to interpret the corrosion of the

bridge decks. Numerical amplitude method depends on the value of the amplitude of the reflected waves from the top layer of reinforcement. The higher the amplitude the better the condition of the bars will be. On the other hand, the lower the amplitude the higher the corrosion the reinforcement bars will be and consequently, the lower condition state the bridge deck will be. The main drawback of this method is its lack of a clear value for the thresholds that define the different categories of corrosion. For example, the profiles of one bridge deck may have amplitude values from 10 dB to -5 dB, where 10 dB represents the best condition and -5 dB represents the worst for that bridge. Meanwhile, another of Bridges' profiles may have amplitude values that range from -5 dB to -40 dB, where -5 dB represents the best condition and -40 dB represents the worst condition. A Microsoft Excel spreadsheet is generated containing some important parameters retrieved from the GPR profiles such as scan number, two-way travel time, and normalized amplitude for each reinforcement rebar.

Then, the depth correction is performed based on the methodology developed by Barnes et al. (2008). The main objective of this step is to remove the effect of the depth on the target data because there is an attenuation of the electromagnetic waves associated with the deeper targets. Depth-corrected amplitudes provide a more accurate assessment of the amplitude values of the reinforcement rebars. The depth correction was performed as follows: the data points were divided into time bins; e.g. 0.5 ns. The 90th percentile point for each time bin is calculated assuming that the chloride content is consistent for the 90th percentile of the normalized amplitude at each time bin, i.e., amplitude values above the 90th percentile are not affected by deterioration. Regression analysis is then applied to fit the 90th percentile points. Correction of data is carried out by forcing the 90th percentile to be zero decibel (dB). After the depth correction, the threshold values should be calculated in order to delineate the areas of corrosion.

The second step of the developed method is the clustering module, whereas a group of bridge decks is used as an input for it. Several clustering algorithms are applied because each algorithm depends on a certain calculation methodology which generates different clusters, and consequently different thresholds. Eight clustering algorithms are utilized which are: K-means, fast K-means, kernel K-means, K-medoids, expectation maximization, fuzzy C-means, X-means, and agglomerative clustering. The multi-objective optimization module takes into consideration any number of bridge decks (based on the available dataset) and it calculates the standardized thresholds based on four objective functions. The first three objective functions tend to find the optimum threshold based on a local search, i.e., dealing with each threshold individually. On the other hand, the fourth objective function tends to find the optimum threshold based on a global search. The multi-objective optimization module incorporates three evolutionary algorithms which are: genetic algorithm, particle swarm algorithm, and shuffled frog-algorithm. Shuffled frog leaping provides proper balance between exploration and exploitation which leads to better quality solutions and faster convergence rate (Tang et al., 2020; Huang and Song, et al., 2019). Genetic algorithm and particle swarm optimization algorithm are selected because they are the two most commonly-utilized meta-heuristics in civil engineering-related applications. They proved their efficiency in dealing with complex and diverse optimization problems such as resource-constrained project scheduling (Nemati-Lafmejani et al., 2019), contractor selection (Ravari et al., 2020) and prediction of construction costs (Lin et al., 2019). The output of this module is the combined Pareto frontier points obtained from the three algorithms where each one of the candidate solutions is represented in a three-dimensional space, i.e., threshold (1), threshold (2), and threshold (3).

Decision-making module is used to calculate the most feasible solution among the optimum solutions obtained from the multi-objective optimization module. Five multi-criteria decision-making techniques are implemented which are: weighted sum model (WSM), complex proportional assessment (COPRAS), VIKOR, grey relational analysis (GRA) and TOPSIS. Each technique provides a distinct ranking for the alternatives. Group decision-making is performed to aggregate the ranking of the alternatives into one final ranking for the alternatives, i.e., obtain the best compromise solution. The alternative with the first ranking represents the standardized thresholds of the GPR. After calculating the thresholds, a corrosion map can be developed for any bridge deck. Surfer 12 is a plotting and mapping software that is utilized to develop the corrosion map for the concrete bridge decks. The obtained percentages of corrosion severities are then fed to the integrated condition assessment model. Due to the size limitations multi-objective optimization and multi-criteria decision making modules are described briefly. Detailed information about the corrosion evaluation method and its different modules can be found in Mohammed Abdelkader et al. (2019a), Mohammed Abdelkader et al. (2019b), Marzouk et al. (2018) and Ata et al. (2017).

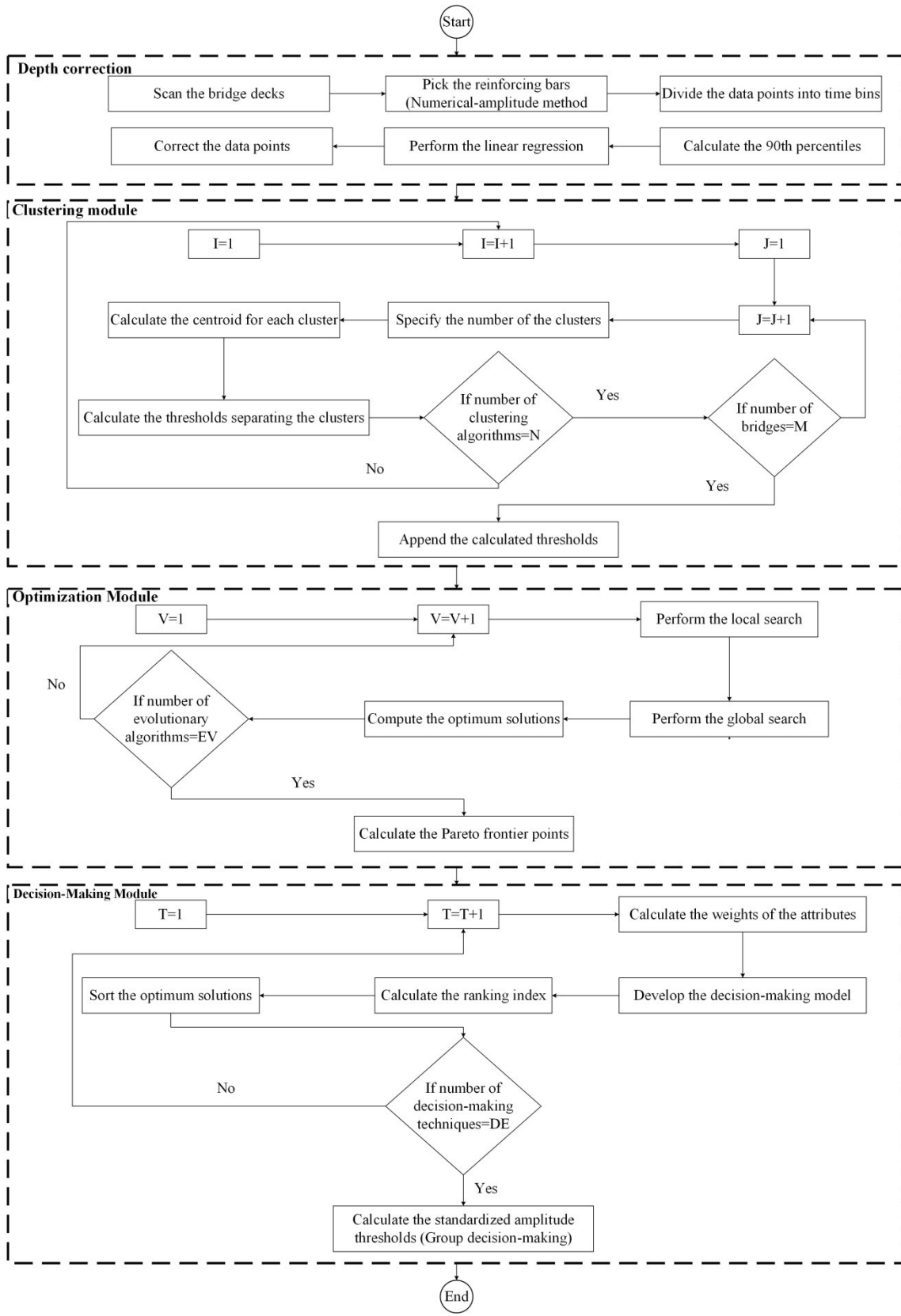


Figure 3.7: Flowchart of the developed corrosion evaluation method

3.5 Integrated Condition Assessment

The method presented in this section provides transportation agencies with an invasive weed optimization fuzzy decision-making framework that supports both element-level and network-level decisions. This is articulated through: modeling the severity levels of the bridge defects separately, designing a bridge deck maintenance prioritization model capitalizing on integrated bridge deck condition index (IBDCI), and formulating a bridge maintenance decision-making strategy. The developed decision-making paradigm is composed of three tiers. It is worth mentioning that the first tier is tackled to improve the flexibility of the developed framework through fitting the preferences of decision-makers, whereas in some cases they are concerned with some type of bridge defects more than the others. It is important to mention that the developed framework deals with five types of bridge defects, namely corrosion, delamination, cracking, spalling, and scaling, and it can be tailored to map other types of bridge defects. The flowchart of the developed framework is depicted in Figure 3.8. As can be seen, the developed framework is composed of three main models, namely weight interpretation, integrated condition assessment, and bridge maintenance decision-making strategy.

In the first model, optimized fuzzy analytical network process (O – FANP) is adopted to compute the weighting vector of the different bridge defects. Preference comparison matrices are the cornerstone of the multi-criteria decision analysis. Thus, they should be dealt with in a way that improves the consistencies of judgments through transforming inconsistent matrices to consistent ones, and minimizes the imprecisions encountered by the classical judgment assignment. Deriving the priority weighting vector is one of the principal issues in the multi-criteria decision analysis (Kou et al., 2016). Kou et al. (2014) highlighted the importance of minimizing the inconsistencies of the pairwise comparison matrices, whereas they developed a

Hadamard product induced bias matrix model for the purpose of improving the consistency ratio of pairwise comparison matrices through addressing the cardinal and ordinal inconsistencies. The developed O – FANP model encompasses single-objective genetic algorithm to generate more coherent judgment matrices that eventually enhances the quality of the decision-making process. In this research, five different fuzzy scales of importance with semantic ranges are experimented such that the optimum one is obtained through formulation a single-objective optimization model that minimizes the consistency ratio of the judgment matrices. Aggregation of the consistent pairwise comparison matrices plays an important role in the derivation of consensus weighting vector (Lin et al., 2020). After the selection of the optimum fuzzy scale, the consistency ratio is computed for each pair-wise comparison matrix developed by each respondent. The pair-wise comparison matrices that are considered in any further analysis stage are only the ones that exhibit a consistency ratio less than 10%. Finally, the judgments of the respondents are aggregated using the geometric mean.

Over the past years, several approaches were presented to compute the weighting priority vector such as Eigen vector method (Saaty, 1977), logarithmic least squared method (Crawford and Williams, 1985) and recently the cosine maximization method (Kou and Lin, 2014). Additionally, there are different FAHP and FANP approaches reported in the literature including: Van Laarhoven and Pedrycz (1983) fuzzy priority approach, Buckley (1985) geometric mean approach, Boender et al. (1989), Chang's (1996) extent analysis approach, Cheng's (1996) entropy-based approach, Mikhailov (2000) Fuzzy Preference Programming approach, and Zeng et al. (2007) arithmetic averaging approach, etc. The developed O – FANP model capitalizes on Chang's extent analysis method that relies on the degree of possibilities of each attribute to compute the priority weights of the bridge defects. Although it allows only triangular fuzzy

numbers to be utilized, it is characterized by its simplicity, lower computational requirements, capacity to deal with both qualitative and quantitative information, and efficiency in solving complex problems in broad variety of diversified fields (Yazdani et al., 2019; Phochanikorn and Tan, 2019). It is worth mentioning that the computational cost is decisive parameter in selecting the appropriate FANP approach, whereas Van Laarhoven and Pedrycz (1983) fuzzy priority method, Buckley (1985) geometric mean method, Boender et al. (1989) method, and Zeng et al. (2007) arithmetic averaging method are often criticized for being computationally expensive (Aydin and Kahraman, 2013; Büyüközkan et al., 2004).

Fuzzy analytical network process is employed to model the bridge defects importance due to its capability to simulate the dependencies between the bridge defects and the condition of the bridge deck (goal) as well as the dependencies of the bridge defects with each other. FANP is also incorporated because most of the defects are corrosion-induced failure modes. Thus, there is a dependency between the bridge defects. The importance weightings are derived based on the data elicited from the questionnaire survey distributed to the experts in the field. The developed survey is designed to sustain two levels of comparison which are: comparison of the main criteria (bridge defects) with respect to the condition of the bridge defect, and comparison of the main criteria (defects) with respect to each other. For instance, each respondent was asked to define the degree of importance of criteria X over the other criteria Y with respect to the goal. An example of the pair-wise comparison of level two is that each respondent is asked to provide the degree of importance of criteria X over criteria Y with respect to a third criteria Z.

The second phase is an invasive weed Optimization-based fuzzy model aims at formulating an IBDCI to be further used in maintenance prioritization of bridge decks. In this model, it is important to define the percentages of each condition category for the bridge defect. For

instance, 40% of the cracks in bridge deck A are in a poor condition or 30% of the spalls in bridge deck B are in a very poor condition. The condition assessment model relies on the integration of two modes of non-destructive evaluation techniques (NDET) for the sake of establishing a computationally accurate and efficient decision-making platform. In it, corrosion is evaluated using ground penetrating radar while the surface defects are analyzed using computer vision-based methods to model their magnitude of severities. The percentages of condition categories of delamination are extracted by the inspection reports provided by the Ministry of Transportation in Quebec. In the inspection reports, delamination is assessed using chain drag or hammer sounding. With regard to corrosion and surface defects, they are evaluated based on the methods delineated in Chapters 4 and 5, respectively.

In the developed invasive weed Optimization-based fuzzy model, Severity levels of the bridge defects are expressed in the form of fuzzy membership functions to capture uncertainties during inspection process, data capturing, transmission and processing.. Moreover, it is preferred over probability distribution because it enables to obtain a severity index for individual bridge defects. Establishing fuzzy inference systems require fine-tuning the membership functions and adjusting the fuzzy rules. The process of manual tuning of the parameters of the fuzzy inference systems is subjective, inconsistent, time-consuming, and case dependent, which yields inferior solutions. This signifies the need for objective-based methods for tuning the membership functions. As such, the developed framework encompasses invasive weed optimization algorithm to automatically calibrate the fuzzy membership functions. This constitutes deriving the optimum shape of fuzzy membership functions (S_D , triangular or trapezoidal), optimum boundaries for each fuzzy membership function of each bridge defect (B_{MD}), and optimum defuzzification technique (DE_FUZZ, centroid or bisector).

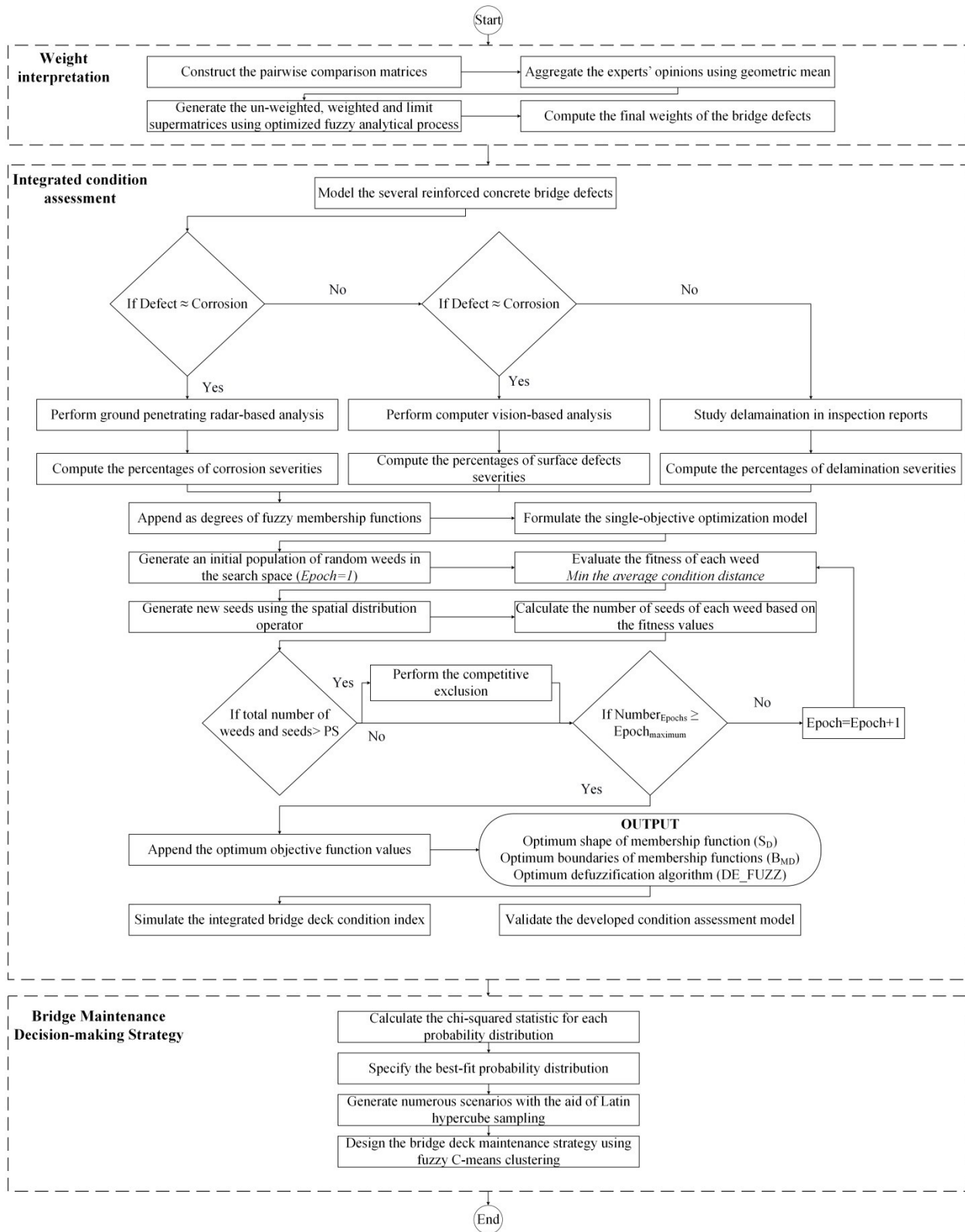


Figure 3.8: Flowchart of the developed bridge intervention prioritization method

These optimum parameters are obtained based on structuring a single-objective invasive weed optimization model which minimizes the absolute distance between IBDCI computed from two different multi-criteria decision making methods. Invasive weed optimization algorithm is preferred over generic algorithm because IWO is an exhaustive search engine that exemplified its capabilities in exploring complex and multi-local search spaces. Moreover, it manifested its superiority over some of the best-performing optimization algorithms such as genetic algorithm, particle swarm optimization algorithm and harmony search algorithm. Furthermore, genetic algorithm is often criticized by the low exploration and exploitation capacity, which leads to the entrapment in local minima than the true optimal solutions (Mohammed Abdelkader et al., 2020c; Asgari et al., 2016; Azizipour et al., 2016).

Group decision making has been adopted by researchers in various disciplines to establish a synchronized solution based on the individual multi-criteria decision making models such as soft consensus cost model developed by Zhang et al. (2019) and weighted-power average operator-based model developed by Li et al. (2018). In this context, the percentages of each condition category represent the degrees of the fuzzy membership functions. They are aggregated using the weighted fuzzy union approach (WFU) to obtain a severity index for each bridge defect separately capitalizing on the calibrated fuzzy membership functions. Then, using the weights fed from the weight interpretation model, the IBDCI can be computed using TOPSIS and grey relational analysis. These two multi-criteria decision making methods are selected because of their efficiency and robustness as well as their different natures (Azimifard et al., 2018; Ma et al., 2019). Thus, they can provide a comprehensive and efficient representation for the physical condition of the bridge deck. It should be mentioned that the final IBDCI used for maintenance prioritization purposes, is the average of IBDCI elicited from TOPSIS and GRA.

The third model is designated for establishing a bridge maintenance decision-making strategy, which enables transportation agencies to map the appropriate intervention action as per the IBDCI. Thus, sufficient amount of inspection records should be present in order to structure an efficient bridge maintenance decision-making strategy. The percentages of condition categories of the bridge defects are assumed random variables that follow certain probability distributions. The best-fit probability distribution is selected based on the Chi-squared test. Then, Latin hypercube sampling is adopted to generate large number of scenarios. Then, these scenarios are evaluated using the integrated using the integrated condition assessment model, and appended in a database.

Latin hypercube sampling (LHS) was initially proposed by Mckay et al. (1979) and it was later improved by Iman and Conover (1982). It is utilized herein to generate random samples drawn from the input probability distributions of condition categories of bridge defects. LHS is a modified stratified scheme of Monte Carlo simulation that enables better coverage and simulation of the variability in the design space of the input probability distributions through reducing the error of sampling. LHS provides faster convergence in estimating the parameter's uncertainties, whereas it requires less number of iterations to attain the same level of statistical accuracy of Monte Carlo simulation (MCS). As such, LHS is recommended over MCS when modeling complex problems, and when time constraint is an issue (Pan et al., 2020; Li et al., 2013). Subsequently, fuzzy C-means clustering is selected as one of the soft clustering algorithms to obtain the thresholds of the IBDCI necessitated to structure the bridge deck maintenance decision-making strategy. The different models of the developed integrated condition driven maintenance prioritization method are discussed briefly within the thesis due to

space limitations. However, detailed information about the models and adopted algorithms can be found in Mohammed Abdelkader et al. (2020g).

3.6 Deterioration Modeling

This section presents two deterioration prediction methods that are built to simulate the future performance of concrete bridge decks. The first deterioration model is based on hybrid Bayesian-based approach while the second one relies on semi-Markov decision process

3.6.1 Hybrid Bayesian-based method

The flowchart of the developed method for bridge deterioration prediction is shown in Figure 3.9. It is a defect-based model which is concerned with bridge elements because they are regarded as the elements that are vulnerable to the highest levels of deterioration. The developed model is a five-stage methodology, whereas it is divided into five main modules which are: data pre-processing module, conditional probabilities module, Bayesian belief network (BBN) module, Metropolis-Hastings module, and stochastic optimization module. The input and output of every stage are depicted in Figure 3.9. The first step of the data-preprocessing module is the definition of the condition states. The deterioration model is constructed based on historical data of the element-level bridge inspections of concrete bridge decks. There are two types of events which are: transition events and censored events. Censored events mean that the observed event which is the sequential change in condition state does not occur during the observation period. In the transition events, the sequential change in the condition states is observed during the observation period (Morcoux et al., 2010). The output of the data processing stage is a group of censored events

The element-level inspection obtained from the Ministry of Transportation in Quebec defines the status (extent of damage) of the bridge elements based on four condition states which are: 1)

condition state 1 (good), condition state 2 (fair), 3) condition state 3 (poor), and 4) condition state 4 (very poor). The bridge inspection data provides the infrastructure managers with information about the current status of the bridge inventory. Moreover, they are used to define future maintenance requirements.

The second step in the first stage is to design the architecture of the BBN. The BBN is composed of nodes and direct links. The nodes are the concrete bridge defects as well as the in-state probabilities. The term “in-state probability” refers to the probability that a certain element remains in a certain condition state i within a certain period of time. The direct links denote the dependencies between the bridge defects in addition to the dependency between the bridge defect and the in-state probabilities.

The developed model is concerned with five types of bridge defects which are: corrosion, delamination, cracking, spalling, and scaling. The in-state probabilities include: P_{11} , P_{22} , and P_{33} . The next step is to define a set of mutually exclusive states for each node. For each one of the five bridge defects, there are four condition states which are: “Good”, “Medium”, “Poor”, and “Very poor”. For the in-state probability, there are two states which are: “Yes”, and “No”. Then, a condition rating index is calculated based on the five bridge defects, and for each event, which helps in specifying whether or not, the bridge element will remain in its condition state.

The marginal probabilities are computed based on the frequency of occurrence of the condition state for a certain bridge defect such as the probability that the corrosion is in a good condition, or the probability that the spalling is in a poor condition. The developed model is concerned with three transition events (TEs) due to the existence of four condition states. The transition events are: the transition from condition state 1 to condition state 2 (TE(1,2)), the transition from

condition state 2 to condition state 3 (TE(2,3)), and the transition from condition state 3 to condition state 4 (TE(3,4)). Transition time is the time that the facility takes to deteriorate from a certain condition state to the next lower condition state. The transition event may not be observed within the analysis period for two main reasons (Destefano and Grivas, 1998):

1. The element may be replaced while it is in its initial condition state, therefore it will not transit to the next condition state, and
2. The analysis period may be not long enough to allow the transition to the lower condition state.

Therefore, the events that are included in the latter stages are only the transition events. Within the developed model, the following set of assumptions is incorporated.

- 1- The transition time is a random variable, whereas it is modeled based on probability distribution.
- 2- Distribution of the transition time is equivalent to the survival function. Survival function is sometimes called “reliability function” where it can be defined as the probability that a bridge element remains in its condition state for at least time (t).
- 3- The transition is assumed to occur in the middle of the inspection period.
- 4- A bridge element deteriorates one stage in unit step (one year), whereas no multi-stage transition is encountered.

The second stage is the conditional probabilities module. The purpose of this module is to calculate the conditional probabilities. The conditional probabilities can be either known or unknown. The conditional probabilities are computed based on the transition time in order to overcome the limitations of the state-based models. An example of the conditional probability is

the probability that delamination becomes in a severe condition given corrosion is in a very severe condition within one year. For the known conditional probabilities, the Anderson-Darling test is performed to select the best-fit distribution of the transition time. The best-fit distribution is the one associated with the smallest Anderson-Darling statistic. Then, the parameters of the probability distribution of the transition time are defined using the maximum likelihood estimation algorithm. Subsequently, the cumulative distributions are obtained, which enables the computation of the probability that a bridge defect x becomes in a condition state i given another bridge defect y is in a condition state j within one year. The unknown conditional probabilities are calculated based on the maximum entropy (ME) principle. The conditional probabilities are calculated based on a single objective function that maximizes entropy of the conditional probabilities. The decision variables are the conditional probabilities, whereas the optimization problem is solved via genetic algorithm. Genetic algorithm is a method that is used to solve problems based on genetic processes of biological organisms, whereas it is mainly based on two operators which are: mutation and crossover to search for the optimum solutions.

The third stage is the Bayesian belief network module. The developed model deals with two sources of uncertainties which are: uncertainty associated with the transition time as mentioned before, in addition to the uncertainty associated with the transition probability. The transition times and in-state probabilities are dealt with as random variables that follow probability distributions, which enables the model to capture the randomness and uncertainties of the deterioration process. This provides more robustness to the stochastic modeling of the presented hybrid Bayesian-based optimization model, which aids in constructing robust and reliable deterioration curves. As such, the conditional probabilities and the marginal probabilities are expressed in the form of probability distributions rather than discrete values. The computerized

tool enables the user to select the number of samples, the type and parameters of both conditional and marginal probabilities. The probability distributions are generated via stratified sampling technique called “Latin hypercube sampling” in order to overcome the limitations of the Monte Carlo sampling technique.

BBN is employed to investigate the relationship between the extent of severity of each of the bridge defects and their effect on the transition process. The joint probability distribution is constructed based on the conditional and marginal probabilities. Finally, the distribution of the in-state probability is generated, and subsequently, the type and the parameters of the probability distribution are defined. The constructed distribution represents the likelihood distribution of the unknown parameters (P_{11} , P_{22} , and P_{33}), which are the in-state probabilities in the present model. The parameters: P_{11} , P_{22} , and P_{33} indicate the probability that the bridge element remains in condition state 1, probability that the probability that the bridge element remains in condition state 2, the probability that the bridge element remains in condition state 3 within one year, respectively.

The fourth stage is the Metropolis-Hastings algorithm module. The Bayesian inference of the posterior distribution is performed via Metropolis-Hastings algorithm. Metropolis-Hastings algorithm is employed to generate the posterior distribution of the in-state probability by integrating two sources of information, which are the prior distribution and the likelihood function obtained from the Bayesian belief network model. The computerized tool enables the user to define the following parameters to calculate the posterior probabilities: 1) number of samples, 2) number of burn-in samples, 3) optimum acceptance rate, 4) parameters of the proposal distribution, and 5) the lag of the autocorrelation function. The previous modules are

repeated for each of the three transition events TE(1, 2), TE(2, 3), and TE(3, 4), whereas the output of the fourth stage is the three posterior distributions for P_{11} , P_{22} , and P_{33} .

The fifth stage is the stochastic optimization model module. To this point, the in-state probabilities are demonstrated in the form of distributions. Thus, the primary objective of the stochastic optimization model is to compute the transition probabilities based on the posterior distributions obtained from the previous module. The stochastic optimization model is designed in order to address the stochastic nature of the decision variables. The transition process of the condition of the bridge element is assumed to be non-homogenous. A variable transition matrix is employed because it is not reasonable to assume the same deterioration pattern for the whole service life.

The service life of the bridge element is divided into a group of zones. In order to fulfill the requirements of the homogeneity of the Markov chain, zoning concept is implemented, whereas a transition probability matrix is calculated for each zone. Within each zone, the Markov chain model and the transition probability matrix are assumed to be homogenous. The decision variables of the stochastic optimization model are the transition probabilities for each zone, whereas they are calculated based on a single objective function that maximizes the joint probability distribution. The transition probabilities are computed using genetic algorithm by sampling from the posterior distributions. The future performance of the bridge element can be forecasted using these transition probabilities.

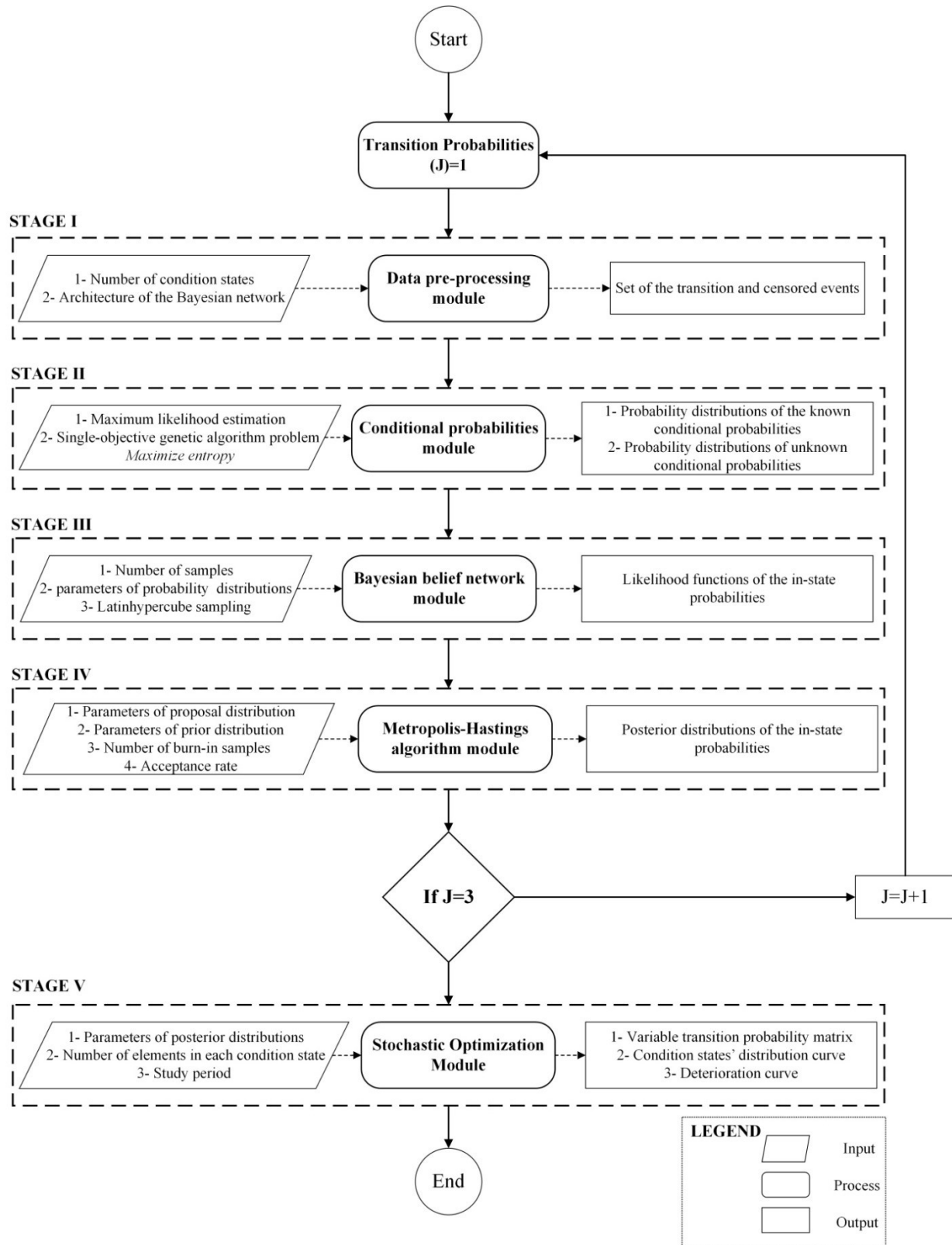


Figure 3.9: Flowchart of the developed hybrid Bayesian-based method for deterioration modeling

Two different architectures of the BBNs are investigated in order to analyze the influence of considering the dependencies on the accuracy of the performance prediction. The developed model utilizes three performance indicators to compare the four deterioration models. The three performance indicators are: root mean-squared error, mean absolute error, and chi-squared statistic (χ^2). The developed method is then compared against the regression-based optimization method to calculate the transition probabilities. The previous method utilizes non-linear optimization to calibrate the Markovian model. In addition to that, the developed method is compared against the gamma and weibull distributions. The different models of the developed hybrid Bayesian-based method are explained briefly herein. Further information about it can be extracted from Mohammed Abdelkader et al. (2019c), Mohammed Abdelkader et al. (2019d) and Mohammed Abdelkader et al. (2018).

3.6.2 Semi Markov-based method

The flowchart of the developed semi Markov-based deterioration method is depicted in Figure 3.10. The developed method considers concrete bridge decks because they are the most deteriorated bridge component. The definition of the condition states is the first step of the developed method. The element-level inspection obtained from the Ministry of Transportation in Quebec defines the status (extent of damage) of the bridge elements based on four condition states. The bridge inspection data provides the infrastructure managers with information about the current status of the bridge inventory. Moreover, they are used to define future maintenance requirements. There are three levels of management in any Bridge Management System which are: element-level, project-level, and network-level (Hammad et al., 2007). The Element-level is the basis for the application of both project-level and network-level. The element-level inspection, i.e., level 2 inspection is used as an input of the deterioration model because failure of

the bridge often occurs due to the failure of one bridge element. The developed model is concerned with modeling the deterioration of concrete bridge decks. The deterioration model is constructed based on a historical data of the element-level bridge inspections of concrete bridge decks.

The second step is to calculate the condition index for each inspection record (event). Previous efforts have been made in order to develop a condition index for concrete bridge decks. The third step is to define the transition events and censored events based on the inspection data. If the transition in condition state occurs after a specific time, therefore the event is right-censored while if the transition in condition state occurs before a specific time, therefore the event is left-censored. In case the transition occurs before and after a specific time, therefore the event is interval-censored (Morcoux et al., 2010).

The fourth step is to develop the deterioration model based on semi-Markov decision process. Latin hypercube sampling is used to calculate the probability distributions of the cumulative waiting time. The most suitable probability distributions of the sojourn times that fit most the data are defined based on goodness of fit tests such as Kolmogorov-Smirnov test, Anderson Darling and chi-squared test. Maximum likelihood estimation algorithm is implemented to estimate the parameters of the probability distributions of the sojourn times. Additional information about the developed semi-Markov based method can be found in Mohammed Abdelkader et al. (2019e).

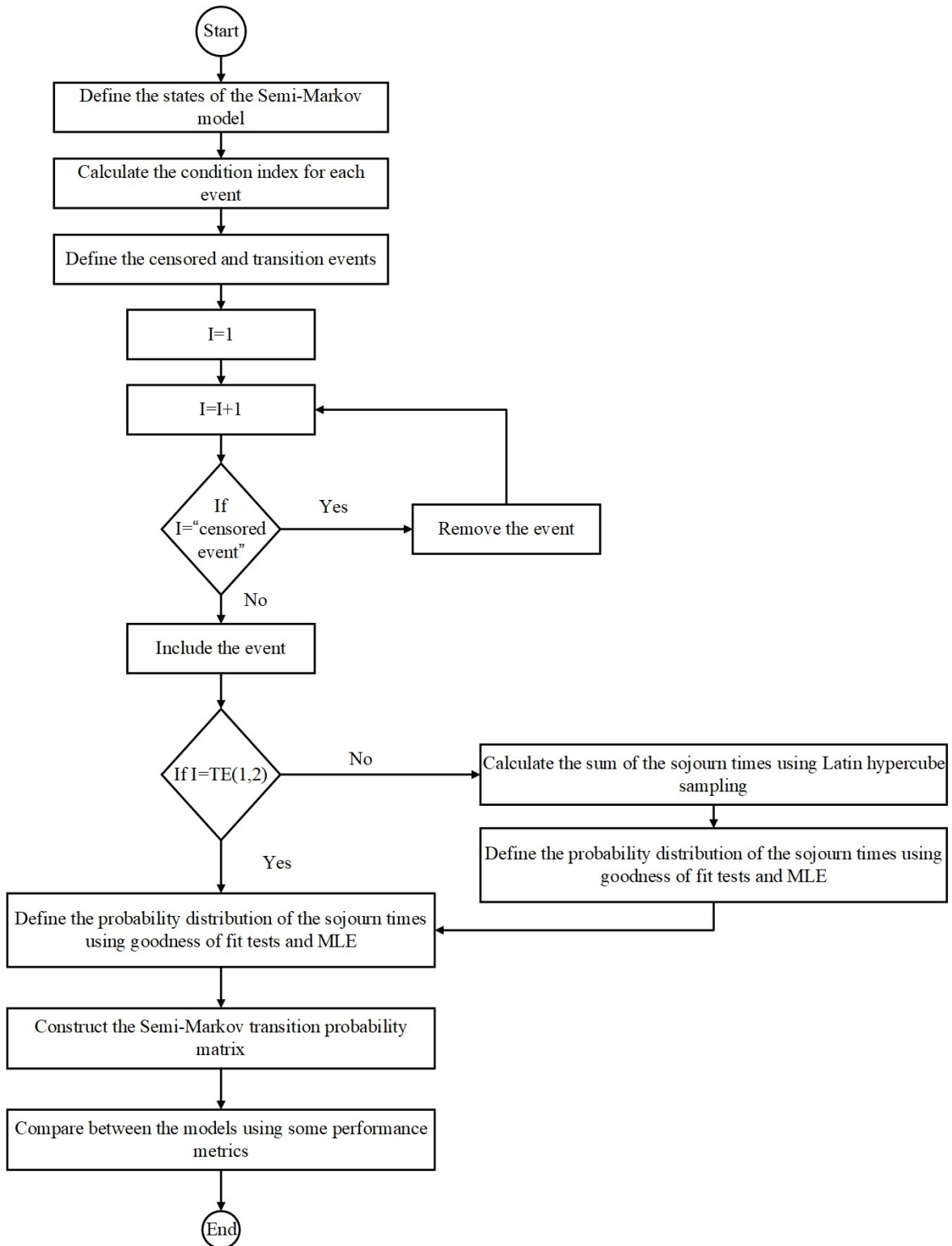


Figure 3.10: Flowchart of the developed semi Markov-based method for deterioration modeling

3.7 Maintenance Optimization

This section describes a resource driven method designated for bridge maintenance optimization at both project and network levels. It encompasses an integration of both operational and strategic planning for the sake of establishing reliable and efficient decision-making platforms. As shown in Figure 3.11, the first tier of the method is an integrative evolutionary-based method for modeling and optimizing resource allocation of bridge deck replacement projects. The output of the first tier is fed alongside other performance aspects parameters into the second one. It involves formulating a multi-objective exponential chaotic differential evolution method for optimizing MR&R plans in both project and network levels.

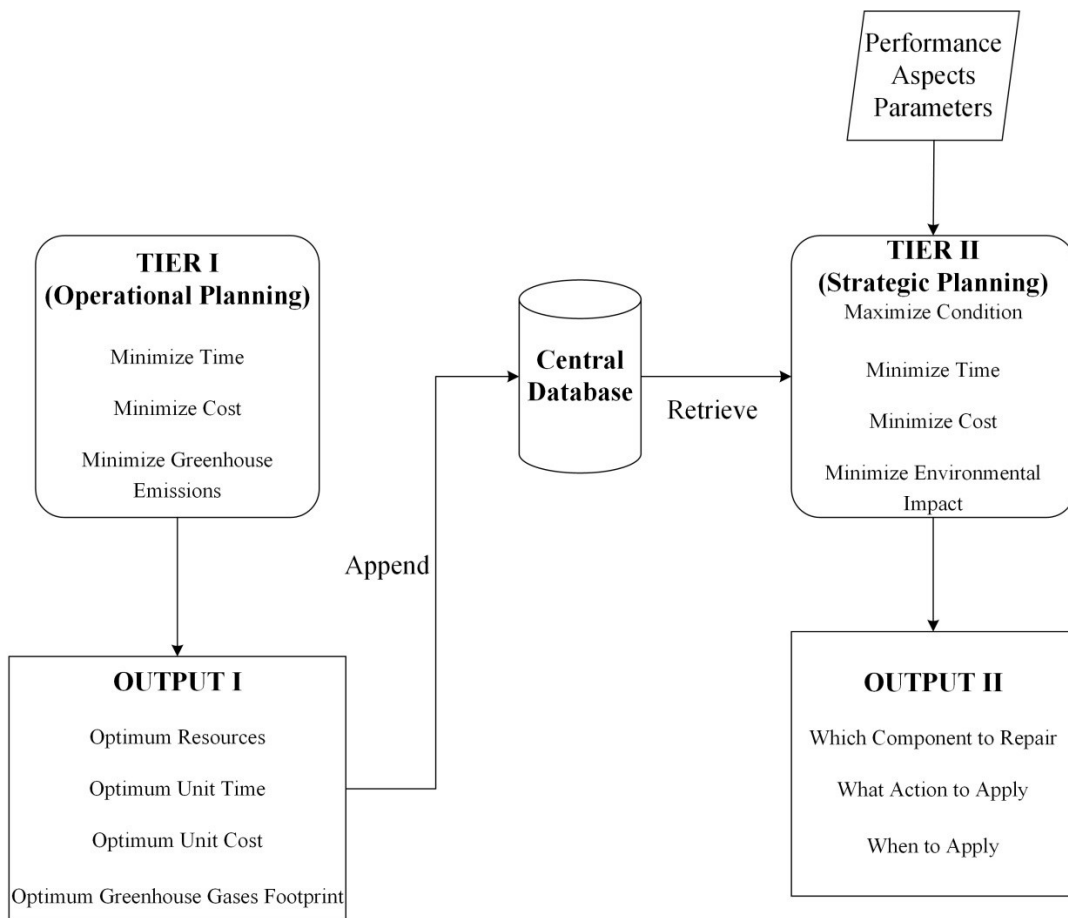


Figure 3.11: Framework of the two-tier method for bridge maintenance planning

3.7.1 Resource planning method

The developed integrative evolutionary-based method is divided into three models, namely discrete event simulation, machine learning and multi-objective optimization (see Figure 3.12). It is designated for modeling and optimizing the performance aspects and utilization rates of limited resources in bridged deck replacement projects (Mohammed Abdelkader et al., 2020h). In the first model, the bridge deck replacement is modeled using STROBOSCOPE simulation platform. The outcomes of this model encompass the performance aspects of the performance aspects of time, cost and greenhouse gases for the different resource allocation plans alongside the utilization rates of resources in the different phases. This output depends on the different input scenarios of resource allocation plans. Martinez (1996) introduced STROBOSCOPE simulation engine to model resourced-based complex operations in diverse fields based on discrete event simulation. It is advised by many researchers because of its programming-based nature, which gives the elements a unique behaviour that provides higher degree of flexibility and extensibility than graph-based simulation platform such as EZStrobe. The first step is to define the logic, constraints, resources and the activities that support the logical sequence required for the bridge deck replacement.

STROBOSCOPE is capable of accommodating both deterministic and stochastic input variables. The productivity rates and direct costs are based on the historical data published in the RSMeans Building Construction Cost Data 2017 (Gordian RSMeans Data, 2017). The fuel consumption rates of the involved construction equipment are adopted from Caterpillar Inc. (2013). The productivity rates and fuel consumptions are assumed stochastic in order to capture the inherent uncertainties and impreciseness associated with the construction processes at the operational level. The productivity rates of the crews and the hourly fuel consumption rates are assumed to

follow normal and triangular distribution, respectively. The distributions were selected due to their simplicity and efficient representation of the input variables in the discrete event simulation model (Kim et al., 2018; Younes et al., 2018). After running the STROBOSCOPE simulation engine, the designated fields from the output report are stored in applicable readable Microsoft Excel format for further analysis. This comprises the involved resources, average utilization factor, standard deviation factor, time, cost and greenhouse gases. The output variables of the performance aspects and utilization rates of resource allocation are represented in the form of normal distributions. In this regard, mean is acceptable in terms of computational complexity and accuracy. The mean of the output distributions is computed to be used as an input for the subsequent computational procedures. The simulation was run 328 times with different resource combination scenarios yielding 328 output files. The Microsoft Excel output files were combined, mapped and appended into the relevant database field.

Simulation models usually invoke numerous iterations, which result in lengthy processing times and CPU intensive simulation process. The presence of large number of activities coupled with the presence of wide resource combinations exhibit a more complex behavior. This high computational complexity results may lead to slow convergence and inferior solutions of the simulation-based optimization models (Parnianifard et al., 2019; Chen et al., 2019). As such, a surrogate model needs to be developed and calibrated to circumvent the shortcomings of the computational time-expensive nature of the discrete event simulation model. The main advantage of the surrogate models is that it capitalizes on the empirical relationships to imitate the input-output behavior of the discrete event simulation process within less computational time and acceptable computational accuracy (Mahmoodian et al., 2018; Song et al., 2018).

The main objective of the second model is to design an efficient, practical and straightforward surrogate machine learning model to mimic the computationally exhaustive discrete event simulation model within an acceptable accuracy. In this regard, the data-driven machine learning is designated for simulating automatically the performance aspects of time, cost and greenhouse gases for the different resource allocation plans in addition to their utilization rates. This comprises two stages, whereas the first surrogate model aims at predicting the efficiency and balance in the utilization of resources through unified metrics based on the number of resources. Then, the utilization rates alongside with the number of resources are fed into a machine learning model to forecast the time, cost and greenhouse gases. The developed model utilizes a hybridization of Elman recurrent neural network and invasive weed optimization algorithm to enhance the prediction accuracy of simulating the afore-mentioned predictors. Training Elman neural networks with meta-heuristic optimization algorithms is a powerful mechanism to improve the search engine of the Elman neural network by addressing the exploration-exploitation trade-off dilemma. The developed model utilizes invasive weed optimization algorithm for both parametric and structural learning. The Elman neural network is trained by designing a variable-length single-objective optimization problem which encompasses a fitness function of minimization of mean absolute percentage error of performance aspects. The steps of the invasive weed optimization algorithm are repeated until satisfying the convergence criteria, i.e., reaching maximum number of iterations. The optimized Elman neural network is appended and utilized to simulate the testing dataset.

The surrogate machine learning model is validated through three phases. The purpose of the first phase is to evaluate the statistical significance of the output of the discrete event simulation model and the machine learning model using Shapiro-Wilk test of normality and Mann-Whitney-

U test. This is done to experiment if the machine learning model can efficiently mimic the discrete event simulation model. The second phase involves its comparison with nine conventional machine learning models reported for their higher accuracies, namely back-propagation artificial neural network, RBNN, GRNN, CONVNET, LSVM, RSVM, GBDT, GP and K – NN. Their performances were evaluated as per mean absolute error, root-mean squared error and mean absolute percentage error. It is worth mentioning that the performances were assessed using split validation and 10-fold cross validation. The K-fold cross validation is used to ensure the training and testing of the entire dataset, which truncates any possibility of over-fitting or over-learning in the pattern recognition phase. The third phase incorporates utilizing non-parametric testing to evaluate the statistical significance level of the outcome of prediction models using the performances of the different folds. Non-parametric tests include Wilcoxon test, Mann-Whitney-U test, Kruskal–Wallis test, binomial sign test and Mood’s median test.

The third model incorporates building a multi-objective differential evolution paradigm to optimize the resources based on the total project duration, total project cost and total greenhouse gases, and subject to the targeted average and dispersion in the utilization of the consumed resources. In this model, the calibrated machine learning models of the previous stage are utilized herein as fitness functions and terms of objective functions. Differential evolution algorithm is exhaustive search engine that demonstrated higher exploration and exploitation capacities in investigating higher-dimension and multi-local spaces (Yagiz et al., 2020; Yu et al., 2018). It is validated through comparisons with a set of well-performing state of the art meta-heuristics, namely multi-objective genetic algorithm, multi-objective particle swarm optimization algorithm, multi-objective dragonfly algorithm, multi-objective grey wolf optimization algorithm, multi-objective Jaya algorithm and multi-objective shuffled frog-leaping algorithm.

The comparisons were conducted as per a set of performance indicators, which included average fitness function values, coefficient of variation of fitness function values, hypervolume indicator, generational distance, spacing, diversity, spread and coverage. These performance metrics can evaluate three main aspects which are: diversity, accuracy and cardinality (Cui et al., 2020; Falahiazar and Shah-Hosseini, 2018). Then, the significance levels of the optimal solutions of the different meta-heuristic optimization algorithms are evaluated using non-parametric testing. Multi-criteria decision making is performed to identify the most feasible solution among the set of Pareto optimal solutions. Shannon entropy is employed to compute the weights of the attributes. Subsequently, Preference Ranking Organization Method for Enrichment Evaluations (PROMETHEE II) is utilized to rank the Pareto optimal solutions according to the net outranking flow. PROMETHEE II is selected over other multi-criteria decision making approaches because of its robustness and efficiency in solving complex problems in diverse fields including optimal site selection of parabolic trough concentrating solar power plant (Wu et al., 2019), sustainability assessment of large scale composite technologies (Makan and Fadili, 2020), and ranking of sub-watersheds threatened by erosion process (Vulević and Dragović, 2017).

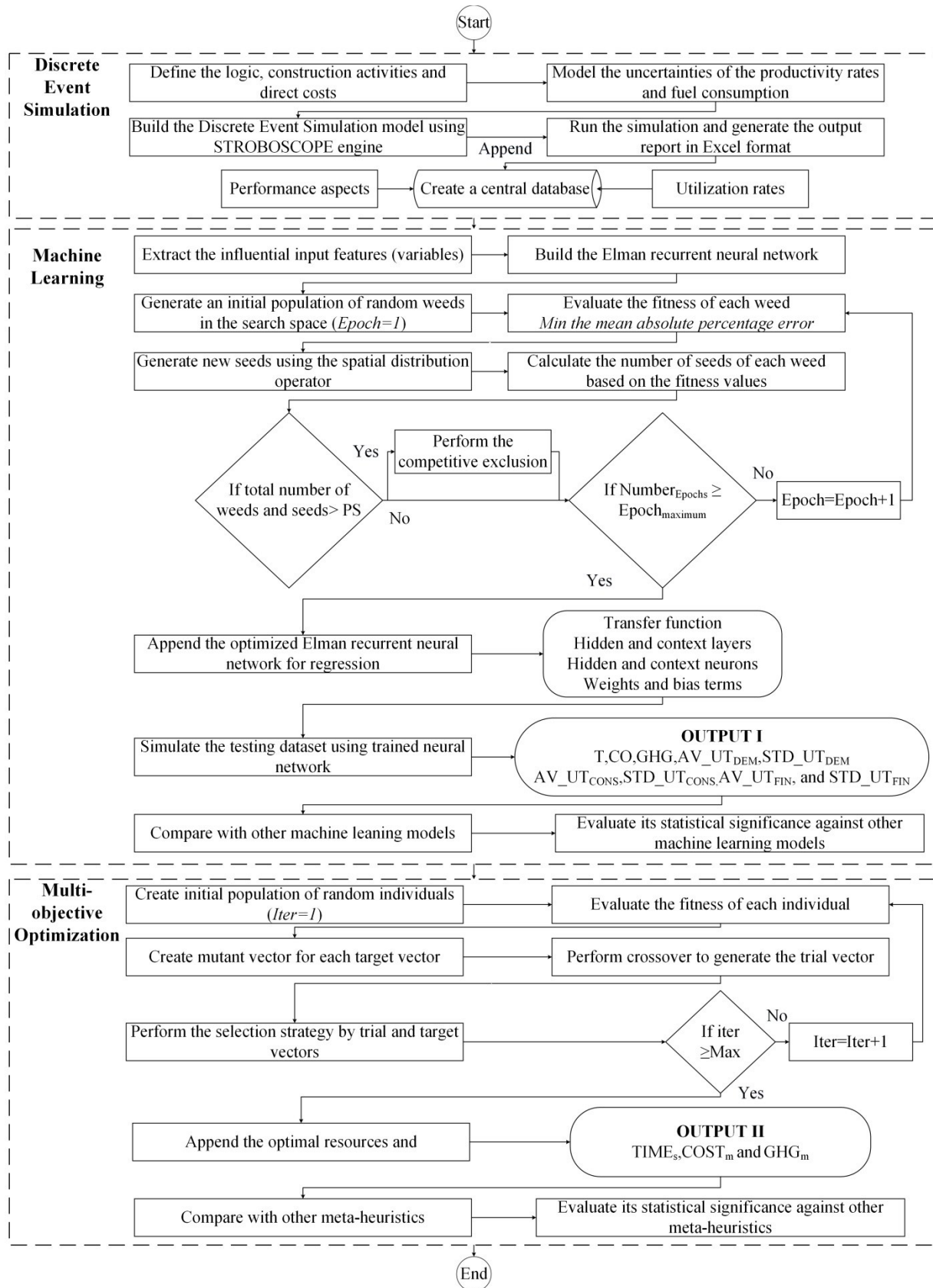


Figure 3.12: Flowchart of the developed integrative evolutionary-based method

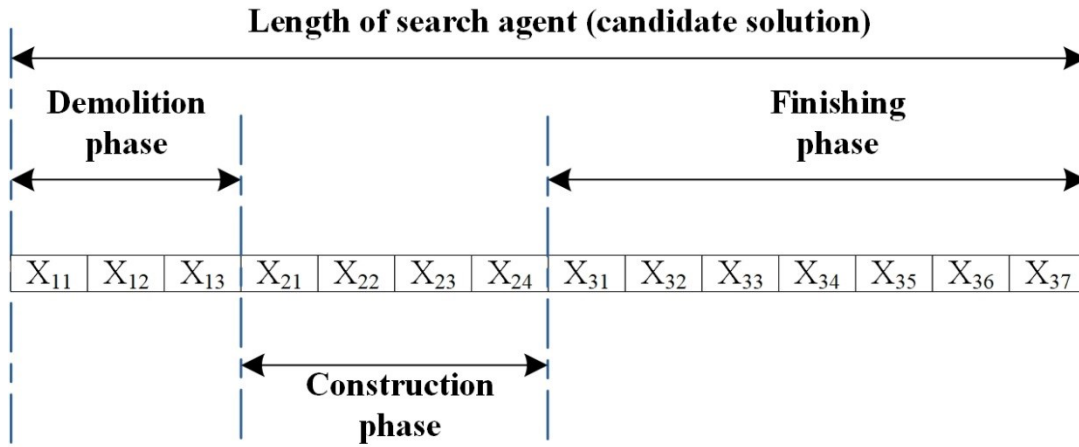
It is expected that the developed integrative evolutionary-based method can provide an efficient multi-objective optimization platform that aids decision-makers to allocate limited resources efficiently through integrating different alternatives and activities in a comprehensive paradigm that enables the fulfilment of targeted objectives and satisfaction of project constraints. It can be also used by the contractors when planning for the resources needed for the bridge deck replacement in an attempt to minimize time, cost and environmental emissions while accommodating the efficiency and uniformity in the utilization of resources. Additionally, it can serve as a template to be used by construction firms in other different construction operations for the purpose of accomplishing better utilization of resources and for minimizing their duration, cost and environmental impact in the delivery of their projects.

- **Multi-objective optimization model**

In the bridge deck replacement process, so many resources, decision variables and constraints are involved. In this regard, a multi-objective differential evolution model is formulated to identify the optimum number of resources such as number of reinforcement crews, number of graders, number of compactors, number of tankers, number of finishers, etc. The nine ENN – IWO models established and calibrated from the previous stage, serve as objective functions, terms of objective functions and constraints.

The solution structure of the multi-objective resource allocation model is depicted in Figure 3.13. As shown in Figure 3.13, the search agent or the candidate solution is structured in the form of a string or vector of elements, whose length denotes the number of decision variables of the multi-objective optimization model. The variable X_{ij} takes integer values range from the minimum allowable number of resources to the maximum allowable number of resources. The length of the vector of decision variables is equal to fourteen, such that this vector encompasses numbers

of hydraulic hammers, loaders and trucks in the demolition phase. It also involves numbers of form crews, rebar crews, stress crews and concrete crews in the construction phase. For the finishing phase, it incorporates numbers of finishing crews, graders, rollers, tankers, finishers, sidewalk finishing crews and painting crews. The vector of optimum solutions is identified capitalizing on minimizing the project duration, project cost and project greenhouse gases as shown in Equations (3.16), (3.17) and (3.18), respectively and satisfying the explicit boundary constraints. The constraints are added to ensure the appropriate efficiency and uniformity (balance) in the utilization of resources as presented in Equations (3.19) and (3.20).



X_{ij} : Number of utilized resources of type i in phase j {1, 2, 3}

Figure 3.13: Schematic representation of a solution structure for resource

$$T_S = \text{Min} [\xi (R_r, P_r)], \forall r \in \{1,2,3,4 \dots \dots \text{CR}\} \quad (3.16)$$

$$C_m = \text{Min} \sum_{r=1}^R R_r \times DC_r \times T_r, \forall r \in \{1,2,3,4 \dots \dots R\} \quad (3.17)$$

$$\text{GHG}_m = \text{Min} \sum_{e=1}^E \text{Cons_Avg}_e \times \gamma_{\text{Diesel}} \times \text{CEF} \times T_e, \forall e \in \{1,2,3,4 \dots \dots E\} \quad (3.18)$$

Subject to;

$$UNI_{AVG_UTIL} = \frac{\sum_{p=1}^{PH} \sum_{r=1}^N UT_{F_{rp}}}{R} \geq C \quad (3.19)$$

$$UNI_{STD_UTIL} = \frac{\sum_{p=1}^{PH} STD_UTIL_p}{PH} \leq B \quad (3.20)$$

Such that;

$$STD_UTIL_p = \sqrt{\frac{\sum_{r=1}^N (AVG_UTIL_p - UT_{F_r})^2}{R}} \quad (3.21)$$

Where;

T_s , C_m and GHG_m stand for the normalized time, normalized cost and normalized greenhouse gas emissions. The time is measured per span while cost and greenhouse gases are measured per square meter. ξ is an operator which represents the discrete event simulation model. R_r and P_r represent the number and productivity of resources, respectively. DC_r indicates the daily direct cost of the resource. T_e represents the actual time spent by the resources in order to account for the in efficient idle periods consumed on site. $Cons_Avg_e$ is average consumption of certain equipment (liters/hour). γ_{Diesel} is density of diesel such that it is assumed 0.832 Kg/l. CEF_e represents the carbon emission factor for diesel, whereas is assumed 3 Kg CO₂-Eq/Kg (Flower and Sanjayan, 2007). $UT_{F_{rp}}$ stands for the utilization rate of the resource r in the phase p . UNI_{AVG_UTIL} represents the unified average utilization rate of resources. UNI_{STD_UTIL} represents the unified standard deviation of utilization rate of resources. AVG_UTIL_p and STD_UTIL_p are the average utilization rate and standard deviation of utilization rate of resources in phase p , respectively. R indicates total number of resources in the project. C and B are threshold values to manage the utilization of resources on site.

- **Multi-criteria decision making**

The objective of the multi-criteria decision making model is to select the best resource allocation plan among the set of Pareto optimal solutions obtained from the multi-objective optimization model. In this regard, Shannon entropy algorithm is applied for the computation of the weighted importance vector of time, cost and greenhouse gases. PROMETHEE II is then employed to rank the resource allocation plans capitalizing on their duration, cost and produced greenhouse gas emissions. Shannon entropy is an objective weighting algorithm that relies on the decision matrix to derive the weighting importance of attributes in an attempt to alleviate the limitations of subjective preference-based weighting algorithms. Entropy is a measure of randomness and uncertainties of information demonstrated by discrete probability distribution, whereas larger amount of information implies smaller uncertainties and entropy values, which indicates that the attribute has higher importance. Entropy can be also utilized to evaluate the degree of dispersion of alternatives associated with a given attribute. In this regard, a higher degree of dispersion implies a greater relative importance of the attribute. The basic computational procedures of the Shannon entropy algorithm can be found in Wu and Hu (2020) and Hafezalkotob and Hafezalkotob (2015).

The family of PROMETHEE approaches were developed by Brans and Vincke (1985) to enable decision makers to establish a ranking of a finite set of alternatives. It is an outranking multi-criteria decision analysis approach that can be applied to generate partial ranking of alternatives (PROMETHEE I) or full ranking of alternatives (PROMETHEE II). A preference function is assigned for each attribute, which enables to determine how much alternative a is preferred over alternative b through mapping the differences in the evaluation of the two alternatives. The preference degrees in the preference functions are represented in a numerical scale ranging from

zero to one, whereas one indicates that alternative a is strongly preferred over alternative b while zero implies indifference preference value between the two alternatives a and b. There are six different types of preference functions including usual criterion, U-shaped (Quasi) criterion, V-shaped criterion, level criterion, V-shaped with indifference (linear) criterion and Gaussian criterion.

In these preference functions, the indifference threshold and preference threshold need to be identified. Indifference threshold (Q) represents the largest deviation that is considered as negligible by the decision maker. Preference threshold (P) denotes the smallest deviation that is regarded as sufficient to generate full preference for the decision maker. A Gaussian threshold (S) is used only in the case of Gaussian preference function. The Gaussian threshold is usually an intermediate value between the indifference threshold and preference threshold. In the present research, V-shaped preference function is selected for the attributes of time, cost and greenhouse gases. It is selected because of its efficiency in dealing with quantitative nature of the present data, which enables to establish a clearer distinction between the evaluations of alternatives. Furthermore, it requires less parameters to be tuned (Brankovic et al., 2018; Kolios et al., 2016). The preference threshold value of each attribute is assumed 60% of the difference between the maximum and minimum performance evaluation (Gervásio and Simões da Silva, 2012). The basic procedures of applying PROMETHEE II are extracted from Brans et al. (1986).

3.7.2 Maintenance planning method

The developed method aims at developing an automated platform that supports both project and network-levels decisions designated for the maintenance budget allocation over a certain planning horizon (Mohammed Abdelkader et al., 2020i). In this method, maintenance plans are considered to be performed by the department of transportation or its agents. The flowchart of

the developed method is depicted in Figure 3.14. As can be seen, the developed method is divided into three main models namely, data input architecturing, multi-objective optimization and hybrid multi-criteria decision-making. In the first model, the first stage is identifying the characteristics of the tackled bridge inventory, which encompasses the type and number of the bridge in the bridge network in addition to the type and number of bridge components in each bridge. In the present research, the lifetime performance of the bridge is demonstrated in the form of three main components, namely deck, pier and abutment. The developed method is designed to deal with short-term and long-term study periods which enable to experiment its performance capacity in both operational and strategic maintenance planning. In this context, the maintenance planning categorizes the intervention strategies into four main types which are: no intervention, minor repair, major rehabilitation and replacement.

The deterioration modeling plays a monumental role in the multi-year maintenance planning at the different decision-making levels. This deterioration mechanism must be properly captured for the different bridge components, whereas each bridge component has a different deterioration trend the other. In the present research, Markov decision process is employed to emulate the deterioration process of the bridge elements because of its capability to handle the uncertainties and vagueness of the deterioration mechanism stemming from the presence of un-observed explanatory variables and in-accurate inspection procedures. The hybrid Bayesian-based described in Chapter 3 approach is adopted to simulate the deterioration process of bridge decks. Regarding the pier and abutment, the transition probabilities are obtained from Hasan (2015).

It should be mentioned that the applied MR&R decision governs both the improvement in the physical condition rating of the bridge element as well as the performance of the bridge element after the employment of the intervention action. The fundamental premise of the condition

improvement functions is that the level of condition performance of the bridge element is improved by an amount that is triggered by the type of the intervention decision. Furthermore, it is worth noting that deterioration transition probability matrices of the bridge element are marked by the application of MR&R action. As such, four deterioration models corresponding to the four intervention actions, are constructed for each bridge component. One of the main objectives of the present research is to address the socio-environmental implications of the maintenance intervention strategies alongside the conventional economic aspects. As such, the user costs, environmental emissions footprint and work zone duration need to be computed. In this context, the work zone duration denotes the length of a time a work activity occupies a certain location. According to the manual on uniform traffic devices (MUTCD), the work duration can be categorized into five main groups namely, mobile, short-duration, short-term stationary, intermediate-term stationary and long-term stationary. The short-duration stands for a work-zone that occupies a location up to one hour while long-term stationary refers to work-zone that occupies a location for more than three days (Datta et al., 2016).

The costs in the bridge's lifecycle cost analysis can be divided into agency costs and user costs. Agency costs refer to the costs incurred by the agency or owner over the lifetime of the facility. User costs refer to costs incurred by the users of the facility as a result of the maintenance operation, which causes traffic disruption or congestion to the normal traffic flow in the facility (Singh and Tiong, 2005). The developed method tackles both agency and user costs in order to establish a holistic analytical platform that enables decision-makers to select the lowest costing alternative. In the developed method, Latin hypercube sampling is utilized to emulate the encountered inherent uncertainties associated with maintenance costs, duration of traffic disruption and environmental impact. These uncertainties are addressed by assuming that the

afore-mentioned parameters are stochastic random variables that follow certain probability distributions. Latin hypercube is stratified sampling scheme that enables better coverage and exploration of the domain of the variations of the input variables. It was stated earlier that the uncertainties of the deterioration process are modeled using the Makrovian model. As such, the developed method is capable to address the uncertainties of the technical, economic, societal and environmental aspects of the maintenance intervention actions, which constitute the main pillars of sustainability-based decision-making process.

The second model is the multi-objective optimization, whereas the developed method deals with multiple objective of maintenance planning. This model is designated for optimizing the MR&R plans through a set of principal objectives which encompass maximization the minimum physical condition rating of the bridge elements, minimization the total intervention costs, minimization the total duration of traffic disruption and minimization of the total environmental impact of the intervention actions. The multi-objective maintenance planning model involves a set of condition and cost constraints that comply with the technical and budget constraints imposed by the transportation agencies. The developed method employs exponential chaotic differential evolution optimization (ECDE) algorithm to optimize the MR&R actions. Chaotic optimization is newly introduced to investigate the maintenance budget allocation of the different assets. In the chaotic processing, the diversity and convergence of the differential evolution are optimized while preserving its original characteristics. The use of chaotic disturbance mechanism enriches the search behavior of the differential evolution capitalizing on amplifying both of its exploration and exploitation. This prevents the differential evolution algorithm from being stagnated in local minima and premature convergence especially in the presence of multimodal search spaces that encompass multiple local minima. In this regard, the multimodal search space is considered as a

substantial challenge for the optimization algorithm to explore in an attempt to find the global optimum solution.

Another advantage of the chaotic mapping is the generated improvement in the diversity of the population. This takes place because the values of the operators are calibrated adaptively over the course of the optimization process which in turn improves the convergence of the differential evolution algorithm. Additionally, the chaotic search saves the computational time consumed in fine-tuning the algorithm's operators to be used in improving the computational efficiency of optimization. Another competitive advantage of the optimization algorithms is that it is less sensitive than the conventional optimization algorithms to the initial setting of values which successively enhances the stability and robustness of the optimization search mechanism (Anter and Ali, 2020; Hekimoğlu, 2019; Mirjalili and Gandomi, 2017). In the present research, the chaotic operations are employed for optimizing the initialization of population and generating chaotic variable sequence for the mutation scaling factor and crossover probability. The strategy of the exponential chaotic mutation scaling factor is formulated based on the integration of exponential distribution function and chaotic maps. The exponential scheme facilitates the efficient exploration of the search space so that the search agents move faster and at distant positions from each other, which in turn aids in converging to the global optimum solution within less number of iterations.

The developed method investigates nine different chaotic maps to find out the most efficient one. These chaotic maps are logistic, Singer, sinusoidal, sine, iterative, Chebyshev, cubic, logistic-sine and circle. The exponential chaotic optimization algorithm is validated through comparisons against state of art meta-heuristics namely, genetic algorithm, particle swarm optimization algorithm, invasive weed optimization algorithm, differential evolution (DE) algorithm, Jaya

algorithm, teaching-learning optimization algorithm and biogeography-based algorithm. The evaluation process of the developed multi-objective chaotic differential evolution optimization model is three-folded. In the first fold, the evaluation comparisons are carried out capitalizing on a set of performance metrics including: minimum and average fitness function values in addition to hypervolume indicator, generational distance, inverted generational distance, spacing and maximum Pareto front error. These performance metrics are capable of judging three main aspects of optimization algorithms which are: diversity, accuracy and cardinality. The second fold is designed for the purpose of evaluating the significance levels of the optimal solution. In this regard, Shapiro-Wilk test is used at first to study the normality of the data at significance level (α) of 0.05. Subsequently, parametric or non-parametric tests are performed relying on the assessment of normality of the data for statistical significance comparison. The third aims at establishing an integrative reflection on the performances of the multi-objective evolutionary algorithms (MOEA) with respect to the accuracy and stability. This is addressed through the average ranking method that is fed by the output generated from the first fold.

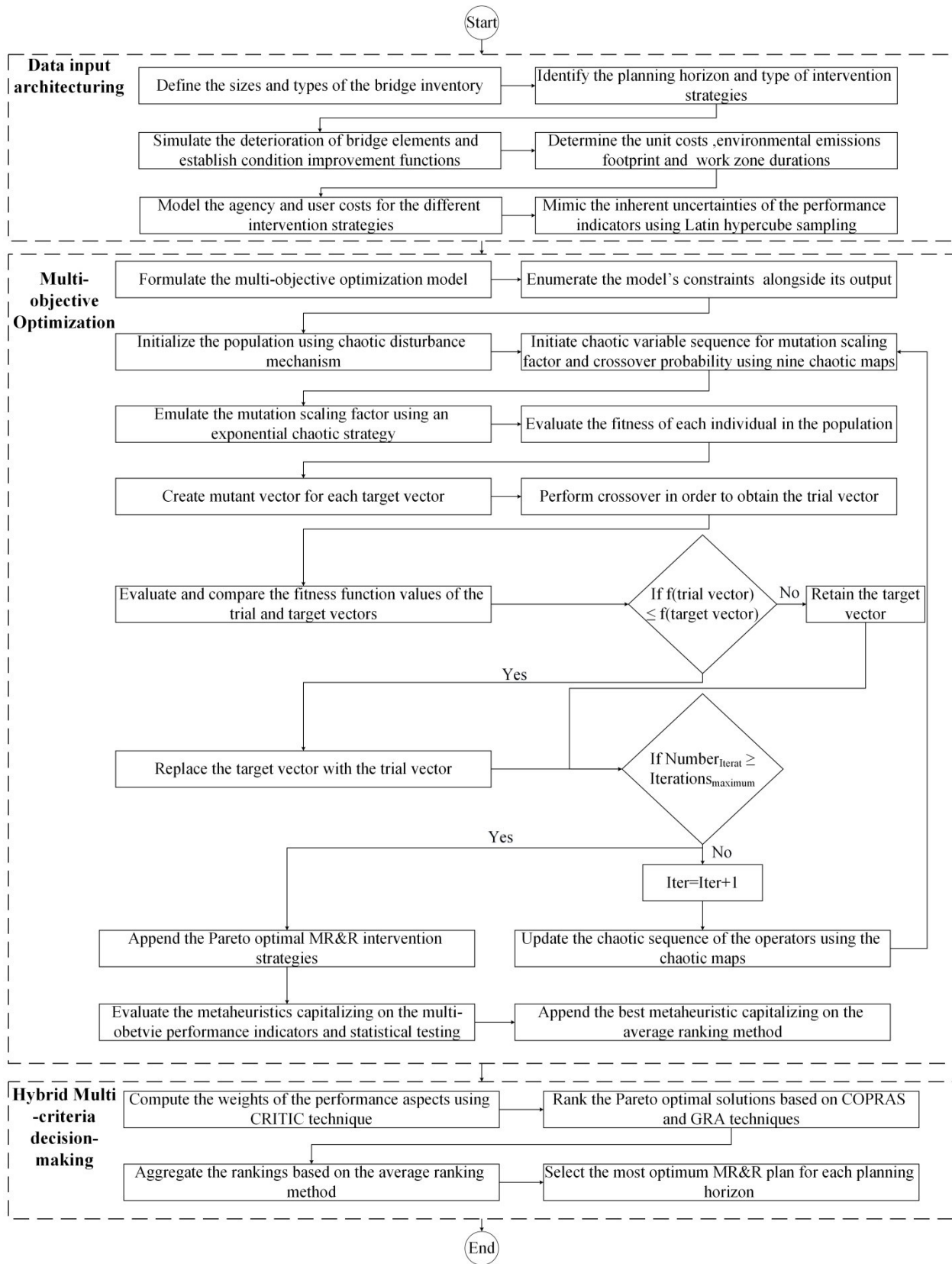


Figure 3.14: Flowchart of the developed maintenance planning method

The third model is the hybrid multi-criteria decision-making which is designed for the purpose of selecting the most optimum MR&R plan for each study period among the set of Pareto optimal solutions. In this model, the weights of the performance aspects are obtained objectively based on the CRITIC technique to overcome the subjective preferences in the weights' assignment. In this algorithm, the information of the criteria is signified by not only the standard deviation of the criteria but also the correlation between the attributes. In this study, a hybrid multi-criteria decision-making approach is proposed to provide a robust and comprehensive ranking of the Pareto optimal solutions. In this regard, complex proportional assessment and grey relational analysis are coupled to generate a final ranking of the Pareto optimal solutions using the average ranking method. COPRAS and GRA are selected because they proved their efficiency in dealing with complex problems of decision-making (Valipour et al., 2017; Ma et al., 2019). Furthermore, they require less parameters than other MCDM approaches in their computational procedures. Additionally, the two MCDM approaches are of different computational nature which paves the way for creating a comprehensive ranking of the solutions.

- **Multi-objective optimization model**

This section describes the different features and constraints of the multi-objective optimization model.

Formulation of the multi-objective optimization problem

The developed multi-objective optimization model considers both project and network-level decisions in the planning of MR&R actions while satisfying the condition rating and budget constraints. In this context, it enables to determine which bridge component to repair, what intervention action to apply and when to perform the intervention action. The solution structure of the multi-objective maintenance planning is depicted in Figure 3.15. As shown in Figure 3.15,

the search agent or the candidate solution is structured in the form of a string of elements, whose length denotes the number of decision variables of the multi-objective optimization model. The variable X_{ijt} takes integer values that range from one to four depending on the type of the intervention action, whereas X_{ijt} of 1, 2, 3 and 4 correspond to no intervention, minor repair, major rehabilitation and replacement, respectively. For instance, minor repair of bridge deck includes crack sealing, patching and removing of spalled or delaminated concrete. Major rehabilitation includes strengthening by adding additional plates or girders in addition to increasing bridge deck thickness.

Additionally, it is worth noting that the developed method can tackle project and network-level decisions by modeling the timely MR&R plans for element i in bridge j at time t . In the present study, a set of principal multiple objectives are modeled for the purpose of multi-year maintenance planning. The objective functions tend to maximize the condition performance level of the bridge elements, minimize the total life-cycle maintenance costs, minimize the duration of traffic disruption and minimize the environmental impact as displayed in Equations (3.22), (3.23), (3.24) and (3.25), respectively.

$$CR = \text{Max} \begin{cases} \min \text{cond}_{\text{deck}} = F[Mt_d, t_d] \text{ |for } d = 1, 2, 3 \dots \dots \dots D \\ \min \text{cond}_{\text{pier}} = F[Mt_p, t_p] \text{ |for } p = 1, 2, 3 \dots \dots \dots P \\ \min \text{cond}_{\text{abutment}} = F[Mt_{ab}, t_{ab}] \text{ |for } ab = 1, 2, 3 \dots \dots \dots AB \end{cases} \quad (3.22)$$

$$TLCC = \text{Min} \sum_{t=1}^T \sum_{j=1}^J \sum_{i=1}^I \frac{TAC_{ijt}}{(1+r)^t} + \frac{TUC_{ijt}}{(1+r)^t} \quad (3.23)$$

$$TDTT = \text{Min} \sum_{t=1}^T \sum_{j=1}^J \sum_{i=1}^I DTT_{ijt} \quad (3.24)$$

$$TEI = \text{Min} \sum_{t=1}^T \sum_{j=1}^J \sum_{i=1}^I EI_{ijt} \quad (3.25)$$

Subject to the following constraints:

$$CR \geq CR_{\min} \quad (3.26)$$

$$TLCC \leq BUD_{\text{available}} \quad (3.27)$$

$$TC_t \leq BUD_t \quad (3.28)$$

$$STD_{MC} \leq STD_{\text{thre}} \quad (3.29)$$

$$\text{Num}_{\text{Interv}} \leq \text{Num}_{\text{thre}} \quad (3.30)$$

Such that;

$$EI_{ijt} = T1 \times \left(\frac{Eghg}{Eghg_{\text{sum}}} \right) + T2 \times \left(\frac{Eap}{Eap_{\text{sum}}} \right) + T3 \times \left(\frac{Epm}{Epm_{\text{sum}}} \right) + T4 \times \left(\frac{Eep}{Eep_{\text{sum}}} \right) + T5 \\ \times \left(\frac{Eod}{Eod_{\text{sum}}} \right) + T6 \times \left(\frac{Es}{Es_{\text{sum}}} \right) \quad (3.31)$$

$$STD_{MC} = \sqrt{\frac{\sum_{r=1}^N (AVG_MC - TC_t)^2}{N}} \quad (3.32)$$

Where;

CR represents the minimum condition rating for all bridge components in all bridges across the planning horizon. It is worth mentioning that the minimum function is adopted instead of the average function because the average function fails to capture the presence of failure in the bridge elements. $\text{min cond}_{\text{deck}}$, $\text{min cond}_{\text{pier}}$ and $\text{min cond}_{\text{abutment}}$ represent the condition

performances of deck, pier and abutment, respectively. Mt_d , Mt_p and Mt_{ab} represent the type of intervention action applied to deck, pier and abutment, respectively. t_d , t_p and t_{ab} depict the time sequences of intervention action applied to deck, pier and abutment, respectively. D, P and AB stand for the total numbers of decks, piers and abutments, respectively.

TLCC depicts the total life-cycle maintenance costs and it is equal to the summation of the discounted maintenance costs applied at time instant t . TAC_{ijt} and TUC_{ijt} depict the total agency and user costs of the intervention action for element i in bridge j at time t . r stands for the monetary discount rate and it is assumed 6% (Xie et al., 2018). TDDT represents the total duration of traffic disruption. DDT_{ijt} stands for the duration of traffic disruption encountered from the MR&R action performed to element i in bridge j at time t . The work zone durations for the different intervention actions are derived from Lindly and Clark (2004) and resource planning developed in the previous section.

TEI is the total environmental impact from the intervention action. EI_{ijt} stands for the environmental impact of the MR&R action performed to element i in bridge j at time t . It is equal to the weighted aggregation of the potentials of the various environmental emissions produced during the intervention process. T1, T2, T3, T4, T5 and T6 indicate the severity percentages of greenhouse gases, sulfur dioxide, particular matter, eutrophication particles, ozone depleting particles and smog, respectively. E_{ghg} , E_{ap} , E_{pm} , E_{ep} , E_{od} and E_s represent potentials of greenhouse gases, sulfur dioxide, particular matter, eutrophication particles, ozone depleting particles, and smog, respectively. $E_{ghg_{sum}}$, $E_{ap_{sum}}$, $E_{pm_{sum}}$, $E_{ep_{sum}}$, $E_{od_{sum}}$, and $E_{s_{sum}}$ represent potential sum of the greenhouse gases, sulfur dioxide, particular matter, eutrophication particles, ozone depleting particles, and smog, respectively. T1, T2, T3, T4, T5 and T6 are

assumed 0.3, 0.1, 0.1, 0.1, 0.3 and 0.1, respectively. The potentials of the six environmental emissions are obtained Athena impact Estimator 5.4.0103 and the developed resource planning method. More information about the modeling of the environmental emissions can be found in Marzouk et al. (2017).

CR_{min} is the minimum allowable condition rating any bridge element is allowed to reach. $BUD_{available}$ denotes the available budget limit for all intervention actions of all bridge elements. TC_t denotes the total maintenance cost at instant t . BUD_t is the yearly budget limit of the intervention actions. STD_{MC} represents the standard deviation of the MR&R expenditures over the planning horizon. STD_{thre} is a threshold that corresponds to the maximum allowable standard deviation of the MR&R costs. AVG_{MC} is the average maintenance costs over the planning horizon. This constraint is imposed to establish a balanced MR&R cost profile as much as possible through minimizing the variations and fluctuations of the MR&R expenditures over the course of the study period. Num_{Interv} is the number of intervention actions for all bridge elements. Num_{thre} is the maximum allowable number of visits over the time horizon. This constraint is assigned to decrease the number of intervention visits, which in turn minimizes the traffic disruption.

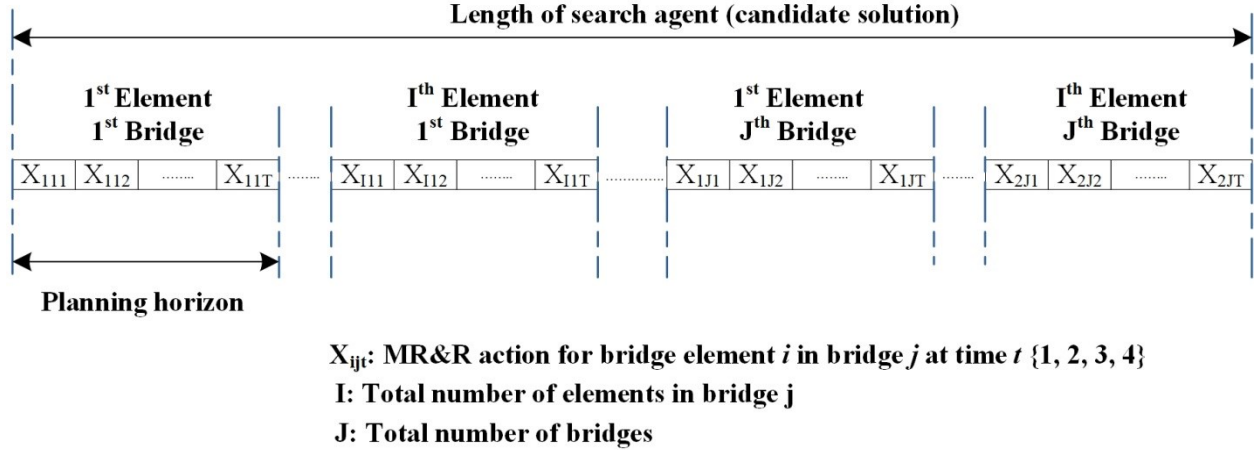


Figure 3.15: Schematic representation of a solution structure for a typical bridge network

Maximization of bridge's condition rating

As mentioned earlier, one of the key objectives of the multi-objective optimization model is to maximize the performance condition rating of the bridge elements. This is accomplished through the deterioration modeling of the bridge elements, which enables to emulate the condition rating of the bridge element over time. In this context, the transition probabilities of the deterioration model are mapped according to the preventive or corrective MR&R action. If the bridge deck undergoes no MR&R action, the transition probability matrix can be defined using Equation (3.33). The transition probability matrices of minor repair, major rehabilitation and replacement are displayed in Equations (3.34), (3.35) and (3.36), respectively (Hong et al., 2013).

$$p_{t,t+1} = \begin{bmatrix} P_{11} & 1 - P_{11} & 0 & 0 \\ 0 & P_{22} & 1 - P_2 & 0 \\ 0 & 0 & P_{33} & 1 - P_{33} \\ 0 & 0 & 0 & 100\% \end{bmatrix} \quad (3.33)$$

$$p_{t,t+1} = \begin{bmatrix} P_{11} & 1 - P_{11} & 0 & 0 \\ P_{11} & 1 - P_{11} & 0 & 0 \\ 0 & P_{22} & 1 - P_{22} & 0 \\ 0 & 0 & P_{33} & 1 - P_{33} \end{bmatrix} \quad (3.34)$$

$$p_{t,t+1} = \begin{bmatrix} P_{11} & 1 - P_{11} & 0 & 0 \\ P_{11} & 1 - P_{11} & 0 & 0 \\ P_{11} & 1 - P_{11} & 0 & 0 \\ 0 & P_{22} & 1 - P_{22} & 0 \end{bmatrix} \quad (3.35)$$

$$p_{t,t+1} = \begin{bmatrix} P_{11} & 1 - P_{11} & 0 & 0 \\ P_{11} & 1 - P_{11} & 0 & 0 \\ P_{11} & 1 - P_{11} & 0 & 0 \\ 0 & P_{11} & 1 - P_{11} & 0 \end{bmatrix} \quad (3.36)$$

Where;

P_{11} , P_{22} and P_{33} represent the probabilities that a bridge element remain in condition state 1, condition state 2 and condition state 3, respectively.

The condition improvement functions are mapped stepping on the type of MR&R action. After applying the minor repair, the condition states 2, 3 and 4 are improved to the condition states 1, 2 and 3, respectively. After the implementation of major rehabilitation, the condition states 2, 3 and 4 are enhanced to the condition states 1, 1 and 2, respectively. If the bridge element is replaced, it will return to its condition state (Hong et al., 2013; Lee et al., 2011).

Minimization of maintenance costs

The maintenance cost is divided into two main components, namely agency and user costs. Agency costs are monetary values incurred by the agency as a result of applying the intervention actions. They are usually estimated as cost per unit area. Table 3.1 represents the agency cost of the intervention actions for the bridge deck. They are adopted from the developed resource planning method and the research study introduced by Shim and Lee (2017). The second component of the maintenance costs is the user cost, which represents the cost incurred by the users or the travelling public during the maintenance activity. This cost is fundamentally attributable to the restriction imposed on the use of the bridge as a result of the MR&R action.

This restriction or construction work induces additional costs and delays because of the additional travel time and vehicle operating costs. The user costs depend primarily on the duration of work zone, average daily traffic and the increase in the accident rate because of the work zone, whereas the increase in the pre-mentioned parameters can result in as substantial increase in the user costs. In the case of bridges associated with high volumes of traffic, the user cost may exceed the agency costs. In the present study the user cost of a work zone is evaluated with respect to travel delay costs, vehicle operating costs and the accident costs (Ehlen and Marshall, 1996).

Table 3.1: Intervention actions and their corresponding unit costs for bridge deck

Type of intervention action	Unit cost (\$/m ²)
Minor repair	107.19
Major rehabilitation	238.86
Replacement	695.76

Exponential chaotic differential evolution algorithm

A revised algorithm that integrates a chaotic and exponential search mechanism with the differential evolution algorithm is proposed to circumvent the shortcomings of the classical meta-heuristic optimization algorithms. In the recent years, chaotic variable sequences generated from chaotic mapping mechanisms have been successfully applied in partial applications. Chaos can be defined as ubiquitous a dynamic non-linear phenomenon that exhibits infinite periodic movements in non-linear systems, and it is characterized by its irregularity, intrinsic stochastic property, randomness and ergodicity.

Ergodicity property is an outstanding feature of chaotic systems that describes dynamical systems that has the same behavior averaged over time as averaged over space of all the system's space. This property enables to transit and search every state and node in the finite search space within certain range without repetition through a deterministic formulation. Chaos can be also viewed as a highly unpredictable and unstable motion of dynamical systems in a finite search plane. Thus, a non-linear system can be called chaotic if it exhibits sensitive-dependence on the initial conditions of the chaotic processing, and experiences infinite unstable periodic motions across the non-linear system. This is expected to amplify the search behavior and diversity of the generated solutions in the multimodal objective search space, which in turn prevents the differential evolution from premature convergence to local optimum solutions (Tharwat et al., 2019; Sayed et al., 2018).

In this research, nine different types of chaotic map sequences are experimented, namely logistic map, sine map, sinusoidal map, singer map, circle map, cubic map, iterative map, Chebyshev map, logistic-sine map (Anter and Ali, 2020; Demir et al., 2020; Tharwat et al., 2019).

Differential evolution with chaotic sequences

The population initialization, mutation scaling factor and crossover probability are key factors affecting the convergence of the differential evolution algorithm and quality of final solutions. As such, the developed method adopts chaotic population initialization and chaotic operators to alleviate the shortcomings of conventional meta-heuristics through amplifying the search mechanism of the differential evolution optimization algorithm. This due to the fact the chaotic variables can travel ergodically over the whole search space of interest. Random initialization is the most commonly-utilized approach to generate initial population. However, this approach may lead search agents to be far away from the population. In this context, chaotic population

initialization is at first carried out to enhance the diversity of the initial population which enables the differential evolution to prevent local optimum solutions and find global optimum solutions. This is accomplished by generating an D-Dimensional vector $Z_0 = [Z_{01}, Z_{02}, Z_{03} \dots \dots \dots Z_{0D}]$, such that each of its elements is random number in the range $[0, 1]$. Then, chaotic queues $[Z_1, Z_2, Z_3 \dots \dots \dots Z_{NP}]$ are generated based on the designated chaotic map. Then, the chaotic queues are mapped to the desired optimized parameters' range.

With respect to the crossover probability and mutation scaling factor, the chaotic dynamics is incorporated for the purpose of their tuning. As mentioned earlier, the search performance of the differential evolution is significantly influenced by the control parameters of crossover probability and mutation scaling factor, whereas proper setting of their values plays a monumental role in the success of their important. The difficulty arises from the methods of selection of optimum parameter values which are usually capitalized on empirical evidence and practical experience. These trial and fine-tuning-based methods require high computational effort because of the large number of runs needed for the optimum setting of parameters of differential evolution scheme. Additionally, these control parameters are constant across the whole exploration process. Thus, the mutation scaling factor and crossover probability can't guarantee the optimization's ergodicity in the search space. In the light of forgoing, the crossover probability and mutation scaling factor are modeled and tuned as chaotic variables to substitute the random numbers of the classical algorithm through establishing a self-adaptive dynamic parameter control mechanism. It is expected that this chaotic dynamics-based mechanism is capable of amplifying the search behaviour by improving the balance between the exploration and exploitation during the disturbance process. The chaotic sequences of the crossover probability based on the circle map can be formally expressed as follows.

$$CR_{G+1} = CR_G + b - \frac{a}{2\pi} \times \sin(2\pi CR_G) \text{mod}(1) \quad \text{such that } G = [1, 2, 3 \dots \dots G_{\max}] \quad (3.37)$$

With respect to the mutation scaling factor, it is tuned based on hybridization of the merits of both chaotic sequences and exponential distribution. From one side, the nature of exponential scheme presents a faster mechanism to explore the design space. From the other side, chaotic behavior avoids optimization problems from stagnation in local optimum. This in turn is expected to accomplish faster convergence and better solutions. The strategy of exponentially-decreasing chaotic mutation scaling factor based on the logistic-sine map is formulated as follows.

$$F_{G+1} = [(e^{\frac{-2G}{G_{\max}}}) \times (F_{\max} - F_{\min})] + [(\beta \times F_G \times (1 - F_G) + \frac{(4 - \beta)}{4} \times \sin(\pi F_G)) \text{mod}(1)] \times F_{\min} \quad (3.38)$$

Where;

F_{\min} and F_{\max} stand for the initial and final mutation scaling factors, respectively. $\text{mod}(\cdot)$ is the modulus operator.

- **Hybrid multi-criteria decision-making**

This objective is designed for selecting the best solutions among the set of Pareto optimal solutions. In this context, CRITIC technique is utilized to compute the weighting importance vector of the condition performance level, total life-cycle maintenance costs, the duration of traffic disruption and the environmental impact (Diakoulaki et al., 1995). This objective weighting approach is data dependent, and deals directly with the decision matrix when deriving the weights of attributes. Thus, it doesn't need pairwise comparison matrices or decision-maker's judgements like subjective referencing-based techniques. The objective weight of the attributes

signifies the real features and amount of information stored in each one. This technique is based on two dimensions generated from the measures of performance of criteria in the multi-criteria decision analysis, namely comparative intensity and conflict. The first dimension is captured by the standard deviation which analyzes the measure performance of the evaluated alternatives in each criteria separately. The second dimension is tackled by the correlation coefficient between each pair of attributes. COPRAS and GRA are incorporated to sort the optimal solutions based on a different theoretical concept, whereas COPRAS relies on the utility degrees of the different alternatives for their ranking. On the other hand, GRA is established based on the grey theory, and it utilizes the grey relational grade to analyze the reference series and the alternative series. Each technique produces a distinct ranking from the other. Thus, average ranking (AR) method is applied to derive the final global ranking of the optimal solutions for the sake of accurate and comprehensive assessment. It provides an integrative view of the performances of an algorithm from the perspectives of accuracy and robustness. This is accomplished through computing the mean and standard deviation of the ranks (Yu et al., 2018).

▪ **Computation of search space size**

The search space size plays a fundamental role in selecting the optimization algorithm designated for optimizing bridge maintenance plans. Programming a maintenance preservation plans requires dealing with large numbers of components in a bridge network using a set of possible MR&R strategies. The number of possible combinations for a maintenance programming model can be computed using Equation (3.39)

$$SOL_SZ = (N_{repair})^{N_{Comp} \times T} \quad (3.39)$$

Where;

SOL_SZ represents the solution search space size and it is computed using the number of possible combinations due to the discrete nature of decision variables. N_{Comp} and N_{repair} indicate number of possible combinations and number of possible MR&R actions, respectively. T stands for length of study period. It is worth mentioning that Equation (3.39) is used on condition that more than one bridge component can be visited each year. The well-known complexity classes in computational complexity theory comprise P, NP, and NP – hard. P or polynomial problems stands for the problems which can be solved in a polynomial time by a deterministic Turing machine. NP stands for non-deterministic polynomial time and it refers to a complexity class of decision problems which cannot be solved in a feasible polynomial time but can be verified in a polynomial time by a deterministic Turing machine. NP – hard are the most complex class of problems in computer science. They can be defined as a class of problems which are not only hard to solve but cannot be verified in polynomial time (Pokharel, 2020; Zhang et al., 2018).

The SOL_SZ is 1.15×10^{58} in the case of presence of a bridge network 22 components, four possible MR&R actions and 35-year study period. As such, the presence of computationally expensive search space, large number of objective functions, combinatorial nature of optimization maintenance optimization problem, and existence of hard constraints that cannot be violated call for the implementation of efficient optimization search algorithm. It is worth mentioning that solving discrete optimization problems is much more complex and harder than solving continuous optimization problems (Le et al., 2019; Su et al., 2018). This state of affairs causes exact optimization methods to fail to solve the present NP – hard problem and meta-heuristics need to be applied to search for the near-exact optimal solutions (Petroodi et al., 2019; Bagloee and Sarvi, 2018).

CHAPTER IV: COMPUTER AIDED APPLICATIONS

4.1 Overview

All the previous developed methods are automated as standalone computer applications with partially autonomous linkage between them. They are automated using a computerized platform that encompasses a hybridization of C#.net and Matlab programming languages. It is expected that the automated paradigm is capable of exploiting the compatibility and versatility capabilities of C#.net and the superior computational capacity of the Matlab. The developed computer aided application works off-line. However, it may be extended in the future to work as on-line web application. This chapter presents interactive screens of some programmed computer applications for surface defects evaluation, deterioration modeling and maintenance optimization. Additionally, it provides sample of the source code written for the programming of the developed methods.

4.2 Autonomous Surface Defects Evaluation

The developed methods are programmed in Microsoft Visual Studio 2010, Microsoft SQL server 2010, visual C#.net, and Matlab. C#.net is a simple, modern, and object-oriented language, which is derived from C and C++. C#.net language is utilized due to its effectiveness, and flexibility of integration with other modules (Qu et al., 2011). The developed model incorporates a programming language, which is C#.net in addition to a scripting language, which is Matlab. The windows application is designed using Microsoft Visual Studio 2010, which helps to integrate the developed model with the Matlab scripts. Three references were added in order to be able to communicate with other programs:

- 1- “MSBNx” which is a COM reference used to communicate with the Microsoft belief networks software.

- 2- “MLApp” which is a COM reference used to communicate with Matlab scripts.
- 3- “Microsoft.Office.Interop.Excel” which is a .net reference used to communicate with Microsoft Excel files.

The developed computerized platform for automated recognition of surface defects gives the user the flexibility to select between the single restoration process and hybrid restoration process in the image restoration based on the developed filtering protocol (see Figure 4.1). Then, by clicking the “Import” button, the restored image is displayed. The next module is the contrast enhancement, whereas the user is asked to specify the adjusting ratio and margin parameter. As shown in Figure 4.1, the min-max gray level discrimination method is capable of discriminating the gray intensities in the potential defected and non-defected regions. The interface of the feature extraction model for bridge defects recognition in the computerized platform is shown in Figure 4.2. By clicking “View” button, the singular values vector for the different images are displayed and By clicking “Plot”, the distribution of singular values are plotted.

The interface of the developed SVD – ENN – IWO model for defects recognition is depicted in Figure 4.3. In the computerized platform, the user is asked to identify the ranges of the optimization hyper parameters of Elman neural network alongside the parameters of invasive weed optimization algorithm. As can be seen, the upper bounds of number of hidden layers, context layers, hidden neurons and context neurons are assumed 15. The output of this model is obtained by pressing the “View” button. In the surface defects evaluation model, the interface of the spalling detection model is presented in Figure 4.4. The user is asked to specify the entropy index of the Renyi’s entropy segmentation model as well as the parameters of the invasive weed optimization algorithm. The outcome of this module is the optimum threshold, Kapur and Renyi’s entropy fitness function values, set of performance indicators in addition to the

segmented image (See Figure 4.4). The interface of the developed feature extraction model for surface defects evaluation is depicted in Figure 4.5. The automated platform gives the user the flexibility to select between Haar, Daubechies 1, Symlet 1 and Coiflet 5 wavelet transforms to build the frequency domain feature vector set. In the present study, Haar wavelet transform is selected. By clicking “View” button, the singular values of the spatial domain features alongside the energies of wavelet sub-bands of frequency domain features retrieved from the gray-level images are computed.

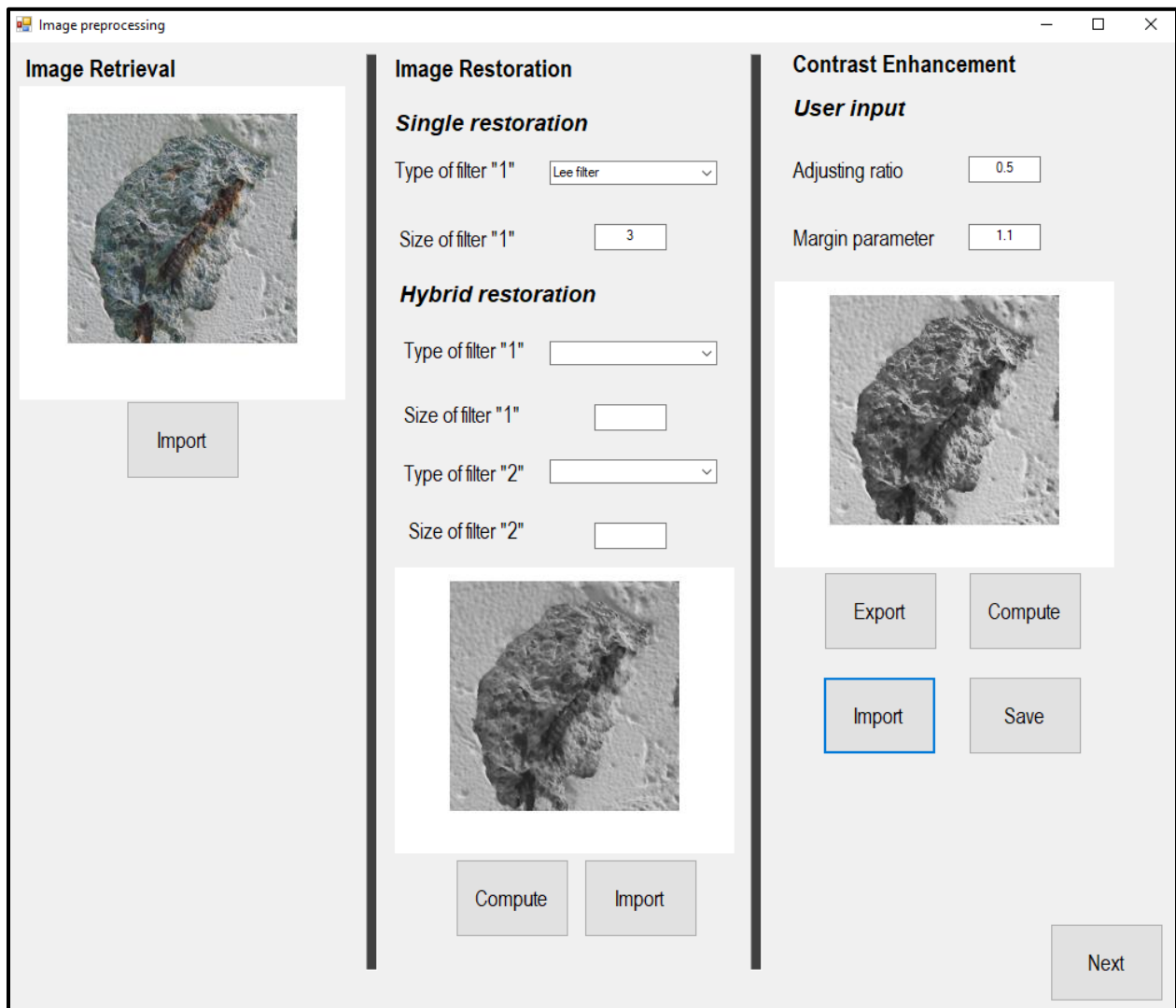


Figure 4.1: Interface of the developed preprocessing module of surface defects

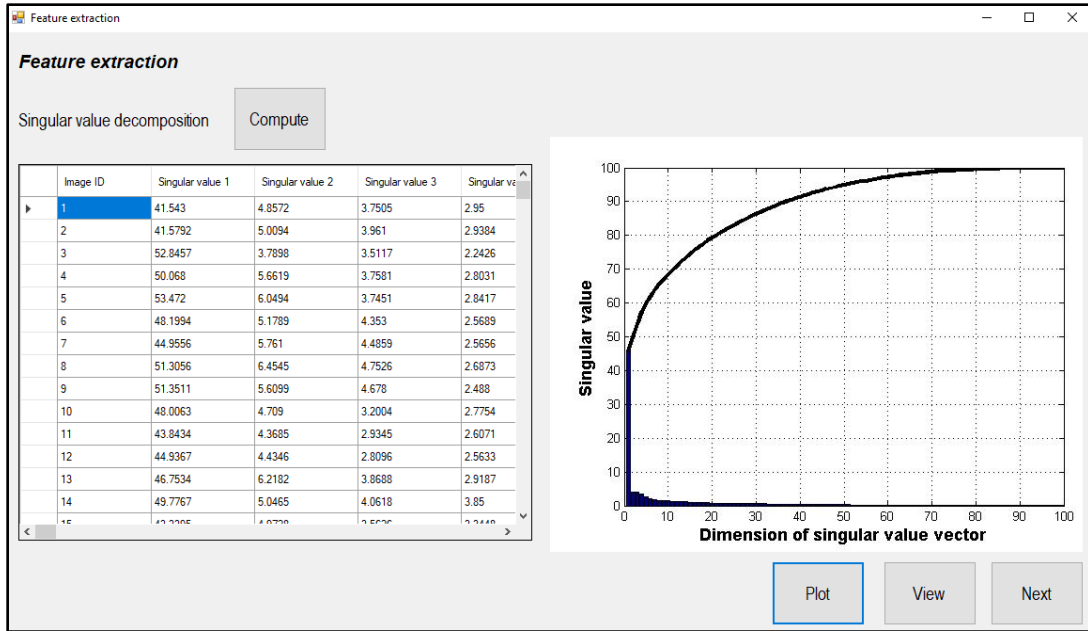


Figure 4.2: Interface of the developed feature extraction model for bridge defects recognition

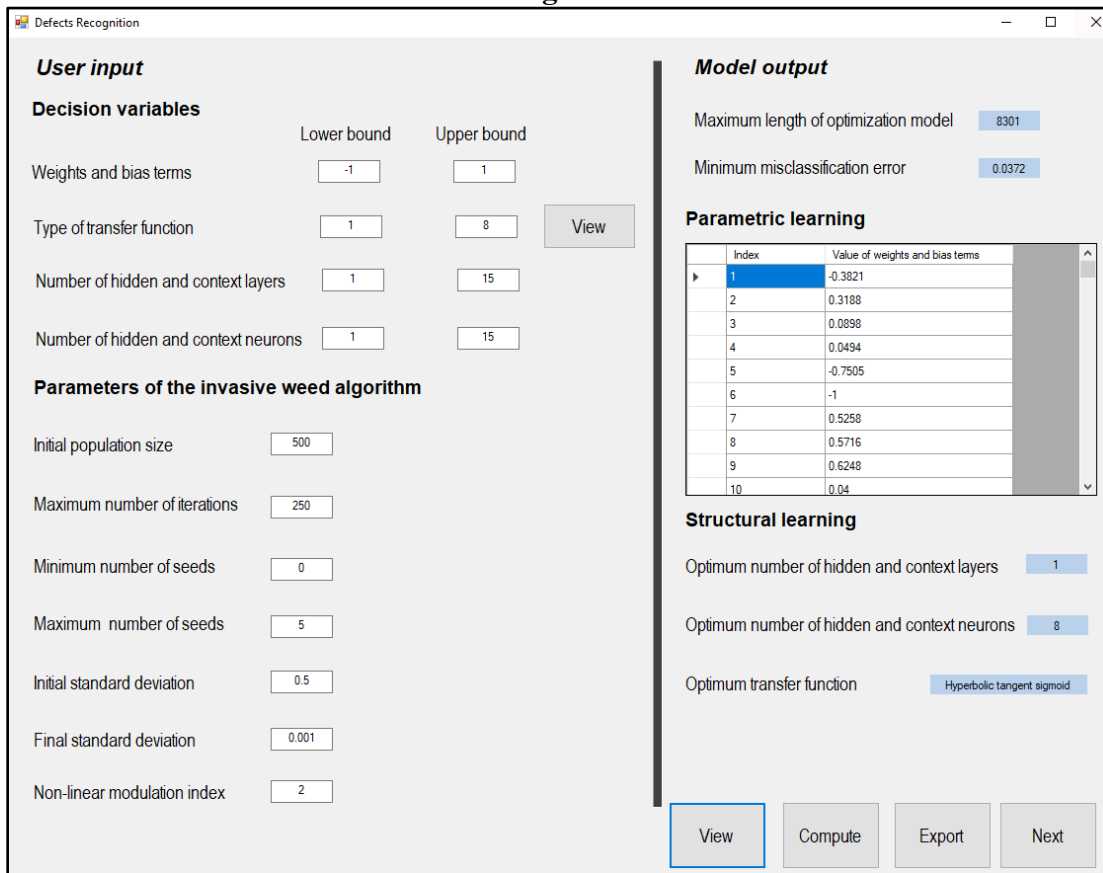


Figure 4.3: Interface of the developed SVD – ENN – IWO model for bridge defects recognition

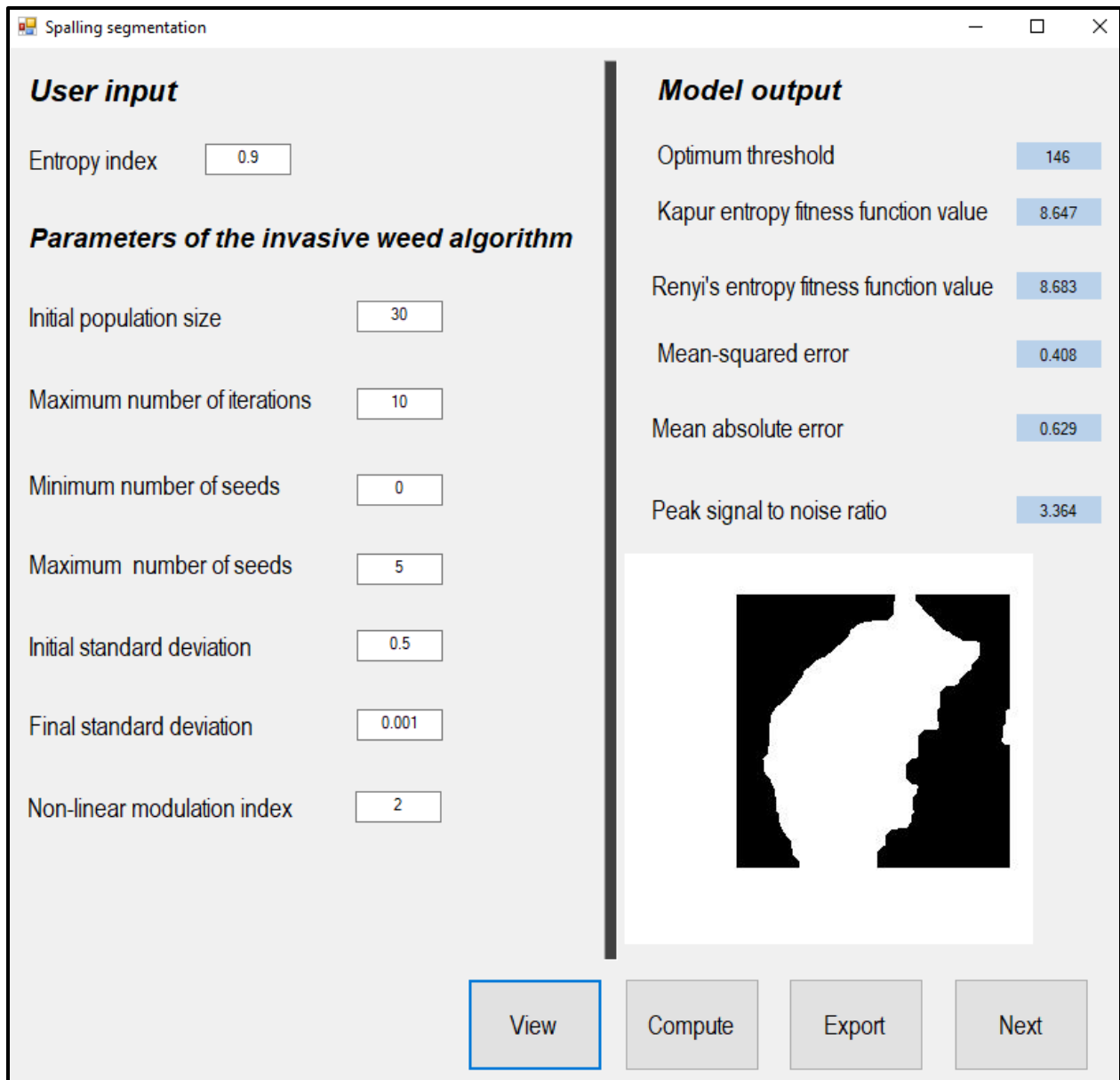


Figure 4.4: Interface of the developed spalling detection model

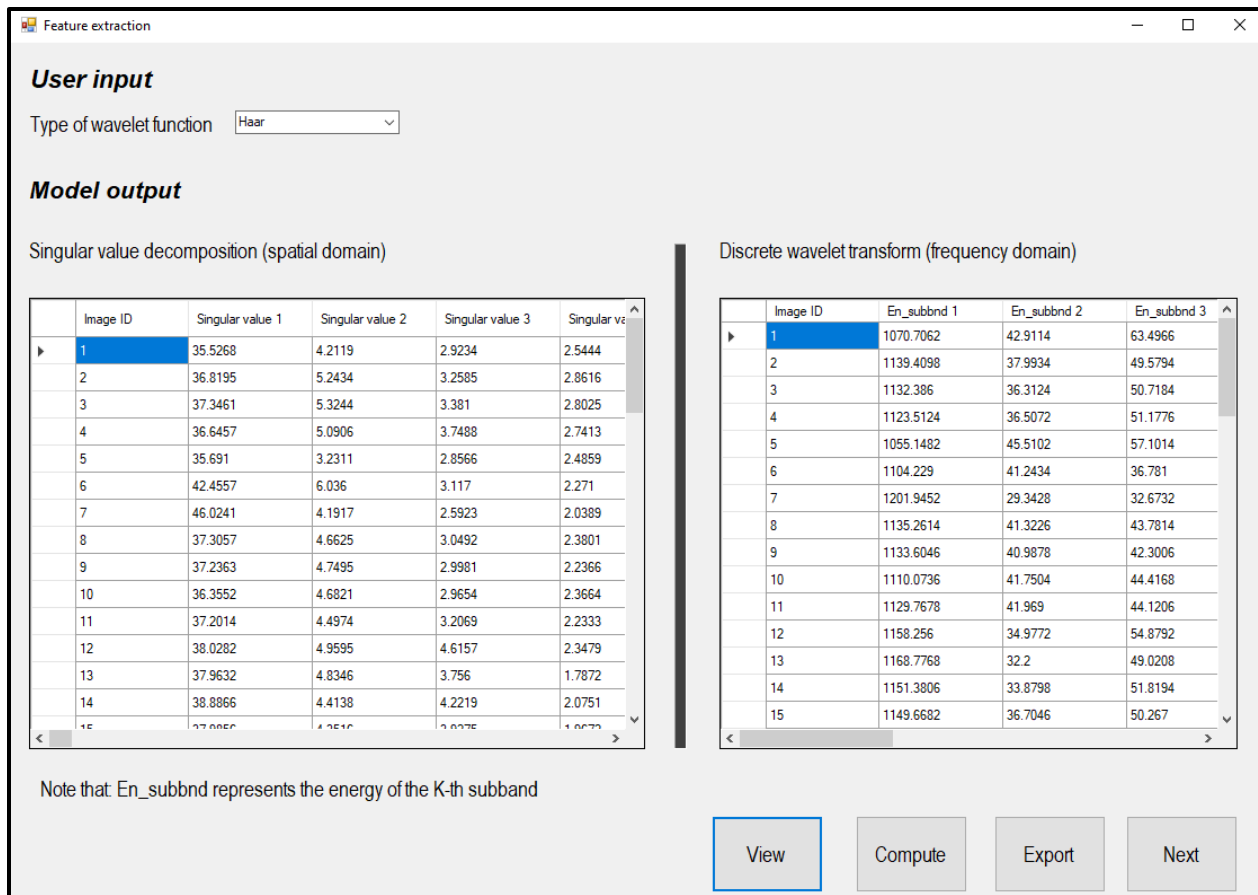


Figure 4.5: Interface of the developed feature extraction model for bridge defects evaluation

4.3 Autonomous Deterioration Modeling

A sample of the C#.net written in the standalone computer application designated for deterioration modeling is shown in Figure 4.6. The shown code enables the developed platform to access the inference engine and the nodes of the Bayesian belief network. The automated paradigm enables the user to calculate the known conditional probabilities. As shown in Figure 4.7, the “Import” button enables the user to enter the events and the transition time associated with each event in a Microsoft Excel sheet. Then, by clicking “View” button, the automated tool calculates the conditional probability, defines the type of the probability distribution of the transition time in addition to the parameters of the probability distributions.

For the unknown conditional probabilities, they are calculated based on the maximum entropy approach. As shown in Figure 4.8, the user is asked to specify the following parameters: population size, number of iterations, crossover rate, mutation rate, number of elites, type of parents' selection strategy, and the tournament size in the case of the tournament selection strategy. The computerized tool enables the user to choose between three parents' selection strategies which are: roulette wheel strategy, tournament selection strategy, and uniform selection strategy.

```
Microsoft.Office.Interop.Excel.Range mycells;

myexcel.Workbooks.Open(@"C:\Users\abdelkader\Desktop\Automation\LHS1.xlsx");

myexcel.Visible = true;

MYWORKSSET = myexcel.Worksheets.Item[1];

mycells = MYWORKSSET.Cells;
MSBN aMSBN = new MSBN();

Model modelCat = aMSBN.Models.Add("Cat", Directory.GetCurrentDirectory() + @"..\..\..\P12.dsc",
Directory.GetCurrentDirectory() + @"..\..\..\loadererror.log");

Node nodeTransition = modelCat.ModelNodes["Transition"];
Node nodeCorrosion = modelCat.ModelNodes["Corrosion"];
Node nodeDelamination = modelCat.ModelNodes["Delamination"];
Node nodeCracking = modelCat.ModelNodes["Cracking"];
Node nodeSpalling = modelCat.ModelNodes["Spalling"];
Node nodePopout = modelCat.ModelNodes["Popout"];

Dist aDist = nodeTransition.get_Dist();
```

Figure 4.6: A sample of the C#.net code written for the deterioration model platform

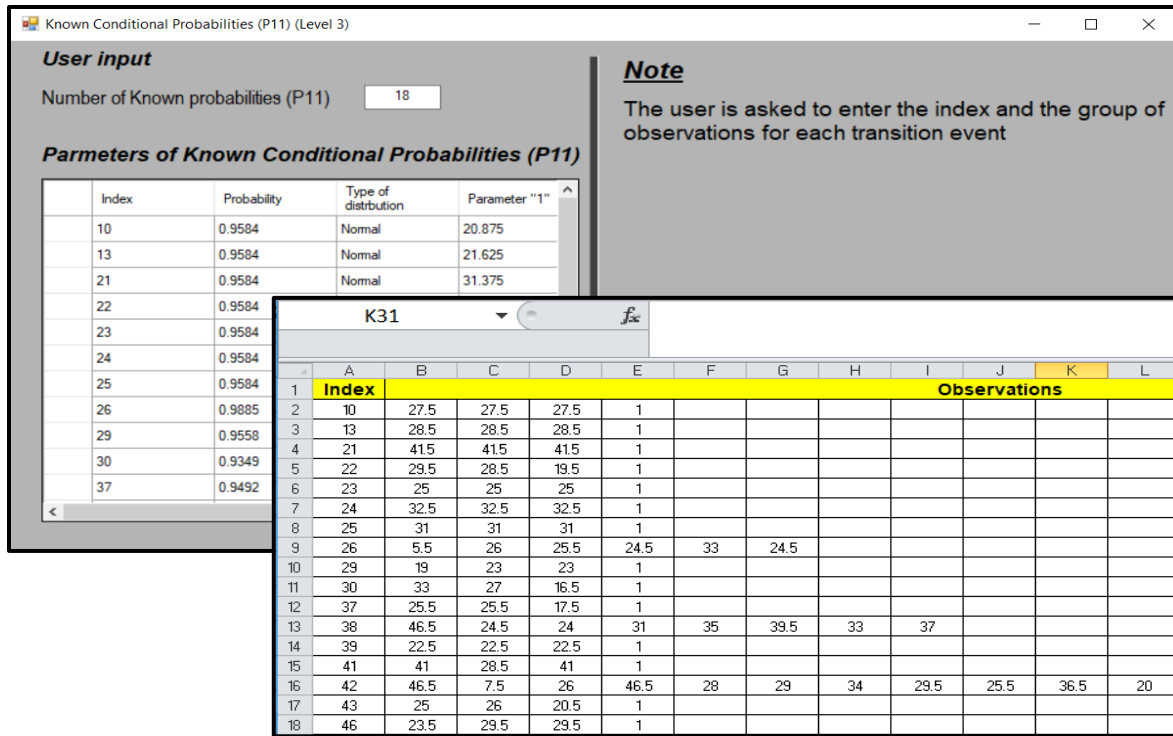


Figure 4.7: Interface and output of the conditional probabilities module

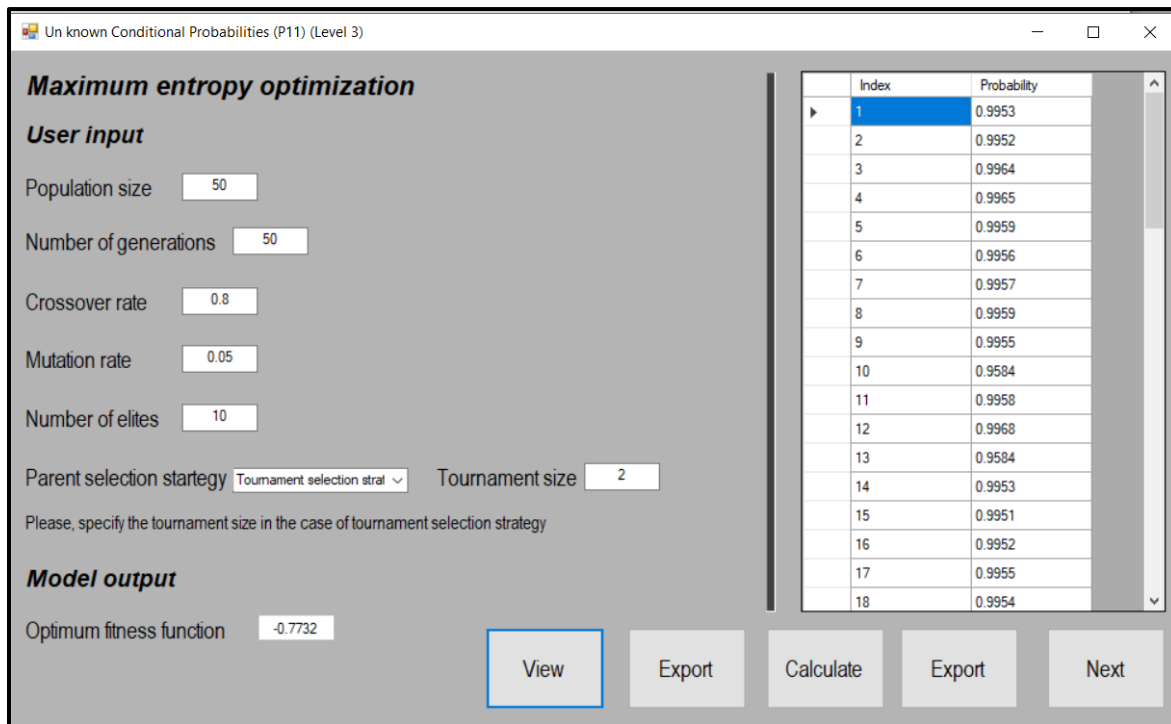


Figure 4.8: Interface of the unknown conditional probabilities module

The interface of the Metropolis-Hastings algorithm module is shown in Figure 4.9. By clicking the “View” button, three types of output are provided. First, the values of the samples of the in-state probability P_{11} are then shown in the data-grid view. The second output of the Metropolis-Hastings module is a group of trace plots for the in-state probabilities. The trace plots are as follows: posterior distributions, sampling process, convergence of the mean, and autocorrelation function.

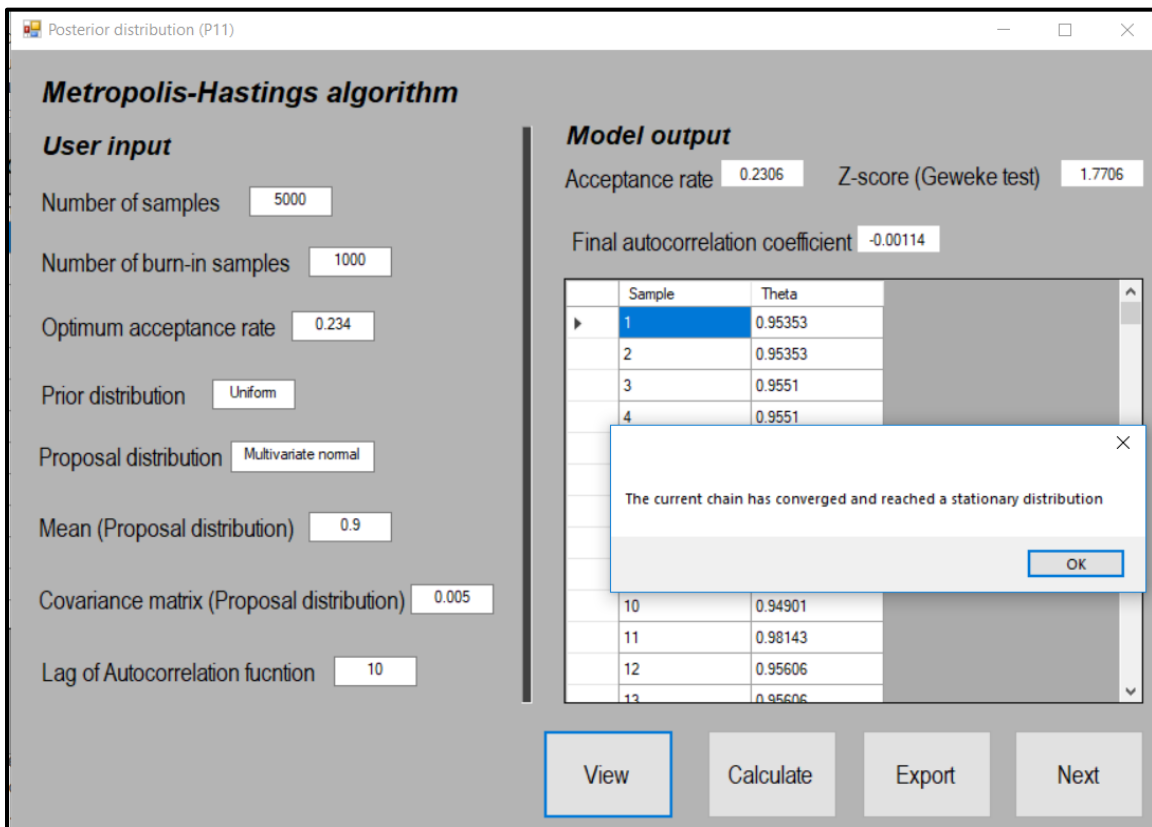


Figure 4.9: Interface of the Metropolis-Hastings algorithm model

The final output of the stochastic optimization module is the transition probabilities for each zone. The interface of the stochastic optimization model is illustrated in Figure 4.10. The stochastic optimization module enables the user to define the following: 1) number of elements in each condition state, 2) study period, and 3) parameters of the genetic algorithm. The user first

clicks the “Import” button, which enables he/she to enter the number of elements in each condition state in a Microsoft Excel sheet. By clicking the “View” button, three types of outputs are provided. The outputs of the model encompass optimum fitness function value, transition probability matrix for each zone, and convergence graph.

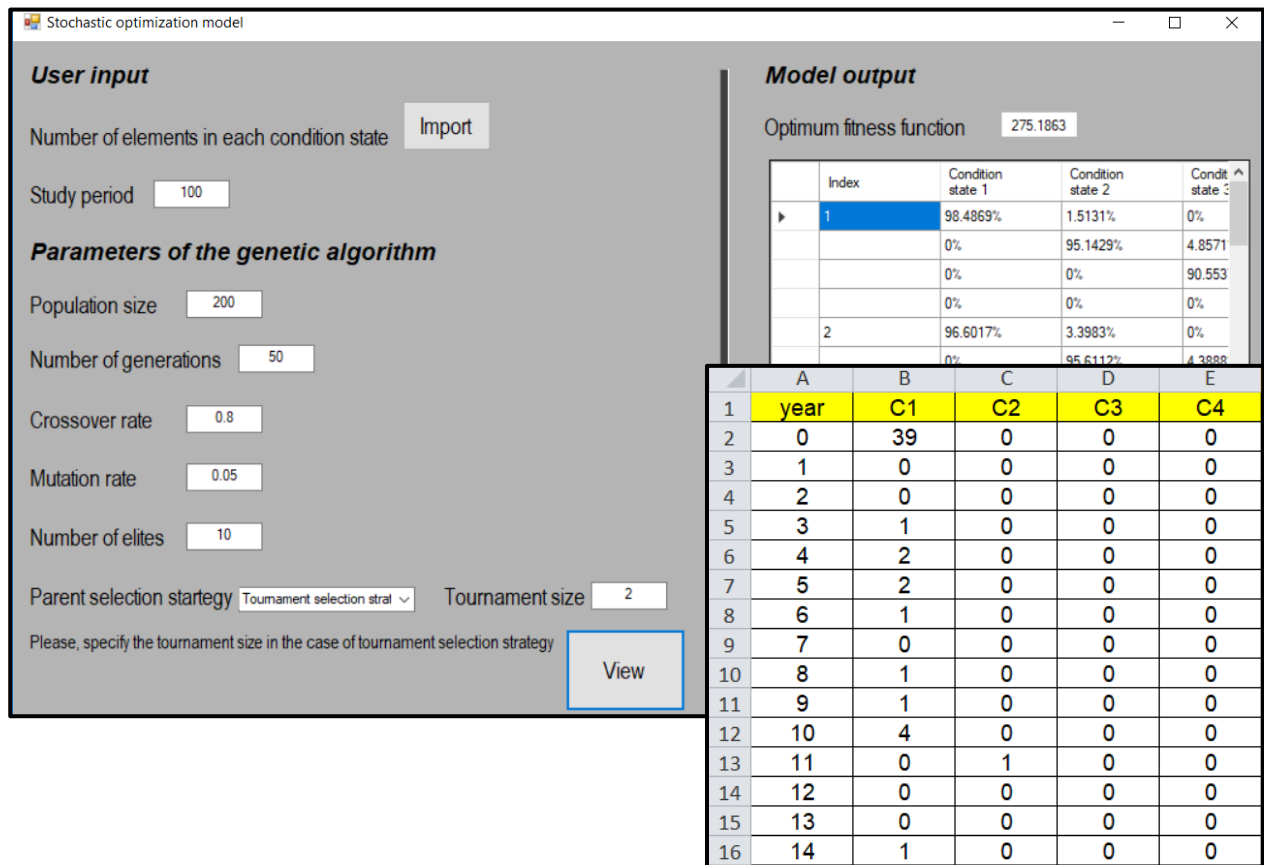


Figure 4.10: Interface of the stochastic optimization model

The performance metrics interface is depicted in Figure 4.11. The developed tool enables the user to define the number of training and testing cases. The “Import” button enables the user to enter the age and condition rating for both the training and testing cases in a Microsoft Excel sheet. The automated tool incorporates a database for the different values of the chi-squared statistic at different degrees of freedom at a significance level of 5%. By clicking the “Calculate” button, the values of RMSE, MAE, and χ^2 for both training and testing cases. Moreover, a

message box will pop-up indicating that the null hypothesis is rejected. Otherwise, the null hypothesis is accepted. In the present study, the value of the chi-squared statistic is smaller the chi-squared critical value. Therefore, the null hypothesis is accepted. In other words, the observed condition ratings of the bridge decks are consistent with the predicted condition ratings.

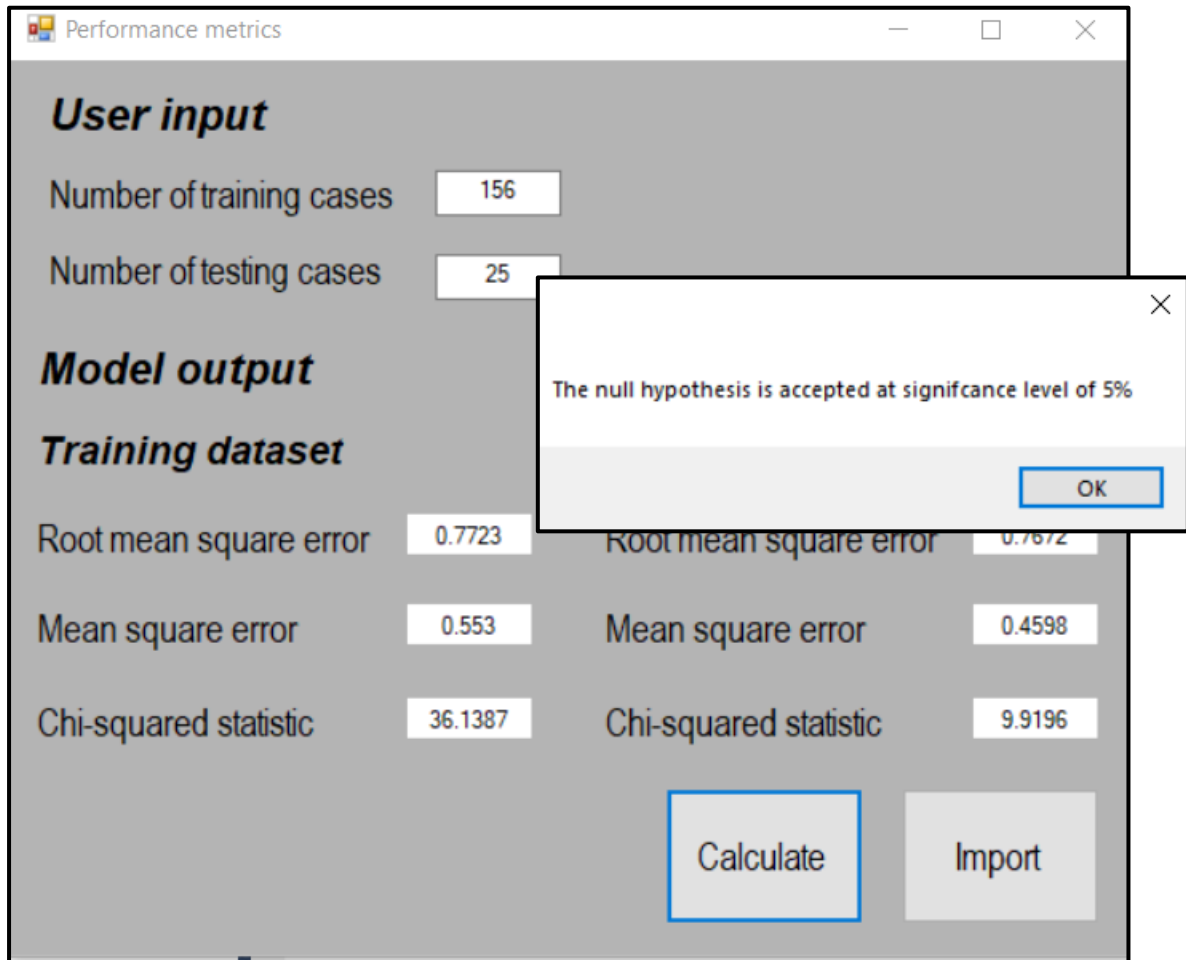


Figure 4.11: Interface of the performance metrics computation module

be 15. The automated platform also gives the user the flexibility to identify the minimum allowable average utilization rate and maximum allowable standard deviation of utilization rate of resources.

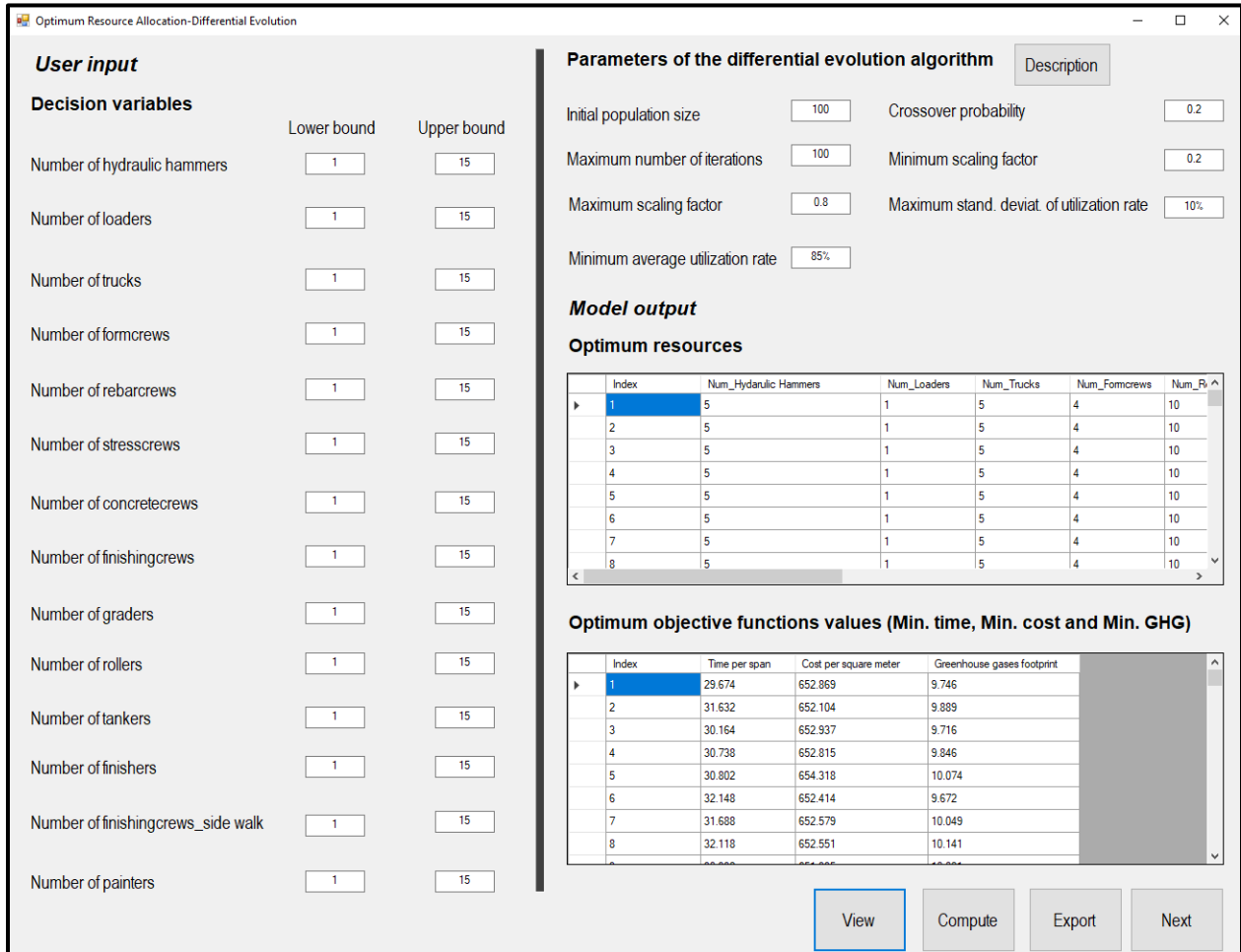


Figure 4.13: User interface of the multi-objective differential evolution model for resource allocation

Figure 4.14 demonstrates the interface designated for the multi-objective maintenance model. In it, the user is asked to define the length of study period, maximum number of visits for each element, minimum acceptable performance condition of element, maximum available budget, maximum yearly-budget and maximum standard deviation of costs. With respect to the parameters of the exponential chaotic differential evolution algorithm, the user is asked to

specify the initial population size, maximum number of iterations, minimum and maximum scaling factors, value of initial chaotic number, and type of chaotic mechanism.

User input

Length of study period: 35

Maximum number of visits per element: 10

Minimum acceptable element condition rating: 64.04

Maximum available budget: 1000000

Maximum yearly budget: 250000

Standard deviation of costs: 20000

Parameters of the chaotic exponential differential evolution algorithm

Initial population size: 50 Minimum scaling factor: 0.2

Maximum number of iterations: 1700 Type of chaotic map: [Dropdown menu]

Maximum scaling factor: 0.8 Initial chaotic number: [Input field]

Model output

List of optimum solutions

Index	Element 1_Year 1	Element 1_Year 2	Element 1_Year 3	Element 1_Year 4	E
1	1	1	1	1	1
2	1	1	1	2	1
3	1	1	1	2	1
4	1	1	1	2	1
5	1	1	1	2	1
6	1	1	1	2	1
7	1	1	1	2	1

Corresponding optimum objective function values

Index	Condition index	Total cost	Environmental impact	Time of disruption
1	64.7957	36597.5387	0	11.8884
2	64.0999	42406.8335	0	13.8698
3	64.2116	37342.8855	0	11.8884
4	64.2116	37445.937	0	11.8884
5	64.2116	37037.1207	0	11.8884
6	64.2116	37136.7967	0	11.8884
7	64.0999	37084.2207	0	11.8884
8	64.2116	36784.7968	0	11.8884
9	64.2116	36934.1043	0	11.8884
10	64.2116	37136.7967	0	11.8884

Buttons: View, Compute, Export

Figure 4.14: Interface of the developed ECDE-based models for maintenance planning of bridge network

CHAPTER V: TESTING AND VALIDATION

5.1 Overview

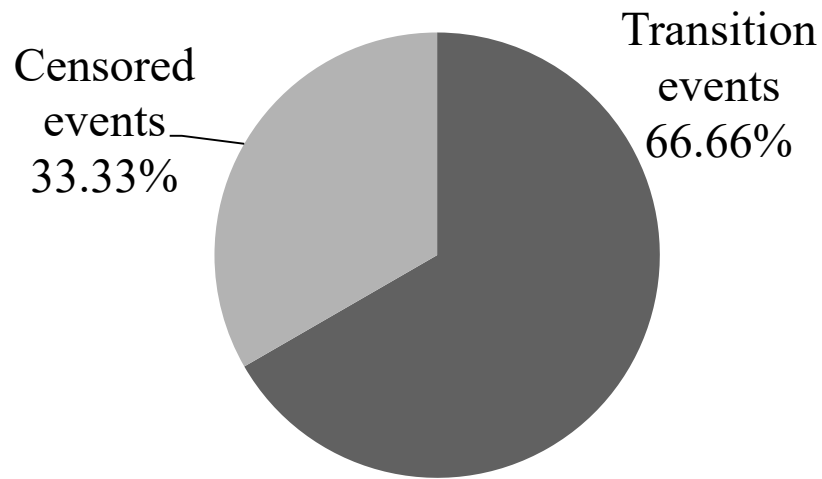
The present chapter comprises testing and validation of the computer applications developed in chapter 4 based on the developed integrated method in chapter 3. Each of the developed methods is validated using different list of case studies. The images utilized to train and test the developed methods for surface defects evaluation are captured from three bridge decks in Montreal and Laval, Canada using Sony DSC-H300 digital camera of 20.1 megapixel resolution. For the defects detection model, a dataset comprising 265 real-world images are used as an input to experiment the developed method such that 200 images are used for training while the remaining 65 images are used for testing. For the defects recognition, the data set is composed of 264 images, whereas 215 and 49 images are utilized for training and testing the model, respectively. The dataset used for testing was generated randomly and not used in training. The images were captured in different weather conditions for the purpose of establishing automated detection and recognition models that are invariant to the lighting conditions.

The second method designated for corrosion evaluation considers four bridge decks in North America: three of them are in Quebec, Canada, and one of them is in New Jersey, United States. The four bridges are denoted as bridge “A”, bridge “B”, bridge “C”, and bridge “D”. In this regard, two bridge decks are analyzed in detail. The first is a bridge located on the Chemin Saint-Grégoire in municipality Les Cèdres that overpasses Autoroute 20, Quebec, Canada. The bridge was constructed in 1965 with a total length of 65 meters, and the width of the bridge decks is 13 meters. The second case study is a bridge located in Boulevard Lévesque Est that overpasses Auto route 25 in the city of Laval. The bridge was constructed in 1966 where the length of the

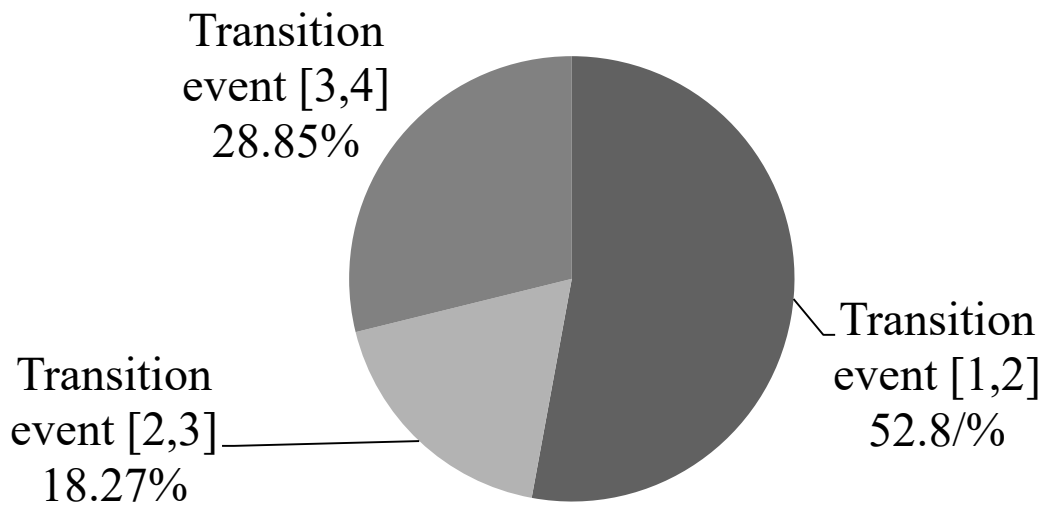
bridge is 55 meters while the width of the bridge is 8 meters (Mohammed Abdelkader et al., 2019a).

The developed method for deterioration modeling utilizes 181 inspection records from the Ministry of Transportation in Quebec, Canada. One hundred fifty six are used for training the model, while the remaining twenty five records are used for testing the model. Out of the 156 inspection records, there are 104 transition events and 52 censored events, whereas the number of events for the TE(1, 2), TE(2, 3), and TE(3, 4) are 55, 19 and 30, respectively (see Figure 5.1)

In the developed surrogate machine learning model, 80% (262) and 20% (66) of the dataset are utilized for training and testing the prediction models, respectively. The developed maintenance planning method is performed for optimum maintenance planning of a group of bridge elements in Quebec. The targeted bridge elements encompass ten bridge decks, seven piers and five abutments. A five-year, twenty five-year and thirty-five year maintenance plans are developed for the sake of testing the capacity of the developed method to handle the short-term and long-term multi-year maintenance planning. The age of the bridge elements ranges from 1970 to 2004 with average age of 27.05 years for the five-year and twenty five-year study periods. More deteriorated bridges of average 33.09 years are considered in the case of thirty-five year study period to better experiment the capabilities of the developed maintenance optimization method. All the computations of the machine learning and optimization algorithms took place on a laptop with an Intel Core i7 CPU, 2.2 GHz and 16 GB of memory



(a) Transition and censored events



(b) Types of transition events

Figure 5.1: Breakdown of transition and censored events

5.2 Validation of Developed Computer Aided Applications

▪ Assessment of Surface Defects

This section enumerates the implementation of the methods developed for restoration of bridge defects images alongside detection and evaluation of surface defects.

Restoration of bridge defects images

Sample of the free-noise bridge defects images is shown in Figures 5.2 and 5.3. Sample of the degraded bridge defects images with different types of noises is depicted in Figures 5.4 and 5.5. Figures 5.4 and 5.5 contain images corrupted with Gaussian noise, speckle noise, salt and pepper noise, combination of Gaussian and speckle noises, combination of Gaussian and salt and pepper noises and combination of speckle and salt and pepper. As shown in Figures 5.4 and 5.5, the combination of noises amplifies the degradation in the qualities of the bridge defects images, which requires a higher capacity restoration method. For the separate noise recognition module, the output of this model is if the image contains speckle, Gaussian, salt and pepper or doesn't contain noise. The neural network is composed of four output neurons for the four previous states, whereas the output is expressed in the form of a binary vector.

One hundred images are used for training the separate noise recognition module while the thirty five images are used for its testing in the split validation. The decision variables of the developed ENN – IWO model are as follows: maximum numbers of hidden and context layers are 10 while the maximum numbers of hidden and context neurons are 10. Thus, maximum length of the optimization problem is 2137. The number of iterations is assumed 250 while the initial population size is assumed 150. The maximum and minimum numbers of seeds are 5 and 0, respectively. The initial and final standard deviations are assumed 0.5 and 0.001, respectively. The convergence of the ENN – IWO model for separate noise recognition is depicted in Figure 5.6. The least misclassification error achieved by ENN – IWO model is equal to 0.05. In addition to that, the developed optimization model stabilizes 191, which exemplifies the higher capacity of the developed model to search for the optimum structure and parameters of the ENN.



(a) Spalling-Image "A"



(b) Spalling-Image "B"



(c) Spalling-Image "C"



(d) Spalling-Image "D"

Figure 5.2: Sample of bridge defects images



(a) Spalling-Image "E"



(b) Spalling-Image "F"

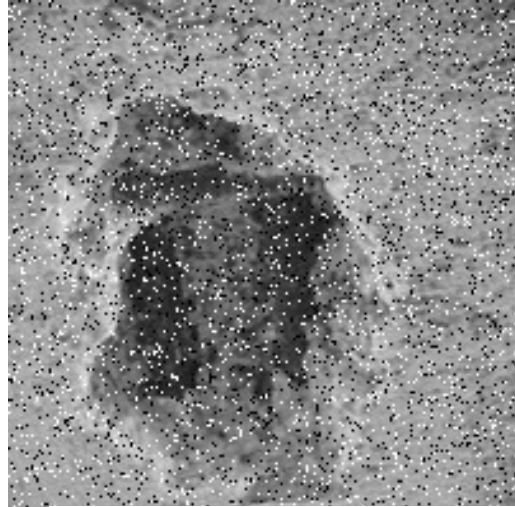


(c) Spalling-Image "G"

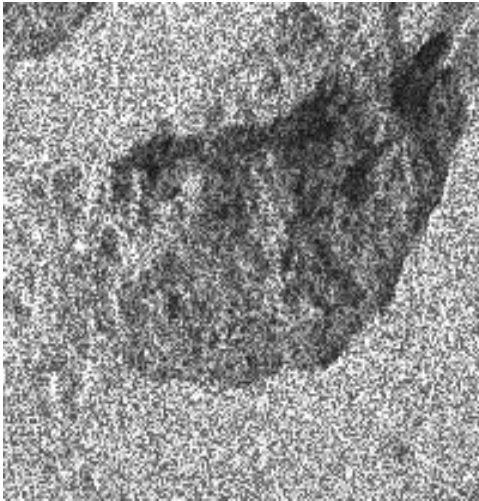
Figure 5.3: Another sample of bridge defects images



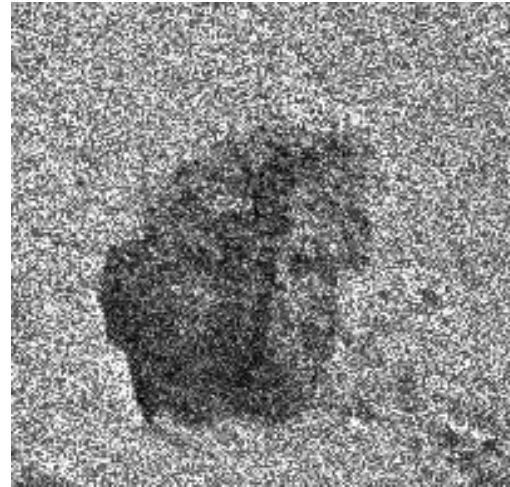
(a) Gaussian noise



(b) Salt and pepper noise

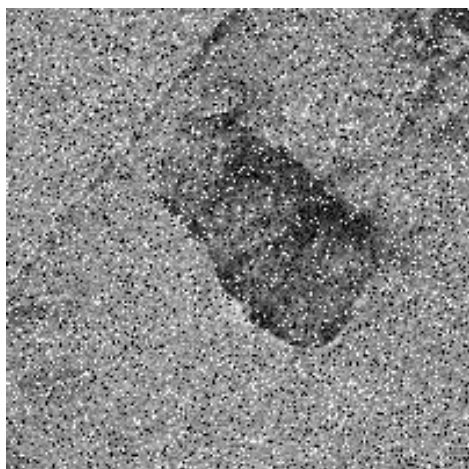


(c) Speckle noise

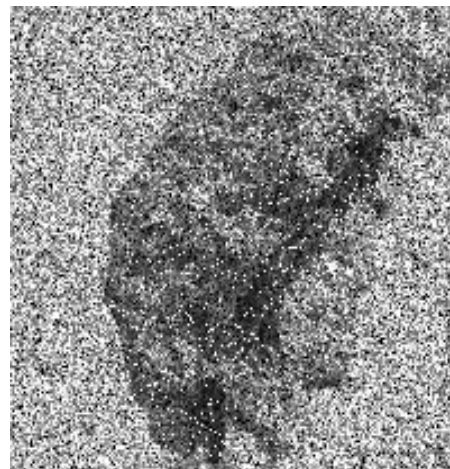


(d) Combination of Gaussian and speckle noises

Figure 5.4: Corrupted images by (a) Gaussian noise, (b) salt and pepper noise, (c) speckle noise and (d) combination of Gaussian and speckle noises



(a) Combination of Gaussian and salt and pepper noises



(b) Combination of speckle and salt and pepper noises

Figure 5.5: Corrupted images by (a) combination of Gaussian and salt and pepper noises, and (b) combination of speckle and salt and pepper noises

The optimum structure of the ENN is one hidden layer, one context layer, seven hidden neurons and seven context neurons. The optimum transfer function is the hyperbolic tangent sigmoid function. The performance comparisons for the five classification models using split validation and 10-fold cross validation are described in Tables 5.1 and 5.2, respectively. It was found that, the developed separate noise recognition model outperformed other classification models for the six performances indicators in both split validation and 10-fold cross validation. Random forest achieved the second best performance, while discriminant analysis and artificial neural network attained the lowest values for the performance indicators. In the cross validation model, the developed ENN – IWO model attained accuracy, sensitivity, specificity, precision, F-measure and Kappa coefficient of 95.28%, 95.24%, 98.07%, 95.25%, 95.43% and 0.935, respectively. On the other hand, accuracy, sensitivity, specificity, precision, F-measure and Kappa coefficient of discriminant analysis were equal to 83.45%, 83.41%, 93.84%, 83.42%, 83.57% and 0.768, respectively.

Non-parametric tests were conducted to provide a thorough assessment of the noise classification models by examining the significant difference in the accuracies among the different classifiers. Wilcoxon test, Mann-Whitney-U test, Kruskal–Wallis test, binomial sign test, and Mood’s median test of the noise classification models are recorded in Table 5.3. Results indicate that the P – values of the pairs (ENN – IWO, discriminant analysis), (ENN – IWO, K-nearest neighbors), (ENN – IWO, random forest), (ENN – IWO, support vector machines) and (ENN – IWO, artificial neural network) for all the tests are less than 0.05, which implies that there are statistically significant differences between the performance of the proposed noise classification model and other classification models.

The second model is the restoration of bridge defects images identified from the previous stage. The output of this model is a filtering protocol, which incorporates the optimum design of filters for each noise type. In order to provide a fair comparison between the different meta-heuristic optimization algorithms, the population size and number of iterations are assumed 10 and 40, respectively. Different initializations of parameters were experimented for the different meta-heuristics in order to search for their optimum values. Each meta-heuristic was run ten times independently in order to avoid unstable solutions due to random initialization of population. The developed restoration model was compared with other models reported in the literature based on the de-noising performance of ten different types of images to examine its robustness in restoration of degraded images.

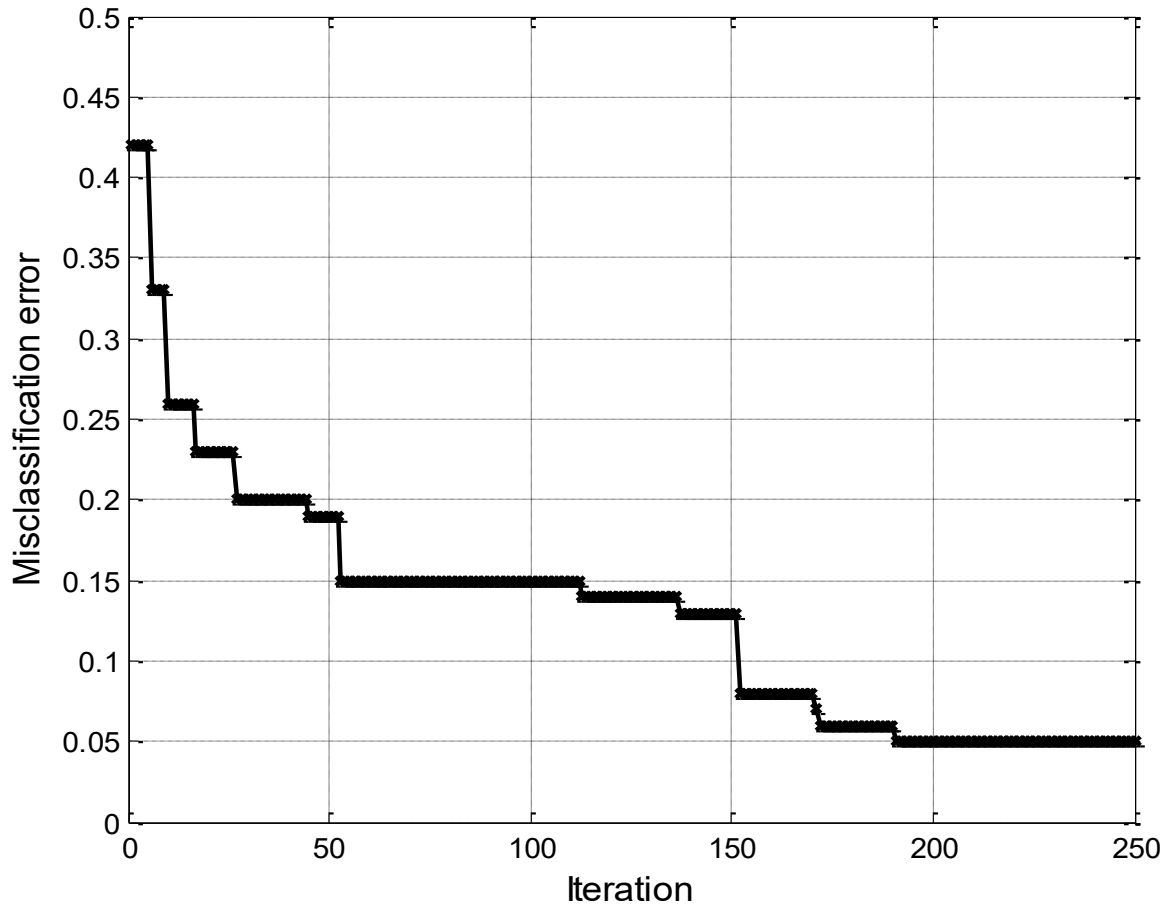


Figure 5.6: Convergence of the ENN – IWO separate noise recognition model

Table 5.1: Comparison of the performance metrics of the six classification models for separate noise recognition based on split validation

Type of classifier	Accuracy	Sensitivity	specificity	Precision	F-measure	Kappa coefficient
DA	83.7%	83.7%	94.26%	83.7%	83.7%	0.77
KNN	85.93%	85.93%	95.08%	85.93%	85.93%	0.801
RF	91.85%	91.85%	97.21%	91.85%	91.85%	0.887
SVM	86.67%	86.67%	95.36%	86.67%	86.67%	0.813
ANN	84.44%	84.44%	94.53%	84.44%	84.44%	0.781
ENN-IWO	95.56%	95.56%	98.5%	95.56%	95.56%	0.937

Table 5.2: Comparison of the performance metrics of the six classification models for separate noise recognition based on 10-fold cross validation

Type of classifier	Accuracy	Sensitivity	specificity	Precision	F-measure	Kappa coefficient
DA	83.45%	83.41%	93.84%	83.42%	83.57%	0.768
KNN	85.67%	85.63%	94.65%	85.65%	85.80%	0.799
RF	91.57%	91.53%	96.77%	91.55%	91.71%	0.884
SVM	86.41%	86.37%	94.93%	86.38%	86.54%	0.811
ANN	84.19%	84.14%	94.10%	84.16%	84.31%	0.779
ENN – IWO	95.28%	95.24%	98.07%	95.25%	95.43%	0.935

Table 5.3: Statistical comparison of the developed noise classification model against other models based on non-parametric tests

Type of classifier	Wilcoxn	Mann-Whitney-U	Kruskal-Wallis	Binomial sign	Mood's median
Discriminant analysis, ENN – IWO	H ₁ (P – value = 5.39×10^{-7})	H ₁ (P – value = 1.17×10^{-6})	H ₁ (P – value =0)	H ₁ (P – value =0)	H ₁ (P – value = 1×10^{-3})
K-nearest neighbors, ENN – IWO	H ₁ (P – value = 5.39×10^{-7})	H ₁ (P – value = 6.06×10^{-3})	H ₁ (P – value = 6×10^{-3})	H ₁ (P – value =0)	H ₁ (P – value = 1×10^{-3})
Random Forest, ENN – IWO	H ₁ (P – value = 5.39×10^{-7})	H ₁ (P – value = 1.83×10^{-2})	H ₁ (P – value = 1.8×10^{-2})	H ₁ (P – value =0)	H ₁ (P – value = 1×10^{-3})
Support vector machines, ENN – IWO	H ₁ (P – value = 5.39×10^{-7})	H ₁ (P – value = 1.83×10^{-2})	H ₁ (P – value = 1.8×10^{-2})	H ₁ (P – value =0)	H ₁ (P – value = 1×10^{-3})
Artificial neural network, ENN – IWO	H ₁ (P – value = 5.39×10^{-7})	H ₁ (P – value = 6.93×10^{-7})	H ₁ (P – value =0)	H ₁ (P – value =0)	H ₁ (P – value = 1×10^{-3})

The overall performance of the different developed restoration model is investigated through comparison against other restoration models as shown in Table 5.4. These models are evaluated as per the average of the peak signal to noise ratio (APSNR), average of mean-squared error (AMSE), average of normalized absolute error, (ANAE) and average of image enhancement factor (AIEF) for the ten images. The developed restoration model achieved superior de-noising results when compared against other optimization-based restoration models and conventional restoration models. MDE achieved the second best performance followed by DE algorithm. On the other hand, non-linear programming-based model attained the least restoration performance among the optimization-based models. The APSNR, AMSE, ANAE and AIEF of the MFO algorithm are 25.36, 176.32, 0.059 and 7.18, respectively.

MDE algorithm attained APSNR, AMSE, ANAE and AIEF of 25.23, 177.59, 0.059 and 6.9, respectively. For the DE algorithm, the values of APSNR, AMSE, ANAE and AIEF are 24.94, 180.71, 0.06 and 6.82, respectively. The APSNR, AMSE, ANAE and AIEF of the non-linear programming are 20.3, 415.34, 0.099 and 3.09, respectively. This highlights that the evolutionary algorithms provide better filtering performance when compared to exact optimization models, which illustrates that exact optimization algorithms fail to solve discrete and complex optimization problems. For the conventional restoration models, Wiener and lee filter are the best two performing restoration models while mode filter achieved the least filtering performance. The APSNR, AMSE, ANAE and AIEF of the Wiener filter are 22.73, 290.04, 0.093 and 4.26, respectively. Mode filter achieved APSNR, AMSE, ANAE and AIEF of 14.14, 2701.5, 0.284 and 0.53, respectively. This manifests that the developed restoration model using MFO algorithm provided holistic and consistent superior filtering capacity over the conventional restoration models.

The utmost objective of the developed method is to develop a filtering protocol, which incorporates the optimum filters to deal with each type of the different noises. Table 5.5 describes the optimum filter(s) for each noise type(s). As shown in Table 5.5, conventional filters of size 3×3 are more efficient in removing separate noises than the combination of noises. Moreover, a filter of size 3×3 provides better de-noising outcome than a filter of size 4×4 . In addition to that, it is worth mentioning that, the application of a set of filters in a certain sequence can improve the restoration process when compared to single filters in the case of images corrupted with a combination of noises. For example, the optimum hybrid filter in the case of images corrupted by a combination of Gaussian and speckle noises is to apply Wiener filter of size 3×3 followed by Lee filter of size 3×3 . Moreover, the optimum hybrid filter in the case of images corrupted with a combination of speckle and salt and pepper noises is to apply Lee filter of size 3×3 followed by Wiener filter of size 3×3 . This also demonstrates that the application of two filters in two different sequences yields different restoration results.

Table 5.4: Overall performance evaluation of the different types of restoration models

Restoration model	APSNR	AMSE	ANAE	AIEF
DE algorithm	24.94	180.71	0.06	6.82
MDE algorithm	25.23	177.59	0.059	6.9
PSO algorithm	24.56	184.26	0.061	6.71
IWO algorithm	24.32	186.57	0.062	6.65
MFO algorithm	25.36	176.32	0.059	7.18
GOA	23.92	191.71	0.064	6.54
GWO algorithm	25.11	178.72	0.059	6.86
GA	24.52	184.91	0.062	6.7
Nonlinear programming	20.3	415.34	0.099	3.09
Median filter	20.23	418.92	0.106	3.1
Gaussian filter	18.72	884.72	0.154	1.38
Weiner filter	22.73	290.04	0.093	4.26
Average filter	20.97	355.99	0.104	3.86
Mode filter	14.14	2701.5	0.284	0.53
Lee filter	22.47	241.72	0.09	5.17
Frost filter	21.68	291.38	0.096	4.34

Table 5.5: Filtering protocol for different types of noises

Type of noise	Restoration model	Optimum design of filter(s)
Gaussian	MFO algorithm	Wiener filter of size 3×3
Salt and pepper	MFO algorithm	Median filter of size 3×3
Speckle	MFO algorithm	Lee filter of size 3×3
Combination of Gaussian and speckle noises	MFO algorithm	Wiener filter of size 3×3 followed by Lee filter of size 3×3
Combination of Gaussian and salt and pepper noises	MFO algorithm	Median filter of size 3×3
Combination of Speckle and salt and pepper noises	MFO algorithm	Lee filter of size 3×3 followed by Wiener filter of size 3×3

Recognition of surface Defects

The developed method is validated using Dataset I and Dataset II to test its robustness towards different types and natures of images.

1. Dataset I

The developed SVD – ENN – IWO method is utilized for the defects detection and recognition. In this regard, two datasets are generated from Dataset I for the sake of defects detection and recognition. The developed SVD – ENN – IWO method utilizes singular value decomposition for the purpose of dimensionality reduction and extracting the most significant features in images. In the singular value decomposition, , an input image of size 100×100 pixels can be reduced to a feature vector of size 1×100. For instance, the distribution of singular values of image Spalling-Image displayed in Figure 5.3.c is depicted in Figure 5.7. In this regard, the first few diagonal elements contain the most considerable amount of information while the tail end of the feature vector incorporates lesser information. It can be inferred that the first 50 dimensions

are able to preserve substantial amount of information (approximately 95% of the total inform present in the image).

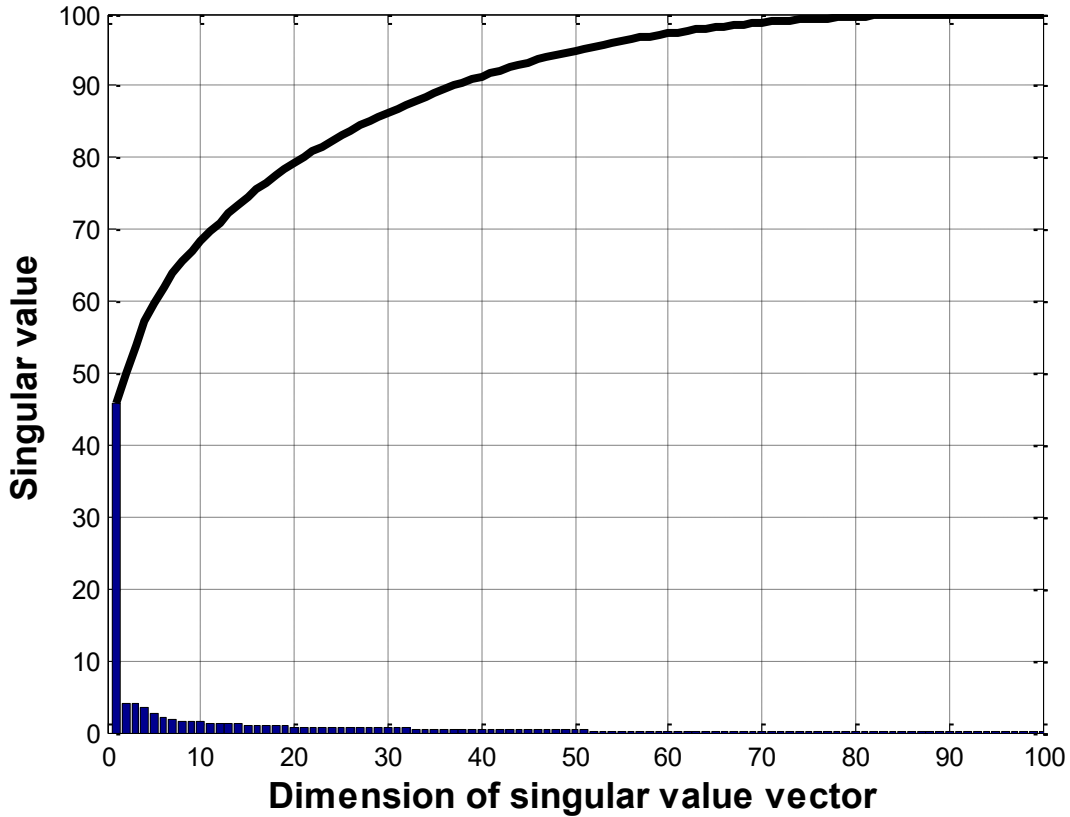


Figure 5.7: Distribution of the singular values for image image Spalling-Image “G”

In the SVD – ENN – IWO model, the feature vector of 100 singular values is used as an input to establish its training. Since the performance of the Elman neural network is significantly influenced by its parameters such as number of hidden layers, number of context layers, number of hidden neurons, number of context neurons, type of transfer functions, moment value, bias terms and weights of the connections between neurons. The present study relies on the IWO to establish a proper setting for the tuning parameters of the Elman neural network. The optimization parameters of the developed SVD – ENN – IWO model for defects detection are as

follows. The maximum number of hidden and context layers are 5. Also, the maximum number of hidden and context neurons are five. Eight transfer functions are investigated and the values of weights and bias terms are real numbers between -1 and 1. Therefore, the maximum length of the optimization problem is 759.

The parameters of the IWO algorithm are as follows: the number of iterations and the initial population size are assumed 500 and 250, respectively. The maximum and minimum numbers of seeds are 5 and 0, respectively. The initial and final standard deviations are assumed 0.5 and 0.001, respectively. The convergence of the developed SVD – ENN – IWO model for defects detection is shown in Figure 5.8. The least misclassification error achieved by SVD – ENN – IWO model equals to zero. Moreover, the optimization model stabilizes at iteration 120 which demonstrates the superior search capability of the IWO algorithm. The optimum structure of the ENN is as follows: the optimum numbers of hidden and context layers are one while the optimum number of hidden and context neurons are one. The optimum transfer function is the Elliot symmetric sigmoid transfer function.

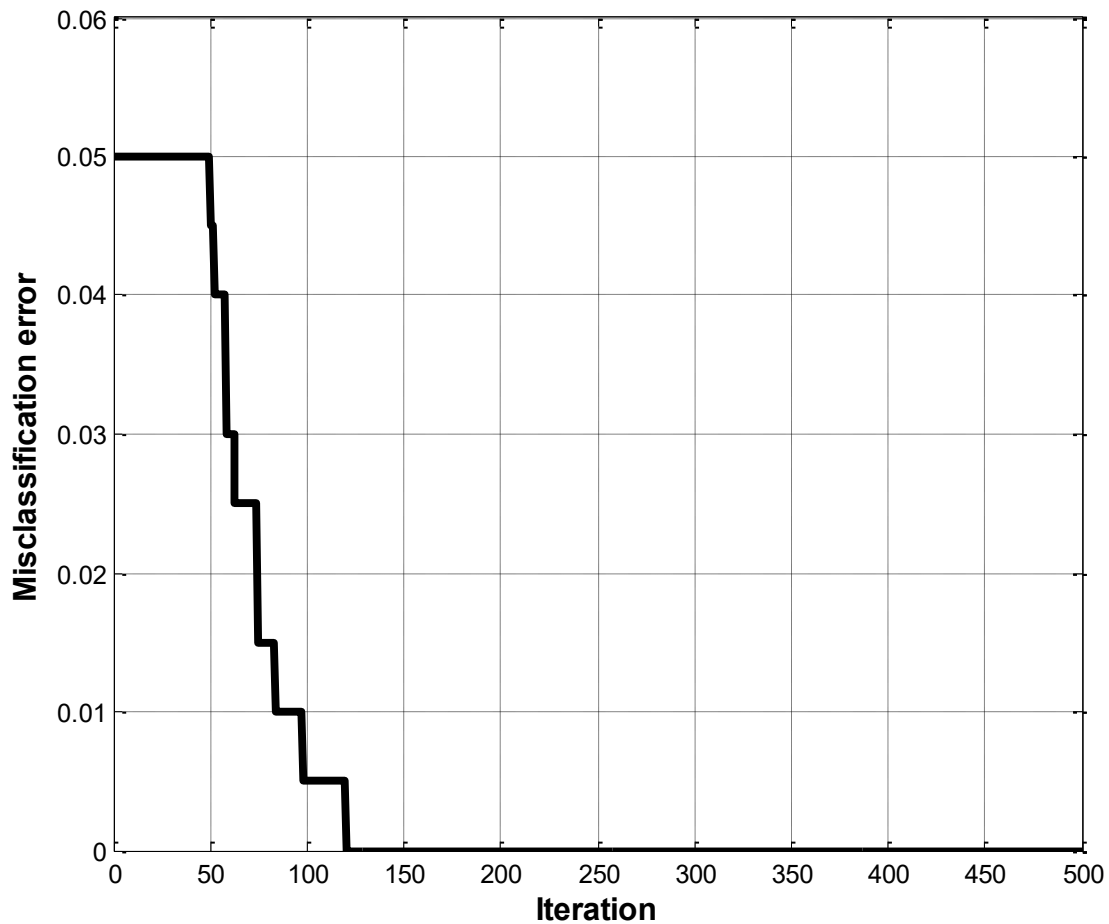


Figure 5.8: Convergence of the SVD – ENN – IWO model for defects detection based on dataset I

The convergence of developed SVD – ENN – IWO model for defects recognition is depicted in Figure 5.9. The minimum misclassification error achieved by the SVD – ENN – IWO model equals to 0.0372. Furthermore, the IWO algorithm stabilizes at iteration 292, which illustrates the capability of the IWO algorithm in exploring the search space. The optimum topology of the ENN is as follows: optimum numbers of hidden and context layers are one while the optimum number of hidden and context neurons are eight. The optimum transfer function is the hyperbolic tangent sigmoid transfer function

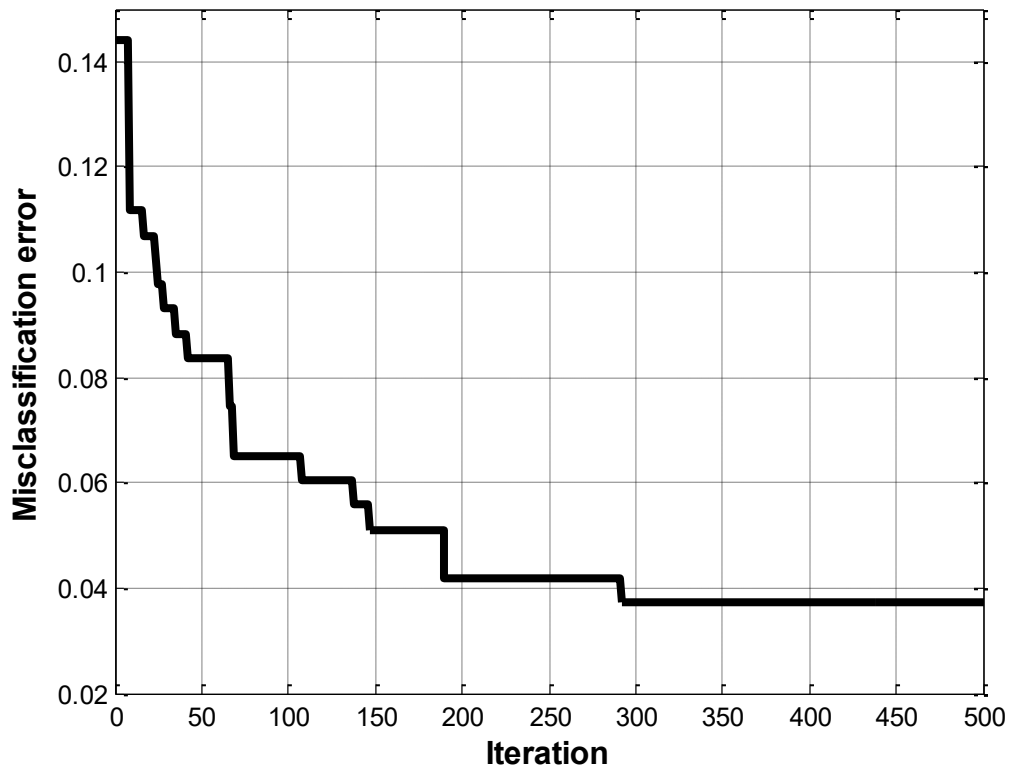


Figure 5.9: Convergence of the SVD – ENN – IWO model for defects recognition

The performance accuracies of the prediction models based on 10-fold cross validation are recorded in Tables 5.6. It is worthy to note that developed model outperformed other prediction models based on split validation and 10-fold cross validation. With regards to cross validation, artificial neural network yielded the lowest prediction outcome. In the context, the developed model managed to establish an average improvement in the performance indicators by 24.85% when compared against the ENN model. The prediction accuracies of the cross validation and testing accuracies are close to each other which evinces that the developed method don't suffer from over fitting. The receiver operating characteristics curves for the different prediction models are depicted in Figure 5.10. The ROC curves are utilized to visually compare the performance of the prediction models. A larger area under ROC curve indicates a better performance of the prediction model. In this context, the ROC curve of the SVD – ENN – IWO

lies above other classifiers. This implies that AUC for SVD – ENN – IWO is larger than other classifiers. Thus, the developed model provides better classification performance than other models. This evinces the significant enhancement in the classification accuracy achieved by the implementation of the developed model.

Table 5.6: Performance evaluation of the prediction models for defects detection based on entire dataset I using 10-fold cross validation

Prediction model	overall accuracy	F-measure	Kappa coefficient	Balanced accuracy	Matthews correlation coefficient	Area under curve
Discriminant analysis	91.79%	94.71%	0.685	93.14%	0.712	0.931
K-nearest neighbors	80.12%	87.21%	0.418	88.39%	0.512	0.884
Random Forest	93.35%	95.77%	0.688	83.74%	0.689	0.837
Support vector machines	93.75%	95.91%	0.747	92.55%	0.758	0.926
Decision tree	89.25%	93.65%	0.425	69.5%	0.427	0.695
Artificial neural network	85.85%	91.72%	0.236	60.75%	0.237	0.608
Elman neural network	90.83%	94.41%	0.588	82.4%	0.593	0.824
CONVNET	95.74%	97.14%	0.811	88.55%	0.812	0.89
AlexNet	76.14%	84.46%	0.357	86.27%	0.464	0.863
VGG16	75.79%	84.21%	0.352	86.09%	0.461	0.861
VGG19	59.59%	71.20%	0.182	58.27%	0.341	0.583
CaffeNet	72.44%	81.73%	0.31	84.25%	0.427	0.843
SVD – ENN – IWO	97.65%	98.35%	0.906	94.94%	0.907	0.949

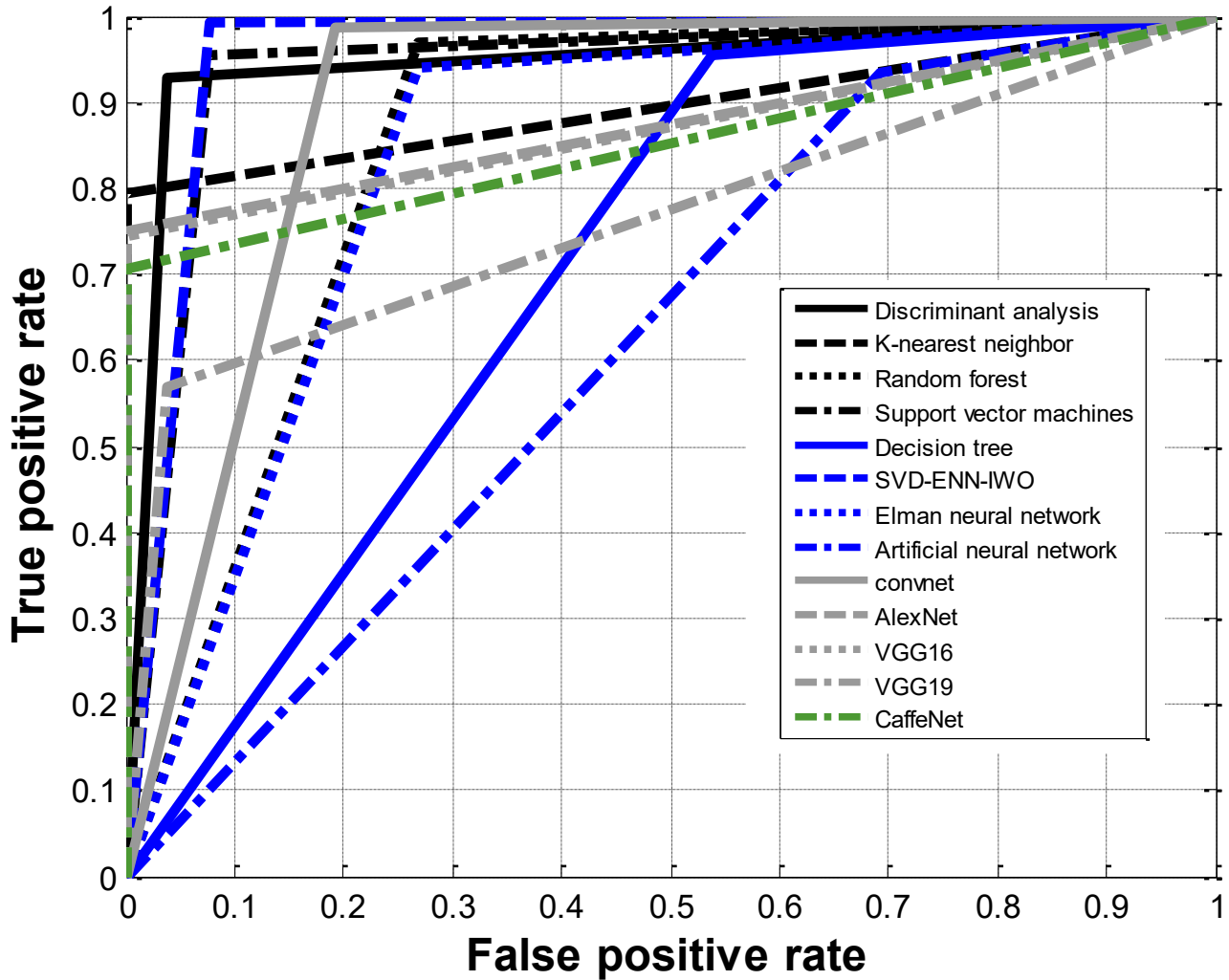


Figure 5.10: ROC curves of the prediction models for defects detection based on entire dataset I

The classification performances evaluations of the prediction models for bridge defects recognition based cross validation are recorded in Tables 5.7. The developed SVD – ENN – IWO model outperformed other prediction models attaining overall accuracy, F-measure, Kappa coefficient, balanced accuracy, Matthews’s correlation coefficient and area under curve of 95.5%, 95.5%, 0.914, 96.49%, 0.937 and 0.904, respectively. It managed to improve the classification performance indicators by values ranging from 10.7% to 37.44% when compared against the artificial neural network.

2. Dataset II

Table 5.8 reports the performance evaluations of the prediction models for bridge defects detection based on 10-fold cross validation. The developed model outperformed other prediction models such that it achieved overall accuracy, F-measure, Kappa coefficient, balanced accuracy, Matthews's correlation coefficient and area under curve of 99.45%, 97.32%, 0.969, 98.1%, 0.97 and 0.981, respectively. VGG19 outperformed CONVNET and other pre-trained networks yielding overall accuracy, F-measure, Kappa coefficient, balanced accuracy, Matthews's correlation coefficient and area under curve of 95.38%, 81.37%, 0.788, 95.7%, 0.8 and 0.957, respectively. In this context, the developed model generated an average improvement in the classification performance evaluation of 12.18% with reference to VGG16. It is computed according to the average of improvements achieved in each of the classification performance indicators.

Table 5.7: Performance evaluation of the prediction models for defects recognition based on entire dataset using 10-fold cross validation

Prediction model	overall accuracy	F-measure	Kappa coefficient	Balanced accuracy	Matthews correlation coefficient	Area under curve
Discriminant analysis	80.45%	80.45%	0.597	85.03%	0.714	0.783
K-nearest neighbors	78.20%	78.20%	0.633	83.35%	0.68	0.865
Random Forest	85.80%	85.80%	0.715	89.06%	0.794	0.828
Support vector machines	89.24%	89.24%	0.791	91.66%	0.846	0.854
Decision tree	89.64%	89.64%	0.79	91.94%	0.851	0.845
Artificial neural network	83.33%	83.33%	0.665	87.16%	0.754	0.756
Elman neural network	85.93%	85.93%	0.696	89.19%	0.795	0.743
CONVNET	89.02%	89.02%	0.768	91.51%	0.841	0.766
AlexNet	93.58%	93.58%	0.879	94.96%	0.91	0.922
VGG16	94.38%	94.38%	0.895	95.56%	0.922	0.929
VGG19	93.25%	93.25%	0.873	94.72%	0.905	0.921
CaffeNet	94.06%	94.06%	0.889	95.34%	0.917	0.909
SVD – ENN – IWO	95.5%	95.5%	0.914	96.49%	0.937	0.904

Table 5.8: Performance evaluation of the prediction models for defects detection based on entire dataset II using 10-fold cross validation

Prediction model	overall accuracy	F-measure	Kappa coefficient	Balanced accuracy	Matthews correlation coefficient	Area under curve
CONVNET	92.39%	42.2%	0.397	64.18%	0.485	0.642
AlexNet	95.37%	81.12%	0.786	95.14%	0.796	0.951
VGG16	95.3%	81.11%	0.785	95.65%	0.798	0.956
VGG19	95.38%	81.37%	0.788	95.7%	0.8	0.957
CaffeNet	95.27%	81.08%	0.785	95.86%	0.798	0.958
SVD – ENN – IWO	99.45%	97.32%	0.969	98.1%	0.97	0.981

The average ranking method is adopted for the sake of establishing an integrative representation of the performances of the prediction models for bridge defects detection and recognition based on datasets I and II. The mean and standard deviation of rankings of the prediction models are reported in Table 5.9. It is revealed that the developed model achieved the highest rank and satisfactory standard deviation of rankings. In this regard, its mean and standard deviation are equal to 1.22 and 0.92, respectively. Results also demonstrate that VGG16 achieved the second ranking followed by AlexNet and then CaffeNet. It is also found that the transfer learning-based deep neural networks generated an overall prediction performance better than the trained from scratch network. In the light of the previous analysis, it is revealed that the developed method was capable of providing a holistic and significant better classification scheme than other prediction models for both defects detection and recognition.

Table 5.9: Mean and standard deviation of rankings obtained by the prediction models

Prediction model	Mean of rankings	Standard deviation of rankings
CONVNET	4.39	1.74
AlexNet	3.61	0.68
VGG16	3	0.94
VGG19	4.28	1.66
CaffeNet	3.67	1
SVD – ENN – IWO	1.22	0.92

Modeling of surface defects severities

Sample of the used spalling images is shown in Figure 5.11. The developed spalling detection model capitalizes on the accommodation of Kapur entropy and Renyi’s entropy objective functions. A comparative analysis of the different segmentation models for the 60 images is recorded in Table 5.10. The comparison is carried out based on the average values of MSE, MAE, PSNR, Ov_ACC, F – measure, BACC and MCC. It is worth mentioning the differences in the values of the image quality indicators between the different spalling segmentation models due to the fact that the developed detection method deals with bi-level thresholding problems. As shown in Table 5.10, the developed model achieved very promising results. It can be observed that the developed model outperformed other spalling detection models achieving MSE, PSNR, MAE, Ov_ACC, F – measure, BACC and MCC of 0.399, 0.621, 3.56, 90.448%, 90.981%, 91.343% and 0.818, respectively. It can be also inferred that K-means clustering, fuzzy C-means clustering and expectation maximization algorithms provided similar efficiency in detecting spalling pixels in images. Region growing failed to detect efficiently the spalling such that it

attained MSE, PSNR, MAE, Ov_ACC, F – measure, BACC and MCC of 0.411 0.633, 3.433, 76.538%, 81.033%, 83.319% and 0.595, respectively.

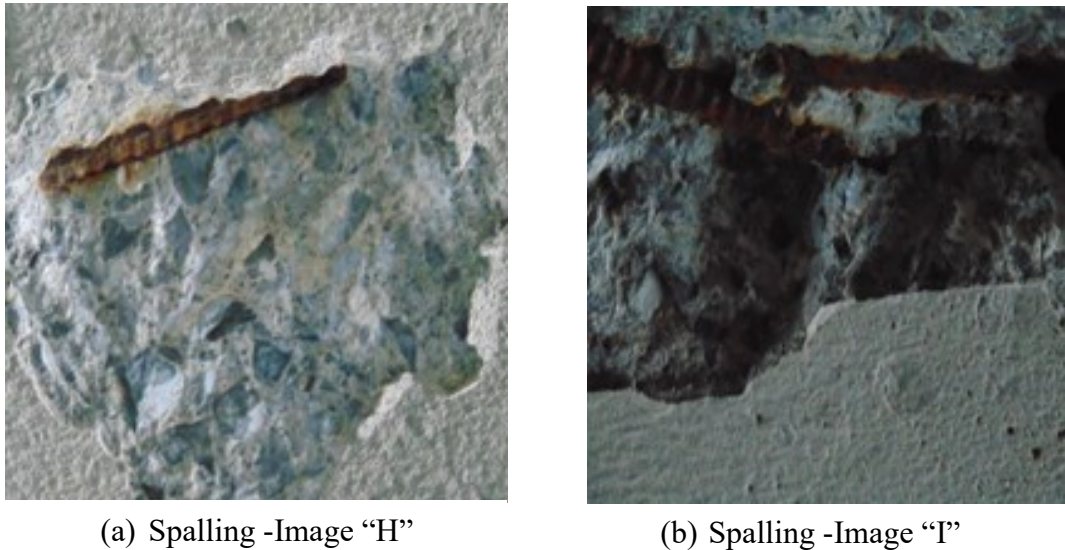


Figure 5.11: Sample of the spalling images

Two-tailed Student's t-tests were performed to evaluate the significance levels of the segmentation performances for the different spalling detection models. The tests were conducted using the image quality indicators and classification performance metrics. Statistical comparisons between the spalling detection models capitalizing on balanced accuracy are reported in Table 5.11. The tests are conducted at significance level (α) of 0.05. The performed student's t-tests examine the null hypothesis (H_0), which is that there is no significant difference between the segmented images obtained from each pair of spalling detection models. On the other hand, the alternative hypothesis (H_1) assumes that there is a significant difference between the segmented images obtained from each pair of the of spalling detection models. If the P – value is less than the significance level, then the null hypothesis is rejected in favor of the

alternative hypothesis. Nevertheless, if the P – value is more than the significance level, thus the null hypothesis is accepted.

The elements of the upper triangle in Table 5.11 are reflected in the lower triangle. As shown in Table 5.11, the P – values of the pairs (developed model, Otsu), (developed model, K-means clustering), (developed model, fuzzy C-means clustering), (developed model, region growing) and (developed model, expectation maximization) are less than 0.05, which implies that the null hypothesis (H_0) is rejected, which manifests that the developed model significantly outperformed other spalling segmentation models stepping on balanced accuracy. It can be also concluded from Table 5.11 that the P – values of the pairs (K-means clustering, fuzzy C-means clustering), (K-means clustering, expectation maximization) and (fuzzy C-means clustering, expectation maximization) are more than 0.05, which implies that the null hypothesis (H_0) is accepted. Thus, there are no statistical significant differences between these spalling segmentation models based on the balanced accuracy.

Table 5.10: Performance comparison between the different spalling detection models

Segmentation model	MSE	MAE	PSNR	Ov_ACC	F – measure	BACC	MCC
Developed model	0.399	0.621	3.56	90.448%	90.981%	91.343%	0.818
Otsu	0.423	0.645	3.297	81.919%	83.849%	84.475%	0.659
K-means clustering	0.42	0.641	3.335	84.321%	85.225%	85.136%	0.617
Fuzzy C-means clustering	0.419	0.642	3.322	84.228%	85.208%	85.141%	0.694
Region growing	0.411	0.633	3.433	76.538%	81.033%	83.319%	0.595
Expectation maximization	0.419	0.641	3.334	84.302%	85.227%	85.141%	0.694

Clearer visual comparisons between the different spalling detection models are conducted, whereas any pixel that has a value equal to one is appended as spalling. Otherwise, if the pixel is equal to zero it is considered as non-spalling. Figures 5.12, 5.13 and 5.14 depict the binarized images using the different spalling segmentation models for spalling images “A”, “F” and “I”, respectively. By examining the differences between the segmented images, it can be inferred that the developed spalling detection method generates a better well-separated spalling pixels from the background when compared against other segmentation models.

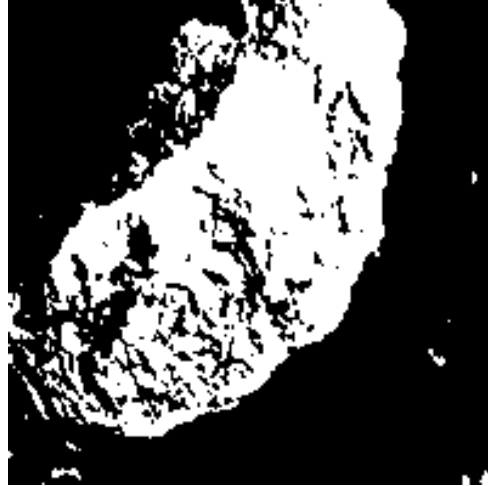
The second model is the quantification of spalling area. The developed ENN – IWO model is compared against a set of baseline models. The convergence curve of the developed ENN – IWO model for predicting spalling area based on original dataset is shown in Figure 5.15. As shown in Figure 5.15, the least mean absolute percentage error achieved by the invasive weed optimization algorithm is 3.97%. A performance comparison between the different prediction methods based on the original dataset is described in Table 5.12. It is worth mentioning that the RMSE is measured in cm^2 . The developed ENN – IWO model attained the highest prediction accuracy with respect to other prediction models reported in the literature, whereas MAPE, RMSE and RMSPE are equal to 4.07%, 76.061 and 0.065, respectively. Pre-trained deep learning networks outperformed the trained from scratch deep neural network, whereas VGG16 achieved MAPE, RMSE and RMSPE of 6.774%, 93.176 and 0.184, respectively. On the level of conventional machine learning models, Elman neural network provided the highest prediction accuracies followed by radial basis neural network and then generalized regression neural network. In this regard, back back-propagation artificial neural network yielded the lowest prediction accuracies attaining MAPE, RMSE and RMSPE of 26.203%, 276.936 and 0.519, respectively.

Table 5.11: Statistical comparison between the different spalling detection models using balanced accuracy

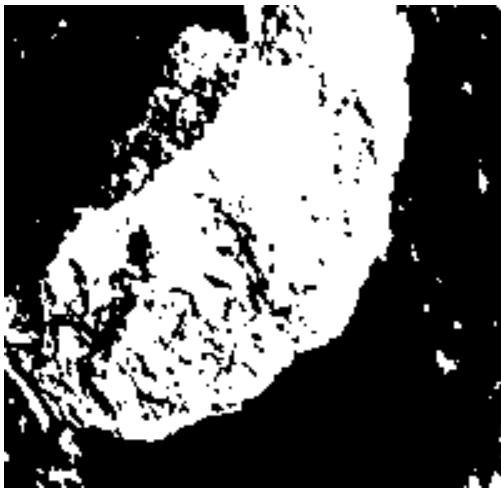
Pair of segmentation models	Developed model	Otsu	K-means clustering	Fuzzy C-means clustering	Region growing	Expectation maximization
Developed model	H_0 (P – value=1)	H_1 (P – value = 5.59×10^{-7})	H_1 (P – value = 2.65×10^{-6})	H_1 (P – value = 2.31×10^{-6})	H_1 (P – value = 6.07×10^{-7})	H_1 (P – value = 2.53×10^{-6})
Otsu		H_0 (P – value=1)	H_0 (P – value = 2.2×10^{-1})	H_0 (P – value = 2.13×10^{-1})	H_0 (P – value = 7.86×10^{-2})	H_0 (P – value = 2.12×10^{-1})
K-means clustering			H_0 (P – value=1)	H_0 (P – value = 8.46×10^{-1})	H_1 (P – value = 1.89×10^{-2})	H_0 (P – value = 7.89×10^{-1})
Fuzzy C-means clustering				H_0 (P – value=1)	H_1 (P – value = 1.74×10^{-2})	H_0 (P – value = 9.55×10^{-1})
Region growing					H_0 (P – value=1)	H_1 (P – value = 1.71×10^{-2})
Expectation maximization						H_0 (P – value=1)



(a) Developed method



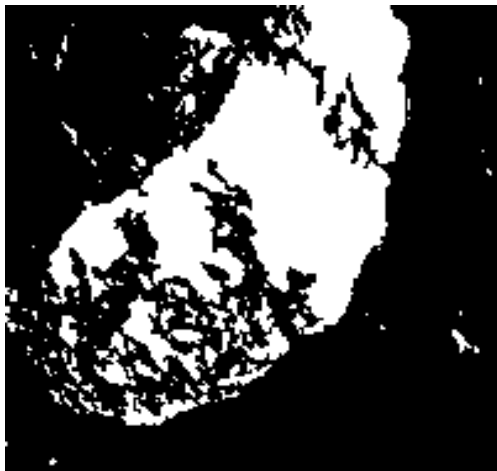
(b) Otsu



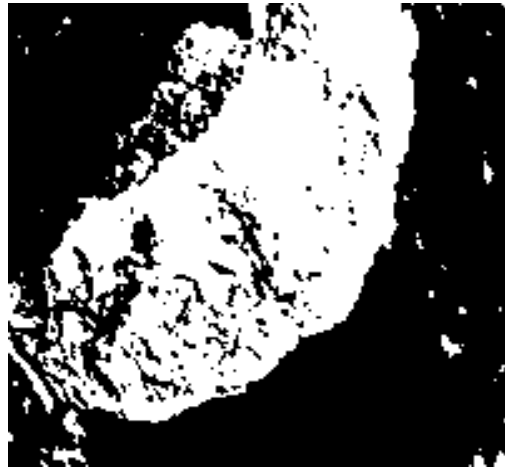
(c) K-means clustering



(d) Fuzzy C-means clustering



(e) Region growing



(f) Expectation maximization

Figure 5.12: Segmentation outcome of different detection models for spalling-Image “A”

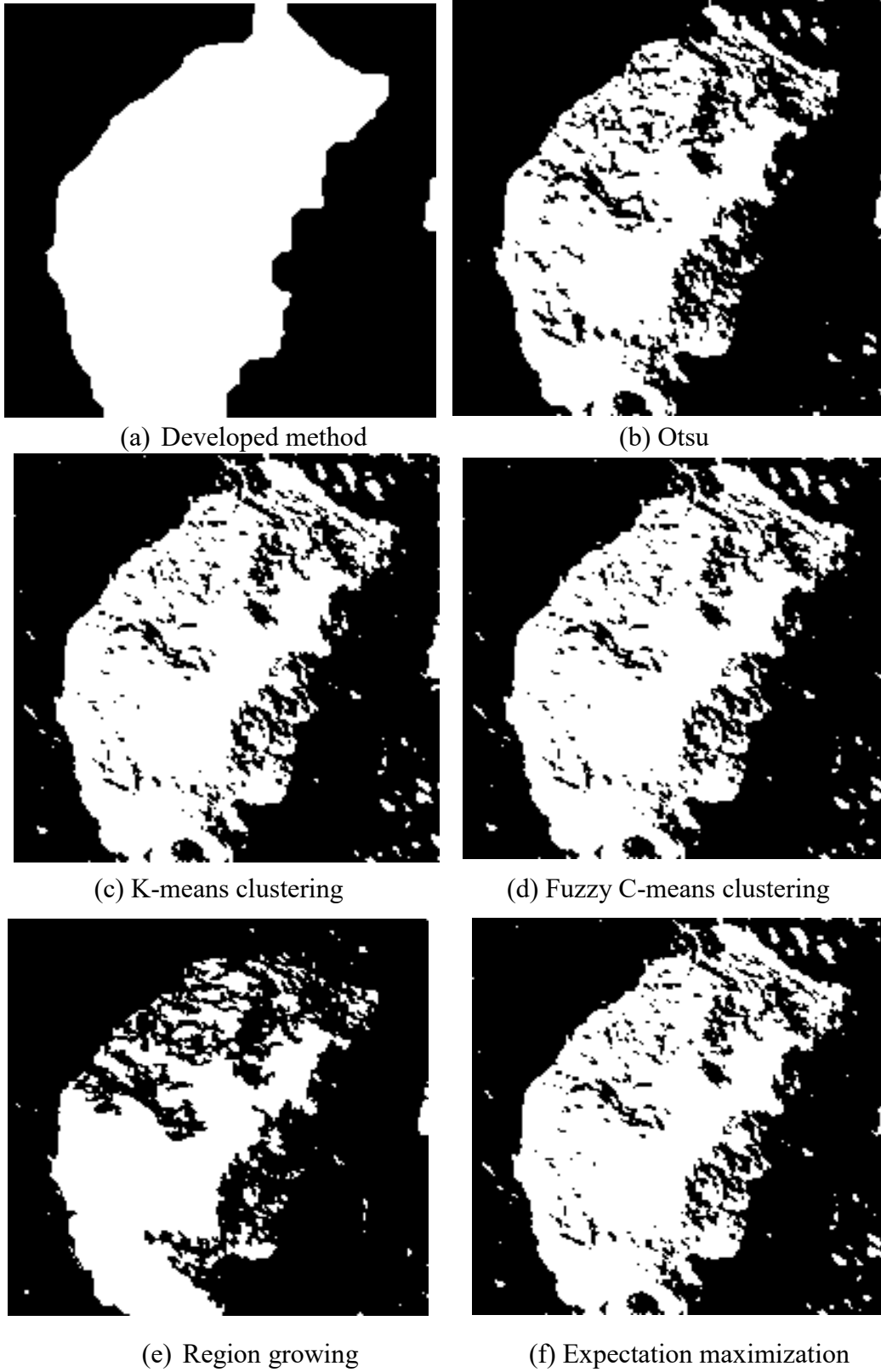


Figure 5.13: Segmentation outcome of different detection models for spalling-Image “F”



(a) Developed method



(b) Otsu



(c) K-means clustering



(d) Fuzzy C-means clustering



(e) Region growing



(f) Expectation maximization

Figure 5.14: Segmentation outcome of different detection models for spalling-Image “I”

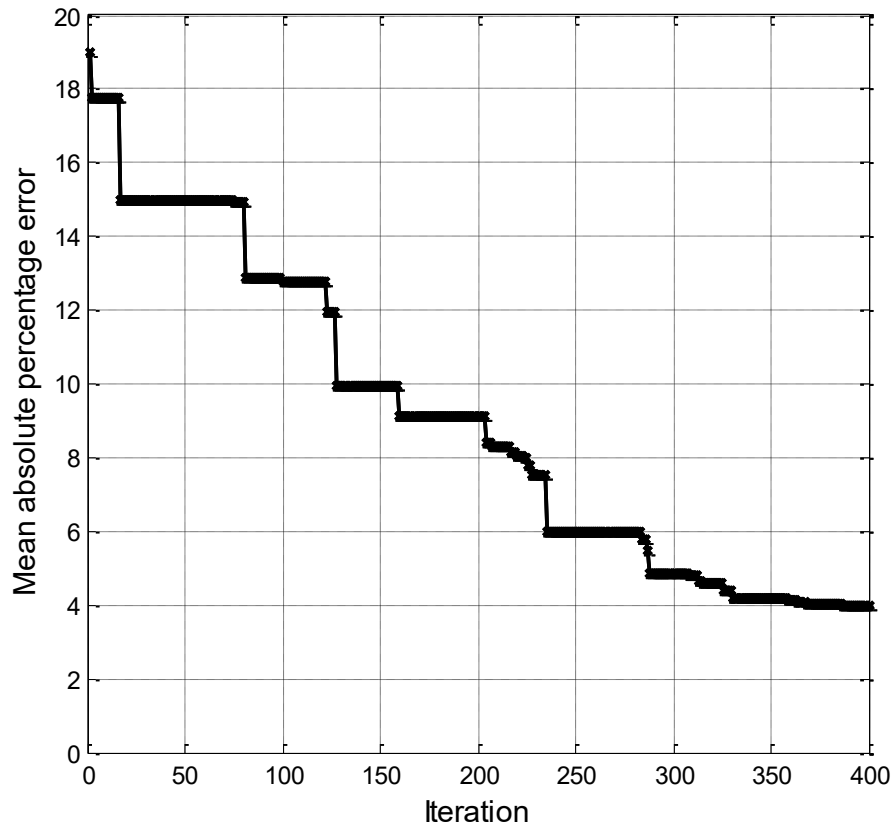


Figure 5.15: Convergence Curve of the developed ENN – IWO model for predicting spalling area based on original dataset

In order to further evaluate the prediction models, the original dataset is augmented for the sake of establishing more robust and generalized spalling interpretation models. In this regard, the augmented dataset is composed of 565 images, whereas 450 images (80%) are utilized for training the prediction models while the remaining 115 images (20%) are used for their testing. A performance comparison between the prediction models based on the augmented dataset is reported in Table 5.13. It can be inferred that the developed model provided the highest prediction accuracies such that it attained MAPE, RMSE and RMSPE of 4.625%, 81.257 and 0.087, respectively. On the level of deep learning models, CONVNET outperformed the pre-trained deep learning networks achieving MAPE, RMSE and RMSPE of 5.218%, 83.797 and

0.105, respectively. It is observed also that AlexNet, VGG16, VGG19 and CaffeNet generated very close prediction accuracies. With respect to the conventional machine learning models, Elman neural network and radial basis neural network accomplished the highest prediction performance while artificial neural network and generalized regression provided the highest prediction error. In this regard, it can be interpreted the developed model outperformed the conventional Elman neural network based on original and augmented datasets. This can be explained by the facts that the developed model offers two layers of improvement over the conventional Elman recurrent neural network, which are the application of singular value decomposition and discrete wavelet transform for efficient feature extraction in addition to employing invasive weed optimization algorithm to enhance the search mechanism of Elman neural network by magnifying the exploration-exploitation trade-off. In view of different sources of testing and validation in addition to box plots and statistical analysis tests, the developed method is not case dependent and can be applied in similar applications.

The third model is designated for establishing a severity rating system of spalling based on its area and depth. In this regard, spalling area and depth are assumed as random variables in order to generate large number of possible scenarios. The best-fit distribution is the one which is associated with the lowest Anderson Darling statistic. The probability distributions and their corresponding rankings and Anderson Darling statistics are depicted in Table 5.14. As shown in Table 5.14, logistic and exponential achieved the lowest and highest Anderson Darling statistics, respectively. In this context, logistic is the best-fit distribution and its location and scaling factors are assumed 979.37 and 102.25, respectively. It is worth mentioning that loglogistic is the best-fit distribution of spalling depth and its location and scaling factors are assumed 1.58 and 0.28, respectively.

Table 5.12: Performance comparison between the prediction models based on the original dataset

Prediction model	Mean absolute percentage error	Root mean-squared error	Root mean squared percentage error
ENN – IWO	4.07%	76.061	0.065
Artificial neural network	26.203%	276.936	0.519
Elman neural network	18.043%	175.96	0.333
Generalized regression neural network	19.669%	198.707	0.359
Radial basis neural network	18.349%	176.041	0.335
CONVNET	9.362%	108.276	0.198
AlexNet	6.824%	93.184	0.186
VGG16	6.774%	93.176	0.184
VGG19	6.791%	93.303	0.182
CaffeNet	6.8%	93.209	0.184

A sample of the cluster memberships of spalling area obtained from the fuzzy C-means clustering algorithm are displayed in Table 5.15. In fuzzy C-means clustering, the data point is assigned to the cluster with the highest degree of membership. As shown in Table 5.15, the data point 1013.186 is assigned to “Cluster 2” since it is accompanied by the maximum degree of membership of 0.461. Additionally, the data point 760.253 is assigned to “Cluster 1” because it has the maximum degree of membership of 0.901. The thresholds utilized to describe the severity levels of spalling area and depth are presented in Table 5.16. The severity level of spalling is expressed in the form of percentage of zone area. It can be observed that if the

spalling area is between 45% and 55%, this implies that the bridge deck is in a “Poor” condition. Furthermore, it can be concluded that if spalling depth is more than 10 millimeters. Then, the bridge deck is in a “Very Poor” condition category.

Table 5.13: Performance comparison between the prediction models based on the augmented dataset

Prediction model	Mean absolute percentage error	Root mean-squared error	Root mean squared percentage error
ENN – IWO	4.625%	81.257	0.087
Artificial neural network	13.791%	225.2	0.231
Elman neural network	11.513%	216.306	0.225
Generalized regression neural network	13.775%	225.106	0.233
Radial basis neural network	12.183%	209.37	0.22
CONVNET	5.218%	83.797	0.105
AlexNet	6.394%	89.728	0.108
VGG16	6.395%	89.726	0.108
VGG19	6.393%	89.723	0.108
CaffeNet	6.393%	89.715	0.108

Table 5.14: Anderson Darling tests for probability distributions of spalling area

Probability distribution	Anderson Darling statistic (A²)	Rank
Normal	2.545	3
Logistic	1.76	1
Loglogistic	2.843	4
Gamma	3.744	5
Largest extreme value	4.827	6
Exponential	18.05	7
Weibull	1.891	2

Table 5.15: Sample of the cluster memberships of spalling area obtained from fuzzy C-means clustering algorithm

Data point	Degree of membership				Assigned Cluster
	Good	Medium	Poor	Very Poor	
1013.186	0.048	0.461	0.445	0.044	Medium
855.934	0.172	0.766	0.047	0.014	Medium
1126.234	0.001	0.004	0.989	0.004	Poor
1265.121	0.009	0.024	0.127	0.837	Very Poor
760.253	0.901	0.077	0.015	0.005	Good
1140.675	0.004	0.015	0.957	0.022	Poor
928.617	0.003	0.99	0.004	0.001	Medium

Table 5.16: Severity rating system of spalling based on its area and depth

Condition category	Spalling area	Spalling depth
Good	Less than 35%	Less than 3.7 mm
Medium	Between 35% and 45%	Between 3.7 and 6.1 mms
Poor	Between 45% and 55%	Between 6.1 and 10 mms
Very Poor	More than 55%	More than 10 mm

▪ **Assessment of corrosion severities**

GSSI RADAN7 software is used to pick the amplitude values of the top reinforcing rebars as shown in Figure 5.16. RapidMiner 7.5 is one of the platforms used to perform the clustering algorithms. The clustering model is divided into eight main sub modules, whereas the clustering algorithm is performed using the "clustering" submodule (see Figure 5.17). The number of optimization steps is assumed 100 for all the clustering algorithms. The clusters obtained from the expectation maximization clustering algorithm are shown in Figure 5.18. Y-axis 1 represents the amplitude values of bridge "A". X-axis represents the four condition categories of "Good", "Medium", "Poor" and "Very Poor". Threshold values obtained from the expectation maximization clustering algorithm of bridge "A" are -25.538, -10.964, and -2.767, respectively.

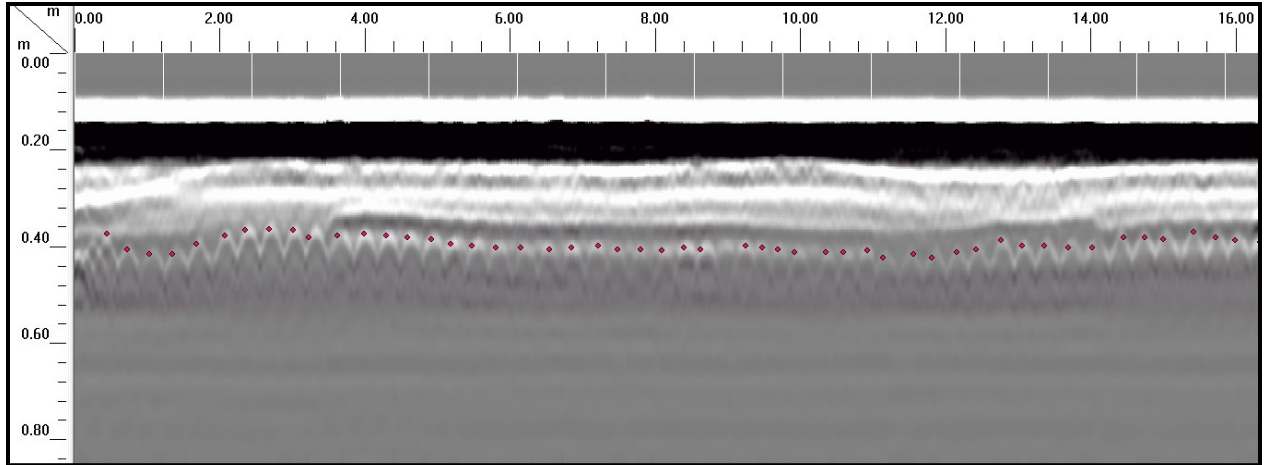


Figure 5.16: Picking the amplitude values of the top reinforcing rebar

Due to the difference in the thresholds obtained from the different clustering algorithms, the multi-objective optimization module is performed based on the four objective functions defined in chapter 4. In order to provide a fair comparison between the optimization algorithms, 20 independent optimization runs are carried out with different initializations for the multi-objective shuffled frog leaping algorithm, multi-objective particle swarm algorithm and multi-objective genetic algorithm. The initial parameters of the utilized meta-heuristics are adopted from previous literature. These parameters are adapted by modifying each of them one at a time to come up with the optimum configuration of parameters capitalizing on their performance. A sample of the optimum solutions obtained from the SFL is shown in Table 5.17. SFL generated very promising results when compared against the genetic algorithm, and the particle swarm optimization algorithm.

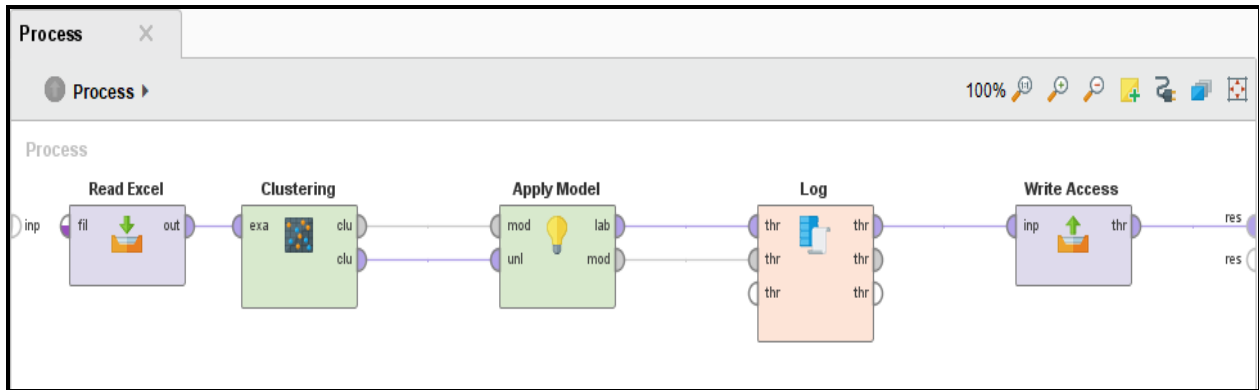


Figure 5.17: Interface of the RapidMiner platform

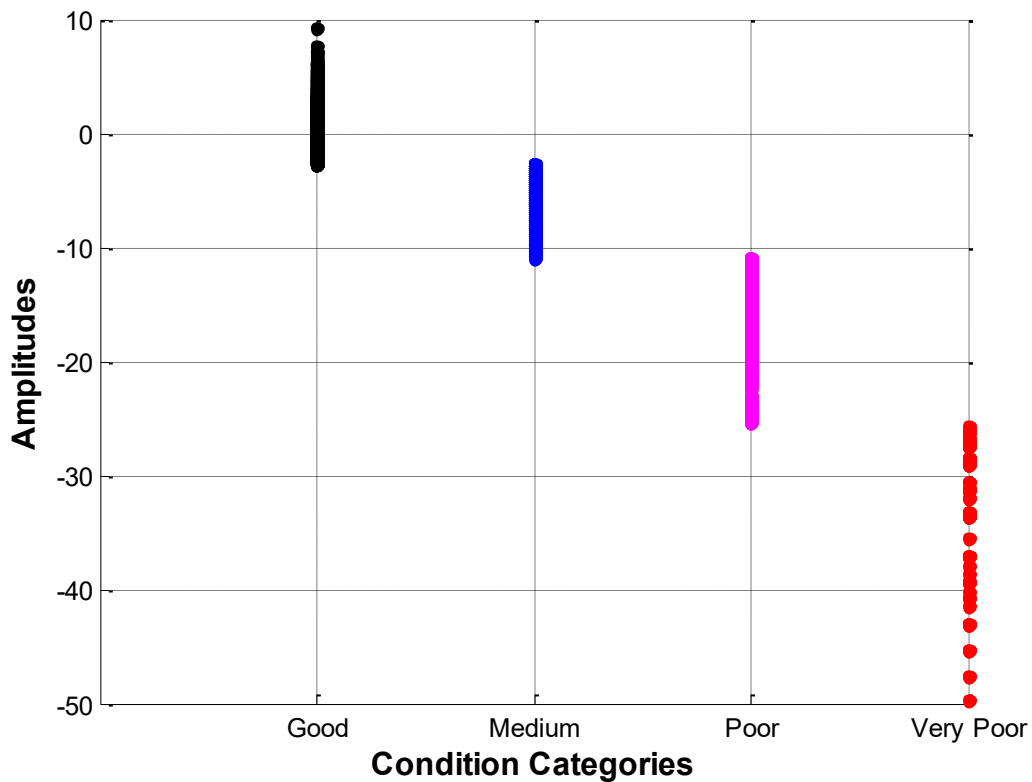


Figure 5.18: Clusters obtained from expectation maximization clustering algorithm

A sample of the Pareto frontier points for one of the runs is shown in Figures 5.19 and 5.20. Twenty seven Pareto frontier points are obtained from the three evolutionary algorithms, i.e., 12 points from the shuffled frog leaping algorithm, 10 points from the genetic algorithm, and 5 points from the particle swarm algorithm. The black bubbles, blue bubbles, and red bubbles

represent the Pareto frontier points of the shuffled frog leaping algorithm, genetic algorithm, and particle swarm algorithm, respectively. As shown in Figures 5.19 and 5.20, SFL generates the most feasible optimal solutions. However, a further detailed analysis is conducted to compare between the optimization algorithms

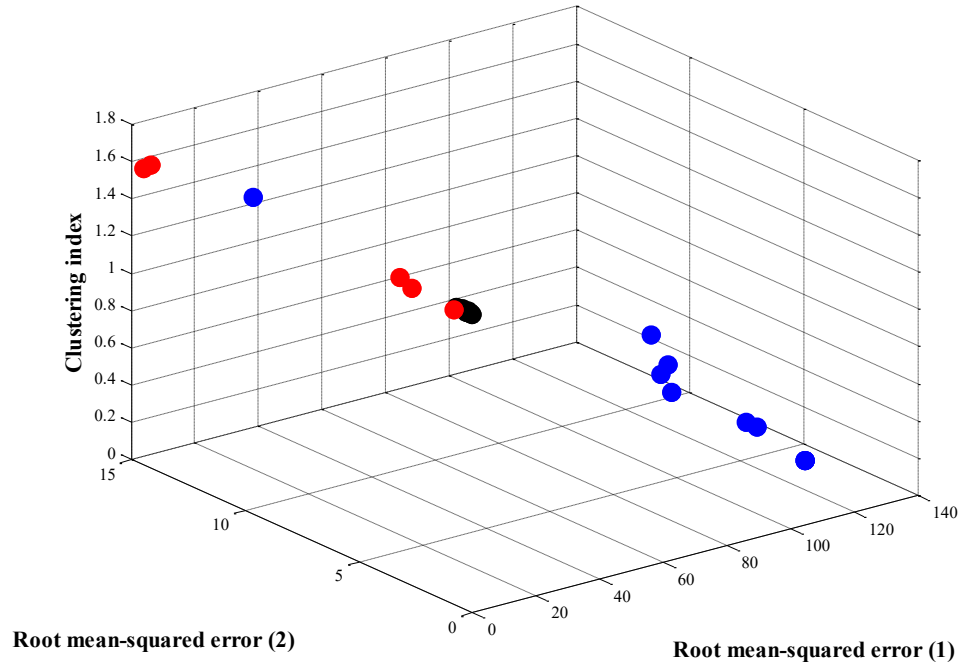
A comparison between shuffled frog-leaping, particle swarm algorithm and genetic algorithm based on the output of the 20 runs is illustrated in Table 5.18. The numbers mentioned herein represent the average values. Shuffled frog-leaping algorithm achieved the lowest objective function value regarding objective functions 1 and 3 while the genetic algorithm had the lowest objective function value regarding the objective functions 2 and 4. The worst objective function value of shuffled frog-leaping algorithm is better than other evolutionary algorithms for the first three objective functions. However, genetic algorithm has a better worst objective function value for the fourth objective function. The mean value obtained employing SFL is better than the other two algorithms regarding the first three objective functions while GA achieved the best mean value for the fourth objective function. SFL has the lowest standard deviation in terms of the four objective functions. A lower standard deviation indicates higher stability of the algorithm while a higher mean value indicates more accuracy of the optimization algorithm.

GA has the lowest coefficient of variation for the first objective function while SFL has the lowest coefficient of variation for the remaining three objective functions. SFL has the largest hypervolume indicator (84.87%) followed by particle swarm optimization algorithm and finally the genetic algorithm. In terms of the inverted generational distance, SFL has the least inverted generational distance (0.0034) when compared to other algorithms. For the processing time, the average processing times of the shuffled frog leaping algorithm, particle swarm algorithm and genetic algorithm are 131.97 minutes, 97.048 minutes and 88.143 minutes. Thus, SFL has the

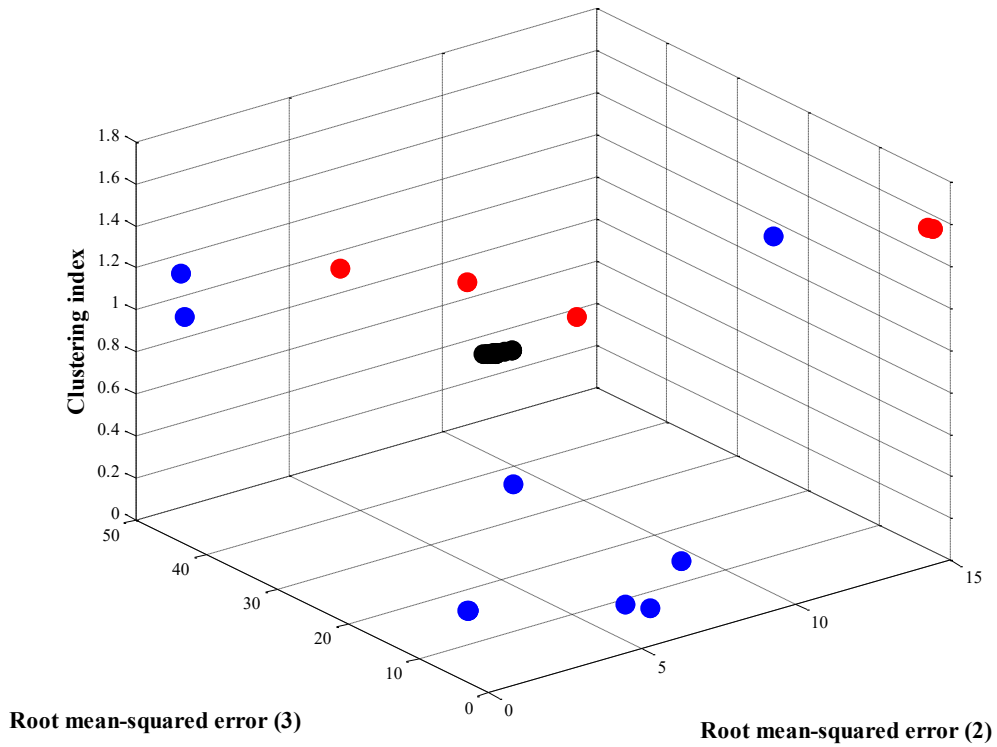
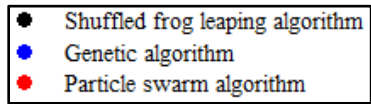
longest average computational time while genetic algorithm has the shortest average computational time.

Table 5.17: Sample of the optimal solutions of the shuffled frog leaping algorithm

Optimal Amplitudes	RMSE₁	RMSE₂	RMSE₃	CLU
[-16.6637, -8.7673, -2.9887]	0.5281	0.5306	0.0493	1.6003
[-16.729, -8.8339, -2.9277]	0.1644	0.1597	0.3885	1.6008
[-16.7505, -8.882, -2.8774]	0.0446	0.1082	0.6887	1.6001
[-16.8005, -8.8227, -3.0706]	0.2334	0.2223	0.4068	1.6018
[-16.7911, -8.8046, -2.9266]	0.1814	0.323	0.3947	1.6001
[-16.8363, -8.8094, -2.9632]	0.433	0.2962	0.1913	1.6018
[-16.7611, -8.8676, -2.844]	0.0423	0.0282	0.8545	1.6
[-16.6637, -8.7673, -2.9887]	0.5281	0.5306	0.0493	1.6003



(a)



(b)

Figure 5.19: Pareto frontier points of the three adopted evolutionary algorithms- A

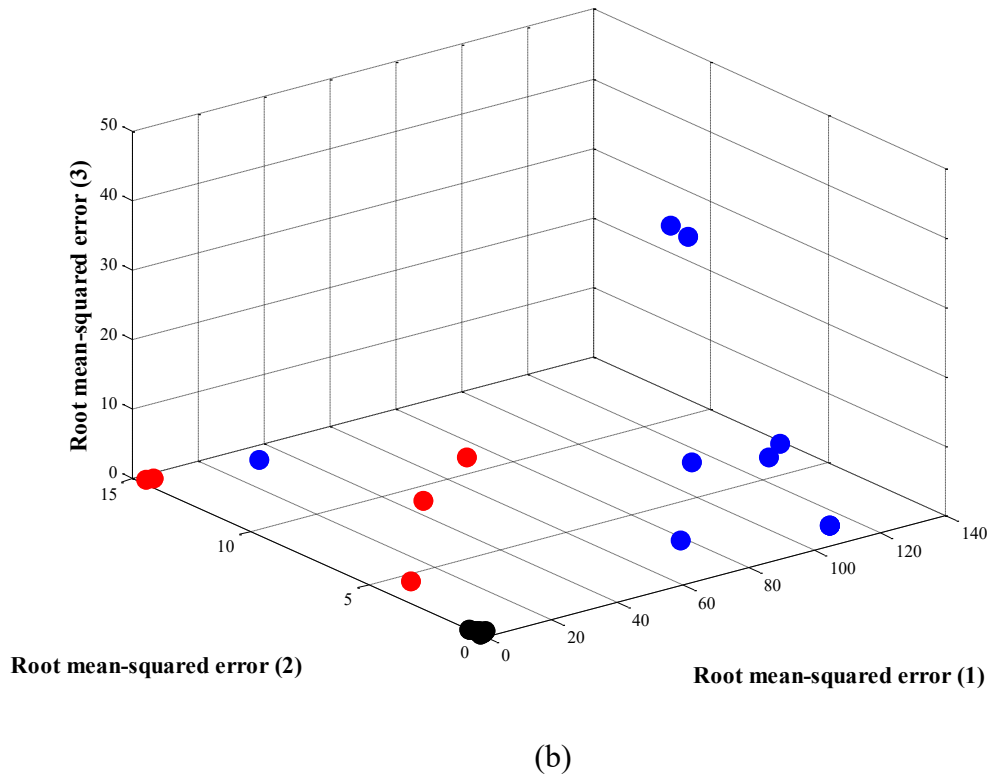
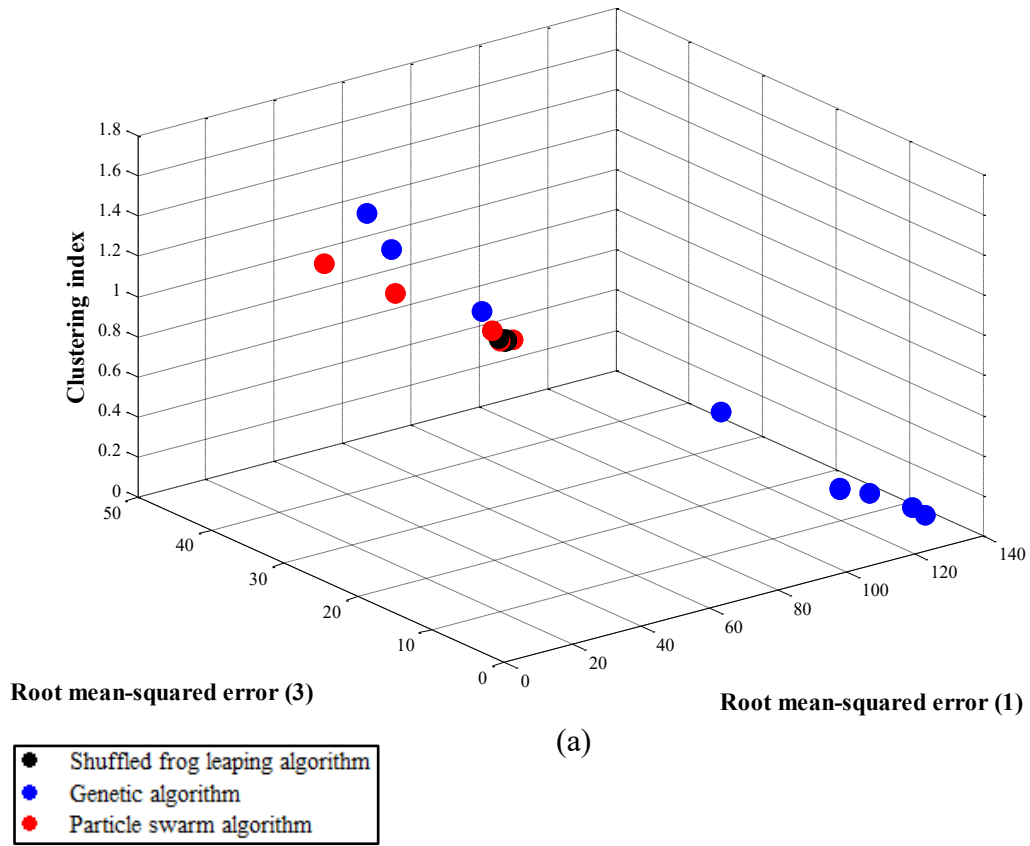


Figure 5.20: Pareto frontier points of the three evolutionary algorithms- B

Table 5.18: Comparison between shuffled frog-leaping, particle swarm algorithm and genetic algorithm for the twenty runs

Index	Objective function	Shuffled frog-leaping	Particle swarm optimization	Genetic algorithm
Minimum	RMSE ₁	0.0187	0.0423	65.4994
	RMSE ₂	0.0282	0.8257	0.0044
	RMSE ₃	0.0019	0.3135	1.3756
	CLU	1.5998	1.5804	0.1321
Maximum	RMSE ₁	0.6957	3.0568	127.4886
	RMSE ₂	0.7561	14.5401	10.9924
	RMSE ₃	0.8545	24.6486	49.2263
	CLU	1.6018	1.6036	1.5843
Mean	RMSE ₁	0.2598	1.2496	89.1582
	RMSE ₂	0.3177	7.2220	3.2343
	RMSE ₃	0.3259	8.7193	12.3022
	CLU	1.6006	1.5907	0.6197
Standard deviation	RMSE ₁	0.196	1.1312	34.197
	RMSE ₂	0.2312	6.0043	3.5267
	RMSE ₃	0.2755	9.6845	18.1101
	CLU	0.0008	0.0081	0.4647
Coefficient of variation	RMSE ₁	0.7546	0.9052	0.3836
	RMSE ₂	0.7280	0.8314	1.0904
	RMSE ₃	0.8453	1.1107	1.4721
	CLU	0.0005	0.0051	0.7498
Hypervolume indicator	84.87%	70.65%	50.58%
Inverted generational distance	0.0034	0.011	0.0037
Computational time (minutes)		131.97	97.0482	88.143

The decision-making module is implemented to select the best solution among the Pareto frontier points obtained from the multi-objective optimization module. There are four attributes which are: RMSE₁, RMSE₂, RMSE₃, and CLU whereas the weights of the attributes are calculated based on the Shannon entropy method. The weights of the four attributes (RMSE₁, RMSE₂, RMSE₃, and CLU) are 22.11%, 27.23%, 34.83%, and 15.82%, respectively. The calculations of the weights of the attributes are illustrated in Table 5.19. A sample of the solution ranking obtained

from TOPSIS is depicted in Table 5.20. Each one of the decision-making provided a distinct ranking for the solutions. For instance, TOPSIS selected the solution [-16.7619, -8.8161, -2.9744] as the best solution. On the other hand, COPRAS selected the solution [-16.729, -8.8339, -2.9727] as the best solution. Thus, group decision-making is essential to aggregate the rankings obtained from the several multi-criteria decision-making techniques based on a single objective optimization problem. Genetic algorithm is implemented where the population size and the number of generations are assumed 100. The crossover rate, and the mutation rate are assumed 0.8, and 0.1, respectively. Based on the decision-making module, the standardized thresholds of amplitude rating system are: -16.7619, -8.8161, and -2.9744 decibels.

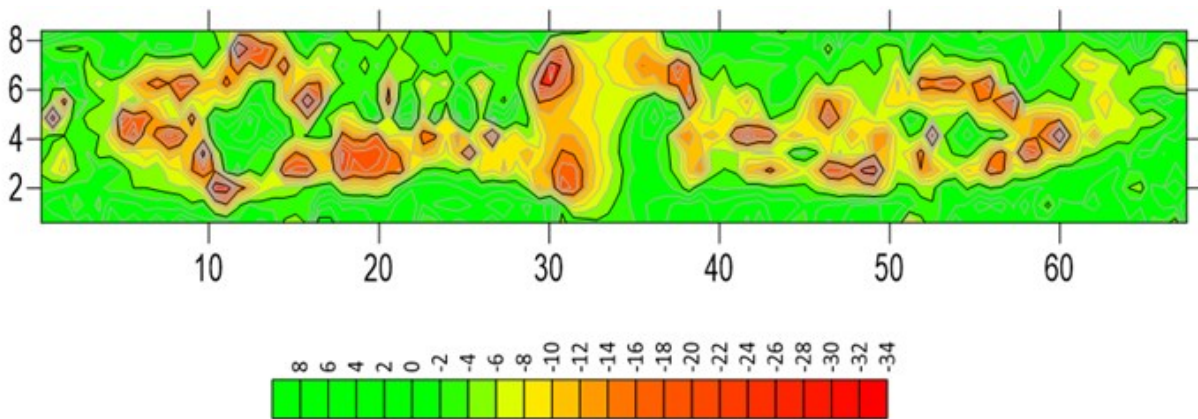
A corrosion map of a zone of the bridge deck “A” is depicted in Figure 5.21. As can be seen, the area percentages of the “Good”, “Medium”, “Poor” and “Very Poor” categories are: 45.78%, 34.26%, 12.98%, and 6.98%, respectively. The corrosion map of a zone of the bridge deck “B” is depicted in Figure 5.22. As shown in Figure 5.22, the area percentages of the “Good”, “Medium”, “Poor”, and “Very Poor” condition categories are: 41.3%, 43.18%, 10.35%, and 5.17%, respectively. In this context, the corrosion maps are developed based on the standardized amplitude rating system of [-16.7619, - 8.8161, -2.9744].

Table 5.19: Entropy values, variation coefficients, and the weights of the attributes

Index	RMSE₁	RMSE₂	RMSE₃	CLU
Entropy value (e_j)	0.476	0.355	0.175	0.625
variation coefficient (d_j)	0.523	0.6447	0.824	0.374
weights of the attribute (w_j)	22.11%	27.23%	34.83%	15.82%

Table 5.20: Sample of the solutions' ranking obtained from TOPSIS

Solution (decibels)	Evolutionary algorithm	s_i^+	s_i^-	c_i^*	Solution ranking
[-16.7619, - 8.8161, -2.9744]	SFL	0.03318	0.28816	0.89673	1
[-16.729, -8.8339, -2.9727]	SFL	0.03315	0.28773	0.89669	2
[-16.705, -8.882, -2.8774]	SFL	0.03321	0.287303	0.89636	4
[-29.2791, -8.5982, -3.5222]	GA	0.03397	0.28581	0.89377	17
[-35.5542, -8.8618, -3.5443]	GA	0.0332	0.28798	0.89661	15
[-29.1454, -8.6766, -5.5362]	GA	0.227	0.1491	0.3964	26
[-17.3076, -6.2511, -2.9412]	PSO	0.15622	0.2444	0.61006	24
[-16.7866, -9.0109, 1.4294]	PSO	0.11914	0.206	0.63356	21
[-16.751, -6.2662, -3.1229]	PSO	0.15537	0.2435	0.6105	23



Good	Medium	Poor	Very Poor
45.78%	34.26%	12.98%	6.98%

Figure 5.21: Corrosion map of the first bridge deck

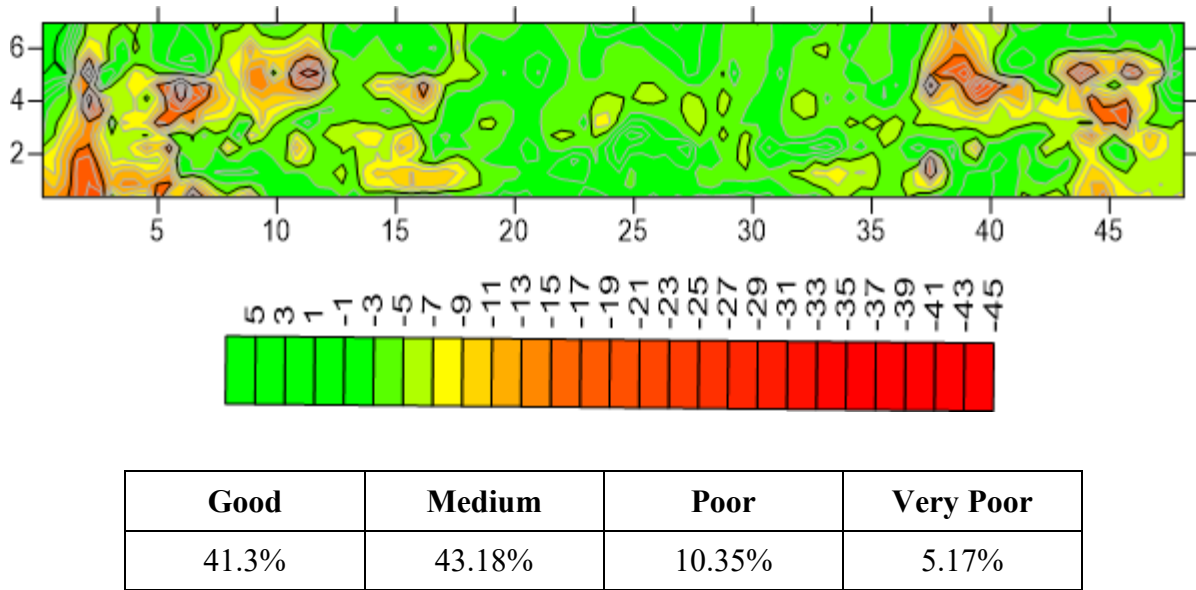


Figure 5.22: Corrosion map of the second bridge deck

▪ **Integrated condition assessment**

The first stage of the developed framework is to compute the weighting vector of the bridge defects capitalizing on O – FANP. A questionnaire survey is designed to get feedback from the experts based on two levels of comparison, where the experts were asked to determine how important is bridge defect A when compared with bridge defect B with respect to the condition of the bridge deck. For the second level of comparison, the experts were asked to identify how important is bridge defect A when compared to bridge defect B with respect to bridge defect C. A total of 35 responses were received from 40 experts, which implies a response rate of 87.5%. The respondents are site engineers with experience of 5-10 years. They are aware of the different construction practices of bridges as well as the different concrete defects.

In the designed survey, the experts were asked to fill out the pair-wise comparison matrices based on five linguistic terms, which are: equally important (EI), moderately important (MI),

strongly important (SI), very strongly important (VSI), and absolutely important (AI). The developed framework utilizes NSGA – II to determine the optimum fuzzy scale among the set of five triangular fuzzy scales. The population size and number of iterations are assumed 10 and 30, respectively. Tournament selection is the parent selection strategy. The crossover rate and the mutation rate are assumed 0.8 and 0.05, respectively. The convergence of the optimum fuzzy scale selection model is presented in Figure 5.23. As can be seen, the minimum OVR_CONST achieved is 1.88%. Moreover, the optimization model stabilizes at iteration 8 which demonstrates the success of NSGA – II in searching for the optimum fuzzy scale. TFS#3 is selected as the optimum fuzzy scale, and it is the one used in any further computations. Table 5.21 and Table 5.22 illustrate a sample of the pair-wise comparison matrices for the first level of comparison and second level of comparison (with respect to corrosion), respectively using TFS#3. It should be mentioned that the optimization model provided a significant enhancement in the OVR_CONST from 20.38% to 1.88%, which aids in establishing more efficient condition assessment models.

After the calculation of the optimum linguistic scale, the pair-wise comparison matrices that achieved a consistency ratio more than 10% are removed from any further calculations. The considered pair-wise comparison matrices are only the ones that achieved a consistency ratio less than 10%. The opinions of the experts are aggregated based on the geometric mean. The opinions of the experts are aggregated based on the geometric mean using Equation. The aggregated pair-wise comparison matrices are analyzed using Chang’s extent analysis method to compute the weights of the five bridge defects. Table 5.23 presents a sample of the constructed un-weighted supermatrix, weighted supermatrix, and limit supermatrix. Based on the limit supermatrix, the weights of the corrosion, delamination, cracking, spalling and scaling are:

33.411%, 22.816%, 16.735%, 23.467%, and 3.569%, respectively. This implies that corrosion has the largest weight followed by spalling while scaling had the lowest weight of importance. The second model is the integrated condition assessment. The weights of the bridge defects are fed from the weight interpretation model. The first phase of the integrated condition assessment model is the automated calibration of fuzzy membership functions of the bridge defects. The percentages of severities of bridge defects alongside with their importance weightings are integrated to compute the BDSIs and IBDCI. These percentages constitute the degrees of fuzzy membership functions of bridge defects. The percentages of severities of corrosion are interpreted using the ground penetrating radar while the severities of surface defects are analyzed using computer vision-based methods. Delamination severities are captured from the inspection reports.

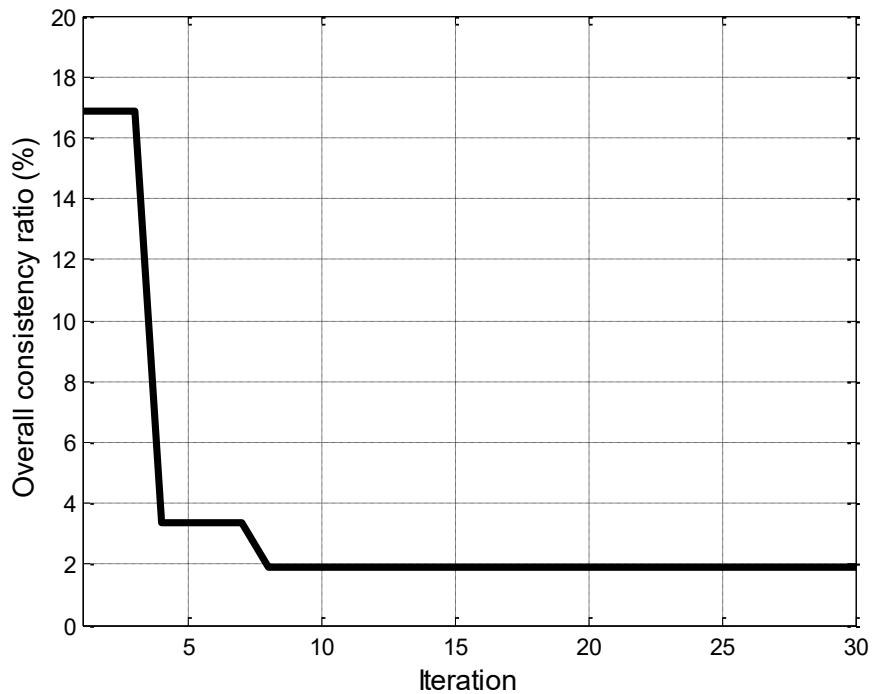


Figure 5.23: Convergence of the NSGA – II for optimum fuzzy scale computation

Table 5.21: Sample of the pair-wise comparisons with respect to the condition of the bridge deck

Bridge defects	Corrosion	Delamination	Cracking	Spalling	Scaling
Corrosion	(1, 1, 1)	(1, 1, 1)	(1, 1, 1.5)	(1, 1.5, 2)	(1, 1.5, 2)
Delamination	(1, 1, 1)	(1, 1, 1)	(1, 1, 1.5)	(1, 1, 1.5)	(1, 1, 1.5)
Cracking	(2/3, 1, 1)	(2/3, 1, 1)	(1, 1, 1)	(1, 1, 1.5)	(1, 1, 1.5)
Spalling	(1/2, 2/3, 1)	(2/3, 1, 1)	(2/3, 1, 1)	(1, 1, 1)	(1, 1, 1)
Scaling	(1/2, 2/3, 1)	(2/3, 1, 1)	(2/3, 1, 1)	(1, 1, 1)	(1, 1, 1)

Table 5.22: Sample of the pair-wise comparisons with respect to the corrosion

Bridge defects	Delamination	Cracking	Spalling	Scaling
Delamination	(1, 1, 1)	(1, 1, 1)	(1, 1.5, 2)	(1, 1.5, 2)
Cracking	(1, 1, 1)	(1, 1, 1)	(1, 1, 1)	(1, 1, 1)
Spalling	(1/2, 2/3, 1)	(1, 1, 1)	(1, 1, 1)	(1, 1, 1)
Scaling	(1/2, 2/3, 1)	(1, 1, 1)	(1, 1, 1)	(1, 1, 1)

IWO algorithm is adopted for the automated calibration of fuzzy membership functions. This comprises optimizing the shape of fuzzy membership function of bridge defects, the boundaries of fuzzy membership functions and defuzzification technique. The length of the optimization model varies within the iterations as a result of the optimization of S_D , whereas its maximum length is 32. The initial population size and maximum number of iterations are assumed 100 and 100, respectively. The minimum and maximum numbers of seeds are assumed 0 and 5, respectively. The initial and final values of the standard deviation are assumed 0.01 and 0.5, respectively. The non-linear modulation index is assumed two. The convergence curve of the invasive weed optimization model is depicted in Figure 5.24. The minimum ACDT achieved by the IWO algorithm is 4.878×10^{-6} . Furthermore, the optimization model stabilizes at iteration 22. This exemplifies the higher capacity of the IWO algorithm in optimizing the fuzzy membership functions of the bridge defects.

Table 5.23: Un-weighted supermatrix, weighted supermatrix, and limit supermatrix of the different affecting bridge defects

With respect to	Un-weighted supermatrix					weighted supermatrix					limit supermatrix				
	Goal	C1	C2	...	C5	Goal	C1	C2	...	C5	Goal	C1	C2	...	C5
Goal	0	0	0	0	0	0	0	0	0	0	0	0	0	0	0
C1	0.306	0	0.429	...	0.392	0.306	0	0.429	...	0.392	0.334	0.334	0.334	...	0.334
C2	0.186	0.179	0	...	0.117	0.186	0.179	0	...	0.117	0.228	0.228	0.228	...	0.228
C3	0.16	0.417	0.254	...	0.058	0.16	0.417	0.254	...	0.058	0.167	0.167	0.167	...	0.167
C4	0.293	0.373	0.26	...	0.431	0.293	0.373	0.26	...	0.431	0.234	0.234	0.234	...	0.234
C5	0.053	0.029	0.056	...	0	0.053	0.029	0.056	...	0	0.035	0.035	0.035	...	0.035

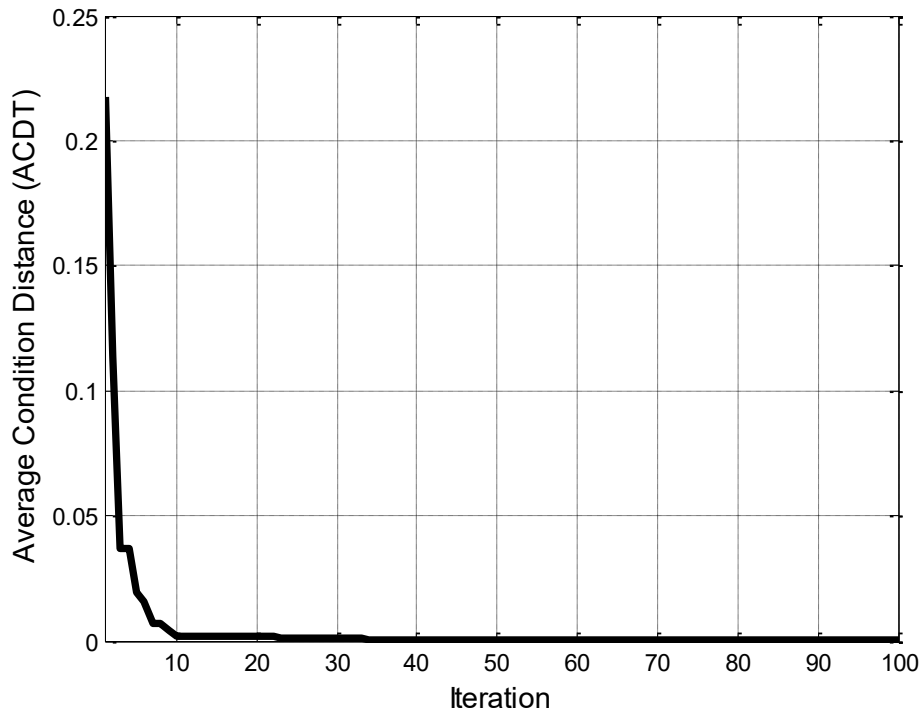


Figure 5.24: Convergence of invasive weed optimization algorithm for the automated calibration of fuzzy membership functions

The developed automated calibration model is validated through comparison with genetic algorithm and nonlinear programming (NLP). Genetic algorithm is considered as the benchmark meta-heuristic that most of the optimization algorithms are compared with to signify their performance. Ten independent runs were carried out in order to account for the randomness of the meta-heuristic optimization algorithms and to establish a robust comparison between the optimization algorithms. The population size and number of iterations are assumed 100 for both in order to establish a fair comparison with the invasive weed optimization model. Tournament selection is the parent selection strategy. Two-point crossover is utilized such that the crossover rate is assumed 0.8 while the mutation rate is assumed 0.1. A comparative analysis between the invasive weed optimization algorithm, genetic algorithm and non-linear programming is depicted in Table 5.24. IWO algorithm achieved the lowest objective function value while NLP attained

the highest objective function value (4.709). It can be also noticed that the IWO algorithm provided lowest maximum and mean values of the ACDT. Furthermore, IWO algorithm achieved lowest coefficient of variation than the GA. A lower coefficient of variation implies better quality and less variability in the generated optimum solutions. The convergence curve of the genetic algorithm optimization model is presented in Figure 5.25. It can be inferred that the minimum attained ACDT is 0.0192. Moreover, the optimization model stabilizes at iteration 53. In the light of foregoing, it can be interpreted that IWO algorithm significantly outperformed the genetic algorithm and non-linear programming. Additionally, it required more iterations to stabilize compared against the IWO algorithm.

Table 5.24: A comparative analysis between the performances of IWO, GA and NLP

Index	IWO	GA	NLP
Minimum	4.878×10^{-6}	1.92×10^{-2}	4.709
Maximum	1.6×10^{-4}	2.782×10^{-1}
Mean	3.32×10^{-5}	5.93×10^{-1}
Coefficient of variation	0.4756	1.2561

It is worth mentioning that the present optimization problem consists of discrete and continuous decision variables. Discrete optimization problems are combinatorial problems, which are subsequently considered as non-deterministic polynomial time (NP)-hard problems. Mathematical optimization algorithms often fail to deal with NP-hard problems. NLP is performed based on the active set algorithm. NLP provided the least performance compared to IWO algorithm and GA. This manifests that the NLP fails to solve the NP -hard problems with a large number of decision variables especially discrete decision variables and non-linear objective functions. NLP failed to find the global optimum solutions because, in the case of large-scale and

complex problems, the exact solutions methods are inefficient to explore the design search space, and the meta-heuristic algorithms can serve as a better alternative to find the optimal solutions.

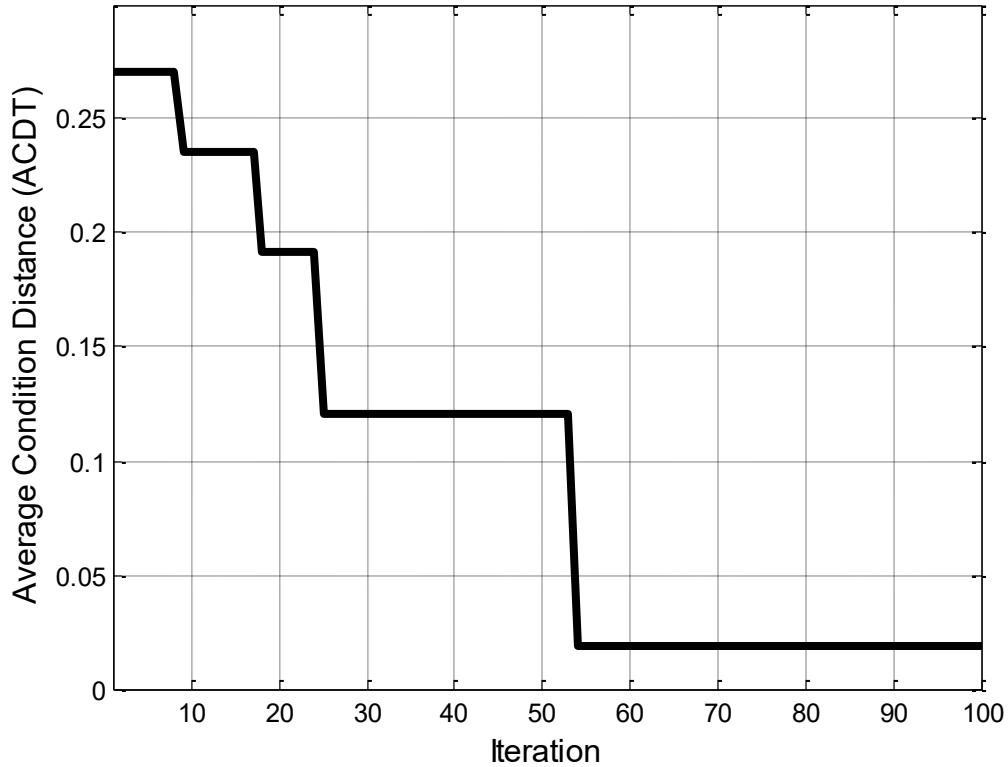


Figure 5.25: Convergence of genetic optimization algorithm for the automated calibration of fuzzy membership functions

The optimized parameters of the fuzzy membership functions are presented in Table 5.25. As can be seen, the optimum shape of fuzzy membership function is triangular distribution. The optimum defuzzification technique is the bisector method. It can be also concluded that the optimized boundaries of the fuzzy membership functions of the bridge defects are different from each other. For instance, the distributions of the very poor, poor, good and medium categories for corrosion are (0, 25.647), (0, 25.647, 55.206), (25.647, 55.206, 100), and (25.647, 55.206, 100), respectively. On the other hand, the distributions of the very poor, poor, good and medium

categories for spalling constitute (0, 37.91), (0, 37.91, 67.636), (37.91, 67.636, 100), and (67.636, 100), respectively. The calibrated membership functions of the corrosion are displayed in Figure 5.26. The black, magenta, red and blue fuzzy sets denote the “Very Poor”, “Poor”, “Medium” and “Good” categories, respectively.

Table 5.25: Optimized parameters of the fuzzy membership functions using the invasive weed optimization algorithm

Parameter	Description	Value
S_D	Shape of the membership function	Triangular
B_{11}	Very Poor fuzzy set in corrosion	(0, 25.647)
B_{21}	Poor fuzzy set in corrosion	(0, 25.647, 55.206)
B_{31}	Medium fuzzy set in corrosion	(25.647, 55.206, 100)
B_{41}	Good fuzzy set in corrosion	(55.206, 100)
B_{12}	Very Poor fuzzy set in delamination	(0, 30.364)
B_{22}	Poor fuzzy set in delamination	(0, 30.364, 61.834)
B_{23}	Medium fuzzy set in delamination	(30.364, 61.834, 100)
B_{24}	Good fuzzy set in delamination	(61.834, 100)
B_{13}	Very Poor fuzzy set in cracking	(0, 25.958)
B_{23}	Poor fuzzy set in cracking	(0, 25.958, 56.101)
B_{33}	Medium fuzzy set in cracking	(25.958, 56.101, 100)
B_{34}	Good fuzzy set in cracking	(56.101, 100)
B_{41}	Very Poor fuzzy set in spalling	(0, 37.91)
B_{42}	Poor fuzzy set in spalling	(0, 37.91, 67.636)
B_{43}	Medium fuzzy set in spalling	(37.91, 67.636, 100)
B_{44}	Good fuzzy set in spalling	(67.636, 100)
B_{51}	Very Poor fuzzy set in scaling	(0, 29.541)
B_{52}	Poor fuzzy set in scaling	(0, 29.541, 58.531)
B_{53}	Medium fuzzy set in scaling	(29.541, 58.531, 100)
B_{54}	Good fuzzy set in scaling	(58.531, 100)
DE_FUZZ	Defuzzification method	Bisector

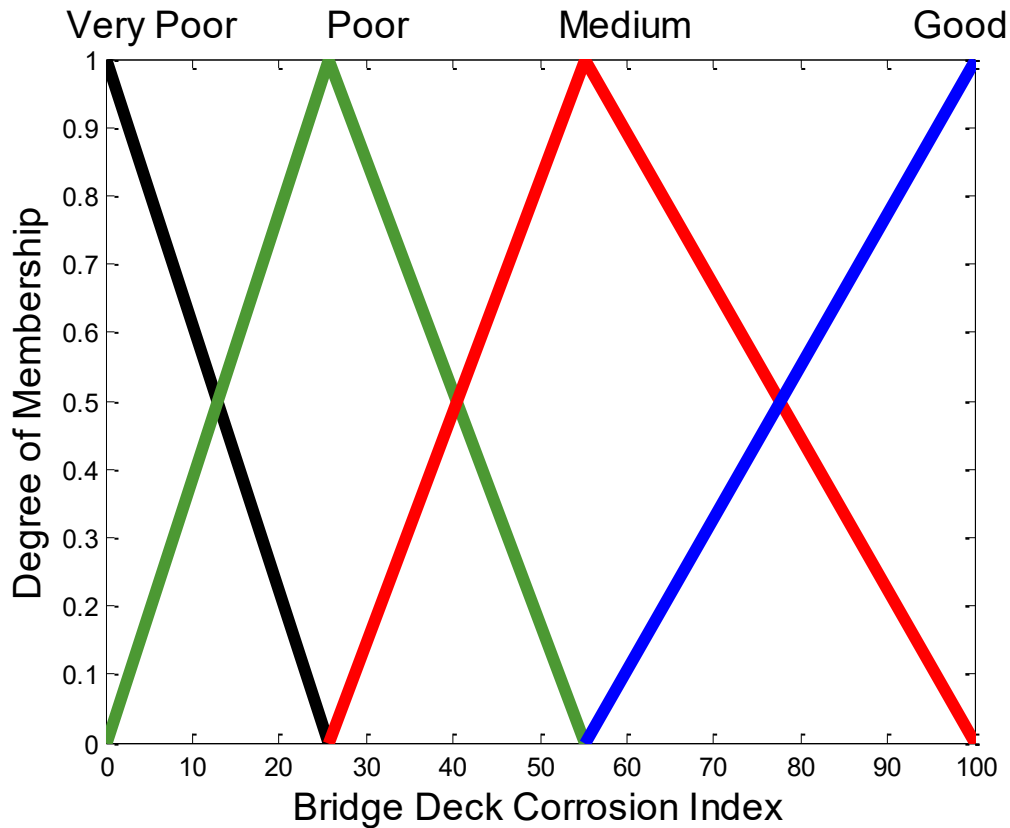


Figure 5.26: Calibrated fuzzy membership functions of corrosion

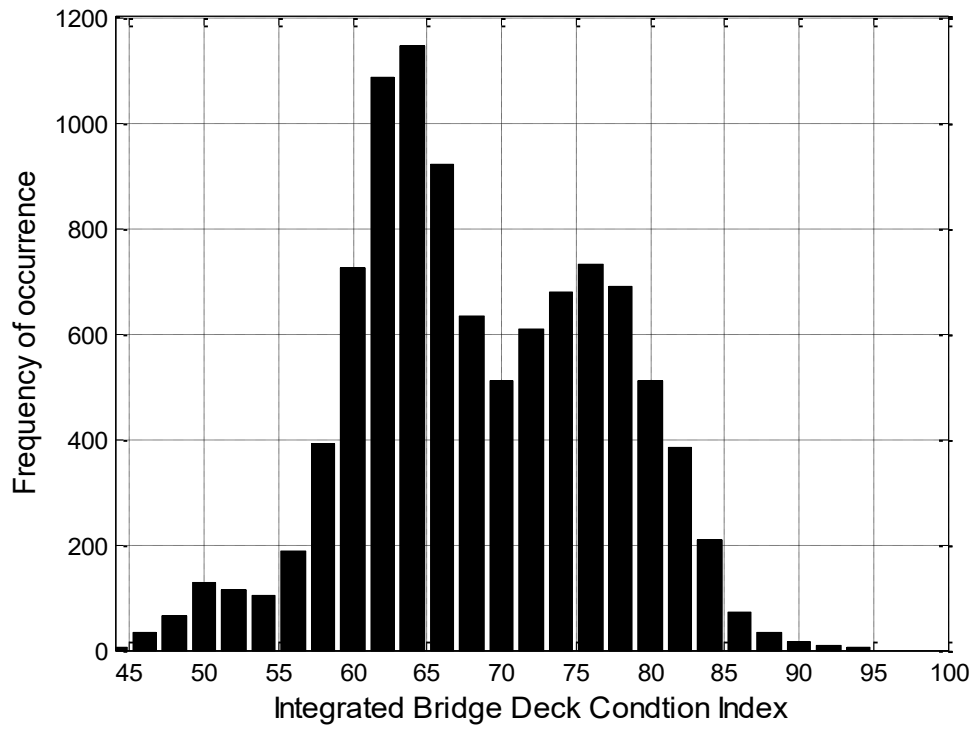
The third model is the bridge maintenance decision-making strategy, which opts at structuring an intervention platform of bridge decks capitalizing on the IBDCI in addition to designing a severity rating system for each of the five bridge defects separately. A database is established using 10 bridges scanned using the ground penetrating radar alongside other 35 inspection records. This dataset is used to append the percentages of severities of the bridge defects for the purpose of identification the best-fit distribution. In this context, Chi-squared test is implemented to define the best-fit distribution of each condition category. The chi-squared critical value at significance level of 0.05 is 60.481. A sample of the identified best-fit distributions for some condition categories is illustrated in Table 5.26. The best-fit distribution is the one associated with the lowest chi-squared statistic. The chi-squared statistic for the best-fit distribution of the

“Very Poor” condition category of corrosion is 2.746. Additionally, the chi-squared statistic for the best-fit distribution of the “Poor” condition category of scaling is 54.396. This indicates that the exponential distribution better fits the “Very Poor” condition category of corrosion than the uniform distribution fits “Poor” condition category of scaling.

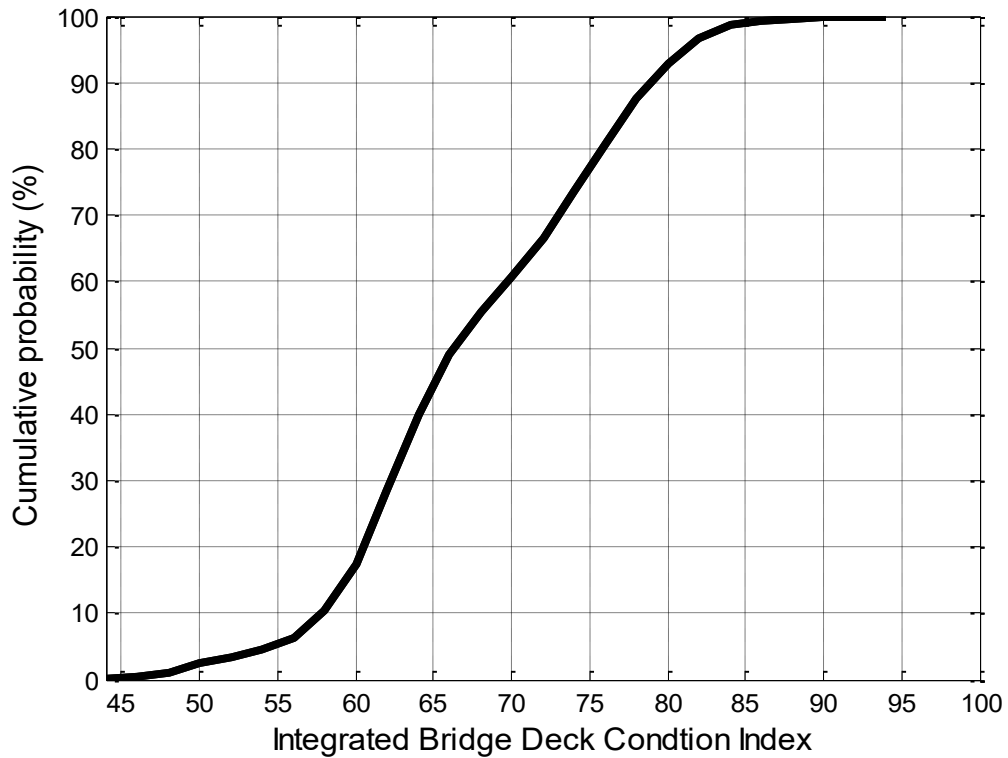
It can be also interpreted that the best-fit distribution for the “Good” category of corrosion is uniform distribution while the best-fit distribution of the “Medium” category of spalling follows exponential distribution. Latin hypercube sampling is adopted to generate a large number of random scenarios of the severity percentages of defects based on the best-fit distribution. The histogram generated from Latin hypercube sampling is constructed based on 10,000 iterations. Figure 5.27.a depicts the histogram of the IBDCI generated using Latin hypercube sampling. Figure 5.27.b represents the cumulative distribution of the IBDCI. The simulations of the LHS signify that there is a probability 90.37% that the IBDCI lies between 50 and 80.

Table 5.26: A sample of chi-squared test for some bridge condition categories

Condition category	Bridge defect	Chi-squared statistic	Best-fit distribution
Good	Corrosion	51.219	Uniform
Very poor	Corrosion	2.746	Exponential
Very poor	Delamination	40.289	Exponential
Medium	Cracking	12.92	Exponential
Medium	Spalling	50.54	Exponential
Poor	Scaling	54.396	Uniform



(a) Output of the Latin hypercube sampling



(b) Cumulative distribution of the integrated bridge deck condition index

Figure 5.27: Histogram and cumulative distribution of the IBDCI using Latin hypercube sampling

The rating systems of the BDCI, BDDI, BDCRI, BDSPI, BDSCI and IBDCI are established based on fuzzy C-means clustering algorithm. The maximum number of iterations and fuzzifier constant are assumed 9,000 and 3, respectively. A sample of the cluster memberships obtained from the FCM algorithm is depicted in Table 5.27. In the fuzzy C-means clustering algorithm, the data point is assigned to the cluster that has the maximum degree of membership. For instance, the data point of IBDCI 59.149 is assigned to “Cluster 2” because it has the maximum degree of membership of 0.5937. Furthermore, the data point of IBDCI 78.48 is assigned to “Cluster 4” because it is associated with the maximum degree of membership (0.8489).

Table 5.28 describes the rating systems of the bridge defects based on their corresponding BDSI. As shown in Table 5.28, if the BDCRI is less than 57.223. Then, the bridge deck experience very severe cracking. It can also be interpreted that if the BDSPI lies between 65.916 and 83.81. Thus, the bridge deck suffers from severe spalling. Table 5.29 enables the decision makers to interpret the severity levels of the bridge defects they are mostly concerned with capitalizing on the corresponding BDSI. Table 5.29 demonstrates the bridge deck intervention recommendations as per the IBDCI. As shown in Table 5.29, if the IBDCI is less than 60.318 this implies that the bridge deck needs replacement. Moreover, if the IBDCI is between 60.318 and 67.769. Thus, the bridge deck requires rehabilitation.

For the bridge located in the Chemin Saint-Grégoire in municipality Les Cèdres, the output of the bridge deck corrosion model is depicted in Figure 5.28. The cyan membership function represents the resultant fuzzy set of the bridge defects based on the interpreted severity levels of the bridge defects. This fuzzy set is defuzzified to obtain the bridge deck severity index for each of the defects. The degrees of membership of the resultant fuzzy set are obtained based on the percentages of condition categories of the bridge defects. As shown in Figure 5.28, the

percentages of severities of corrosion are extracted from the displayed corrosion map. As such, the resultant fuzzy set of corrosion is established, and the BDCI is found to be equal to 70.552, which implies that the bridge deck suffers from medium corrosion. It can be also inferred from that the BDDI, BDCRI, BDSPI and BDSCI are equal to 57.443, 43.42, 72.923 and 41.137, respectively. This indicates the bridge deck suffers from severe delamination, very severe cracking, severe spalling and very severe scaling. Then, the IBDCI is computed capitalizing on the weights of the bridge defects and the BDSIs. The IBDCI is found to be equal to 60.844 out of 100. This implies that the bridge deck requires rehabilitation.

Table 5.27: A sample of the cluster memberships obtained from the FCM algorithm

Data point	Degree of membership				Assigned Cluster
	Good	Medium	Poor	Very Poor	
59.149	0.0559	0.0858	0.2646	0.5937	Very Poor
75.73	0.4140	0.3956	0.1141	0.0764	Good
66.768	0.1215	0.2783	0.4421	0.1581	Poor
63.186	0.0109	0.0193	0.9406	0.0292	Poor
70.583	0.1215	0.6565	0.1440	0.0780	Medium
70.194	0.1327	0.6018	0.1738	0.0918	Medium
81.586	0.6687	0.1740	0.0900	0.0674	Good
78.508	0.8548	0.0845	0.0354	0.0252	Good
57.764	0.0203	0.0301	0.0773	0.8724	Very Poor
75.197	0.3506	0.4556	0.1168	0.0770	Good
78.48	0.8489	0.0881	0.0368	0.0262	Good
58.516	0.0430	0.0649	0.1826	0.7095	Very Poor

The developed bridge deck corrosion model using the ground penetrating radar is validated through comparison with the results obtained from the half-cell potential. Half-cell potential is a non-destructive technique that relies on the potential difference between a reference electrode and the reinforcement rebars to evaluate the corrosion in concrete structures. It is criticized by being inefficient to deal with epoxy coated reinforcement (Elsener et al., 2003). A comparison

between the corrosion evaluated from both ground penetrating radar is described in Table 5.30. As shown in Table 5.30, the percentages of “Good”, “Medium”, “Poor” and “Very Poor” categories interpreted using half-cell potential are 62%, 33.6%, 3.7% and 0.14%, respectively. The BDCI obtained from ground penetrating radar and half-cell potential are 70.552 and 83.135, respectively. As such, the overall severity levels of corrosion from ground penetrating radar and half-cell potential are “Medium” and “Good”, respectively. In this context, it can be concluded that the differences in the overall corrosion assessment obtained from the models manifest the higher capacity of ground penetrating radar in detecting and evaluating corrosion. This is compatible with the recommendations provided by Gucunski et al. (2013), Barnes and Trottier (2004), and Cardimona et al. (2000) who preferred ground penetrating radar over half-cell potential with respect to modelling the deterioration in the reinforced concrete bridges.

The developed integrated condition assessment model is then compared against the models established by Alsharqawi et al. (2018), and Dinh and Zayed (2016). Alsharqawi et al. (2018) introduced a quality function deployment-based model to calculate an integrated condition index. The bridge deck achieved a condition index of 22.77%, which meant that the bridge deck needs was in a poor condition and requires repair based on a three-point scale. Dinh and Zayed (2016) computed a bridge deck corrosiveness index for the same bridge deck and it was 60.26 out of 100. The bridge deck was given grade “D”, which indicated the bridge deck is very unhealthy and intervention is strongly recommended based on a five-point scale. The differences in the IBDCI obtained from the developed model with respect to the afore-mentioned models can be attributed to three main reasons. The developed model defines the bridge intervention strategy based on an evaluation of a set of defects, whereas developing a bridge intervention strategy based on a single defect often fails to provide an accurate insight about the condition of the

bridge deck. Additionally, the developed condition assessment model is based on the integration of ground penetrating radar and computer vision technologies for better capturing the severity levels of surface defects. Furthermore, some models don't model the uncertainties arise from the vagueness and subjectivity provided by experts' judgements, and the inherent uncertainties encountered during the evaluation of bridge defects' severities. Lack of modelling of these uncertainties sometimes induces unrobust and inefficient condition assessment models.

For the second bridge located in Boulevard Lévesque Est, based on the integrated condition assessment model, BDCI, BDDI, BDCRI, BDSPI and BDSCI are 80.657, 77.599, 95.171, 89.066 and 95.53, respectively, This signifies that the bridge deck experience slight corrosion, medium delamination, slight cracking, medium spalling and slight scaling. Then, IBDCI is envisioned based on the afore-mentioned bridge defects severity indices as well as the relative importance weightings of the bridge defects. The IBDCI is equal to 82.964, which manifests that the bridge deck doesn't need intervention. A two-fold comparison is conducted between the condition ratings obtained by the developed framework and the ones from the inspection ratings. The IBDCI is converted to a scale from one to four in order to establish a fair comparison between the two models.

Table 5.28: Rating systems of the bridge defects based on their severity indices

Range of the BDSI	Bridge defect	Extent of severity
Less than 42.721	Corrosion	The bridge deck suffers from very severe corrosion.
Between 42.721 and 58.29		The bridge deck suffers from severe corrosion.
Between 58.29 and 75.381		The bridge deck suffers from medium corrosion.
More than 75.381		The bridge deck suffers from slight corrosion.
Less than 55.211	Delamination	The bridge deck suffers from very severe delamination.
Between 55.211 and 69.963		The bridge deck suffers from severe delamination.
Between 69.963 and 78.073		The bridge deck suffers from medium delamination.
More than 78.073		The bridge deck suffers from slight delamination.
Less than 57.227	Cracking	The bridge deck suffers from very severe cracking.
Between 57.227 and 79.153		The bridge deck suffers from severe cracking.
Between 79.153 and 89.453		The bridge deck suffers from medium cracking.
More than 89.453		The bridge deck suffers from slight cracking.
Less than 65.916	Spalling	The bridge deck suffers from very severe spalling.
Between 65.916 and 83.81		The bridge deck suffers from severe spalling.
Between 83.81 and 91.734		The bridge deck suffers from medium spalling.
More than 91.734		The bridge suffers from slight spalling.
Less than 57.512	Scaling	The bridge deck suffers from very severe scaling.
Between 57.512 and 74.707		The bridge deck suffers from severe scaling.
Between 74.707 and 81.938		The bridge deck suffers from medium Pop-out.
More than 81.938		The bridge suffers from slight scaling.

Table 5.29: Bridge intervention recommendations based on the IBDCI

Range of IBDCI	Category	Corresponding Intervention action
Less than 60.318	Very Poor	Total bridge deck replacement is needed
Between 60.318 and 67.769	Poor	The bridge deck requires rehabilitation
Between 67.769 and 76.651	Medium	The bridge deck requires repair
More than 76.651	Good	The bridge deck doesn't need intervention

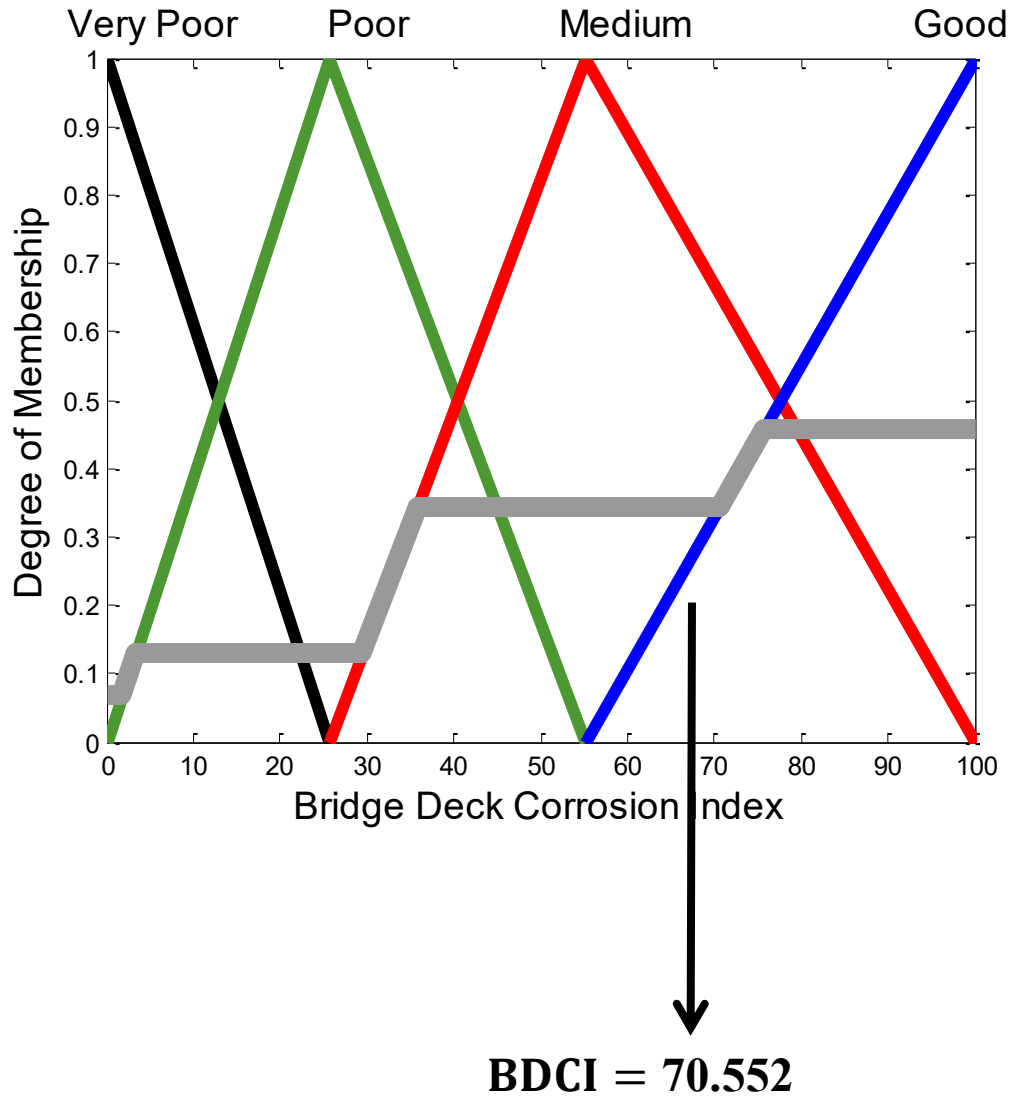


Figure 5.28: Output of the corrosion model for the first bridge deck

Table 5.30: A comparison between corrosion evaluation using ground penetrating radar and half-cell potential

Method	Condition category				BDCI	Overall severity level
	Good	Medium	Poor	Very poor		
Ground penetrating radar	45.78%	34.26%	12.98%	6.98%	70.552	“Medium”
Half-cell potential	62%	33.6%	3.7%	0.14%	83.135	“Good”

The developed integrated condition assessment model is implemented for the intervention prioritization of sub network of five bridge decks. Table 5.31 presents the BDSIs, IBDCI and prioritization rankings. It is worth mentioning that the bridge maintenance prioritization is envisioned on the IBDCI, whereas a lower IBDCI implies a more deteriorated bridge deck that needs urgent intervention. As such, it possesses a higher ranking with respect to the others. “Bridge 1” has the highest ranking while “Bridge 2” provided the lowest ranking, whereas the IBDCI of “Bridge 1” and “Bridge 2” are 60.844 and 82.964, respectively. It is expected that the developed model can provide an efficient decision-making platform that aids transportation agencies for bridge maintenance prioritization in both element and network levels.

Table 5.31: Bridge maintenance prioritization for a sub network of bridges

Bridge ID	BDCI	BDDI	BDCRI	BDSPI	BDSCI	IBDCI	Ranking
Bridge 1	70.552	57.443	43.42	72.923	41.137	60.844	1
Bridge 2	80.657	77.599	95.171	89.066	95.53	82.964	5
Bridge 3	71.023	78.033	80.092	97.404	74.241	74.339	2
Bridge 4	77.636	80.947	75.987	93.77	49.631	75.881	3
Bridge 5	83.708	74.464	90.102	93.994	80.836	79.61	4

- **Modeling of deterioration of bridge decks**

The posterior distributions for each of the three in-state probabilities are computed using the Metropolis-Hastings algorithm. The developed method utilizes a multi-variate normal distribution as a proposal distribution and a uniform distribution as a prior distribution. The posterior distributions of P_{33} is shown in Figures 5.29. As shown in Figures 5.29, the posterior distributions of the in-state probabilities are normal distributions. The values of the mean of three posterior distributions of P_{11} , P_{22} , and P_{33} are: 0.9552, 0.9597 and 0.9211, respectively. The values of the standard deviation of the three posterior distributions are small, whereas the values of the standard deviation of the three posterior distributions of P_{11} , P_{22} , and P_{33} are: 0.01348, 0.01328 and 0.01361, respectively.

The trace plot for the 5,000 samples P_{33} is depicted in Figures 5.30 After setting 1,000 burn-in samples, the present study generated 5,000 samples for each one of the three in-state probabilities. This figure provides a simulation of the three in-state probabilities within each iteration. The trace plot of the mean convergence of P_{33} is shown in Figure 5.31. They describe the variation of the mean within iterations. The mean of the posterior distribution almost stabilizes within the first 500 iterations, which proves that the Markov chain has converged. The autocorrelation function of P_{33} is depicted in Figures 5.32. Trace plots of the autocorrelation function depict how the autocorrelation coefficient decays. As shown in Figure 5.32, the values of the correlation coefficient for the posterior distributions of P_{11} , P_{22} , and P_{33} are very small within the last iteration, which proves that the chains have converged.

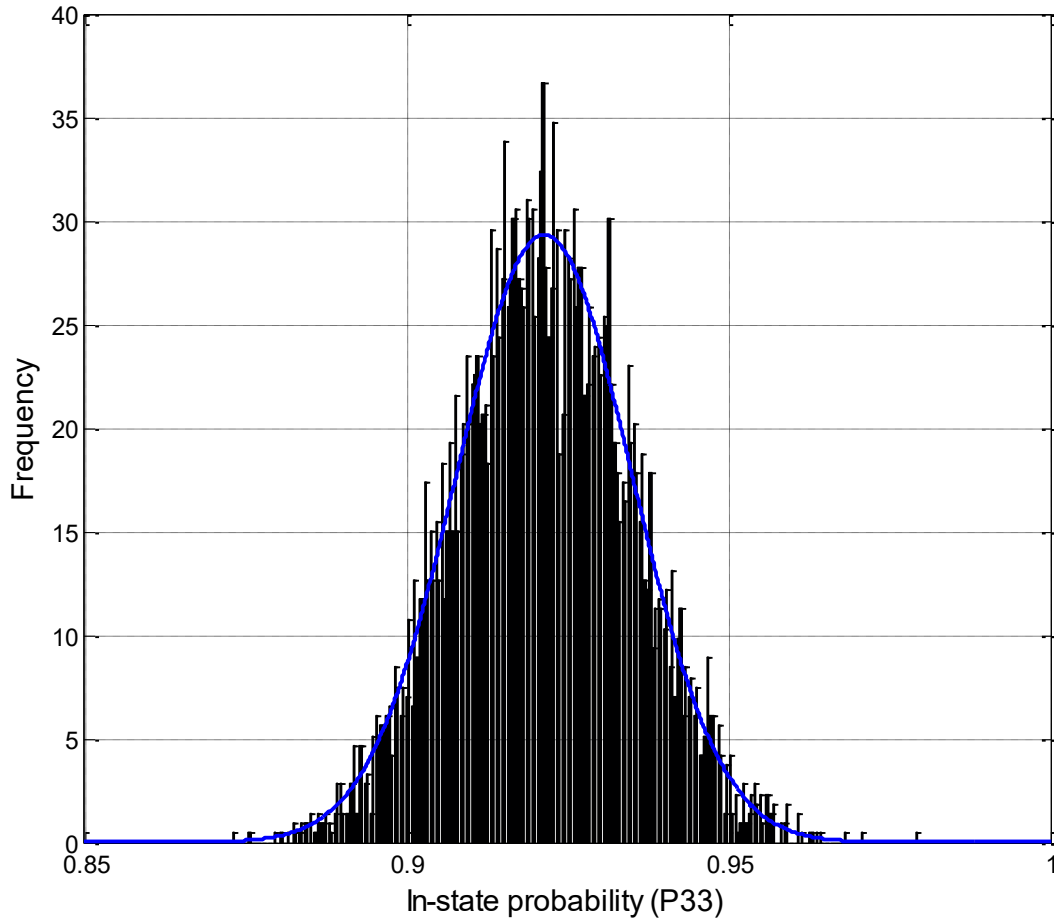


Figure 5.29: Posterior distribution of the in-state probability P_{33}

In addition to the trace plots, three convergence diagnostics are presented acceptance rate, Z-score of Geweke test, and the final autocorrelation coefficient. The acceptance rate is 0.2306, Z-score is 1.7706, and final autocorrelation coefficient is -0.00114 for the in-state probability P_{11} . If the calculated probabilities satisfy the three tests, a message box will appear indicating that the current chain has converged. Otherwise, a message box will appear indicating that the current chain did not converge. Results indicated that the constructed chain of P_{11} satisfies the three convergence diagnostics, which means that the current chain has converged. Since, the Markov

chains fulfill the convergence diagnostics. Thus, the type and parameters of the prior and proposal distributions are correctly defined.

The convergence curve of the stochastic optimization model is depicted in Figure 5.33, whereas the optimum fitness function value equals to 275.1863. The fitness function starts to stabilize starting from iteration 39. The calculated transition probability matrices are then shown in the data-grid view. All values of the transition probabilities are depicted in Table 5.32. The deterioration of the bridge deck does not follow the same pattern along the study period whereas the transition probabilities of the zones are different from each other. The deterioration curve and condition states distribution are depicted in Figure 5.34. As shown in Figure 5.34.a, condition state 1 is the dominant condition state. Then, condition state 4 becomes the dominant condition state.

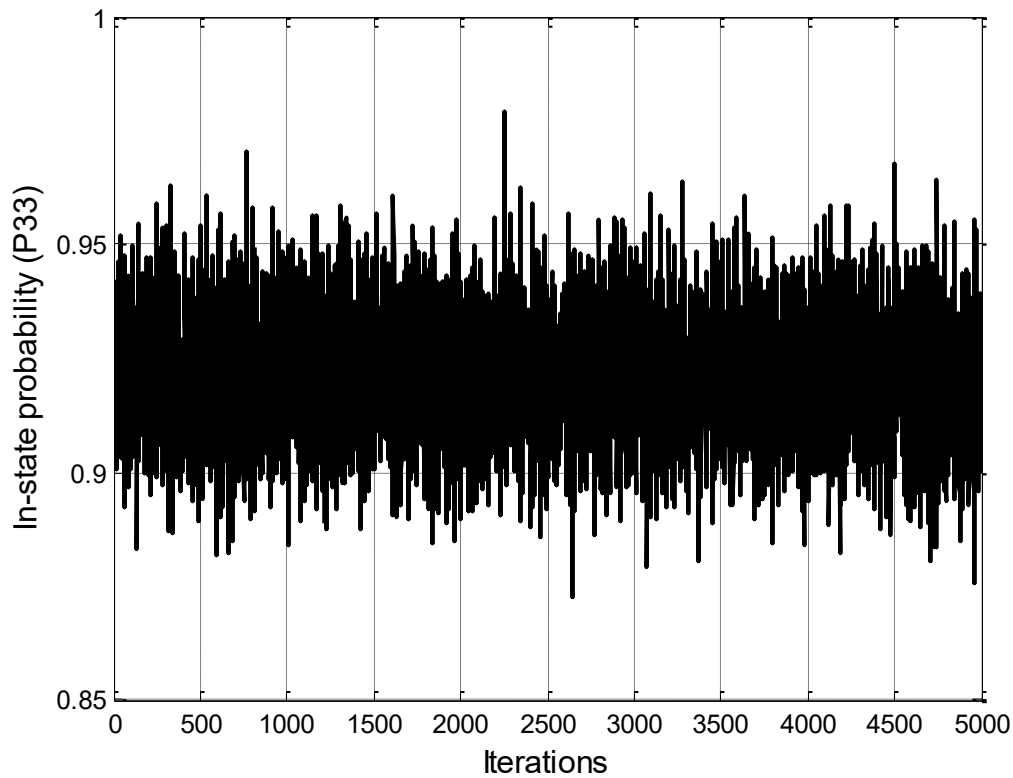


Figure 5.30: Trace plot of the in-state probability P_{33}

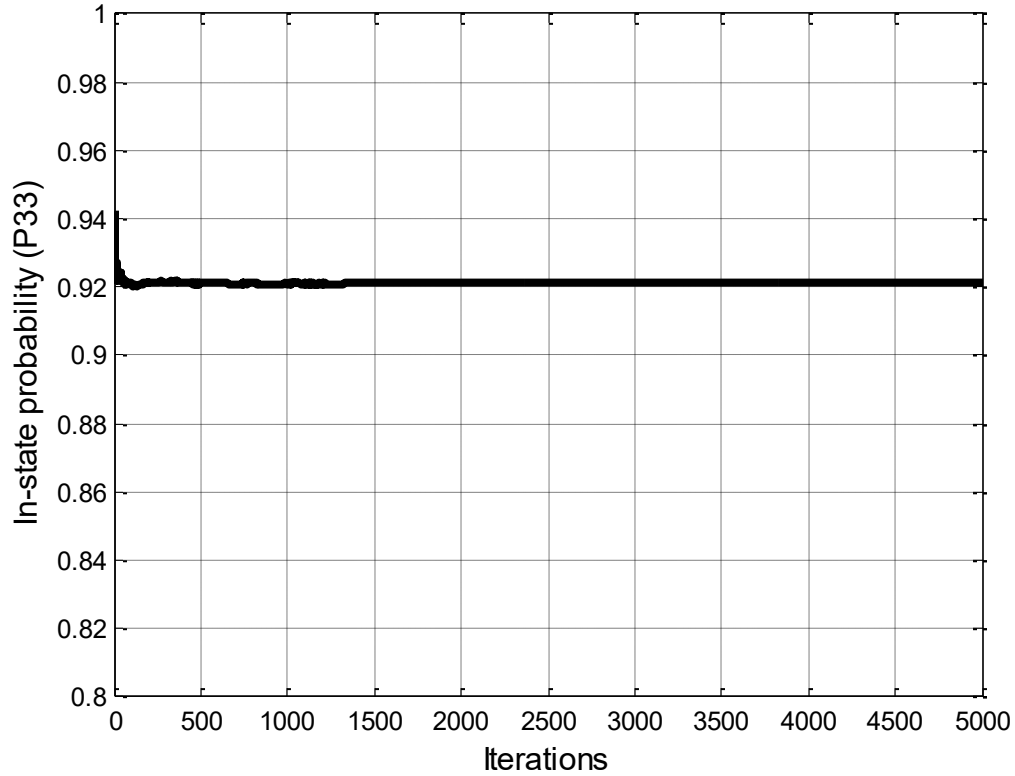


Figure 5.31: Trace plot of the mean convergence of the in-state probability P_{33}

The developed hybrid Bayesian-based model is denoted as hybrid Bayesian-based model-1 (H – B1), which is based on the Bayesian belief network that modelled the independencies between bridge defects. Another model is developed following the same procedures of the developed model except for the architecture of the Bayesian belief network. For the second model, the bridge defects are assumed to be independent on each other. The second model is denoted as hybrid Bayesian-based model-2 (H – B2). The comparison between the two models enables to investigate the effect of dependencies on the prediction accuracy of the condition of bridge decks (deterioration mechanism). The regression-based optimization model is denoted as RBO. As such, the transition probabilities obtained using the regression-based optimization method are shown in Equation (5.1). The parameters of the weibull and gamma distributions are calculated using the maximum likelihood estimation algorithm. The scale and shape parameters

of the weibull distribution are 84.2378 and 5.0643, respectively. The scale and shape parameters of the gamma distribution are 21.767 and 3.5521, respectively.

$$p^{t,t+1} = \begin{bmatrix} 0.855 & 0.145 & 0 & 0 \\ 0 & 0.918 & 0.082 & 0 \\ 0 & 0 & 0.912 & 0.088 \\ 0 & 0 & 0 & 1 \end{bmatrix} \quad (5.1)$$

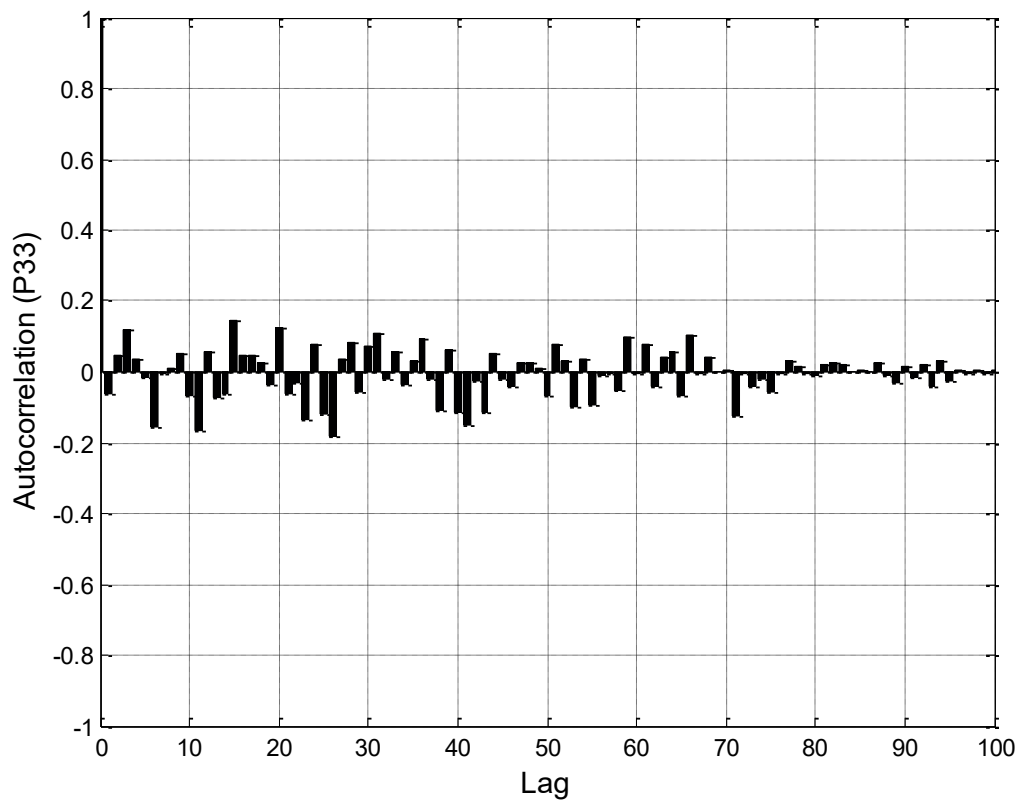


Figure 5.32: Trace plot of the autocorrelation function for the in-state probability P_{33}

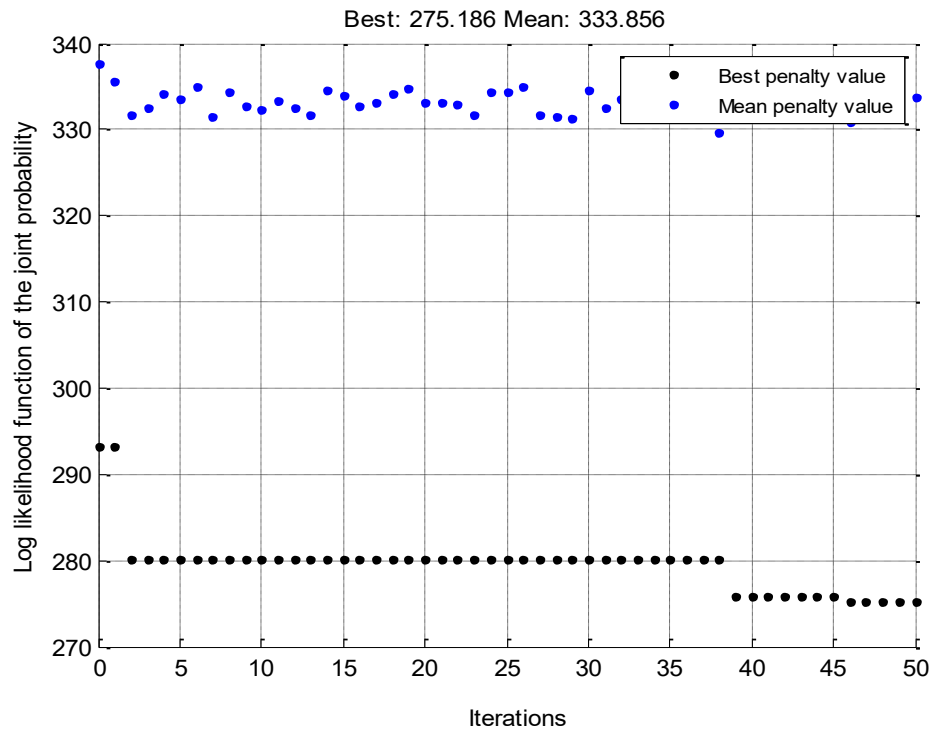
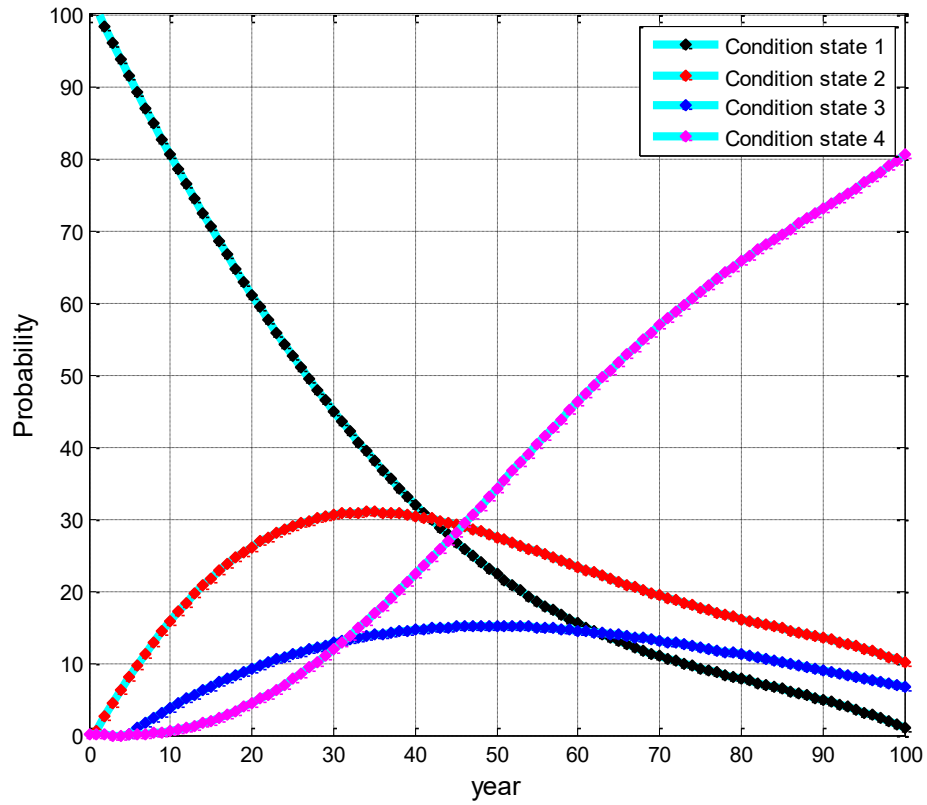


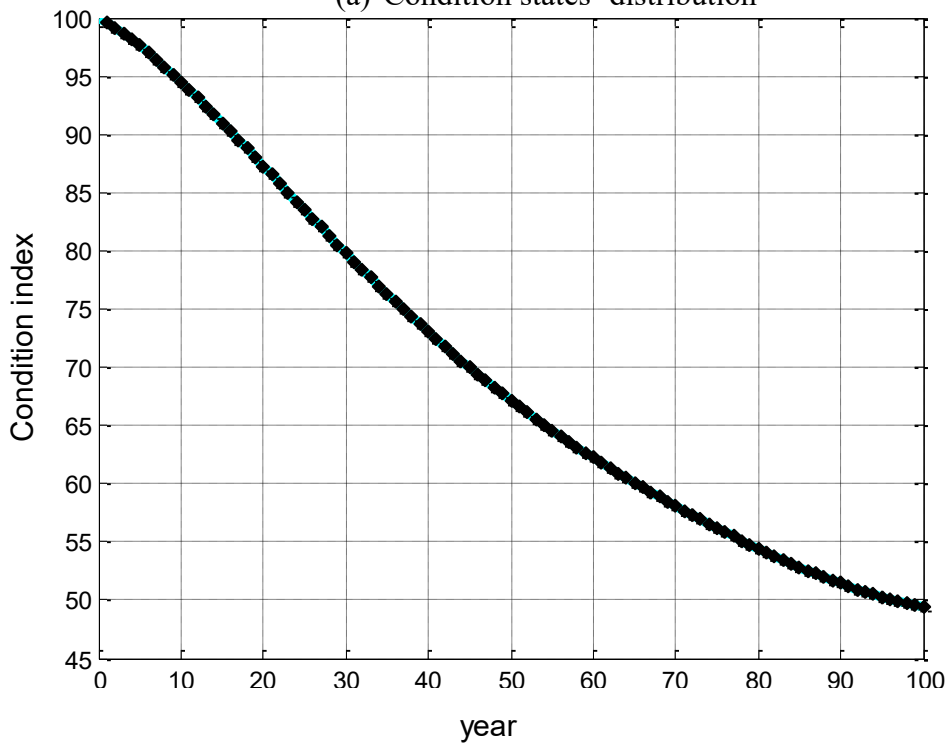
Figure 5.33: Convergence curve of the negative log likelihood of the unknown transition probabilities

Table 5.32: Calculated transition probabilities for each zone

Zone	Year	In-state probabilities			Zone	Year	In-state probabilities		
		P11	P22	P33			P11	P22	P33
Zone 1	1-5	98.487%	95.134%	90.554%	Zone 11	51-55	97.503%	95.497%	90.57%
Zone2	6-10	96.602%	95.611%	92.113%	Zone 12	56-60	94.689%	95.985%	92.642%
Zone 3	11-15	99.225%	96.193%	91.571%	Zone 13	61-65	97.425%	96.274%	92.593%
Zone 4	16-20	95.666%	95.288%	91.012%	Zone 14	66-70	95.231%	95.053%	93.418%
Zone 5	21-25	95.751%	95.848%	91.093%	Zone 15	71-75	96.95%	97.065%	91.7%
Zone 6	26-30	97.402%	94.552%	93.658%	Zone 16	76-80	95.131%	94.76%	91.5%
Zone 7	31-35	98.914%	96.444%	94.323%	Zone 17	81-85	94.038%	96.155%	92.265%
Zone 8	36-40	94.086%	94.397%	93.44%	Zone 18	86-90	95.428%	96.324%	93.755%
Zone 9	41-45	95.846%	94.397%	93.44%	Zone 19	91-95	93.816%	96.075%	91.411%
Zone 10	46-50	99.33%	96.096%	91.63%	Zone 20	96-100	95.224%	96.399%	91.191%



(a) Condition states' distribution



(b) Deterioration curve

Figure 5.34: Condition states' distribution and deterioration curve of the hybrid Bayesian model

A comparison between different deterioration models is shown in Table 5.33. The chi-squared critical value at 180 degrees of freedom and a significance level of 5% equals to 212.304. In terms of RMSE, H – B1 achieved the lowest RMSE (RMSE = 0.7716). On the other hand, gamma distribution achieved the highest RMSE (RMSE = 1.4584). Thus, H – B1 achieved the best performance based on RMSE. For MAE, H – B1 provided the lowest MAE (MAE = 0.5401) followed by hybrid Bayesian-based model-2 and then the semi-Markovian model. On the other hand, gamma distribution achieved the highest MAE (MAE = 0.9899). Thus, H – B1 provided the best performance according to MAE. The gamma and weibull distributions fail to pass the chi-squared test because the chi-squared critical value ($x_{\text{Crit}}^2 = 212.304$) is larger than the chi-squared statistic. H – B1 provided the best performance according to x^2 ($x^2 = 46.0583$) followed by H – B2 ($x^2 = 62.5$), and then the semi-Markovian model ($x^2 = 89.75$). Based on the previous statistics, H – B1 outperformed other models in terms of RMSE, MAE, and x^2 .

It is worth mentioning that H – B1 outperformed the model H – B2 for all the performance metrics, which proves that modeling the interaction between the bridge defects provides more accurate results. Moreover, H – B1 outperformed the weibull distribution and gamma distribution models which proves the superiority of the time-based models over the state-based models in modeling the deteriorations process of the bridge elements, which proves the conclusion derived by Ravirala and Grivas (1995) that it is more reasonable to model the deterioration process as a function of time. As per the previous comparison, the developed model surpassed other deterioration models for both training and testing datasets, which the infrastructure managers can benefit from in deciding the optimal intervention actions, which the infrastructure managers can benefit from in deciding the optimal intervention actions. Deterioration prediction is one of the most crucial parameters in maintenance optimization

models. Thus, infrastructure managers need reliable prediction models such as the hybrid Bayesian-based optimization model to forecast the condition of the bridge elements, whereas the early diagnosis of the deterioration scenarios helps in optimizing maintenance, repair and rehabilitation activities for both project and network levels.

Table 5.33: Comparison between the different deterioration models

Model	RMSE	MAE	χ^2
Hybrid Bayesian-based model- 1 (H – B1)	0.7716	0.5401	46.0583
Hybrid Bayesian-based model- 2 (H – B2)	0.8572	0.542	62.5
Semi-Markov model	0.9748	0.5966	89.75
Regression-based optimization model (RBO)	1.1489	0.8066	69
Weibull	1.4527	0.9834	356
Gamma	1.4584	0.9889	356.6667

▪ **Optimization of maintenance plans**

This section is divided into two sections. The first part enumerates the results of the developed method for allocation limited resources in bridge deck replacement projects. The second part reports the implementation results of the developed method for optimizing bridge maintenance plans.

Resource allocation of bridge deck replacement projects

The case study is for a bridge that is composed of 8 lanes and 20 spans. The length of the span and width of the lane are 20 and 3.75 metres, respectively. Table 5.34 describes the lower and upper bounds for the output variables of the discrete event simulation model that were used to generate the machine learning surrogate model. The output variables include: time per span (T_S),

cost per square meter (C_m), greenhouse gases per square meter (GHG_m), average utilization rate of demolition phase (AVG_UTIL_{DEM}), and standard deviation of utilization rate of demolition phase (STD_UTIL_{DEM}), average utilization rate of construction phase (AVG_UTIL_{CONST}), standard deviation of utilization rate of construction phase (STD_UTIL_{CONST}), average utilization rate of finishing phase (AVG_UTIL_{FINISH}) and standard deviation of utilization rate of finishing phase (STD_UTIL_{FINISH}). For instance, the lower and upper bounds of the output variable GHG_m are 11.214 and 24.047, respectively. The next phase is to build the surrogate machine learning model using the simulation dataset to construct a reliable approximation of the STROBOSCOPE model.

Table 5.34: Boundary condition of the output variables from discrete event simulation model

Output variable	Boundary conditions
Time per span (T_s , days/span)	4.572-50.909
Cost per square meter (C_m , \$/square meter)	344.351-794.027
Greenhouse gases per square meter (GHG_m , Kg CO ₂ -Eq./square meter)	11.214-24.047
Average utilization rate of demolition phase (AVG_UTIL_{DEM} , %)	72.931-99.989
Standard deviation of utilization rate of demolition phase (STD_UTIL_{DEM} , %)	2.01-38.142
Average utilization rate of construction phase (AVG_UTIL_{CONST} , %)	60.451-90.141
Standard deviation of utilization rate of construction phase (STD_UTIL_{CONST} , %)	10.408-43.543
Average utilization rate of finishing phase (AVG_UTIL_{FINISH} , %)	84.91-99.958
Standard deviation of utilization rate of finishing phase (STD_UTIL_{FINISH} , %)	3.018-12.365

Table 5.35 records the performance evaluation metrics of greenhouse gases as per 10-fold cross validation. The developed ENN – IWO model provided the highest performance, such that

MAPE, MAE and RMSE are equal to 4.873%, 78.466 and 39.515, respectively. K – NN, GBDT and RSVM provided the second highest performance according to MAPE, MAE and RMSE, respectively. GP provided the lowest prediction accuracies, whereas MAPE, MAE and RMSE equal to 24.879%, 5.713 and 4.117, respectively. Back-propagation artificial neural network is the most widely-used algorithm in machine learning applications. when compared against the ANN model in greenhouse gases prediction, the ENN – IWO accomplished an enhancement in the reduction of MAPE, MAE and RMSE by 44.421%, 46.203% and 40.298%, respectively. With respect to the cross validation, It can be inferred that the developed ENN – IWO outperformed the remainder of the machine learning models with respect to three performance indicators attaining; MAPE, MAE and RMSE 7.417%, 1.701 and 1.293, respectively. On the contrary, GP provided the lowest prediction accuracies, such that MAPE, MAE and RMSE are equal to 28.113%, 6.473 and 4.669, respectively. This highlights that the developed prediction model outperformed other machine learning models by accomplishing lower prediction errors for the different output variables according to split validation and 10-fold cross validation.

The third model is multi-objective differential evolution to find the optimum combinations of resources. The search space size is computed using the number of possible solutions ($15^{14} = 2.92 \times 10^{16}$). The minimum allowable average utilization rate and maximum allowable standard deviation of utilization rate of resources are assumed 85% and 10%, respectively. This state of affairs necessitates the implementation of efficient meta-heuristic for the purpose of exhaustive search of possible resource allocation plans while accommodating the allowable utilization constraints. The set of optimal solutions obtained from the multi-objective particle swarm optimization model and multi-objective differential evolution optimization model are depicted in Figures 5.35 and 5.36, respectively. The performance design space is defined as the set of all

design points represented by the design (decision) variables that satisfy the constraints. The feasible performance space represents the set of objective function values elicited from every feasible design. The non-dominated Pareto optimal solutions attained from the multi-objective particle swarm optimization model and multi-objective differential evolution optimization model are shown in Figures 5.37.a and 5.37.b, respectively. As can be seen, the differential evolution algorithm attained notable lower T_s , C_m and GHG_m compared to the particle swarm optimization algorithm.

Table 5.35: Performance comparison between the different machine learning models for the prediction of greenhouse gases based on 10-fold cross validation

Type of machine learning model	Mean absolute percentage error	Mean absolute error	Root-mean squared error
ENN – IWO	7.417%	1.701	1.293
ANN	13.501%	3.202	2.191
RBNN	13.132%	3.425	2.283
GRNN	12.284%	3.385	2.391
CNN	9.813%	1.988	1.612
LSVM	10.218%	2.105	1.681
RSVM	9.457%	2.196	1.458
GBDT	9.302%	1.841	1.514
GP	28.113%	6.473	4.669
K – NN	9.096%	1.874	1.497

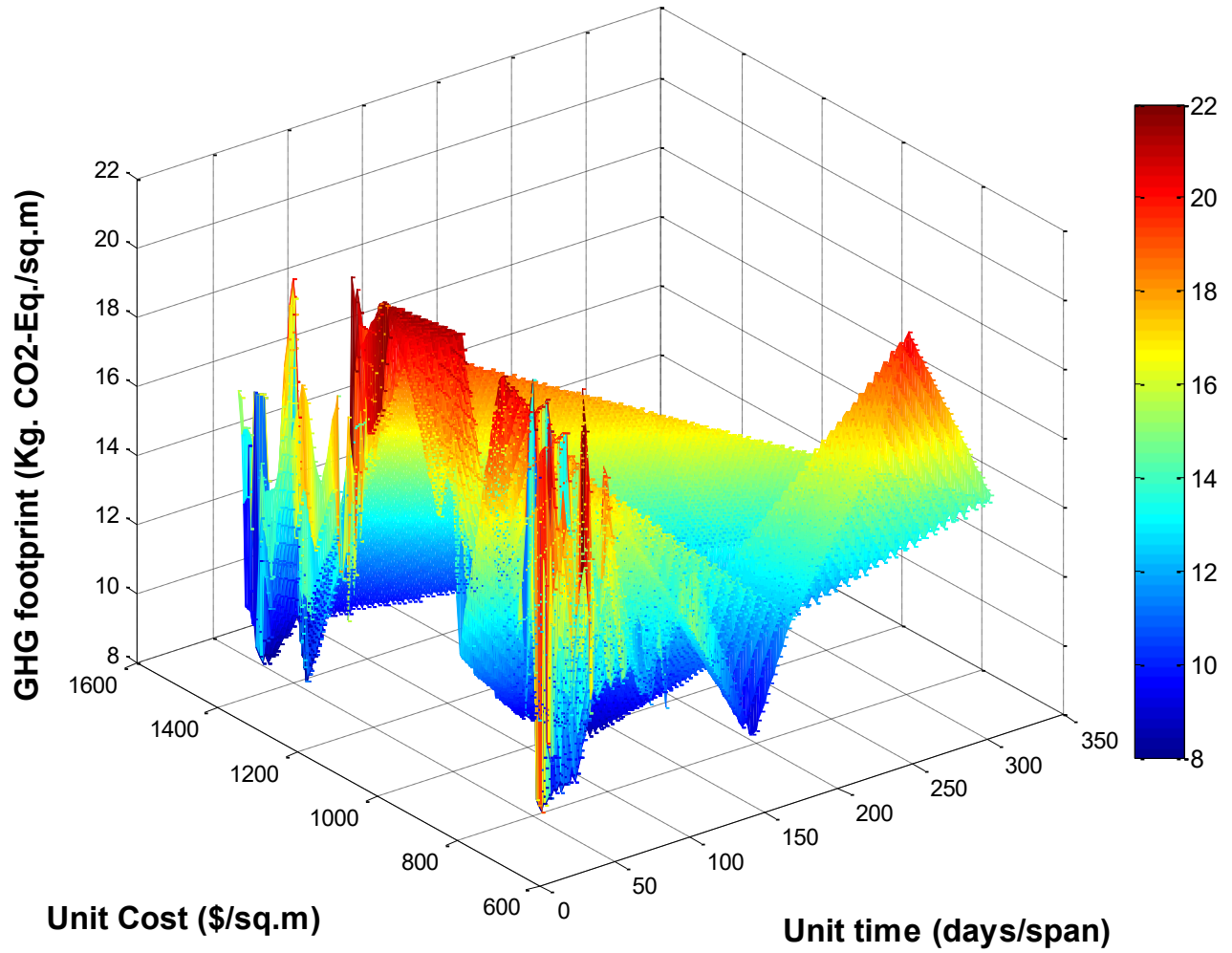


Figure 5.35: 3D optimal surface obtained from the multi-objective particle swarm optimization model

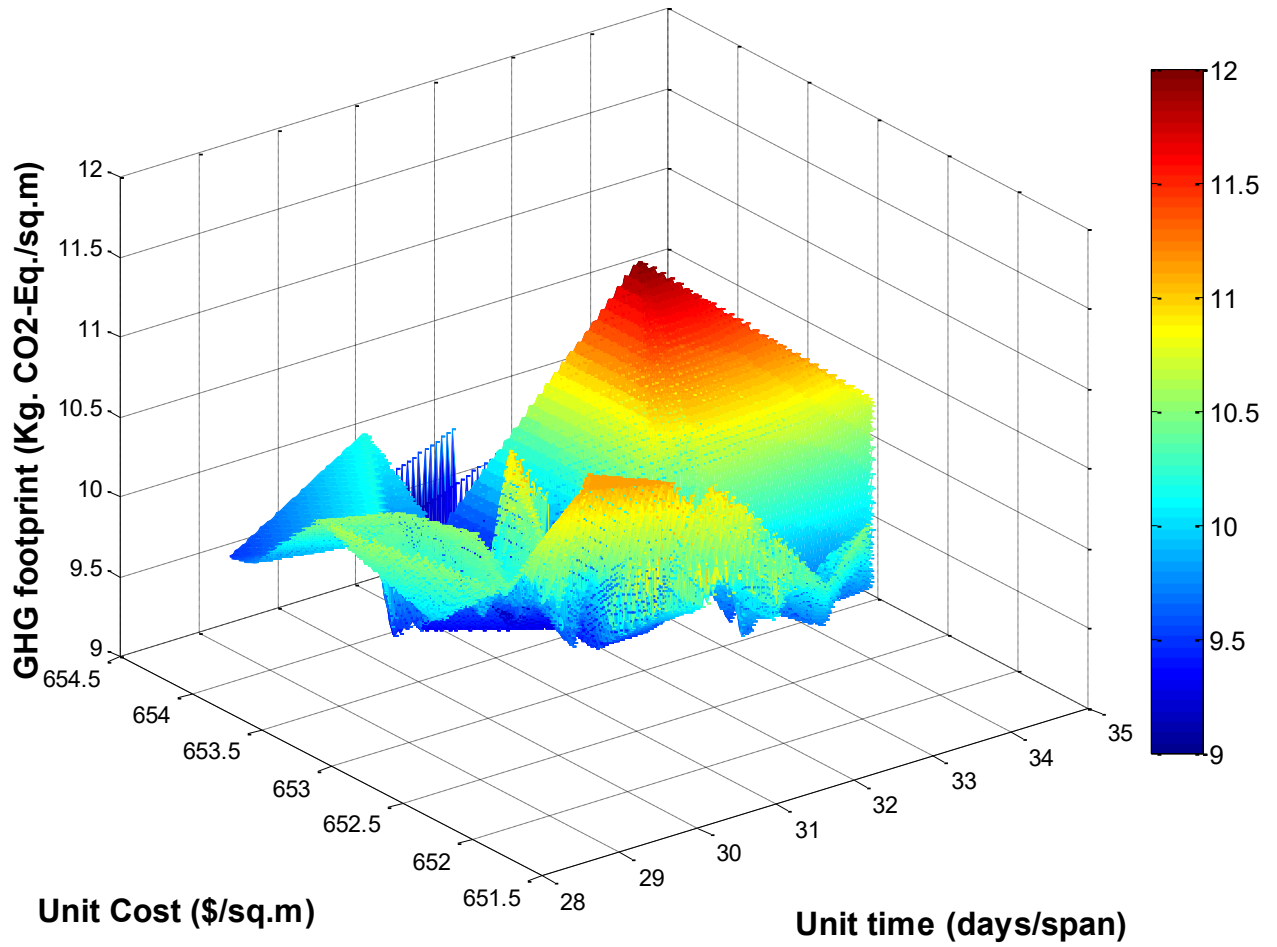
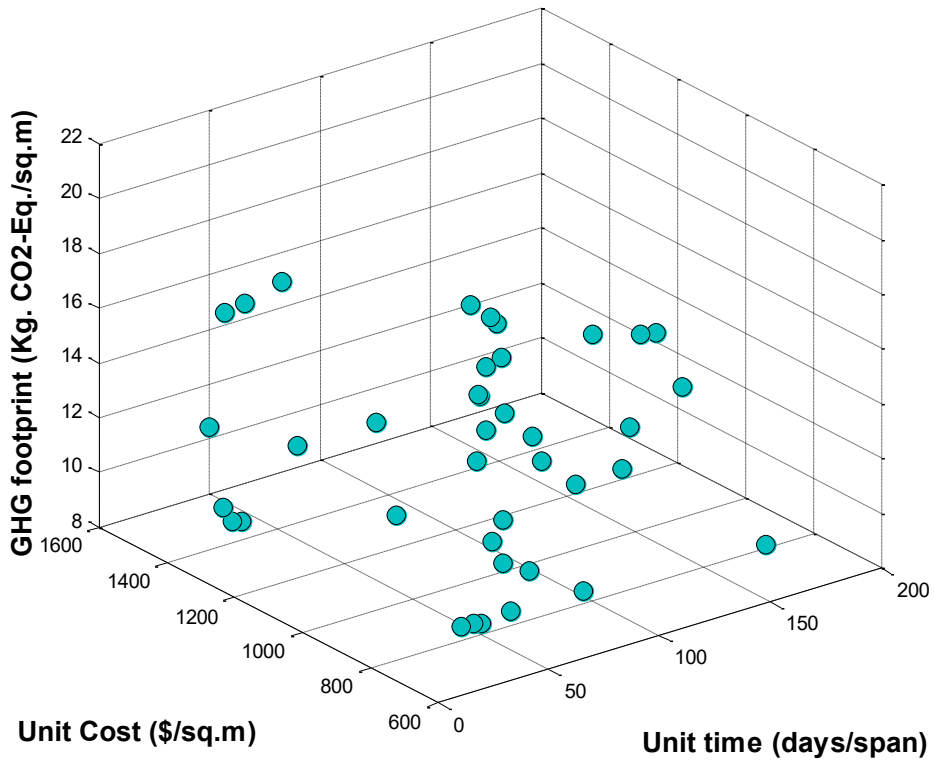
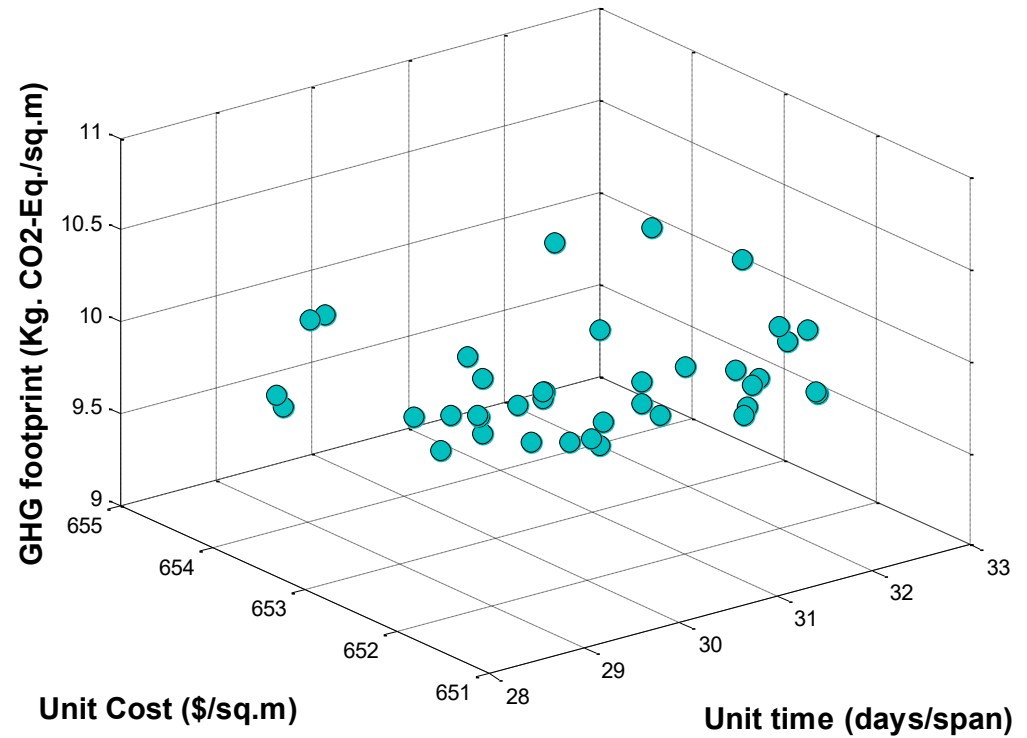


Figure 5.36: 3D optimal surface obtained from the multi-objective differential evolution model



(a) Pareto optimal solutions computed from the multi-objective particle swarm optimization model



(b) Pareto optimal solutions computed from the multi-objective differential evolution model

Figure 5.37: Pareto optimal solutions computed from the multi-objective particle swarm optimization model and multi-objective differential evolution model

1 The multi-criteria decision making model is employed to select the best solution among the
 2 Pareto frontier points obtained from the multi-objective optimization model. It constitutes three
 3 attributes, namely T_S , C_m and GHG_m , whereas the weights of the attributes are calculated based
 4 on the Shannon entropy method. The calculations of the weights of the attributes are presented in
 5 Table 5.36. As shown in Table 5.36, the weights of T_S , C_m and GHG_m are 44.588%, 27.102%
 6 and 28.31%, respectively. PROMETHEE II is employed to generate a full ranking of the resource
 7 allocation plans. The preference threshold values of T_S , C_m and GHG_m are equal to 73.51,
 8 490.134 and 8.058, respectively. A sample of the solution ranking obtained from the
 9 PROMETHEE II is depicted in Table 5.37. The best solution is the one which provides the
 10 highest net flow. As can be seen, the solution [5, 1, 5, 4, 10, 7, 10, 5, 5, 8, 10, 6, 5, 1] is selected
 11 as the best solution. It yields T_S , C_m and GHG_m of 29.742, 652.918 and 9.719, respectively and a
 12 net flow $\phi(a)$ of 0.2213. Furthermore, this solution achieved UNI_{AVG_UTIL} and UNI_{STD_UTIL} of
 13 95.133% and 9.533%, respectively. This demonstrates that the developed resource allocation
 14 method is capable of minimizing time, cost and greenhouse gases while accommodating the
 15 uniformity in the utilization of resources. The solution [5, 2, 5, 4, 6, 7, 7, 1, 4, 9, 7, 4, 4, 5]
 16 achieved the fourteenth rank such that, it attained T_S , C_m and GHG_m of 30.469, 652.567 and
 17 10.208, respectively and a net flow $\phi(a)$ of 0.2123.

18 **Table 5.36: Entropy values, variation coefficients, and the weights of the attributes**

Index	T_S	C_m	GHG_m
Entropy value (e_j)	5.7502	5.7706	5.7691
variation coefficient (d_j)	0.00895	0.00544	0.00568
weights of the attribute (w_j)	44.588%	27.102%	28.31%

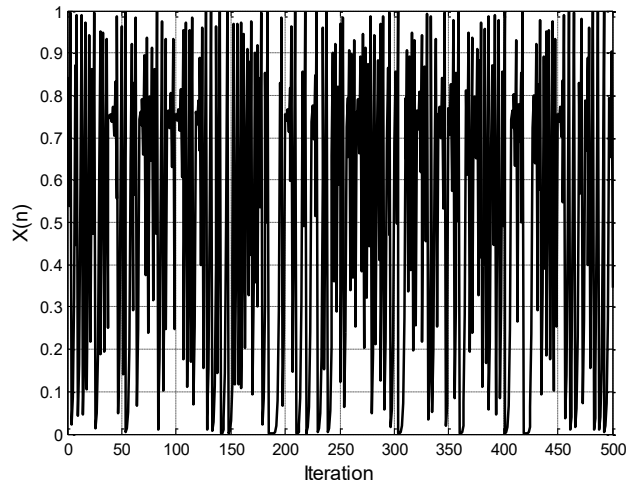
Table 5.37: Sample of the solutions' rankings obtained from PROMETHEE II

Optimum solution	Optimum objective function values	Meta-heuristic	Net flow ($\sigma(a)$)	Ranking
[5, 1, 5, 4, 10, 7, 10, 5, 5, 8, 10, 6, 5, 1]	[29.742, 652.918, 9.719]	MODE	0.2213	1
[5, 1, 5, 4, 10, 7, 10, 4, 5, 10, 10, 6, 5, 1]	[30.304, 652.817, 9.762]	MODE	0.2165	8
[5, 2, 5, 4, 6, 7, 7, 1, 4, 9, 7, 4, 4, 5]	[30.469, 652.567, 10.208]	MODE	0.2123	14
[5, 2, 1, 6, 7, 6, 6, 2, 4, 11, 6, 8, 4, 4]	[28.685, 1422.838, 12.731]	MODA	0.2078	29
[3, 4, 4, 5, 7, 5, 3, 5, 4, 12, 5, 7, 5, 2]	[40.896, 658.032, 10.781]	MOSFL	0.2066	32

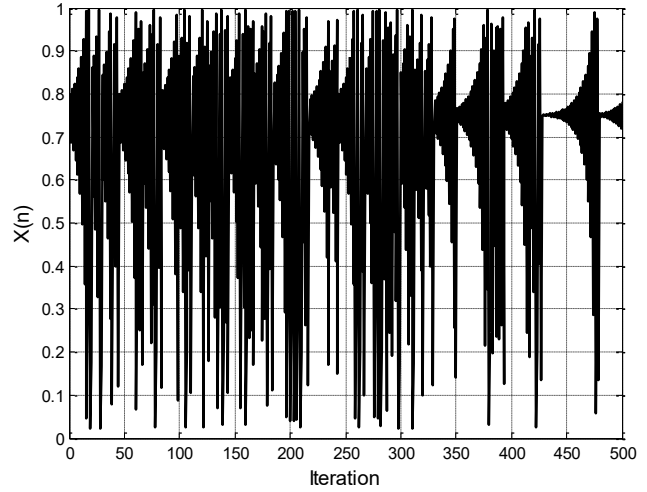
Maintenance planning of bridges

The parameters of the user costs are as follows. The length of affected bridges is 600 meters. The normal traffic speed is 100 km/hr. The reduced traffic speeds in the case of minor repair, major repair and replacement are 80, 50 and 30, respectively. The initial average daily traffic is 10,000 vehicles per day. The percentage of trucks from average daily traffic is 3.1%. The traffic growth is selected to be 1.1%/year. Hourly time value of passenger car driver and truck driver are assumed \$14.21/hr and \$29.22/hr, respectively. The operating costs of passenger car and truck are 17.24/hr and \$39.67/hr, respectively. The normal accident rate and accident rate during the work zone are assumed 1.56% and 2.58%, respectively. The average cost per accident is assumed \$126,120. Maintenance costs, environmental emissions footprint and work zone durations are assumed to be normally distributed such that the stochastic nature of these random variables is mimicked using Latin hypercube sampling of 1000 iterations.

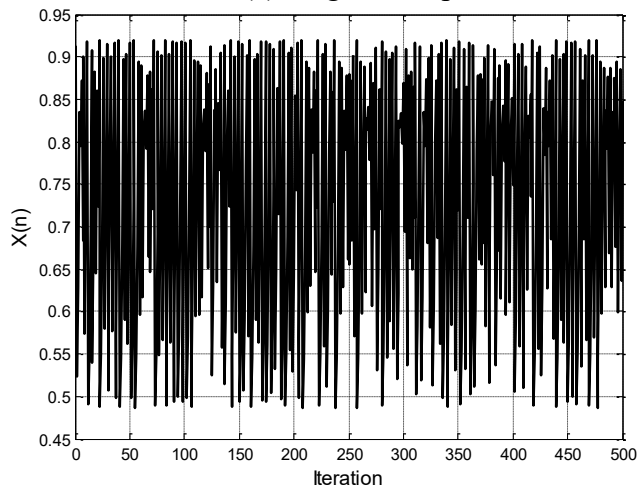
After the definition and quantification of the performance aspects of maintenance management of bridges, the second model is the exponential chaotic multi-objective differential evolution model which aims at structuring the optimum maintenance schedule of bridges over the multi-year planning period while accommodating the multiple performance constraints. The initial value of all chaotic maps is assumed 0.7 (Sayed et al., 2018; Saxena et al., 2018). Figures 5.38 and 5.39 describe the behavior of the nine chaotic maps for 500 iterations. As can be seen, the chaotic dynamics enable the chaotic operators to travel ergodically across the search space. For instance, the chaotic sequences of control parameters in the singer map exhibit rapid transitions within close number of iterations. In the sinusoidal map, the chaotic variable sequences vary from 0.5 to 0.95. This provides an advantage over constant control parameters through providing full and efficient exploration of the search space.



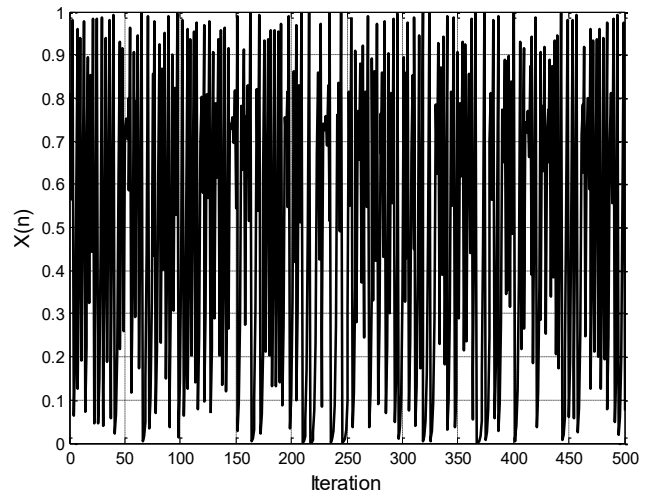
(a) Logistic map



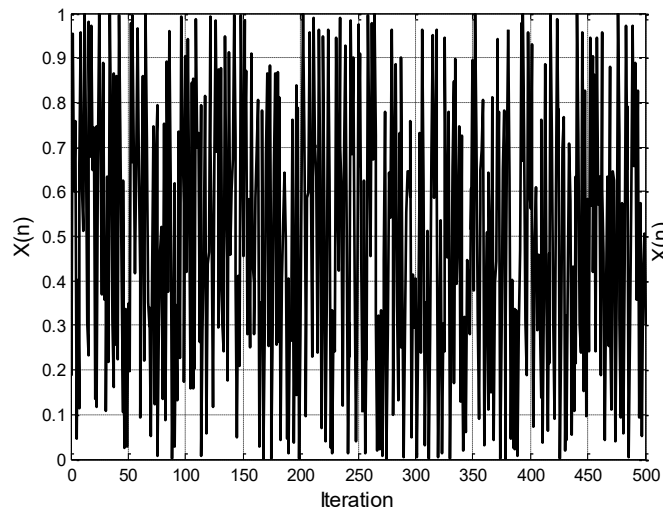
(b) Singer map



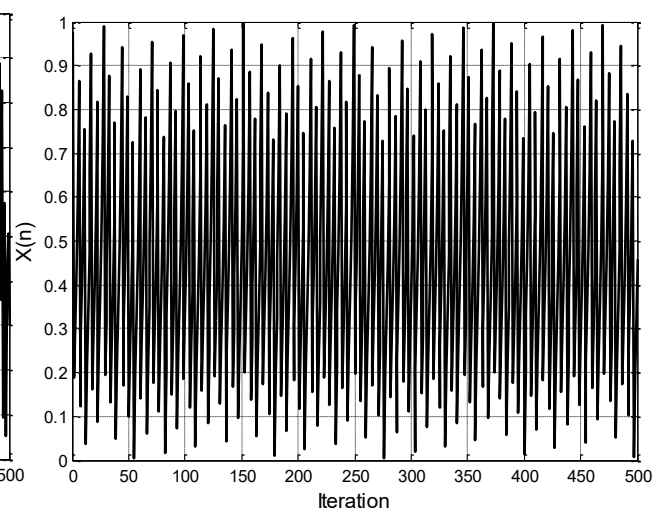
(c) Sinusoidal map



(d) Sine map

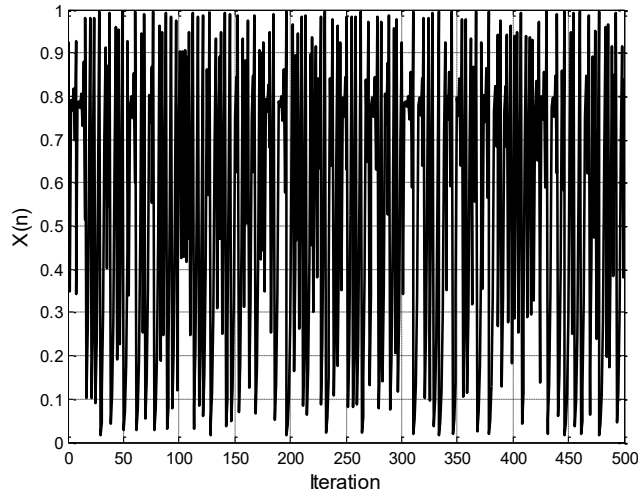


(e) Iterative map

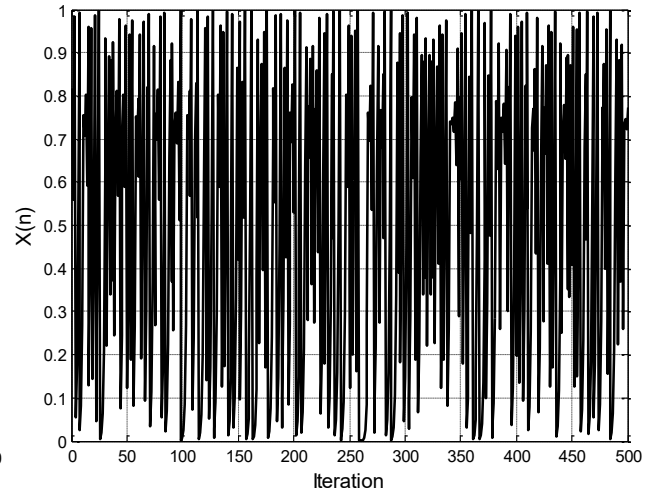


(f) Chebyshev map

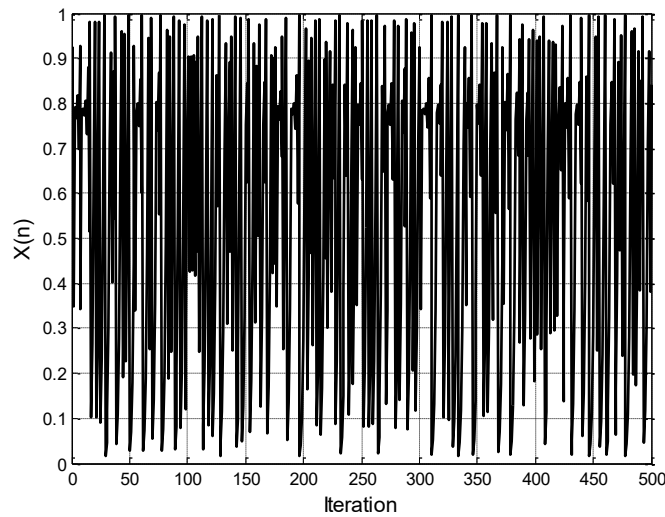
Figure 5.38: Behavior of different chaotic maps



(a) Circle map



(b) Logistic-sine map



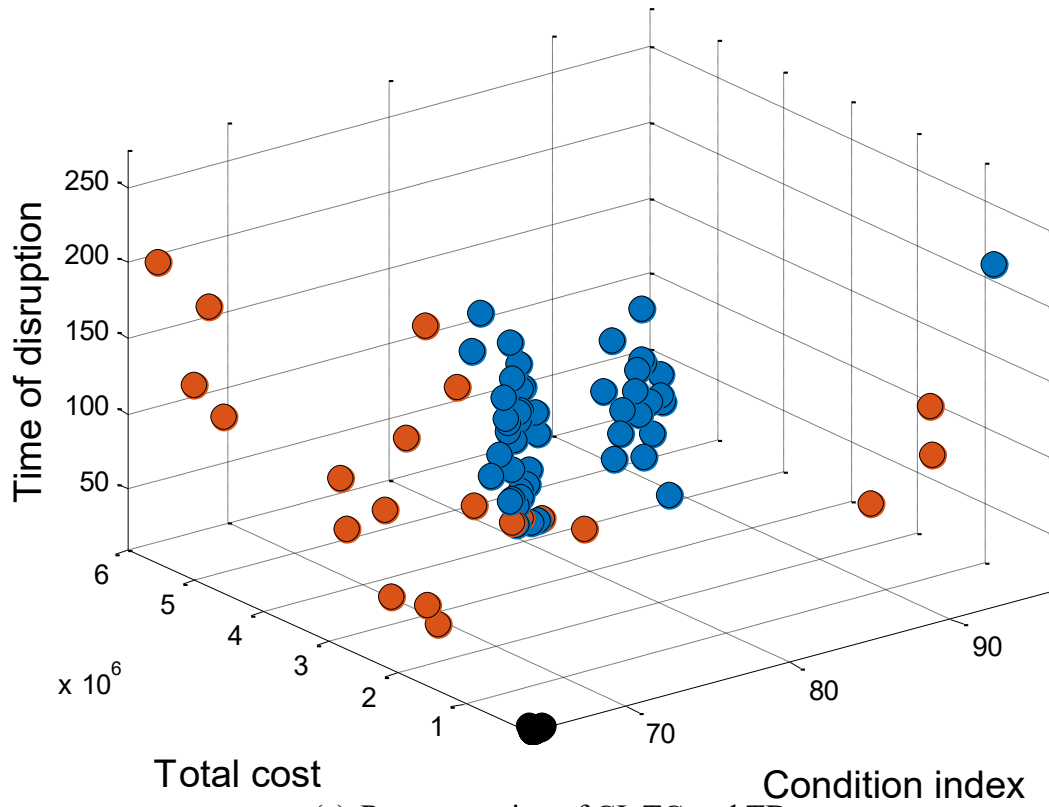
(c) Cubic map

Figure 5.39: Behavior of different chaotic maps (Continued)

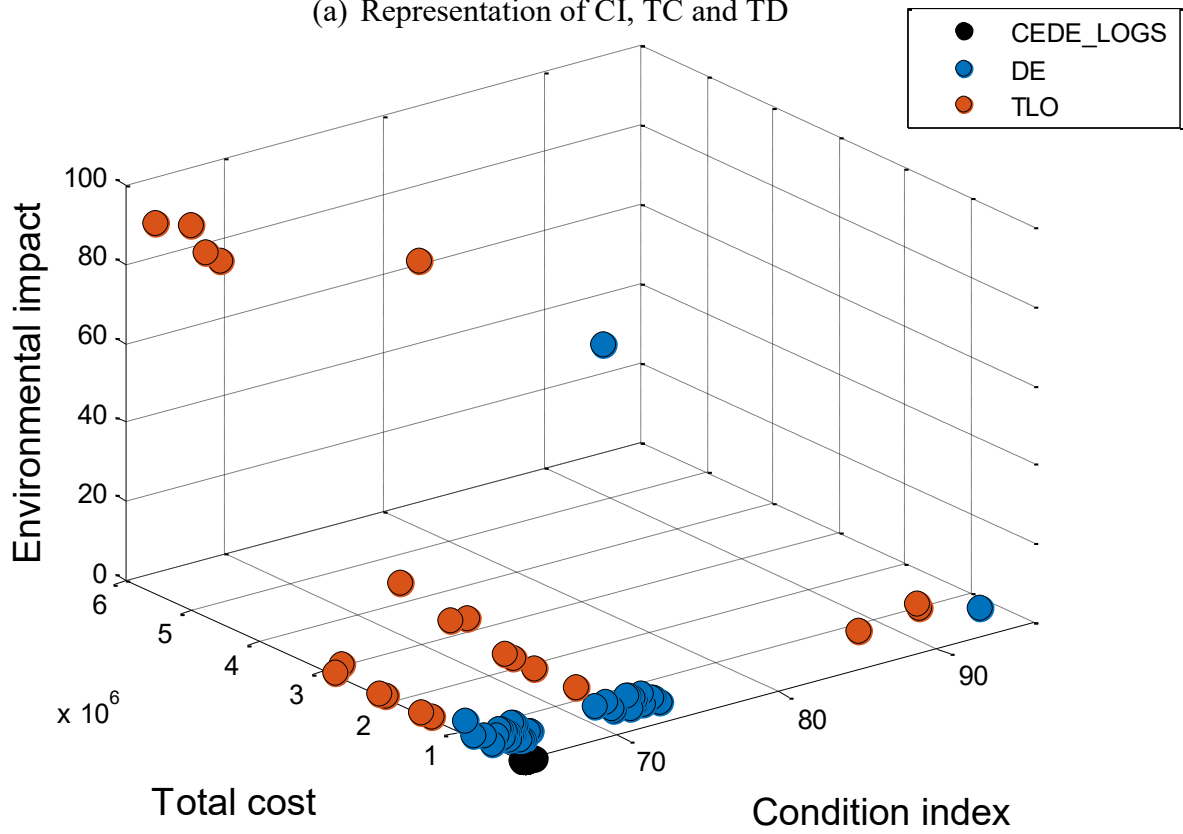
In order to provide a fair comparison between the different meta-heuristic optimization algorithms, the initial population size is assumed 50. The numbers of iterations for the five-year, twenty five-year and thirty-five year study periods are assumed 1000, 1500 and 1700, respectively. Different initializations of parameters were experimented for the different meta-heuristics in order to search for their optimum setting of values. Each meta-heuristic was run five times independently in order to avoid unstable solutions due to random initialization of

population. The set of optimal solutions obtained from the multi-objective exponential chaotic differential evolution model based on the logistic-sine map alongside the multi-objective differential evolution optimization model and multi-objective teaching learning optimization model for the twenty five-year study horizon are depicted in Figures 5.40 and 5.41. The variables “CI”, “TC” “EI” and “TD” denote performance condition index, maintenance costs, duration of traffic disruption and environmental impact, respectively. Four figures are generated to cover all possible combinations of the four performance aspects of the multi-objective optimization model. The generated maintenance plans satisfy a minimum performance condition threshold of 64.04. The maximum available budget is \$1000,000. Furthermore, the maximum yearly-budget and maximum standard deviation of costs are set to \$250,000 and \$20,000, respectively.

As can be seen, the ECDE model is capable of achieving significant reduction in the maintenance expenditures, traffic disruption and adverse environmental implications when compared against the classical meta-heuristics. For the thirty five-year maintenance plan, the optimal solutions of the ECDE-based cubic, ECDE-based logistic-sine, ECDE-based circle and ECDE-based sine models are presented in Figure 5.42. It should be mentioned that all the exponential chaotic optimization models achieved environmental impact of zero. Thus, the performance aspects of condition, maintenance cost and traffic disruption are displayed. In this context, it can be inferred that the exponential chaotic differential evolution models attained promising results in terms of the four governing performance metrics. Furthermore, it should be reported that the classical optimization algorithms failed to find the optimum solutions within the boundaries and constraints for the maintenance planning model of thirty five-year study period.

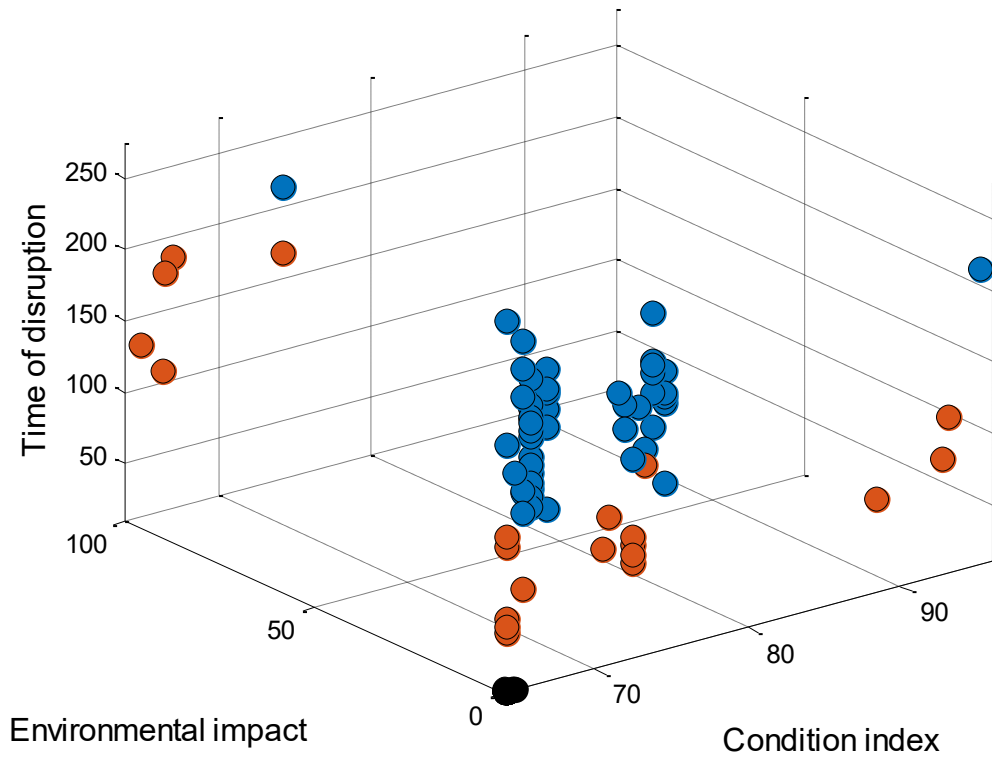


(a) Representation of CI, TC and TD

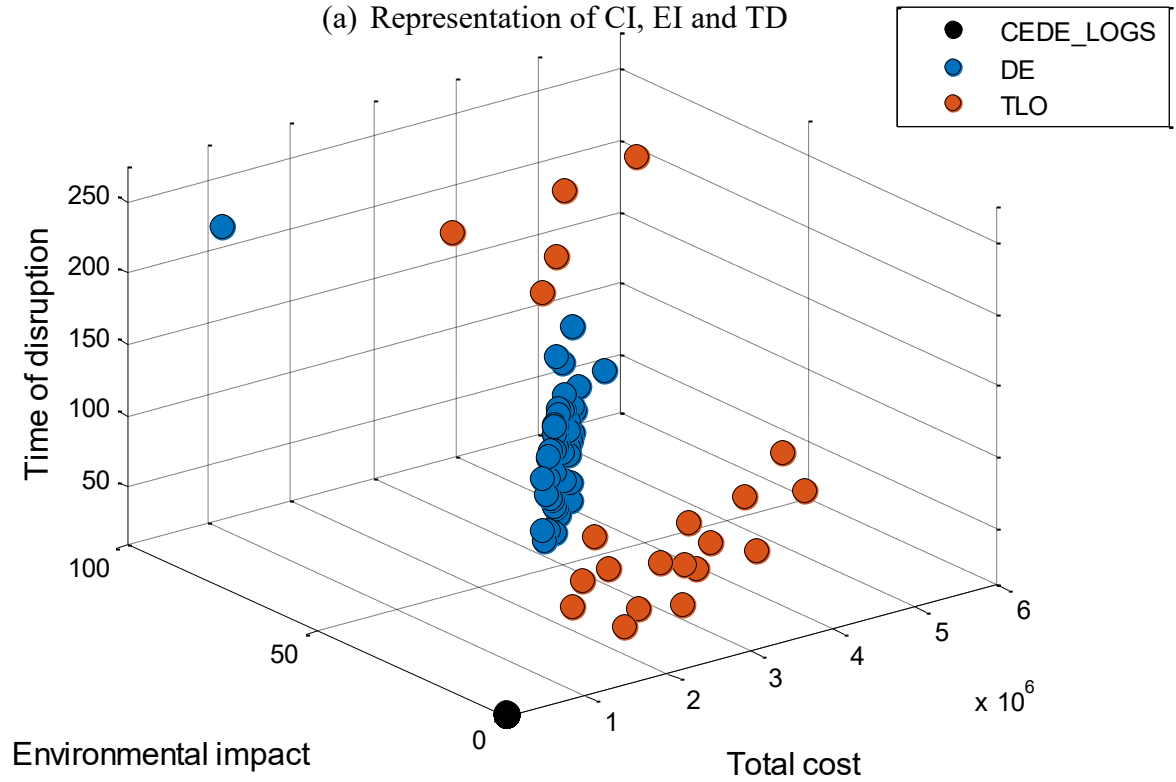


(b) Representation of CI, TC and EI

Figure 5.40: Optimum maintenance plans of the twenty five-year study period



(a) Representation of CI, EI and TD



(b) Representation of TC, EI and TD

Figure 5.41: Optimum maintenance plans of the twenty five year-study period (Continued)

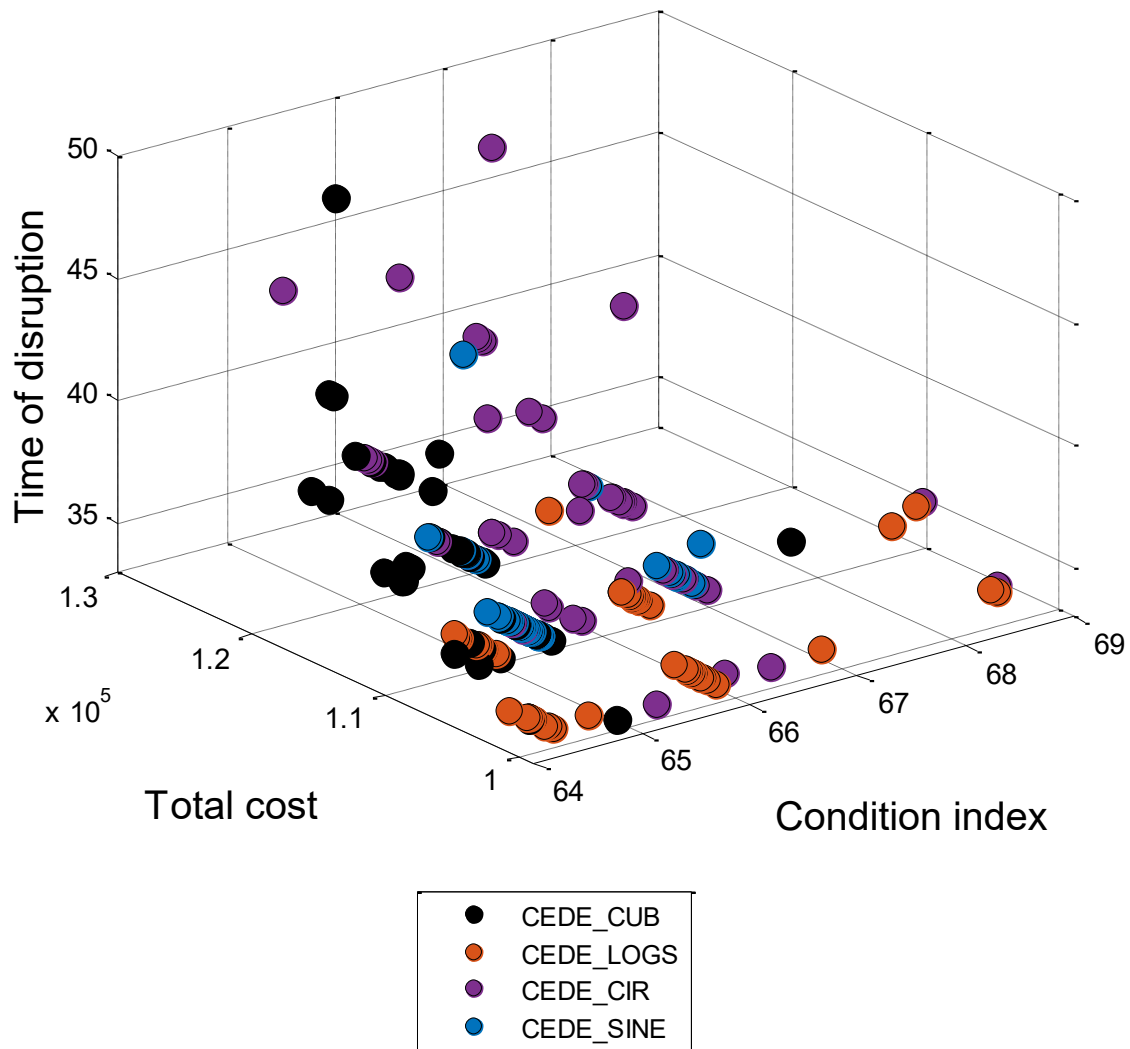


Figure 5.42: Optimum maintenance plans of the thirty five-year study period

Tables 5.38 and 5.39 are presented to establish an in-depth comparison between the different meta-heuristic algorithms for the maintenance planning of the thirty five-year study period. They are evaluated capitalizing on the minimum fitness function values (Min), average fitness function values (Avg), hypervolume indicator, generational distance (GD), inverted generational distance, spacing (S) and maximum Pareto front error (MPFE). It should be mentioned that the best performing meta-heuristic optimization algorithm is the one which yields higher values of

hypervolume indicator, in addition to lower values of generational distance, inverted generational distance, spacing and maximum Pareto front error. The bold values represent the best achieved values of the performance indicators. It can be interpreted that the ECDE-based logistic model achieved the highest minimum condition rating, ECDE-based cubic model achieved the lowest minimum total maintenance cost. Additionally, ECDE-based sinusoidal model, ECDE-based cubic model, ECDE-based logistic-sine model and ECDE-based circle model yielded the lowest minimum environmental impact. With respect to the average performance of the objective function values, ECDE-based circle model provided the highest average condition rating. Moreover, ECDE-based sinusoidal model achieved the lowest average maintenance cost and environmental impact.

In terms of hypervolume indicator, ECDE-based sinusoidal model provided the largest hypervolume indicator (98.4%). On the other hand, ECDE-based cubic model attained the lowest hypervolume indicator (96.4%). ECDE-based logistic, ECDE-based sinusoidal and ECDE-based Chebyshev models provided the best generational distance, inverted generational distance and maximum Pareto front error. On the other hand, ECDE-based cubic model provided the highest generational distance and inverted generational distance. Additionally, ECDE-based circle model attained the worst maximum Pareto front error. With respect to spacing metric, ECDE-based logistic, ECDE-based sinusoidal, ECDE-based sine, ECDE-based iterative, ECDE-based Chebyshev and ECDE-based circle models provided the lowest spacing. Nonetheless, ECDE-based logistic-sine model provided the highest spacing.

Table 5.38: Performance comparison between the different multi-objective meta-heuristics for maintenance planning of the thirty five-year study period

Performance metric	Object. function	MOEDE Logistic	MOEDE Singer	MOEDE Sinusoidal	MOEDE Sine	MOEDE Iterative
Minimum	CR	66.02	64.30	65.11	64.81	65.85
	TLCC	108450.79	163632.75	99495.98	104997.22	109656.6
	TDTT	0	0	0	0	0
	TEI	37.65	39.63	33.68	35.67	37.65
Average	CR	66.02	64.3	65.11	65.2	65.85
	TLCC	108450.79	163925.64	99495.98	107554.82	109672.74
	TDTT	0	0	0	0	0
	TEI	37.65	39.63	33.68	36.06	37.65
Hypervolume indicator	98	98	98.4	97.7	98
Generational distance	0	79.17	0	451.25	5.91
Inverted generational distance	0	292.89	0	2557.6	16.14
Spacing	0	4.75×10^{-4}	0	0	0
Maximum Pareto front error	0	2005.07	0	9020.5	138.19

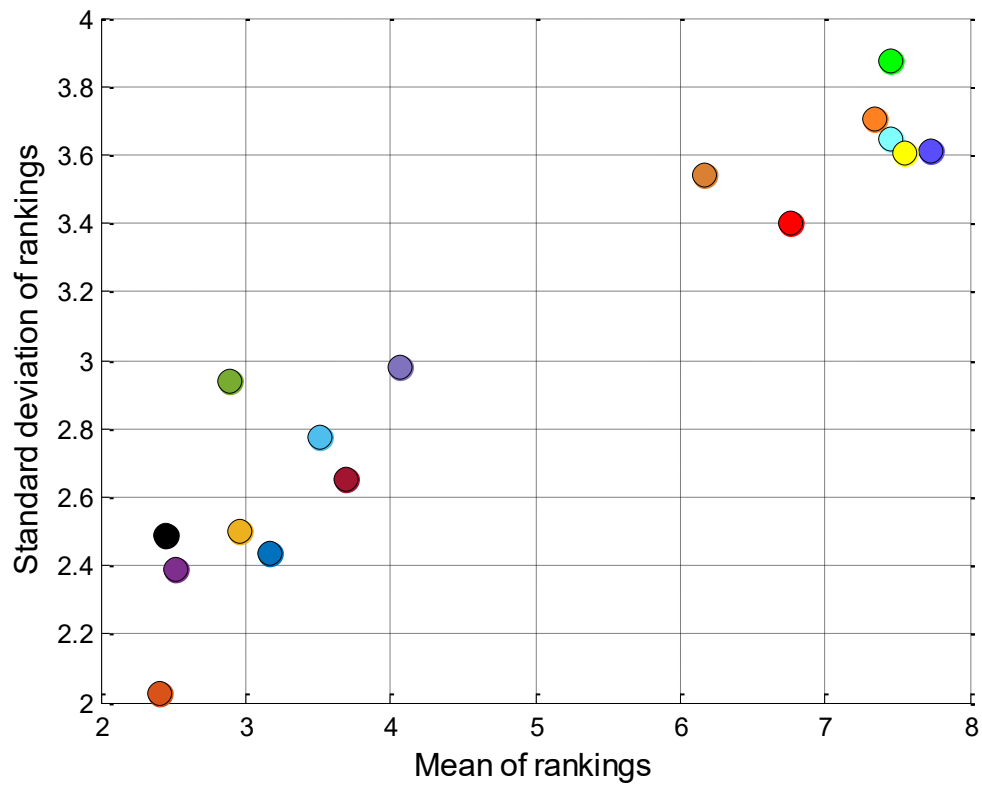
Table 5.39: Performance comparison between the different multi-objective meta-heuristics for maintenance planning of the thirty five-year study period (Continued)

Performance metric	Objective function	MOEDE Chebyshev	MOEDE Cubic	MOEDE Logistic-sine	MOEDE Circle
Minimum	CR	64.81	64.10	64.31	64.81
	TLCC	882308.26	99394.74	100187.32	99810.60
	TDTT	0	0	0	0
	TEI	55.48	33.68	33.68	33.68
Average	CR	64.81	64.71	65.46	66.12
	TLCC	882308.26	110403.66	103834.35	111667.16
	TDTT	0	0	0	0
	TEI	55.48	37.65	34.56	37.93
Hypervolume indicator	97.4	96.4	98	97.1
Generational distance	0	1163.2	595.52	1120.3
Inverted generational distance	0	6579.7	3214.05	5939.33
Spacing	0	2.7×10^{-3}	1.8×10^{-2}	0
Maximum Pareto front error	0	16866	12118	21382

The average ranking method is utilized to establish a comprehensive and unified comparison between the meta-heuristic optimization algorithms. This comparison integrates their performances with respect to all multi-objective quality indicators in both short-term and long-term planning. The results of the average ranking method are displayed in Figure 5.43. As shown

in Figure 5.43, there is significant improvement in both the mean of rankings and standard deviation of rankings attained by the exponential chaotic differential evolution models when compared against the conventional optimization algorithms. According to the conducted analysis, it can be found that ECDE-based sinusoidal achieved the first rank followed by the ECDE-based logistic and then the ECDE-based iterative. In this context, ECDE-based sinusoidal model achieved μ_a and σ_a of 2.41 and 2.03, respectively. With respect to the conventional optimization algorithms, DE algorithm provided the tenth rank followed by the TLO while Jaya algorithm provided the sixteenth rank, whereas Jaya algorithm provided μ_a and σ_a of 7.72 and 3.61, respectively. This evinces that the exponential chaotic differential evolution optimization model achieves higher accurate results and demonstrates more stable performance when compared against the classical meta-heuristics.

The box plots based on the hypervolume indicator of the multi-objective maintenance planning of the twenty-five year study period are depicted in Figure 5.44. The box plots enable analyzing the robustness of the different meta-heuristics through mapping the distribution and skewness of the numerical data. The robustness of the algorithm is one of the main aspects to judge the performance of meta-heuristics. It can be derived the exponential chaotic differential evolution optimization model sustain more consistent hypervolume across the different runs. Additionally, the DE and TLO algorithms experience more perturbations in the hypervolume indicator. It can be also found that the ECDE-based sinusoidal model achieved superior HV while TLO yielded the lowest HV.



- ECDE-based logistic
- ECDE-based Singer
- ECDE-based Sinusoidal
- ECDE-based Sine
- ECDE-based Iterative
- ECDE-based Chebyshev
- ECDE-based cubic
- ECDE-based logistic-sine
- ECDE-based circle
- Differential evolution
- Invasive weed optimization
- Biogeography-based optimization
- Teaching-learning optimization
- Genetic algorithm
- Jaya algorithm
- Particle swarm optimization

Figure 5.43: Plot of the average and standard deviation of rankings of the meta-heuristic-based optimization models

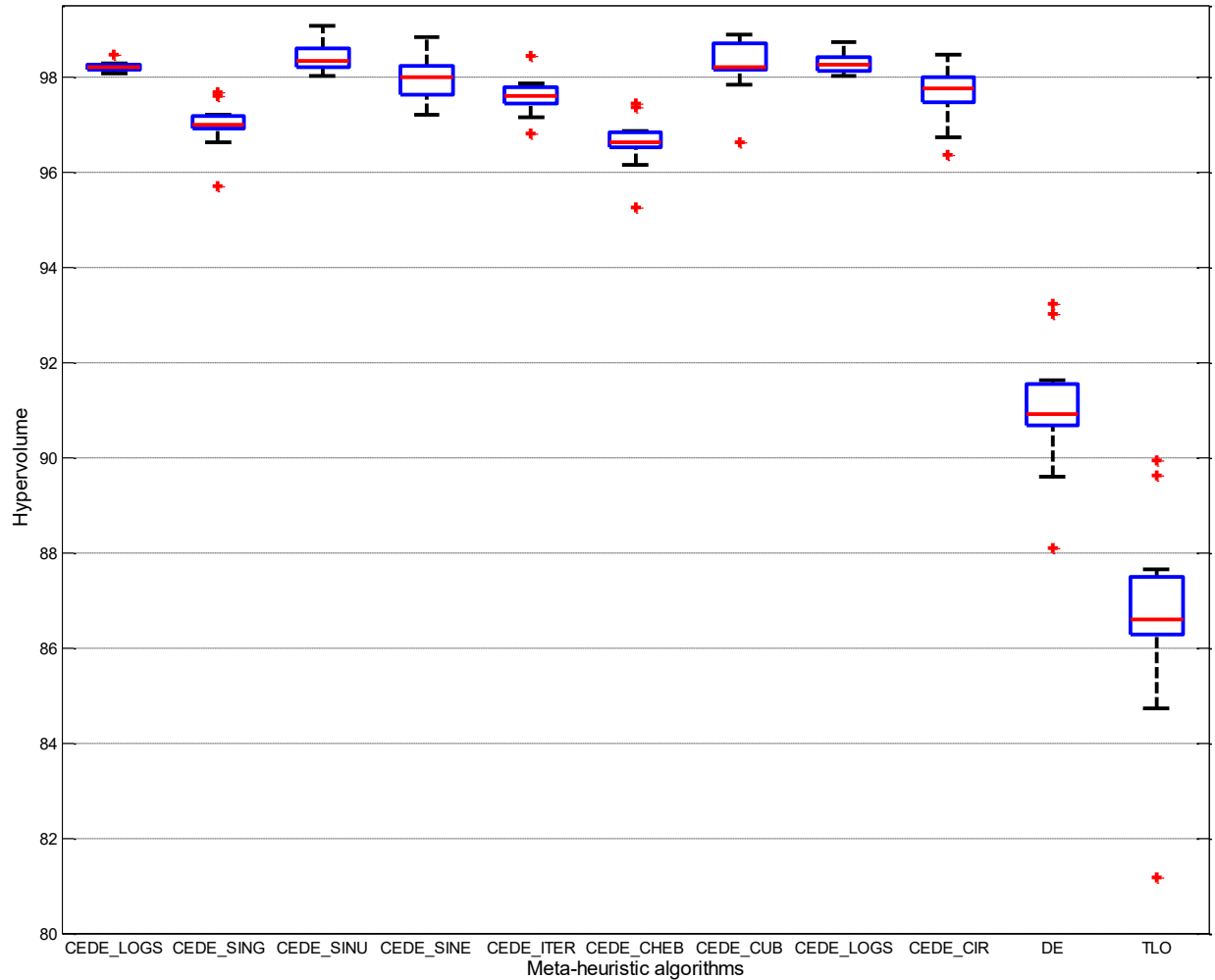


Figure 5.44: Box plots of the hypervolume of the meta-heuristic-based maintenance optimization models

A hybrid multi-criteria decision-making model is designed to select the compromise solution among the set of Pareto optimal solutions. In this context, CRITIC technique is used for deriving the weights of the attributes CR, TLCC, TDDT and TEI. It was concluded that the weights of CR, TLCC, TDDT and TEI are 30.07%, 20.03%, 26.68% and 23.22%, respectively. Furthermore, COPRAS and GRA are applied to rank the Pareto optimal solutions. Each type of the multi-criteria decision-making induces a distinct ranking from the other. In this regard, AR method is employed to formulate a consensus ranking of the Pareto optimal solutions. Sample of the optimal solutions for the five-year, twenty five-year and thirty five-year maintenance planning

horizons are recorded in Tables 5.40, 5.41 and 5.42, respectively. The best maintenance plan for the five-year study period induces CR, TLCC, TDTT and TEI of 72.87, 38805.06, 0 and 33.68, respectively. For the twenty five-year planning horizon, the best solution comprises CR, TLCC, TDTT and TEI of 64.8, 36597.54, 0 and 11.89, respectively. Additionally, The most optimum maintenance plan for the thirty five-year study period induces CR, TLCC, TDTT and TEI of 68.65, 101866.48, 0 and 33.68, respectively. By analyzing the rankings of the optimum solutions, it can be inferred that the disagreement between the rankings of the optimum solutions increases with the increase in the complexity of the multi-objective optimization model, i.e., more lengthy planning horizon. This state of affair necessitates the employment of the AR method for the purpose of obtaining compromise solution.

Table 5.40: Sample of the solutions’ rankings obtained from COPRAS, GRA and AR for the maintenance planning of five-year study period

Objective function values [CR, TLCC, TDTT, TEI]	Utility degree	Grey relational grade	Mean ranking (μ_a)	Final ranking
[72.87, 38805.06, 0, 33.68]	100	71.8	1	1
[72.87, 38858.56, 0, 33.68]	99.98	71.8	4	4
[72.87, 45122.37, 0, 33.68]	88.31	71.17	5	5
[74.15, 899921.57, 0, 33.68]	30.24	60.97	7	7
[74.58, 3374606.95, 0, 263.74]	20.83	47.3	9	9

Table 5.41: Sample of the solutions' rankings obtained from COPRAS, GRA and AR for the maintenance planning of twenty five-year study period

Objective function values [CR, TLCC, TDDT, TEI]	Utility degree	Grey relational grade	Mean ranking (μ_a)	Final ranking
[64.8, 36597.54, 0, 11.89]	99.81	86.13	2	1
[64.21, 36784.8, 0, 11.89]	99.63	86.04	6	5
[64.21, 36786.44, 0, 11.89]	99.6	86.04	9	8
[72.02, 2793796.51, 6, 81.68]	14.85	61.82	102.5	104
[72.45, 3927176.3, 6, 101.64]	14.15	57.92	116	116

Table 5.42: Sample of the solutions' rankings obtained from COPRAS, GRA and AR for the maintenance planning of thirty five-year study period

Objective function values [CR, TLCC, TDDT, TEI]	Utility degree	Grey relational grade	Mean ranking (μ_a)	Final ranking
[68.65, 101866.48, 0, 33.68]	100	74.69	1.5	1
[66.02, 100983.86, 0, 33.68]	99.25	72.74	8	7
[64.34, 100570.04, 0, 33.68]	98.72	71.85	24.5	24
[64.81, 106738.61, 0, 35.67]	94.72	66.27	104.5	106
[64.81, 107575.51, 0, 35.67]	94.51	66.22	116.5	120

CHAPTER VI: CONCLUSION AND FUTURE RESEARCH

6.1 Summary and Conclusions

The thesis introduced a newly developed method for optimization of maintenance plans of reinforced concrete bridge decks. The method and its embedded models are automated in a computational framework developed in C#.net and Matlab environment. It houses a developed set of partially integrated standalone computer applications for the detection and evaluation of surface defects, assessment of corrosion severities, integrated condition assessment, deterioration modeling and optimizing maintenance plans. The contributions of the developed integrated method lie in the following. A self-adaptive surface defects detection and evaluation method that adopted newly-developed hybrid SVD – DWT algorithm for better representation of the spatial and domain features of the image. This method also utilized ENN – IWO for the automated identification of defects and evaluation of their magnitudes of severities in an attempt to alleviate the shortcomings of gradient descent and manual tuning-based models in addition to the computational intensive deep learning models. It significantly outperformed a set of widely-utilized machine learning and deep learning models based on both split and 10-fold cross validation and for different sizes of datasets. When compared against artificial neural networks, the developed models for detection, recognition and evaluation managed to improve the prediction accuracies by 56.08%, 20.2% and 64.23%, respectively. The developed corrosion evaluation method was able to circumvent the limitations of numerical amplitude-based corrosion maps that utilized case dependent clustering algorithms.

The integrated condition assessment method used optimized fuzzy analytical network process model to compute the relative importance weights of defects. It enabled to address the limitations of classical weighting interpretation models through maximizing the overall consistency of the

responses via restructuring the judgment matrices while preserving as much possible information in the original matrices. It capitalized on ground penetrating radar and computer vision technologies to evaluate the extent of severities of the bridge defects. In this context, a variable-length invasive weed optimization model was designed to automatically calibrate the fuzzy membership functions to circumvent the limitations of subjective, tedious and case dependent manual methods of calibration. This method also implicated designing a bridge maintenance decision-making strategy and structuring severity rating systems for the bridge defect severity indices. The developed O – FANP model outperformed classical FANP, whereas it provided a significant improvement in the OVR_CONST of 90.78%. It was found also that the developed model induced mores significant and consistent improvement against visual inspection models created by the MTQ.

The fourth method for deterioration modeling predicts the future performance of concrete bridge based on a hybrid Bayesian-based optimization approach. Bayesian belief network was adopted for the investigation of the degree of influence of the bridge defects on the condition rating. Metropolis Hastings algorithm was employed to capture the uncertainties associated with the transition time and transition probabilities to overcome the deterministic and computationally expensive nature of artificial neural network. In the developed method, a hybrid genetic algorithm-Markovian model was established for emulating the non-homogenous pattern of deterioration process. Results demonstrated that the developed model managed to decrease the prediction error by 59.67% with respect to the most commonly-utilized weibull distribution.

The fifth method is resource driven established for bridge maintenance optimization at both project and network levels. It supports operational and strategic planning in an endeavor to structure more efficient and reliable decision support system. The resource allocation method

encompassed a novel surrogate machine learning model devised in an effort to address the shortcomings of timely and computationally expensive simulation. The maintenance budget allocation method is envisioned on formulating multi-objective exponential chaotic differential evolution model to optimize the MR&R schedule for a large network of bridge elements. In this context, exponential chaotic search mechanism was proposed to circumvent the critical limitations of multi-criteria decision-making-based models, single objective optimization models and classical meta-heuristic-based models. It accommodates performance, economic, social and environmental objective functions to generate short-term and long-term multi-year maintenance timely-maintenance plans with balanced expenditures over the planning period. It comprised the use of Latin hypercube sampling to simulate the encountered inherent uncertainties associated with the modeled performance aspects.

It was concluded that developed ECDE-based Sinusoidal model managed to improve the multi-objective performance diagnostics by 49.15% with reference to the multi-objective genetic algorithm in the five-year study period. ECDE-based Sinusoidal model yielded an enhancement of performance aspects by 24.98% with respect to multi-objective differential evolution in the twenty five-year study period. At the level of thirty five-year study period, classical meta-heuristics failed to find feasible solutions within the imposed constraints of the maintenance budget allocation model. It was found that ECDE-based sinusoidal model significantly surpassed state of art meta-heuristics. This was exemplified capitalizing on achieving P-values of less than 5% for five different types of non-parametric tests.

6.2 Research Limitations

The main limitations of the developed method can be summarized as follows:

- 1- Deterioration model is based on age group. In this regard, several deterioration models can be simulated and categorized according to their age and traffic volume.
- 2- The maintenance budget allocation model considers only deck, piers and abutments.
3. The developed surrogate machine learning model doesn't account for the range and deviation of the output distributions and only accounts for the mean.

6.3 Recommendations for Future Research

Some recommendations are proposed in order to improve the current research study as follows:

- 1- Develop a post disaster optimization model for a bridge network to enhance their restoration ability and minimize associated economic losses.
- 2- Study the implications of surface defects and their propagation over time on stiffness reduction of bridge deck.
- 3- Expand the developments made in this thesis for structural steel bridges and composite steel-concrete bridges.
- 4- Extend the development made here to account for outsourcing maintenance and rehabilitation work.

REFERENCES

1. AASHTO Highways subcommittee on Bridges and Structures. (2011). “*The Manual for Bridge Evaluation: Second Edition*”. American Association of State Highway and Transportation Officials, Washington, D.C, United States.
2. Abu Dabous, S., Yaghi, S., Alkass, S., and Moselhi, O. (2017). “Concrete bridge deck condition assessment using IR Thermography and Ground Penetrating Radar technologies.” *Automation in Construction*, 81, 340–354.
3. Adhikari, R. S., Moselhi, O., and Bagchi, A. (2014). “Image-based retrieval of concrete crack properties for bridge inspection”. *Automation in Construction*, 39(1), 180–194.
4. Agarwal, A., and Kumar, P. (2019). “Advanced BPANN Based Modified Boundary Discriminative Noise Removal Technique for Salt and Pepper Noise Removal. *International Journal of Engineering and Technical Research*, 9(9), 12–20.
5. Agrawal, A. K., Kawaguchi, A., and Chen, Z. (2010). “Deterioration rates of typical bridge elements in New York.” *Journal of Bridge Engineering*, 15(4), 419–429.
6. Ahmad, M. W., Mourshed, M., and Rezgui, Y. (2017). “Trees vs Neurons : Comparison between random forest and ANN for high-resolution prediction of building energy consumption”. *Energy & Buildings*, 147, 77–89.
7. Akay, B. (2013). “A Study on Particle Swarm Optimization and Artificial Bee Colony Algorithms for Multilevel Thresholding.” *Applied Soft Computing*, 13(6), 3066–3091.
8. Al-Allaf, O. N. A. (2011). “Fast BackPropagation Neural Network algorithm for reducing convergence time of BPNN image compression.” *2011 International Conference on Information Technology and Multimedia*, Kuala Lumpur, Malaysia, 14-16 November, 1-6.
9. Alhamdoosh, M., and Wang, D. (2014). “Fast decorrelated neural network ensembles with

- random weights.” *Information Sciences*, 264, 104–117.
10. Ali, G., Elsayegh, A., Assaad, R., El-Adaway, I. H., and Abotaleb, I. S. (2019). “Artificial neural network model for bridge deterioration and assessment.” *Proceedings, Annual Conference - Canadian Society for Civil Engineering*, Laval, Canada, 1–10.
 11. Allah Bukhsh, Z., Stipanovic, I., and Doree, A. G. (2020). “Multi-year maintenance planning framework using multi-attribute utility theory and genetic algorithms.” *European Transport Research Review*, 12(1), 1-13.
 12. Allah Bukhsh, Z., Stipanovic, I., Klanker, G., Connor, A. O., and Doree, A. G. (2019). “Network level bridges maintenance planning using Multi-Attribute Utility Theory.” *Structure and Infrastructure Engineering*, 15(7), 872–885.
 13. Alsharqawi, M., Zayed, T., and Shami, A. (2020). “Ground penetrating radar-based deterioration assessment of RC bridge decks.” *Construction Innovation*, 20(1), 1–17.
 14. Alsharqawi, M., Zayed, T., and Abu Dabous, S. (2018). “Integrated condition rating and forecasting method for bridge decks using Visual Inspection and Ground Penetrating Radar.” *Automation in Construction*, 89, 135–145.
 15. Amini, A., Nikraz, N., and Fathizadeh, A. (2016). “Identifying and evaluating the effective parameters in prioritization of urban roadway bridges for maintenance operations”. *Australian Journal of Civil Engineering*, 14(1), 23-34.
 16. Amiri, M. J. T., Abdollahzadeh, G., and Haghghi, F. (2019). “Bridges Risk Analysis in View of Repair and Maintenance by Multi Criteria Decision Making Method (Case Study : Babolsar Bridges).” *International Journal of Transportation Engineering*, 7(1), 91–114.
 17. Anter, A. M., and Ali, M. (2020). “Feature selection strategy based on hybrid crow search optimization algorithm integrated with chaos theory and fuzzy c-means algorithm for

- medical diagnosis problems.” *Soft Computing*, 24(3), 1565–1584.
18. Asgari, H. R., Haddad, O. B., Pazoki, M., and Loáiciga, H. A. (2016). “Weed optimization algorithm for optimal reservoir operation.” *Journal of Irrigation and Drainage Engineering*, 142(2), 1–11.
 19. Ata, M., Mohammed Abdelkader, E., Abouhamad, M., Serror, M. H., and Marzouk, M. (2017). “On the Use of Ground Penetrating Radar for Bridge Deck Assessment”. *1st International Conference on Computer Science and Application Engineering*, Shanghai, China, 21-23 October, 1-7.
 20. Aydın, S., and Kahraman, C. (2013). “A New Fuzzy Analytic Hierarchy Process and Its A New Fuzzy Analytic Hierarchy Process and Its Application to Vendor Selection Problem.” *Journal of Multiple-Valued Logic and Soft Computing*, 353–371.
 21. Azimifard, A., Moosavirad, S. H., and Ariaifar, S. (2018). “Selecting sustainable supplier countries for Iran’s steel industry at three levels by using AHP and TOPSIS methods.” *Resources Policy*, 57, 30–44.
 22. Azizipour, M., Ghalenoey, V., Afshar, M. H., and Solis, S. S. (2016). “Optimal Operation of Hydropower Reservoir Systems Using Weed Optimization Algorithm.” *Water Resources Management*, 30, 3995–4009.
 23. Badawy, A. M. (2017). “*Assessment of Bridges’ Expansion Joints In Egypt*”. M.Sc. thesis, American University in Cairo, Egypt.
 24. Bagloee, S. A., and Sarvi, M. (2018). “An outer approximation method for the road network design problem.” *PLoS ONE*, 13(3), 1–28.
 25. Baji, H., Yang, W., and Li, C. Q. (2017). “An optimum strengthening strategy for corrosion-affected reinforced concrete structures.” *ACI Structural Journal*, 114(6), 1591–1602.

26. Bangaru, S. S., Wang, C., Zhou, X., Jeon, H. W., and Li, Y. (2020). “Gesture Recognition–Based Smart Training Assistant System for Construction Worker Earplug-Wearing Training.” *Journal of Construction Engineering and Management*, 146(12), 1-12.
27. Barnes, C. L., Trottier, J.-F., and Forgeron, D. (2008). “Improved concrete bridge deck evaluation using GPR by accounting for signal depth– amplitude effects.” *NDT&E*, 41, 427–433.
28. Barnes, C. L., and Trottier, J.-F. (2004). “Effectiveness of Ground Penetrating Radar in Predicting Deck Repair Quantities.” *Journal of Infrastructure Systems*, 10(2), 69–76.
29. Basha, D. K., and Venkateswarlu, T. (2020). “Linear regression supporting vector machine and hybrid LOG filter-based image restoration.” *Journal of Intelligent Systems*, 29(1), 1480–1495.
30. Bhandari, S., Thakur, B., Kalra, A., Miller, W. P., Lakshmi, V., and Pathak, P. (2019). “Streamflow Forecasting Using Singular Value Decomposition and Support Vector Machine for the Upper Rio Grande River Basin.” *Journal of the American Water Resources Association*, 55(3), 680–699.
31. Bhattacharjee, P. S., Fujail, A. K. M., and Begum, S. A. (2017). “A Comparison of Intrusion Detection by K-Means and Fuzzy C-Means Clustering Algorithm over the NSL-KDD Dataset.” *2017 IEEE International Conference on Computational Intelligence and Computing Research (ICCIC)*, Coimbatore, India, 14-16 December, 1-6.
32. Boender, C. G. E., Graan, J. G. d., and Lootsma, F. A. (1989). “Multi-criteria decision analysis with fuzzy pairwise comparisons.” *Fuzzy Sets and Systems*, 29(2), 133–143.
33. Bolar, A., Tesfamariam, S., and Sadiq, R. (2013). “Condition assessment for bridges : a hierarchical evidential reasoning (HER) framework.” *Structure and Infrastructure*

Engineering, 9(7), 648–666.

34. Braglia, M., Castellano, D., Frosolini, M., Gabbrielli, R., Marrazzini, L., and Padellini, L. (2020). “An ensemble-learning model for failure rate prediction.” *Procedia Manufacturing*, 42, 41–48
35. Brankovic, J. M., Markovic, M., and Nikolic, D. (2018). “Comparative study of hydraulic structures alternatives using promethee II complete ranking method.” *Water Resources Management*, 32(10), 3457–3471.
36. Brans, J. P., Vincke, P., and Mareschal, B. (1986). “How to select and how to rank projects : The PROMETHEE method.” *European Journal of Operational Research*, 24, 228–238.
37. Brans, J. P., and Vincke, D. P. (1985). “A Preference Ranking Organisation Method: (The PROMETHEE Method for Multiple Criteria Decision-Making).” *Management Science*, 31(6), 647–656.
38. Bu, G. P., Lee, J. H., Guan, H., Loo, Y. C., and Blumenstein, M. (2015). “Prediction of Long-Term Bridge Performance: Integrated Deterioration Approach with Case Studies.” *Journal of Performance of Constructed Facilities*, 29(3), 1-10.
39. Bu, G. P., Chanda, S., Guan, H., Jo, J., Blumenstein, M., and Loo, Y. C. (2015). “Crack Detection using a Texture Analysis-based Technique for Visual Bridge Inspection.” *Electronic Journal of Structural Engineering*, 14(1), 41–48.
40. Büyüközkan, G., Kahraman, C., and Ruan, D. (2004). “A fuzzy multi-criteria decision approach for software development strategy selection.” *International Journal of General Systems*, 33, 259–280.
41. Callow, D., Lee, J., Blumenstein, M., Guan, H., and Loo, Y. (2013). “Development of hybrid optimisation method for Artificial Intelligence based bridge deterioration model —

- Feasibility study.” *Automation in Construction*, 31, 83–91.
42. Cardimona, S., Willeford, B., Wenzlick, J., and Anderson, N. (2000). “Investigation of bridge decks utilizing ground penetrating radar.” In *International Conference on the Application of Geophysical Technologies to Planning, Design, Construction, and Maintenance of Transportation Facilities*, Missouri, United States of America, 11-15 December.
43. Caterpillar Inc. (2013). *Caterpillar Performance Handbook*, Illinois, United States of America.
44. Cen, J., Zhao, J., Xia, X., and Liu, C. (2017). “Application Research on Convolution Neural Network for Bridge Crack Detection.” *Advances in Computer Science Research*, 74, 150–156.
45. Cha, Y. J., Choi, W., and Büyüköztürk, O. (2017). “Deep Learning-Based Crack Damage Detection Using Convolutional Neural Networks.” *Computer-Aided Civil and Infrastructure Engineering*, 32, 361-378.
46. Chang, B., Tsai, H., and Yen, C. (2016). “Engineering Applications of Artificial Intelligence SVM-PSO based rotation-invariant image texture classification in SVD and DWT domains”. *Engineering Applications of Artificial Intelligence*, 52, 96–107.
47. Chang, D. (1996). “Applications of the extent analysis method on fuzzy AHP.” *European Journal of Operational Research*, 95, 649–655.
48. Chaiyasarn, K., Khan, W., Ali, L., Sharma, M., Brackenbury, D., and DeJong, M. (2018). “Crack detection in masonry structures using convolutional neural networks and support vector machines.” *35th International Symposium on Automation and Robotics in Construction*, Berlin, Germany, 20-25 July, 1-8.

49. Chatterjee, A., and Tsai, Y.-C. (2020). "Training and Testing of Smartphone-Based Pavement Condition Estimation Models Using 3D Pavement Data." *Journal of Computing in Civil Engineering*, 34(6), 04020043.
50. Chen, B., Zhang, X., Wang, R., Li, Z., and Deng, W. (2019). Detect concrete cracks based on OTSU algorithm with differential image. *The Journal of Engineering*, 2019(23), 9088–9091.
51. Chen, X., Wang, W., Xie, G., Hontecillas, R., Verma, M., Leber, A., Bassaganya-Riera, A., and Abedi, V. (2019). "Multi-Resolution Sensitivity Analysis of Model of Immune Response to Helicobacter pylori Infection via Spatio-Temporal Metamodeling." *Frontiers in Applied Mathematics and Statistics*, 5, 1-15.
52. Cheng, C. (1996). "Evaluating naval tactical missile systems by fuzzy AHP based on the grade value of membership function." *European Journal of Operational Research*, 2217(96), 343–350.
53. Chitsaz, N., Azarnivand, A., and Araghinejad, S. (2016). "Pre-processing of data-driven river flow forecasting models by singular value decomposition (SVD) technique." *Hydrological Sciences Journal*, 61(12), 2164–2178.
54. Contreras-nieto, C., Shan, Y., Lewis, P., and Ann, J. (2019). "Bridge maintenance prioritization using analytic hierarchy process and fusion tables." *Automation in Construction*, 101, 99–110.
55. Crawford, G., and Williams, C. (1985). "A note on the analysis of subjective judgment matrices." *Journal of Mathematical Psychology*, 29(4), 387–405.
56. Cui, Z., Zhang, J., Wu, D., Cai, X., Wang, H., Zhang, W., and Chen, J. (2020). "Hybrid many-objective particle swarm optimization algorithm for green coal production problem." *Information Sciences*, 518, 256–271.

57. Datta, T., Gates, T., Savolainen, P., Kay, J., Parajuli, S., and Nicita, N. (2016). *A Guide to Short - Term Stationary, Short - Duration, and Mobile Work Zone Traffic Control, Washington, D.C.*
58. Dawood, T., Zhu, Z., and Zayed, T. (2017). "Machine vision-based model for spalling detection and quantification in subway networks". *Automation in Construction*, 81, 149–160.
59. Demir, F. B., Tuncer, T., and Kocamaz, A. F. (2020). "A chaotic optimization method based on logistic-sine map for numerical function optimization." *Neural Computing and Applications*, 9, 1-13.
60. Deng, X., Hu, Y., and Deng, Y. (2014). "Bridge Condition Assessment Using D Numbers". *The Scientific World Journal*, Article ID 358057, 11 pages.
61. Destefano, P. D., and Grivas, D. A. (1998). "Method for estimating transition probability in bridge deterioration models." *Journal of Infrastructure Systems*, 4(2), 56–62.
62. Dhillon, A., and Verma, G. K. (2019). "Convolutional neural network: a review of models, methodologies and applications to object detection." *Progress in Artificial Intelligence*, 1–28.
63. Diakoulaki, D., Mavrotas, G., and Papayannakis, L. (1995). "Determining objective weights in multiple criteria problems: The critic method." *Computers and Operations Research*, 22(7), 763–770.
64. Di Biasi, M. R., Valencia, G. E., and Obregon, L. G. (2020). "A new educational thermodynamic software to promote critical thinking in youth engineering students." *Sustainability*, 12, 1–17.
65. Dinh, K., and Zayed, T. (2016). "GPR-Based Fuzzy Model for Bridge Deck Corrosiveness Index." *Journal of Performance of Constructed Facilities*, 30(4), 1–14.

66. Dinh, T. H., Ha, Q. P., and La, H. M. (2016). "Computer Vision-based Method for Concrete Crack Detection." In *14th International Conference on Control, Automation, Robotics & Vision*, Phuket, Thailand, 13-15 November, 1-6.
67. Dorafshan, S., Thomas, R. J., Coopmans, C., and Maguire, M. (2018a). "Deep Learning Neural Networks for sUAS-Assisted Structural Inspections: Feasibility and Application." In *2018 International Conference on Unmanned Aircraft Systems*, Dallas, United States of America, 12-15 June, 1-9.
68. Dorafshan, S., Thomas, R. J., and Maguire, M. (2018b). "SDNET2018: An annotated image dataset for non-contact concrete crack detection using deep convolutional neural networks." *Data in Brief*, *21*, 1664–1668.
69. Dromey, L., Ruane, K., Murphy, J. J., O'Rourke, B., and Lacey, S. (2020). "A bridge-rehabilitation strategy based on the analysis of a bridge-inspection data set." *Infrastructure Asset Management*, *7*(1), 25–35.
70. Dung, C. V., and Anh, L. D. (2019). "Autonomous concrete crack detection using deep fully convolutional neural network." *Automation in Construction*, *92*, 52-58.
71. Dung, C. V., Sekiya, H., Hirano, S., Okatani, T., and Miki, C. (2019). "A vision-based method for crack detection in gusset plate welded joints of steel bridges using deep convolutional neural networks." *Automation in Construction*, *102*, 217–229.
72. Ehlen, M. A., and Marshall, H. E. (1996). *The Economics of New-Technology Materials: A Case Study of FRP Bridge Decking*, Gaithersburg.
73. Ellenberg, A., Kontsos, S., Moon, F., and Bartoli, I. (2016). "Bridge related damage quantification using unmanned aerial vehicle imagery." *Structural Control Health Monitoring*, *23*, 1168–1179.

74. Elsener, B., Andrade, C., Gulikers, J., Polder, R., & Raupach, M. (2003). Half-cell potential measurements – Potential mapping on reinforced concrete structures. *Materials and Structures*, 36, 1–11.
75. Falahiazar, L., and Shah-Hosseini, H. (2018). “Optimisation of engineering system using a novel search algorithm: the Spacing Multi-Objective Genetic Algorithm.” *Connection Science*, 30(3), 326–342.
76. Felio, G. (2016). “*Canadian Infrastructure Report Card*”. Canadian Construction Association, Canadian Public Works Association, Canadian Society for Civil Engineering, and Federation of Canadian Municipalities, Canada. <www.canadainfrastructure.ca/downloads/Canadian_Infrastructure_Report_2016.pdf> (06.05.2016).
77. Feng, C., Ju, S., and Huang, H. (2016). “Using a Simple Soil Spring Model and Support Vector Machine to Determine Bridge Scour Depth and Bridge Safety”. *Journal of Performance of Constructed Facilities*, 30(4), 1–14.
78. Fitriani, H., Pratama, M. A. S., Idris, Y., and Tanzil, G. (2019). “Determination of prioritization for maintenance of the upper structure of truss bridge.” *MATEC Web of Conferences*, 276, 01036, 1-10.
79. Fornell, C. (1983). “Issues in the Application of Covariance Structure Analysis: A Comment”. *Journal of Consumer Research*, 9(4), 443–448.
80. Ganesh, A. K., and Kusagur, A. (2018). “Adaptive noise detection using texture feature extraction and random forest classification.” *International Journal of Intelligent Engineering and Systems*, 11(5), 254–264.
81. Gao, Z., Liang, R. Y., and Xuan, T. (2019). “VIKOR method for ranking concrete bridge

- repair projects with target-based criteria.” *Results in Engineering*, 3, 1–9.
82. Gao, Z., and Li, J. (2018). “Fuzzy Analytic Hierarchy Process Evaluation Method in Assessing Corrosion Damage of Reinforced Concrete Bridges.” *Civil Engineering Journal*, 4(4), 843–856.
83. Gervásio, H., and Simões Da Silva, L. (2012). “A probabilistic decision-making approach for the sustainable assessment of infrastructures.” *Expert Systems with Applications*, 39(8), 7121–7131.
84. Goharnejad, H., Mohamadi Naser, M., and Niri, M. Z. (2017). “The Optimization of Energy Supply Systems by Sequential Streamflow Routing Method and Invasive Weed Optimization Algorithm; Case Study: Karun II Hydroelectric Power Plant.” *Journal of Hydraulic Structures*, 3(1), 71–82.
85. Ghodoosi, F., Abu-Samra, S., Zeynalian, M., and Zayed, T. (2018). “Maintenance cost optimization for bridge structures using system reliability analysis and genetic algorithms.” *Journal of Construction Engineering and Management*, 144(2), 1–10.
86. Goli, A., Tirkolaei, E. B., Malmir, B., Bian, G. Bin, and Sangaiah, A. K. (2019). “A multi-objective invasive weed optimization algorithm for robust aggregate production planning under uncertain seasonal demand.” *Computing*, 101(6), 499–529.
87. Gordian RSMeans Data. (2017). Building Construction Cost Data with rsmeans data.
88. Gucunski, N., Imani, A., Romero, F., Nazarian, S., Yuan, D., Wiggenger, H., Wiggenger, H., Shokouhi, P., Taffe, A. and Kutrubes, D. (2013). “*Nondestructive Testing to Identify Concrete Bridge Deck Deterioration*”, Washington DC, United States of America.

89. Guo, Q., Zhang, C., Zhang, Y., and Liu, H. (2016). "An Efficient SVD-Based Method for Image Denoising." *IEEE Transactions on Circuits and Systems for Video Technology*, 26(5), 868–880.
90. Hafezalkotob, A., and Hafezalkotob, A. (2015). "Extended MULTIMOORA method based on Shannon entropy weight for materials selection." *Journal of Industrial Engineering International*, 12(1), 1–13.
91. Hammad, A., Yan, J., and Mostofi, B. (2007). "Recent Development of Bridge Management Systems in Canada." *Annual Conference of the Transportation*, Saskatoon, Canada, 1-19.
92. Hammouche, K., Diaf, M., and Siarry, P. (2008). "A Multilevel Automatic Thresholding Method Based on A Genetic Algorithm For A Fast Image Segmentation." *Computer Vision and Image Understanding*, 109(2), 163–175.
93. Hasan, M. S. (2015). "*Deterioration Prediction of Concrete Bridge Components Using Artificial Intelligence and Stochastic Methods.*" M.Sc. thesis, RMIT University, Australia.
94. Hekimoğlu, B. (2019). "Optimal Tuning of Fractional Order PID Controller for DC Motor Speed Control via Chaotic Atom Search Optimization Algorithm." *IEEE Access*, 7, 38100–38114.
95. Ho, H., Kim, K., Park, Y., Lee, J. (2013) "An efficient image-based damage detection for cable surface in cable-stayed bridges." *NDT&E International*, 58, 18–23.
96. Hoang, N. D., and Nguyen, Q. L. (2019). "A novel method for asphalt pavement crack classification based on image processing and machine learning." *Engineering with Computers*, 35, 487-498.
97. Hoang, N. (2018). "Detection of Surface Crack in Building Structures Using Image Processing Technique with an Improved Otsu Method for Image Thresholding". *Advances in*

Civil Engineering, Article ID 3924120, 10 pages.

98. Hooda, H., Verma, O. P., and Singhal, T. (2015). "Brain tumor segmentation: A performance analysis using K-Means, Fuzzy C-Means and Region growing algorithm." *Proceedings of 2014 IEEE International Conference on Advanced Communication, Control and Computing Technologies*, Ramanathapuram, India, 8-10 May, 1621-1626.
99. Hong, T., Chae, M. J., Kim, D., Koo, C., Lee, K. S., and Chin, K. H. (2013). "Infrastructure Asset Management System for Bridge Projects in South Korea." *KSCE Journal of Civil Engineering*, 17(7), 1551–1561.
100. Hoshyar, A. N., Al-jumaily, A., and Hoshyar, A. N. (2014). "Comparing the Performance of Various Filters on Skin Cancer Images". *Procedia Computer Science*, 42, 32–37.
101. Huang, Q., and Song, W. (2019). "A land-use spatial optimum allocation model coupling a multi-agent system with the shuffled frog leaping algorithm." *Computers, Environment and Urban Systems*, 77, 1-19.
102. Huang, Y.-H. (2010). "Artificial neural network model of bridge deterioration." *Journal of Performance of Constructed Facilities*, 24(6), 597–602.
103. Hussein, A., and AbuTair, A. (2019). "Estimating Bridge Deterioration Age Using Artificial Neural Networks." *International Journal of Engineering and Technology*, 11(1), 29–32.
104. Iman, R. L., and Conover, W. J. (1982). "A distribution-free approach to inducing rank correlation among input variables." *Communications in Statistics-Simulation and computation*, 11(3), 311–334.
105. Jabin, S. (2014). "Stock market prediction by using artificial neural network." *International Journal of Computer Applications*, 99(9), 718–722.

106. Jáuregui, D. V., Tian, Y., and Jiang, R. (2006). “Photogrammetry applications in routine bridge inspection and historic bridge documentation.” *Transportation Research Record*, 1958(1), 24–32.
107. Jha, R. K., and Chouhan, R. (2014). “Noise-induced contrast enhancement using stochastic resonance on singular values”. *Signal, Image and Video Processing*, 8(2), 339–347
108. Jiang, Y. (2010). “Application and Comparison of Regression and Markov Chain Methods in Bridge Condition Prediction and System Benefit Optimization.” *Journal of the Transportation Research Forum*, 49(2), 91-110.
109. Joni, H. H., Alwan, I. A., and Naji, G. A. (2020). “Investigations of the road pavement surface conditions using MATLAB image processing.” *IOP Conference Series: Materials Science and Engineering*, 737(1), 1-9.
110. Kaushik, M., Sharma, R., and Vidhyarthi, A. (2012). “Analysis of Spatial Features in CBIR System.” *International Journal of Computer Applications*, 54(17), 11–15.
111. Kelly, D. L., Youngblood, R. W., and Vedros, K. G. (2010). “*Minimally Informative Prior Distributions for PSA.*” International Probabilistic Safety Assessment and Management. Seattle, United States of America.
112. Khan, M., and Shah, T. (2014). “A Literature Review on Image Encryption Techniques.” *3D Research*, 5(4), 1-25.
113. Kim, H., Bang, S., Jeong, H., Ham, Y., and Kim, H. (2018). “Analyzing context and productivity of tunnel earthmoving processes using imaging and simulation.” *Automation in Construction*, 92, 188–198.

114. Kim, I. H., Jeon, H., Baek, S. C., Hong, W. H., and Jung, H. J. (2018). "Application of crack identification techniques for an aging concrete bridge inspection using an unmanned aerial vehicle." *Sensors*, 18(6), 1–14.
115. Koch, C., Georgieva, K., Kasireddy, V., Akinci, B., and Fieguth, P. (2015). "A review on computer vision based defect detection and condition assessment of concrete and asphalt civil infrastructure." *Advanced Engineering Informatics*, 29(2), 196–210.
116. Kohestani, V. R., & Hassanlourad, M. (2016). "Modeling the mechanical behavior of carbonate sands using artificial neural networks and support vector machines." *International Journal of Geomechanics*, 16(1), 1–9.
117. Kou, G., Ergu, D., Lin, C., and Chen, Y. (2016). "Pairwise comparison matrix in multiple criteria decision making." *Technological and Economic Development of Economy*, 22(5), 738–765.
118. Kou, G., Ergu, D., and Shang, J. (2014). "Enhancing data consistency in decision matrix: Adapting Hadamard model to mitigate judgment contradiction." *European Journal of Operational Research*, 236(1), 261–271.
119. Kou, G., and Lin, C. (2014). "A cosine maximization method for the priority vector derivation in AHP." *European Journal of Operational Research*, 235(1), 225–232.
120. Kruachottikul, P., Cooharajanone, N., Phanomchoeng, G., Chavarnakul, T., Kovitangoon, K., Trakulwaranont, D., and Atchariyachanvanich, K. (2019). "Bridge Sub Structure Defect Inspection Assistance by using Deep Learning". In *2019 IEEE 10th International Conference on Awareness Science and Technology*, Morioka, Japan, 23-25 October.

121. Kumar, S. V., and Nagaraju, C. (2018). "Support vector neural network based fuzzy hybrid filter for impulse noise identification and removal from gray-scale image." *Journal of King Saud University - Computer and Information Sciences*, 1-16.
122. Le, B., and Andrews, J. (2015). "Modelling Railway Bridge Degradation Based on Historical Maintenance Data." *Safety and Reliability*, 35(2), 32–55.
123. Le, D. T., Bui, D. K., Ngo, T. D., Nguyen, Q. H., and Nguyen-Xuan, H. (2019). "A novel hybrid method combining electromagnetism-like mechanism and firefly algorithms for constrained design optimization of discrete truss structures." *Computers and Structures*, 212, 20–42.
124. Lee, J. H., Jin, S. S., Kim, I. H., and Jung, H. J. (2017). "Development of crack diagnosis and quantification algorithm based on the 2D images acquired by Unmanned Aerial Vehicle (UAV)." *The 2017 Congress on Advances in Structural Engineering and Mechanics*, Seoul, Korea, 28 August- 1 Septemeber, 1-6.
125. Lee, J. H., Lee, J. M., Kim, H. J., and Moon, Y. S. (2008). "Machine Vision System for Automatic Inspection of Bridges". *2008 Congress on Image and Signal Processing Machine*, 363–366.
126. Lee, S., Park, W., Ok, S., and Koh, H. (2011). "Preference-based Maintenance Planning for Deteriorating Bridges under Multi-objective Optimisation Framework." *Structure and Infrastructure Engineering*, 7(8), 633–644.
127. Lei, B., Wang, N., Xu, P., and Song, G. (2018). "New Crack Detection Method for Bridge Inspection Using UAV Incorporating Image Processing." *Journal of Aerospace Engineering*, 31(5), 1–13.

128. Li, G., Kou, G., and Peng, Y. (2018). "A Group Decision Making Model for Integrating Heterogeneous Information." *IEEE Transactions on Systems, Man, and Cybernetics: Systems*, 48(6), 982–992.
129. Li, J., Li, A., and Feng, M. Q. (2013). "Sensitivity and Reliability Analysis of a Self-Anchored Suspension Bridge." *Journal of Bridge Engineering*, 18(8), 703–711.
130. Li, Y., Zhao, W., Zhang, X., and Zhou, Q. (2018). "A Two-Stage Crack Detection Method for Concrete Bridges Using Convolutional Neural Networks". *IEICE Transactions on Information and Systems*, E101(12), 3249–3252.
131. Lin, C., Kou, G., Peng, Y., and Alsaadi, F. E. (2020). "Aggregation of the nearest consistency matrices with the acceptable consensus in AHP-GDM." *Annals of Operations Research*, 1–17.
132. Lin, T., Yi, T., Zhang, C., and Liu, J. (2019). Intelligent prediction of the construction cost of substation projects using support vector machine optimized by particle swarm optimization. *Mathematical Problems in Engineering*, Article ID 7631362, 10 pages.
133. Liu, Y., Yuan, Y., Balta, C., and Liu, J. (2020). A Light-Weight Deep-Learning Model with Multi-Scale Features for Steel Surface Defect Classification. *Materials*, 13(20), 1-13.
134. Lindly, J. K., and Clark, P. R. (2004). "Characterizing Work Zone Configurations and Effects." Alabama.
135. Lu, P., Pei, S., and Tolliver, D. (2016). "Regression Model Evaluation for Highway Bridge Component Deterioration Using National Bridge Inventory Data." *Journal of the Transportation Research Forum*, 55(1), 5–16.
136. Lv, Z. Y., Zhang, P., Benediktsson, J. A., and Shi, W. Z. (2014). "Morphological profiles based on differently shaped structuring elements for classification of images with very high

- spatial resolution.” *IEEE Journal of Selected Topics in Applied Earth Observations and Remote Sensing*, 7(12), 4644–4652.
137. Ma, X., Chen, H., Zhang, X., Xing, M., and Yang, P. (2019). “Effect of Asphalt Binder Characteristics on Filler-Asphalt Interactions and Asphalt Mastic Creep Properties.” *Journal of Materials in Civil Engineering*, 31(8), 1–11.
138. Mahdi, I. M., Khalil, A. H., Mahdi, H. A., and Dina, M. M. (2019). “Decision support system for optimal bridge’ maintenance.” *International Journal of Construction Management*, 1–15.
139. Mahmoodian, M., Torres-matallana, J. A., Leopold, U., Schutz, G., and Clemens, F. H. L. R. (2018). “A Data-Driven Surrogate Modelling Approach for Acceleration of Short-Term Simulations of a Dynamic Urban Drainage Simulator.” *Water*, 10(12), 1–17.
140. Makan, A., and Fadili, A. (2020). “Sustainability assessment of large-scale composting technologies using PROMETHEE method.” *Journal of Cleaner Production*, 261, 121244, 1-8.
141. Mao, X., Jiang, X., Yuan, C., and Zhou, J. (2020). “Modeling the Optimal Maintenance Scheduling Strategy for Bridge Networks.” *Applied Sciences*, 10(2), 1–16.
142. Markiz, N., and Jrade, A. (2018). “Integrating Fuzzy-Logic Decision Support With A Bridge Information Management System (BRIMS) at The Conceptual Stage Of Bridge Design.” *Journal of Information Technology in Construction*, 23, 92–121.
143. Martino, N., Maser, K., Birken, R., and Wang, M. (2016). “Quantifying Bridge Deck Corrosion Using Ground Penetrating Radar”. *Research in Nondestructive Evaluation*, 27(2), 112-124.
144. Martino, N., Maser, K., Birken, R., and Wang, M. (2014). “Determining ground

- penetrating radar amplitude thresholds for the corrosion state of reinforced concrete bridge decks.” *Journal of Environmental and Engineering Geophysics*, 19(3), 175–181.
145. Martinez, J. C. (1996). “*STROBOSCOPE State and Resource Based Simulation of Construction Processes*.” PhD. thesis, University of Michigan, United States of America.
146. Martinez, P., Mohamed, E., Mohsen, O., and Mohamed, Y. (2020). “Comparative Study of Data Mining Models for Prediction of Bridge Future Conditions.” *Journal of Performance of Constructed Facilities*, 34(1), 1–9.
147. Marzouk, M., Mohammed Abdelkader, E., and Zayed, T. (2018). “A probabilistic-Based Deterioration Model Using Ground Penetrating Radar”. *35th International Symposium on Automation and Robotics in Construction*, Berlin, Germany, 20-28 July, 1-8.
148. Marzouk, M., Mohammed Abdelkader, E., and Al-Gahtani, K. (2017). “Building information modeling-based model for calculating direct and indirect emissions in construction projects.” *Journal of cleaner production*, 152, 351-363.
149. Mašović, S., and Hajdin, R. (2014). “Modelling of Bridge Elements Deterioration for Serbian Bridge Inventory.” *Structure and Infrastructure Engineering*, 10(8), 976–987.
150. Mavi, R. K., and Standing, C. (2018). “Critical success factors of sustainable project management in construction: A fuzzy DEMATEL-ANP approach.” *Journal of Cleaner Production*, 194, 751–765.
151. Mckay, M. D., Beckman, R. J., and Conover, W. J. (1979). “Comparison of Three Methods for Selecting Values of Input Variables in the Analysis of Output from a Computer Code.” *Technometrics*, 21(2), 239–245.
152. Mehrabian, A. R., and Lucas, C. (2006). “A novel numerical optimization algorithm inspired from weed colonization.” *Ecological Informatics*, 1(4), 355–366.

153. Mikhailov, L. (2000). "A fuzzy programming method for deriving priorities in the analytic hierarchy process." *Journal of the Operational Research Society*, 51, 341–349.
154. Mirjalili, S., and Gandomi, A. H. (2017). "Chaotic gravitational constants for the gravitational search algorithm." *Applied Soft Computing Journal*, 53, 407–419.
155. Mohammed Abdelkader, E., Marzouk, M. and Zayed, T. (2020a). "A self-adaptive exhaustive search optimization-based method for restoration of bridge defects images." *International Journal of Machine Learning and Cybernetics*, 11, 165-1716.
156. Mohammed Abdelkader, E., Moselhi, O., Marzouk, M. and Zayed, T. (2020b). "Hybrid Elman Neural Network and Invasive Weed Optimization Method for Bridge Defects Recognition", *Submitted to: Journal of the Transportation Research Board* (Accepted).
157. Mohammed Abdelkader, E., Moselhi, O., Marzouk, M. and Zayed, T. (2020c). "A Multi-objective Invasive Weed Optimization Method for Segmentation of Distress Images." *Intelligent automation and soft computing*, 26(4), 1-20.
158. Mohammed Abdelkader, E., Moselhi, O., Marzouk, M. and Zayed, T. (2020d). "Entropy-Based Automated Method for Detection and Assessment of Spalling Severities in Reinforced Concrete Bridges", *Journal of Performance of Constructed Facilities*, 35(1), 1-25.
159. Mohammed Abdelkader, E., Moselhi, O., Marzouk, M. and Zayed, T. (2020e). "A Grey Wolf Optimization-Based Method for Detection and Evaluation of Scaling In Reinforced Concrete Bridges", *Submitted to: International Journal of Information Technology and Decision Making*.
160. Mohammed Abdelkader, E., Moselhi, O., Marzouk, M. and Zayed, T. (2020f). "Evaluation of Spalling in Bridges Using Machine Vision Method", *Submitted to: 37th*

International Symposium on Automation and Robotics in Construction (Accepted).

161. Mohammed Abdelkader, E., Marzouk, M. and Zayed, T. (2020g). “An Invasive Weed Optimization-based Fuzzy Decision-making Framework for Bridge Intervention Prioritization in Element and Network Levels.” *International Journal of Information Technology and Decision Making*, 19(5), 1-58.
162. Mohammed Abdelkader, E., Moselhi, O., Marzouk, M. and Zayed, T. (2020h). “An Integrative Evolutionary-based Method for Modeling and Optimizing Resource Allocation of Bridge Deck Replacement Projects”, *Submitted to: Journal of Construction Engineering and Management* (Tentatively accepted).
163. Mohammed Abdelkader, E., Moselhi, O., Marzouk, M. and Zayed, T. (2020i). “A Meta-heuristic Method for Optimizing Bridge Maintenance Plans”, *Submitted to: Journal of Construction Engineering and Management*.
164. Mohammed Abdelkader, E., Marzouk, M., and Zayed, T. (2019a). “An Optimization-Based Methodology for the Definition of Amplitude Thresholds of the Ground Penetrating”. *Soft Computing*, 23, 12063-12086.
165. Mohammed Abdelkader, E., Marzouk, M., and Zayed, T. (2019b). “Mapping Ground Penetrating Radar Amplitudes using Artificial Neural Network and Multiple Regression Analysis Methods”. *International Journal of Strategic Decision Sciences*, 10 (2), 1-23.
166. Mohammed Abdelkader, E., Zayed, T., and Marzouk, M. (2019c). “A Computerized Hybrid Bayesian-Based Approach for Modeling the Deterioration of Concrete Bridge Decks”. *Structure and Infrastructure Engineering*, 25(19), 1178-1199.
167. Mohammed Abdelkader, E., Moselhi, O., Marzouk, M. and Zayed, T. (2019d). “Condition Prediction of Concrete Bridge Decks Using Markov Chain Monte Carlo-Based

- Method”, *7th CSCE International Construction Specialty Conference Jointly with Construction Research Congress*, Laval, Canada, 12-15 June, 1-10.
168. Mohammed Abdelkader, E., Zayed, T., and Marzouk, M. (2019e). “Modelling the Deterioration of Bridge Decks Based on Semi-Markov Decision Process”. *International Journal of Strategic Decision Sciences*, 10(1), 1-23.
169. Mohammed Abdelkader, E., Marzouk, M., and Zayed, T. (2018). “Modeling of Concrete Bridge Decks Deterioration using a Hybrid Bayesian Model”. *CSCE 2018 Annual Conference: Building Tomorrow’s society*, Fredericton, Canada, 13-16 June, 1-8.
170. Moon, H., and Kim, J. (2011). “Inteligent Crack Detecting Algorithm on The Concrete Crack Image Using Neural Network”, *28th International Symposium on Automation and Robotics in Construction (ISARC)*, Seoul, Korea, 1-7.
171. Morcous, G., Lounis, Z., and Cho, Y. (2010). “An integrated system for bridge management using probabilistic and mechanistic deterioration models: Application to bridge decks.” *KSCE Journal of Civil Engineering*, 14(4), 527–537.
172. Moufti, S. A., Zayed, T., and Dabous, S. A. (2014). “Defect-Based Condition Assessment of Concrete Bridges: Fuzzy Hierarchical Evidential Reasoning Approach.” *Transportation Research Record: Journal of the Transportation Research Board*, 2431(1), 1-9.
173. Mulimani, M., and Koolagudi, S. G. (2019). “Segmentation and characterization of acoustic event spectrograms using singular value decomposition.” *Expert Systems with Applications*, 120, 413–425.
174. Muñoz, Y. F., Paz, A., Fuente-Mella, H. D. La, V.Fariña, J., and M.Sales, G. (2016). “Estimating Bridge Deterioration for Small Data Sets using Regression and Markov Models.” *International Journal of urban and Civil Engineering*, 10(5), 1-8.

175. Nagaraju, T. V., Durga Prasad, C., and Murthy, N. G. K. (2020). “Invasive Weed Optimization Algorithm for Prediction of Compression Index of Lime-Treated Expansive Clays.” *Soft Computing for Problem Solving*, 317-324.
176. National Research Council Canada. (2013). “*Critical Concrete Infrastructure: Extending the Life of Canada’s Bridge Network*”. <<http://www.nrc-cnrc.gc.ca/ci-ic/article/v18n1-5>> (20.12.2016).
177. Nemati-Lafmejani, R., Davari-Ardakani, H., and Najafzad, H. (2019). “Multi-mode resource constrained project scheduling and contractor selection: Mathematical formulation and metaheuristic algorithms.” *Applied Soft Computing Journal*, 81, 1-22.
178. Nguyen, T. T., and Dinh, K. (2019). “Prediction of bridge deck condition rating based on artificial neural networks.” *Journal of Science and Technology in Civil Engineering (STCE) - NUCE*, 13(3), 15–25.
179. Ning, J., Zhang, C., Sun, P., Feng, Y. (2019). “Comparative Study of Ant Colony Algorithms for Multi-Objective Optimization.” *Information*. 10(11), 1–19.
180. Nurani, A. I., Pramudyaningrum, A. T., and Fadhila, S. R. (2017). “Analytical Hierarchy Process (AHP), Fuzzy AHP , and TOPSIS for Determining Bridge Maintenance Priority Scale in Banjarsari , Surakarta.” *International Journal of Science and Applied Science: Conference Series*, 2(1), 60–71.
181. Nurdin, A., Kristiawan, S. A., and Handayani, D. (2017). “Determination of the bridge maintenance and rehabilitation priority scale in kabupaten Pinrang.” *Journal of Physics: Conference Series*, 795, 1–7.
182. Omar, T., Nehdi, M. L., and Zayed, T. (2018a). “Infrared thermography model for automated detection of delamination in RC bridge decks.” *Construction and Building*

Materials, 168, 313–327.

183. Omar, T., Nehdi, M. L., and Zayed, T. (2018b). “Rational condition assessment of RC bridge decks subjected to corrosion-induced delamination.” *Journal of Materials in Civil Engineering*, 30(1), 1–13.
184. Pal, S., and Chatterjee, S. (2018). “Mathematical morphology aided optic disk segmentation from retinal images.” *2017 3rd International Conference on Condition Assessment Techniques in Electrical Systems*, Rupnagar, India, 16-18 November, 380-385.
185. Pan, H., Tian, L., Fu, X., and Li, H. (2020). “Sensitivities of the seismic response and fragility estimate of a transmission tower to structural and ground motion uncertainties.” *Journal of Constructional Steel Research*, 167, 1–13.
186. Parnianifard, A., Azfanizam, A. S., Ariffin, M. K. A., Ismail, M. I. S., and Ale Ebrahim, N. (2019). “Recent developments in metamodel based robust black-box simulation optimization: An overview.” *Decision Science Letters*, 8(1), 17–44.
187. Pavithra, D., Saranya, T., Prakash, K., and Soundarya, G. (2018). “Electronic Crack Detection on Concrete.” *International Journal of Advanced Science and Engineering Research*, 3(1), 515–521.
188. Petroodi, S. E. H., Dit Eynaud, A. B., Klement, N., and Tavakkoli-Moghaddam, R. (2019). “Simulation-based optimization approach with scenario-based product sequence in a reconfigurable manufacturing system (RMS): A case study.” *IFAC-PapersOnLine*, 52(13), 2638–2643.
189. Phochanikorn, P., and Tan, C. (2019). “An Integrated Multi-Criteria Decision-Making Model Based on Prospect Theory for Green Supplier Selection under Uncertain Environment : A Case Study of the Thailand Palm Oil Products Industry.” *Sustainability*,

11(7), 1–22.

190. Pokharel, M. (2020). “*Computational Complexity Theory (P , NP , NP-Complete and NP-Hard Problems)*.”, Tribhuvan University, Nepal.
191. Prasanna, P., Dana, K. J., Gucunski, N., Basily, B. B., La, H. M., Lim, R. S., and Parvardeh, H. (2014). “Automated Crack Detection on Concrete Bridges.” *IEEE Transactions on Automation Science and Engineering*, 13(2), 1–9.
192. Prasad, R., Ali, M., Xiang, Y., and Khan, H. (2020). “A double decomposition-based modelling approach to forecast weekly solar radiation.” *Renewable Energy*, 152, 9–22.
193. Prasetyo, E. D. W., Handajani, M., and Ismiyati. (2019). Criteria Analysis, weight and Priority for Handling Bridges in Kudus District using AHP and Promethee II methods. *Journal of Physics: Conference Series*, 1167(1), 012009.
194. Qu, X., Meng, Q., Yuanita, V., and Wong, Y. H. (2011). “Design and implementation of a quantitative risk assessment software tool for Singapore road tunnels.” *Expert Systems with Applications*, 38(11), 13827–13834.
195. Reddy, B. S. K., and Wanjari, S. (2018). “Core strength of concrete using newly developed in situ compressive testing machine.” *Magazine of Concrete Research*, 70(22), 1149–1156.
196. Ranjith, S., Setunge, S., Gravina, R., and Venkatesan, S. (2013). “Deterioration Prediction of Timber Bridge Elements Using the Markov Chain.” *Journal of Performance of Constructed Facilities*, 27(3), 319–325.
197. Rashidi, M., Ghodrat, M., Samali, B., Kendall, B., and Zhang, C. (2017). “Remedial Modelling of Steel Bridges through Application of Analytical Hierarchy Process (AHP).” *Applied Sciences*, 7(2), 1–20.

198. Rathi, V. P. G. P., and Palani, D. S. (2012). "Brain tumor mri image classification with feature selection and extraction using linear discriminant analysis". *International Journal of Information Sciences and Techniques*, 2(4), 1-16.
199. Karbakhsh Ravari, H., Salajeghe, S., and Sheikhy, A. (2020). "Providing optimal decision-making function for efficient selection of a contractor using PSO algorithm in MAPNA." *International Journal of Nonlinear Analysis and Applications*, 11(2), 29–38
200. Ravirala, V., and Grivas, D. A. (1995). "State Increment Method of Life-Cycle Cost Analysis for Highway Management." *Journal of Infrastructure Systems*, 1(3), 151–159.
201. Rodríguez-Fdez, I., Canosa, A., Mucientes, M., Bugar, A. (2015). "STAC: a web platform for the comparison of algorithms using statistical tests." *2015 IEEE International Conference on Fuzzy Systems (FUZZ-IEEE)*, Istanbul, Turkey, 2-5 August.
202. Ryerkerk, M. L., Averill, R. C., Deb, K., and Goodman, E. D. (2016). "Solving Metameric Variable-length Optimization Problems Using Genetic Algorithms." *Genetic Programming and Evolvable Machines*, 128(2), 247-277.
203. Saaty, T. L. (1977). "A scaling method for priorities in hierarchical structures." *Journal of Mathematical Psychology*, 15(3), 234–281.
204. Samsuri, S., Surbakti, M., Tarigan, A. P., and Anas, R. (2019). "A Study on the Road Conditions Assessment Obtained from International Roughness Index (IRI): Roughometer Vs Hawkeye." *Simetrikal Journal of Engineering and Technology*, 1(2), 103–113.
205. Sayed, G. I., Darwish, A., and Hassanien, A. E. (2018). "A New Chaotic Whale Optimization Algorithm for Features Selection." *Journal of Classification*, 35(2), 300–344.
206. Shanavaz, K. T., and Mythili, P. (2016). "A fingerprint-based hybrid gender classification system using genetic algorithm." *International Journal of Computational Vision and*

Robotics, 6(4), 399-413.

207. Saxena, A., Shekhawat, S., and Kumar, R. (2018). "Application and Development of Enhanced Chaotic Grasshopper Optimization Algorithms. " *Modelling and Simulation in Engineering*, 2018, Article ID 4945157, 14 pages.
208. Sharma, S., and Goyal, P. K. (2019). "Fuzzy assessment of the risk factors causing cost overrun in construction industry." *Evolutionary Intelligence*, 1–13.
209. Shim, H. S., and Lee, S. H. (2017). "Balanced Allocation of Bridge Deck Maintenance Budget Through." *KSCE Journal of Civil Engineering*, 21(4), 1039-1046.
210. Shim, H. S., Lee, S. H., and Kang, B. S. (2017). "Pareto front generation for bridge deck management system using bi-objective optimization." *KSCE Journal of Civil Engineering*, 21(5), 1563–1572.
211. Shuang-rui, C., Zheng, S., and Quan-sheng, Y. (2015). "Concrete Crack Width Detecting System for Android Platform." *The Open Civil Engineering Journal*, 9, 846–851.
212. Słoński, M. (2019). "A comparison of deep convolutional neural networks for image-based detection of concrete surface cracks". *Computer Assisted Methods in Engineering and Science*, 26(2), 105–112.
213. Shreyas, S. K., and Dey, A. (2019). "Application of soft computing techniques in tunnelling and underground excavations: state of the art and future prospects." *Innovative Infrastructure Solutions*, 4(1), 1-15.
214. Song, J., Yang, Y., Wu, J., Wu, J., Sun, X., & Lin, J. (2018). "Adaptive surrogate model based multiobjective optimization for coastal aquifer management." *Journal of Hydrology*, 561, 98–111.

215. Stamate, C., Magoulas, G. D., and Thomas, M. S. C. (2015). "Transfer learning approach for financial applications." *ArXiv:1509.02807*, 1–5.
216. Su, L., Trivedi, R., Sapra, N. V., Piggott, A. Y., Verduyck, D., and Vučković, J. V. (2018). "Fully-automated optimization of grating couplers." *Optics Express*, 26(4), 4766.
217. Su, T. (2013). "Application of Computer Vision to Crack Detection of Concrete Structure." *International Journal of Engineering and Technology*, 5(4), 457–46.
218. Suthanaya, P. A., and Artamana, I. B. (2017). "Multi-criteria Approach for Prioritizing Bridge Maintenance in Developing Country (Case Study of Bali Province, Indonesia)." *Asian Journal of Applied Sciences*, 5(2), 410–418.
219. Tang, J., Zhang, R., Wang, P., Zhao, Z., Fan, L., and Liu, X. (2020). "A discrete shuffled frog-leaping algorithm to identify influential nodes for influence maximization in social networks." *Knowledge-Based Systems*, 187, 1-12.
220. Tanwar, S., Ramani, T., and Tyagi, S. (2018). "Dimensionality reduction using PCA and SVD in big data: A comparative case study." *International Conference on Future Internet Technologies and Trends*, Surat, India, 31 August-2 September, 116–125.
221. Tao, W., Tao, D., Xiaohong, Z., and Yiming, S. (2014). "A Research on Detecting and Recognizing Bridge Cracks in Complex Underwater Conditions." *Frattura ed Integrità Strutturale*, 30, 537–544.
222. Tharwat, A., Elhoseny, M., Hassanien, A. E., Gabel, T., and Kumar, A. (2019). "Intelligent Bézier curve-based path planning model using Chaotic Particle Swarm Optimization algorithm." *Cluster Computing*, 22(s2), 4745–4766.
223. Thompson, P. D., Sobanjo, J. O., and Kerr, R. (2003). "Florida DOT project-level bridge management models." *Journal of Bridge Engineering*, 8(6), 345–352.

224. Tong, X., Guo, J., Ling, Y., and Yin, Z. (2011). "A New Image-Based Method for Concrete Bridge Bottom Crack Detection." *2011 International Conference on Image Analysis and Signal Processing*, Wuhan, China, 21-23 October, 1-4.
225. Van Dam, K. H., Nikolic, I., and Lukszo, Z. (2012). *Agent-Based Modelling of Socio-Technical Systems*. Springer.
226. Van Eck, N. J., and Waltman, L. (2010). "Software survey : VOSviewer , a computer program for bibliometric mapping." *Scientometrics*, 84, 523–538.
227. Van Laarhoven, P. J. M, and W.Pedrycz. (1983). "A fuzzy extension of Saaty's priority theory." *Fuzzy Sets and Systems*, 11, 229–241.
228. Valipour, A., Yahaya, N., Md Noor, N., Antuchevičienė, J., and Tamošaitienė, J. (2017). "Hybrid SWARA-COPRAS method for risk assessment in deep foundation excavation project: an Iranian case study." *Journal of Civil Engineering and Management*, 23(4), 524–532.
229. Vulević, T., and Dragović, N. (2017). "Multi-criteria decision analysis for sub-watersheds ranking via the PROMETHEE method." *International Soil and Water Conservation Research*, 5(1), 50–55.
230. Wang, Q., Li, B., and Nie, X. (2019). "Bridge Crack Identification Based on Feature Fusion of Convolutional Neural Networks." *2019 International Conference on Computation and Information Sciences (ICCIS)*, Aljouf, Kingdom of Saudi Arabia, 3-4 July, 1-11.
231. Wang, Y., Zhang, J. Y., Liu, J. X., Zhang, Y., Chen, Z. P., Li, C. G., He, K., and Yan, R. (2019). "Research on Crack Detection Algorithm of the Concrete Bridge Based on Image Processing." *Procedia Computer Science*, 154, 610–616.
232. Wu, D., Yuan, C., Kumfer, W., and Liu, H. (2017). "A life-cycle optimization model

- using semi-markov process for highway bridge maintenance.” *Applied Mathematical Modelling*, 43, 45–60.
233. Wu, Y., Zhang, B., Wu, C., Zhang, T., and Liu, F. (2019). “Optimal site selection for parabolic trough concentrating solar power plant using extended PROMETHEE method: A case in China.” *Renewable Energy*, 143, 1910–1927.
234. Wu, X., and Hu, F. (2020). “Analysis of ecological carrying capacity using a fuzzy comprehensive evaluation method.” *Ecological Indicators*, 113, 1–13.
235. Xie, H. B., Wu, W. J., and Wang, Y. F. (2018). “Life-time reliability based optimization of bridge maintenance strategy considering LCA and LCC.” *Journal of Cleaner Production*, 176, 36–45.
236. Xu, H., Su, X., Wang, Y., Cai, H., Cui, K., and Chen, X. (2019). “Automatic Bridge Crack Detection Using a Convolutional Neural Network.” *Applied Sciences*, 9(14), 1–14.
237. Xuejun, W. and Yan, Z. (2017). “The Detection and Recognition of Bridges’ Cracks Based on Deep Belief Network.” *2017 IEEE International Conference on Computational Science and Engineering (CSE) and IEEE International Conference on Embedded and Ubiquitous Computing (EUC)*, Guangzhou, China, 21-24 July, 768–771.
238. Xuejun, X.U., and Xiaoning, Z. (2013). “Crack detection of reinforced concrete bridge using video image.” *Journal of Central South University*, 20, 2605–2613.
239. Yagiz, S., Yazitova, A., and Karahan, H. (2020). “Application of differential evolution algorithm and comparing its performance with literature to predict rock brittleness for excavatability.” *International Journal of Mining, Reclamation and Environment*, 1–14.
240. Yan, S., Jin, L., Duan, S., Zhao, L., Yao, C., and Zhang, W. (2013). “Power line image segmentation and extra matter recognition based on improved Otsu algorithm.” *2013 2nd*

International Conference on Electric Power Equipment - Switching Technology, Matsue, Japan, 20-23 October, 1-4.

241. Yang, C. C., Soh, C. S., and Yap, V. V. (2018). "A systematic approach in appliance disaggregation using k-nearest neighbours and naive Bayes classifiers for energy efficiency". *Energy Efficiency*, 11, 239–259.
242. Yang, Q., Shi, W., Chen, J., and Lin, W. (2020). "Deep convolution neural network-based transfer learning method for civil infrastructure crack detection." *Automation in Construction*, 116, 103199.
243. Yao, C., Tao, M., Xiaojie, W., and Feng, L. (2016). "A Bridge Crack Image Detection and Classification Method Based On Climbing Robot". *Proceedings of the 35th Chinese Control Conference*, Chengdu, China, 27-29 July, 4037–4042.
244. Yazdani, M., Abdi, M. R., Kumar, N., Keshavarz-ghorabae, M., and Chan, F. T. S. (2019). "Improved Decision Model for Evaluating Risks in Construction Projects." *Journal of Construction Engineering and Management*, 145(5), 1–13.
245. Yeboah, Y., Wu, W., Jie, W. J., and Yu, Z. L. (2015). "Robotic Crack Detection and Classification via AdaBoost-RVM Implementation". *International Journal of Mechanical Engineering and Robotics Research*, 4(4), 361–367.
246. Yoon, Y., and Hastak, M. (2016). "Condition Improvement Measurement Using the Condition Evaluation Criteria of Concrete Bridge Decks." *Journal of Transportation Engineering*, 142(11), 1–8.
247. Younes, T., Ni, F. M., and Tighe, S. (2018). "Risk analysis in paving operations using discrete event simulation : a case study of Taiwan permeable asphalt concrete pavement pilot road project." *International Journal of Pavement Engineering*, 1–11.

248. Yossyafra, Angelia, N., Yosritzal, Meyadtri, and Mazni5, D. I. (2019). “Determining the priority criteria and ranking of provincial bridge maintenance in West Sumatra using a combination of the Fuzzy Analytical Hierarchy Process and VIKOR-Modification methods.” *IOP Conference Series: Materials Science and Engineering* 602, 8-9 November, Padang, Indonesia, 1-9.
249. Yu, C., Li, H., and Wang, X. (2019). “SVD-based image compression, encryption, and identity authentication algorithm on cloud.” *IET Image Processing*, 13(12), 2224–2232.
250. Yu, D., Hong, J., Zhang, J., and Niu, Q. (2018). “Multi-Objective Individualized-Instruction Teaching-Learning-Based Optimization Algorithm.” *Applied Soft Computing*, 62, 288–314.
251. Zambon, I., Vidovic, A., Strauss, A., Matos, J., and Amado, J. (2017). “Comparison of Stochastic Prediction Models Based on Visual inspections of Bridge Decks.” *Journal of Civil Engineering and Management*, 23(5), 553–561.
252. Zeng, J., An, M., and Smith, N. J. (2007). “Application of a fuzzy based decision making methodology to construction project risk assessment.” *International Journal of Project Management*, 25, 589–600.
253. Zhang, H., Kou, G., and Peng, Y. (2019). “Soft consensus cost models for group decision making and economic interpretations.” *European Journal of Operational Research*, 277(3), 964–980.
254. Zhang, H., Yu, H., Zhang, H., and Yang, W. (2017). “Accurate Extraction of Cracks On The Underside Of Concrete Bridges.” In *2017 IEEE International Geoscience and Remote Sensing Symposium (IGARSS)*, Texas, USA, 23-28 July, 2341-2344.
255. Zhang, J., Xie, N., Zhang, X., Yue, K., Li, W., and Kumar, D. (2018). “Machine learning

- based resource allocation of cloud computing in auction.” *Computers, Materials and Continua*, 56(1), 123–135.
256. Zhang, L., Luo, W., and Xu, Y. (2018). “Bridge Crack Image Segmentation Based on Improved Watershed Algorithm”. In *2018 Chinese Control And Decision Conference (CCDC)*, Shenyang, China, 9-11 July, 3537-3541.
257. Zhang, L., Zhou, G., Han, Y., Lin, H. and Wu, Y. (2018). “Application of Internet of Things Technology and Convolutional Neural Network Model in Bridge Crack Detection”. *IEEE Access*, 6, 39442-39451.
258. Zhang, Y., and Wu, L. (2011). “Optimal Multi-Level Thresholding Based on Maximum Tsallis Entropy via an Artificial Bee Colony Approach.” *Entropy*, 13, 841–859.
259. Zhu, J., and Song, J. (2020). “Weakly supervised network based intelligent identification of cracks in asphalt concrete bridge deck.” *Alexandria Engineering Journal*, 59(3), 1307–1317.

APPENDIX I: SAMPLE OF C#.NET CODE

This section provides sample of the written C#.net code to develop the automated platform designated for deterioration modeling of bridge decks.

```
using System;
using System.Collections.Generic;
using System.ComponentModel;
using System.Data;
using System.Drawing;
using System.Linq;
using System.Text;
using System.Windows.Forms;
using Microsoft.Office.Interop.Excel;
using MApp;
namespace WindowsFormsApplication6
{
    public partial class Form5 : Form
    {
        public Form5()
        {
            InitializeComponent();
            textBox15.Text = "150";
        }

        private void button3_Click(object sender, EventArgs e)
        {
            Form6 frm6 = new Form6();

            frm6.Show();
        }

        private void button4_Click(object sender, EventArgs e)
        {
            double nsamples;

            nsamples = double.Parse(textBox15.Text);

            Microsoft.Office.Interop.Excel.Application myexcel = new
Microsoft.Office.Interop.Excel.Application();

            Microsoft.Office.Interop.Excel._Worksheet MYWORKSSET;

            Microsoft.Office.Interop.Excel.Range mycells;

            myexcel.Workbooks.Open(@"C:\Users\abdelkader\Desktop\Automation\ns1.xlsx");

            myexcel.Visible = true;

            MYWORKSSET = myexcel.Worksheets.Item[1];

            mycells = MYWORKSSET.Cells;

            mycells.Item[1, 1].value = nsamples;
        }
    }
}
```

```

private void button1_Click(object sender, EventArgs e)
{
    MApp.MLApp matlab = new MApp.MLApp();

    matlab.Execute(@"run C:\Users\abdelkader\Desktop\Automation\LH1.m");

    matlab.Execute("[thisismyoutput]=mymatlabcode(temp)");
}

private void button5_Click(object sender, EventArgs e)
{
    Microsoft.Office.Interop.Excel.Application myexcel = new
Microsoft.Office.Interop.Excel.Application();

    Microsoft.Office.Interop.Excel._Worksheet MYWORKSSET;

    Microsoft.Office.Interop.Excel.Range mycells;

    myexcel.Workbooks.Open(@"C:\Users\abdelkader\Desktop\Automation\LHS1.xlsx");

    myexcel.Visible = false;

    MYWORKSSET = myexcel.Worksheets.Item[1];

    mycells = MYWORKSSET.Cells;

    int m;

    int n;

    dataGridView1.ColumnCount = 128;

    dataGridView1.RowCount = 150;

    for (m = 1; m <= dataGridView1.RowCount; m++)

        for (n = 0; n < dataGridView1.ColumnCount; n++)
        {

            dataGridView1.Columns[n].Name = "" + (n + 1);

            dataGridView1.Rows[m-1].Cells[n].Value = Math.Round(mycells.Item[m, n
+ 1].value, 4);

        }

    }

    private void dataGridView1_CellContentClick(object sender,
DataGridViewCellEventArgs e)
    {

    }

    private void button2_Click(object sender, EventArgs e)
    {

```

```

        Microsoft.Office.Interop.Excel.Application myexcel = new
Microsoft.Office.Interop.Excel.Application();

        Microsoft.Office.Interop.Excel._Worksheet MYWORKSSET;

        Microsoft.Office.Interop.Excel.Range mycells;

        myexcel.Workbooks.Open(@"C:\Users\abdelkader\Desktop\Automation\p11tt.xlsx");

        myexcel.Visible = true;

        MYWORKSSET = myexcel.Worksheets.Item[1];

        mycells = MYWORKSSET.Cells;
    }
}

using System;
using System.Collections.Generic;
using System.ComponentModel;
using System.Data;
using System.Drawing;
using System.Linq;
using System.Text;
using MSBN3Lib;
using System.IO;
using System.Windows.Forms;

namespace WindowsFormsApplication6
{
    public partial class Form7 : Form
    {
        public Form7()
        {
            InitializeComponent();
        }

        private void button1_Click(object sender, EventArgs e)
        {

        }

        private void button3_Click(object sender, EventArgs e)
        {
            Form8 frm8 = new Form8();

            frm8.Show();
        }

        private void button2_Click(object sender, EventArgs e)
        {
            Microsoft.Office.Interop.Excel.Application myexcel = new
Microsoft.Office.Interop.Excel.Application();

            Microsoft.Office.Interop.Excel._Worksheet MYWORKSSET;

```

```

Microsoft.Office.Interop.Excel.Range mycells;

myexcel.Workbooks.Open(@"C:\Users\abdelkader\Desktop\Automation\LHS1.xlsx");

myexcel.Visible = true;

MYWORKSSET = myexcel.Worksheets.Item[1];

mycells = MYWORKSSET.Cells;
MSBN aMSBN = new MSBN();

Model modelCat = aMSBN.Models.Add("Cat", Directory.GetCurrentDirectory() +
@"\..\..\..\P12.dsc",
Directory.GetCurrentDirectory() + @"..\..\..\loaderror.log");

Node nodeTransition = modelCat.ModelNodes["Transition"];
Node nodeCorrosion = modelCat.ModelNodes["Corrosion"];
Node nodeDelamination = modelCat.ModelNodes["Delamination"];
Node nodeCracking = modelCat.ModelNodes["Cracking"];
Node nodeSpalling = modelCat.ModelNodes["Spalling"];
Node nodePopout = modelCat.ModelNodes["Popout"];
Dist aDist = nodeTransition.get_Dist();

int mm = 150;
int nn = 132;
double[,] esslam = new double[mm, nn];
double[] ahmed1 = new double[mm];
double[] ahmed2 = new double[mm];
double[] ahmed3 = new double[mm];
double[] ahmed4 = new double[mm];
double[] ahmed5 = new double[mm];
double[] ahmed6 = new double[mm];
double[] ahmed7 = new double[mm];
double[] ahmed8 = new double[mm];
double[] ahmed9 = new double[mm];
double[] ahmed10 = new double[mm];
double[] ahmed11 = new double[mm];
double[] ahmed12 = new double[mm];
double[] ahmed13 = new double[mm];
double[] ahmed14 = new double[mm];
double[] ahmed15 = new double[mm];
int n;

int m;

for (m = 0; m <= 149; m++)
{
    for (n = 0; n <= 131; n++)
    {

        esslam[m, n] = mycells.Item[m + 1, n + 1].value;

        if (n <= 63)
        {
            nodeTransition.get_Dist()[n, "Yes"] = esslam[m, n];
            nodeTransition.get_Dist()[n, "No"] = 1 - esslam[m, n];
        }
    }
}

```

```

}

else if (n <= 79)
{
    nodeDelamination.get_Dist()[0, "Yes"] = es slam[m, 64];
    nodeDelamination.get_Dist()[0, "No"] = es slam[m, 65];
    nodeDelamination.get_Dist()[0, "Poor"] = es slam[m, 66];
    nodeDelamination.get_Dist()[0, "VP"] = es slam[m, 67];

    nodeDelamination.get_Dist()[1, "Yes"] = es slam[m, 68];
    nodeDelamination.get_Dist()[1, "No"] = es slam[m, 69];
    nodeDelamination.get_Dist()[1, "Poor"] = es slam[m, 70];
    nodeDelamination.get_Dist()[1, "VP"] = es slam[m, 71];

    nodeDelamination.get_Dist()[2, "Yes"] = es slam[m, 72];
    nodeDelamination.get_Dist()[2, "No"] = es slam[m, 73];
    nodeDelamination.get_Dist()[2, "Poor"] = es slam[m, 74];
    nodeDelamination.get_Dist()[2, "VP"] = es slam[m, 75];

    nodeDelamination.get_Dist()[3, "Yes"] = es slam[m, 76];
    nodeDelamination.get_Dist()[3, "No"] = es slam[m, 77];
    nodeDelamination.get_Dist()[3, "Poor"] = es slam[m, 78];
    nodeDelamination.get_Dist()[3, "VP"] = es slam[m, 79];

    }

```

```

else if (n <= 95)
{
    nodeCracking.get_Dist()[0, "Yes"] = es slam[m, 80];
    nodeCracking.get_Dist()[0, "No"] = es slam[m, 81];
    nodeCracking.get_Dist()[0, "Poor"] = es slam[m, 82];
    nodeCracking.get_Dist()[0, "VP"] = es slam[m, 83];

    nodeCracking.get_Dist()[1, "Yes"] = es slam[m, 84];
    nodeCracking.get_Dist()[1, "No"] = es slam[m, 85];
    nodeCracking.get_Dist()[1, "Poor"] = es slam[m, 86];
    nodeCracking.get_Dist()[1, "VP"] = es slam[m, 87];

    nodeCracking.get_Dist()[2, "Yes"] = es slam[m, 88];
    nodeCracking.get_Dist()[2, "No"] = es slam[m, 89];
    nodeCracking.get_Dist()[2, "Poor"] = es slam[m, 90];
    nodeCracking.get_Dist()[2, "VP"] = es slam[m, 91];

    nodeCracking.get_Dist()[3, "Yes"] = es slam[m, 92];
    nodeCracking.get_Dist()[3, "No"] = es slam[m, 93];
    nodeCracking.get_Dist()[3, "Poor"] = es slam[m, 94];
    nodeCracking.get_Dist()[3, "VP"] = es slam[m, 95];

}

```

```

else if (n <= 111)
{
    nodeSpalling.get_Dist()[0, "Yes"] = es slam[m, 96];
    nodeSpalling.get_Dist()[0, "No"] = es slam[m, 97];
    nodeSpalling.get_Dist()[0, "Poor"] = es slam[m, 98];
    nodeSpalling.get_Dist()[0, "VP"] = es slam[m, 99];

```

```

nodeSpalling.get_Dist()[1, "Yes"] = esslam[m, 100];
nodeSpalling.get_Dist()[1, "No"] = esslam[m, 101];
nodeSpalling.get_Dist()[1, "Poor"] = esslam[m, 102];
nodeSpalling.get_Dist()[1, "VP"] = esslam[m, 103];

nodeSpalling.get_Dist()[2, "Yes"] = esslam[m, 104];
nodeSpalling.get_Dist()[2, "No"] = esslam[m, 105];
nodeSpalling.get_Dist()[2, "Poor"] = esslam[m, 106];
nodeSpalling.get_Dist()[2, "VP"] = esslam[m, 107];

nodeSpalling.get_Dist()[3, "Yes"] = esslam[m, 108];
nodeSpalling.get_Dist()[3, "No"] = esslam[m, 109];
nodeSpalling.get_Dist()[3, "Poor"] = esslam[m, 110];
nodeSpalling.get_Dist()[3, "VP"] = esslam[m, 111];
}

else if (n <= 127)
{
nodePopout.get_Dist()[0, "Yes"] = esslam[m, 112];
nodePopout.get_Dist()[0, "No"] = esslam[m, 113];
nodePopout.get_Dist()[0, "Poor"] = esslam[m, 114];
nodePopout.get_Dist()[0, "VP"] = esslam[m, 115];

nodePopout.get_Dist()[2, "Yes"] = esslam[m, 116];
nodePopout.get_Dist()[2, "No"] = esslam[m, 117];
nodePopout.get_Dist()[2, "Poor"] = esslam[m, 118];
nodePopout.get_Dist()[2, "VP"] = esslam[m, 119];

nodePopout.get_Dist()[3, "Yes"] = esslam[m, 120];
nodePopout.get_Dist()[3, "No"] = esslam[m, 121];
nodePopout.get_Dist()[3, "Poor"] = esslam[m, 122];
nodePopout.get_Dist()[3, "VP"] = esslam[m, 123];

nodePopout.get_Dist()[3, "Yes"] = esslam[m, 124];
nodePopout.get_Dist()[3, "No"] = esslam[m, 125];
nodePopout.get_Dist()[3, "Poor"] = esslam[m, 126];
nodePopout.get_Dist()[3, "VP"] = esslam[m, 127];
}

else if (n <= 131)
{
nodeCorrosion.get_Dist()[0, "Yes"] = esslam[m, 128];
nodeCorrosion.get_Dist()[0, "No"] = esslam[m, 129];
nodeCorrosion.get_Dist()[0, "Poor"] = esslam[m, 130];
nodeCorrosion.get_Dist()[0, "VP"] = esslam[m, 131];
}

Engine inferCat = modelCat.Engine;
double[] z = new double[150];
z[m] = inferCat.Belief("Transition", "Yes");
mycells.Item[m + 1, 133].value = z[m];
}
}
}

```